Stony Brook University

Phenylalanine as a probe for mineral-mediated hydroxyl radical formation

A Dissertation Presented

by

Shawn Charles Fisher

to

The Graduate School

in Partial Fulfillment of the

Requirements

for the Degree of

Doctor of Philosophy

in

Chemistry

Stony Brook University

August 2012

Stony Brook University
The Graduate School

Shawn Charles Fisher

We, the dissertation committee for the above candidate for the
Doctor of Philosophy degree, hereby recommend
acceptance of this dissertation.

Bruce J. Brownawell – Advisor
Associate Professor, School of Marine and Atmospheric Sciences

Dale G. Drueckhammer – Co-Advisor
Professor, Department of Chemistry

Robert C. Kerber – Chair of Defense
Distinguished Professor, Department of Chemistry

Martin A. A. Schoonen
Professor, Department of Geosciences

Sanford R. Simon
Professor, Departments of Biochemistry and Cell Biology and Pathology

This dissertation is accepted by the Graduate School

Charles Taber
Interim Dean of the Graduate School

Abstract of the Dissertation

Phenylalanine as a probe for mineral-mediated hydroxyl radical formation

by

Shawn Charles Fisher

Doctor of Philosophy

in

Chemistry

Stony Brook University

2012

Mineral-induced formation of reactive oxygen species (ROS) can lead to transformations of organic compounds in aqueous solutions and has been tied to human-health related illnesses resulting from inhalation of mineral or pyritic coal dust. This dissertation reports the use of phenylalanine (Phe) as a biologically-relevant probe to better characterize the conditions that control the formation and fate of hydroxyl radical ($^{\cdot}OH$) in suspensions of pyrite, coal, and manganese oxide minerals (MnO_x). An HPLC-MS method involving minimal sample processing was developed that allows for sensitive analysis of both Phe and its specific phenyl hydroxylation product mixture of *ortho*-, *meta*-, and *para*-tyrosine (Tyr) – with *o*-Tyr and *m*-Tyr unique to reaction of Phe with $^{\cdot}OH$. In pyrite mixtures with pure water, $^{\cdot}OH$ was produced at substantial rates for up to ten days in proportion to the surface area of the pyrite. It was shown for the first time that reaction kinetics were much less than first-order in initial Phe concentration, despite the fact that Phe disappearance as a function of time was generally exponential. These results could be rationalized and modeled by considering that the effective

concentration of ·OH in solution is limited by the flux of hydrogen peroxide (H_2O_2) from the pyrite surface, levels of ·OH decrease with higher levels of reactant, and that an increasing fraction of ·OH is consumed by Phe-degradation products as a function of time.

Reaction rates were greatly reduced in pyrite suspension containing simulating lung fluid due to the effects of iron chelating agents (e.g., citrate), higher pH, adsorption of complex ions to active surface iron sites (e.g., phosphate), and competition of solutes for ·OH (e.g., glycine and chloride). The effects of these components on Phe degradation rates in pyrite slurries were tested individually and compared to their expected competition factors, with the difference between Phe and Tyr kinetics predicted by the model attributed to decreased ROS formation. Similarly, suspensions of pyrite in simulated seawater slowed Phe degradation rates relative to salt concentration (8 – 32 parts-per-thousand) indicating competition for ·OH. An initial lag in Phe loss in pyrite slurries with added sea salts was attributed to a higher initial pH of 6.5 to 8.2. The addition of 200 mg L^{-1} and 400 mg L^{-1} of dissolved humic acids to pyrite slurries slowed the hydroxylation of Phe in manner consistent with competition for ·OH, with the modeled exponential decay curve fitting well based on second-order rate constants derived in previous studies.

Phe was readily transformed to the three isomers of Tyr in slurries of pyritic coals. Degradation rates normalized to pyrite mass were faster in pyritic coal than in pure pyrite, despite the fact that the coal organic matrix can act to compete for ·OH produced, which may be related to a greater surface area of framboidal pyrite present in coal. The effect of pH was characterized with a chemostat, where a constant pH was maintained by titration with sodium hydroxide. Constant pH experiments indicated that ·OH in a slurry of pyritic coal can be formed to a greater extent at pH 4.5 than when pH was allowed to drift to around pH 3.3. On the other

hand, a large initial burst of ·OH was observed in a slurry at constant pH 7.4 (the pH at which physiological fluid is buffered), after which there was little evidence for ·OH production.

Phe loss was only observed in presence of synthetic MnO_x with manganese oxidation states of +3 (Mn_2O_3) or +4 (MnO_2), but the lack of Tyr formation could not support a mechanism involving ·OH formation as indicated in experiments with a different probe. Rather, identification of an oxidative decarboxylation product was consistent with a direct electron transfer mechanism as proposed in prior work with MnO_x. These findings show that specificity of Phe conversion to the three Tyr isomers can be useful in excluding false readings of ·OH formation when other, less-selective probes implicate ·OH.

Table of Contents

List of Figures

List of Tables

List of Abbreviations

ROS	Reactive oxygen species
$^{\cdot}OH$	Hydroxyl radical
H_2O_2	Hydrogen peroxide
$O_2^{\cdot -}$	Superoxide
$^{\cdot}OOH$	Hydroperoxyl radical
Phe	Phenylalanine
Tyr	Tyrosine
o-Tyr	*ortho*-Tyrosine
m-Tyr	*meta*-Tyrosine
p-Tyr	*para*-Tyrosine
ΣTyr	Total tyrosine
DOPA	Dihydroxyphenylalanine
MnO_x	Manganese oxides
APF	3'-(*p*-aminophenyl fluorescein)
LCV	Leuco crystal violet
DMPO	5,5-dimethyl-1-pyrroline *N*-oxide
TCE	Trichloroethylene
DNA	Deoxyribonucleic acid
RNA	Ribonucleic acid
HPLC	High performance liquid chromatography
MS	Mass spectrometer
ToF	Time of Flight
ESI+ (or -)	Electrospray ionization, positive (or negative) mode
ESR	Electron spin resonance
3MT	Minerals, Metals, Metaloids, and Toxicology
HRP	Horseradish peroxidase
EDTA	Ethylenediaminetetraacetate
β-ME	beta-Mercaptoethanol
PheH	Phenylalanine hydroxylase
SLF	Simulated lung fluid
SSW	Simulated seawater
HA	Humic acid
NIST	National Institute of Standards and Technology
USGS	United States Geological Survey
CLB	Coal, Lower Bakerstown mine
CWP	Coal workers' pneumoconiosis

Acknowledgments

Thanks to my wife Irene, family, and friends for your love and support.

Thanks to Dr. Martin Schoonen for your assistance, both in the lab and in research development, as well as the financial support.

Special thanks to my advisor Dr. Bruce Brownawell for your seemingly endless patients and dedication to your students. I could not have done this without you.

This work was supported by the National Science Foundation – Integrative Graduate Education Research Traineeship (IGERT) program: Grant Number DGE0549370.

Chapter 1

INTRODUCTION

1.1 Background

Research in this dissertation focused on the development and application of the amino acid phenylalanine (Phe) as a probe to explore conditions that affect formation of reactive oxygen species (ROS) in heterogeneous, cell-free suspensions of minerals (i.e., slurries) in aqueous solutions. Of particular interest in mineral slurries is the formation of hydroxyl radical (·OH), which is the most reactivity species of all ROS and has been implicated in a number of health-related studies involving inhalation exposure to mineral dust (e.g., via inhalation). Although there are many molecular probes available for monitoring ·OH, only a small fraction have been tested in the presence of mineral slurries, and each have strengths and weaknesses. There are several advantages of using Phe (such as high yields of ·OH-specific products, biological relevance, and solubility) to monitor the kinetics of ·OH formation in mineral slurries containing matrices that mimic biological and environmental conditions.

Work on this topic began as a collaborative effort with development of an HPLC-MS analytical method to detect pyrite-induced degradation products of the nucleobase adenine, which for the first-time led to the confirmation of ·OH through identification of unique oxidation products (Cohn et al. 2010). The continued research into hydroxylation products in mineral slurries that led to the development of Phe as a probe was supported by the Minerals, Metals,

Metalloids, and Toxicity (3MT) program at Stony Brook University, New York, which fostered interdisciplinary studies to better understand the effects metals and minerals have on human and animal health. The 3MT program is one of the National Science Foundation's Integrative Graduate Education and Research Traineeships (NSF IGERT) that encourages collaborative research. Many of the experiments conducted for this dissertation were the direct result of collaboration with other trainees and professors who were working to better understand cellular response to the formation and reactivity of mineral-induced ROS. Results from this work contribute to and support studies by Schoonen et al. (2006; 2010), Cohn et al. (2004; 2006a), and Harrington et al. (2011) who continue to expand the field of health-related geochemistry through work with pyrite, pyritic coal, and more recently manganese oxides.

Pyrite (FeS_2) and manganese oxide minerals (MnO_x) are studied because of their abundance in the environment and adverse health effects associated with mine and factory workers. Chronic exposure to pyritic and MnO_x dust has been shown to cause damage to cells through persistently-high levels of ROS and metal dissolution respectively (Elder et al. 2006; van Maanen et al. 1999). The highly reactive nature of ROS in biological systems has been studied extensively and linked to numerous human health problems, including Parkinson's disease (Rao 2009) and lung cancer (Houghton et al. 2008). One of the main exposure interfaces for minerals is the epithelial lining of the lungs, where minerals can trigger an immune response and cause inflammation and an increase in ROS formation. Phagocytes are a type of white blood cell that generate ROS (in particular hydrogen peroxide, H_2O_2) to decompose potentially harmful antigens, pathogens, or particles as they work to defend the body against foreign compounds (Nyberg et al. 1992). This process involves creation of isolated chambers called phagosomes that envelope foreign compounds and destroy them through production of peroxide and reduced pH. The increase in ROS, including $^{\cdot}OH$, associated with this process has the potential to react with a wide spectrum of components within cells, such as lipids, proteins, enzymes, and nucleic acids.

The reactivity of ROS stems from the unpaired electron in the valence shell of the oxygen. ROS can exist as a charged or neutral species, and may contain an odd electron (i.e., radical). The ROS relevant to this study are superoxide ($O_2^{\cdot-}$), H_2O_2, and $^{\cdot}OH$. Superoxide can be formed by a single-electron reduction of molecular oxygen in the presence of a metal catalyst and is stable in the presence of organic compounds (Sawyer and Valentine 1981). In this study,

interest in $O_2^{\cdot -}$ does not extend beyond its role as an intermediate reactant which is further reduced to form H_2O_2. Hydrogen peroxide is a strong oxidant and energetically unstable (even in pure solution), though spontaneous decomposition to water and oxygen is generally slow without a catalyst present (Jung et al. 2009). Reaction rates between H_2O_2 and organic compounds in aqueous solution also tend to occur slowly. The single-electron reduction of H_2O_2 by way of catalysis (e.g., a transition metal) is energetically favorable and could lead to the formation of $^{\cdot}OH$ or hydroperoxyl radical ($^{\cdot}OOH$) (Walling 1975). In contrast to $O_2^{\cdot -}$ and H_2O_2, $^{\cdot}OH$ is transient (with a half-life of nanoseconds) and will rapidly oxidize most organic and many inorganic compounds.

Analytical detection of most ROS is only possible through measurement of a resulting reaction product. Probes have recently been adapted to detect H_2O_2 (with leuco crystal violet (LCV) (Cohn et al. 2005)) and $^{\cdot}OH$ (with 3'-(*p*-aminophenyl) fluorescein (APF) (Cohn et al. 2009)) in pyrite and pyritic coal slurries (as well as MnO_x (unpublished)), which allowed for quantification of ROS-flux following incubations. However, fluorescence monitoring can be limited by solution chemistry, and single wavelength measurement of fluorescence lacks the specificity of analysis or level of product confirmation available from HPLC-fluorescence or HPLC-MS. Identification by electron spin resonance (ESR) of $^{\cdot}OH$ using the molecular spin-trap 5,5-dimethyl-1-pyrroline *N*-oxide (DMPO) has also been conducted in pyrite slurries, though quantification of $^{\cdot}OH$ concentration was not possible (Cohn et al. 2006c) and measurements are subject to interferences. The same study also showed rapid decomposition of RNA occurs in pyrite slurries, presumably a result of reaction with $^{\cdot}OH$ (though a degradation pathway or specific reaction products could not be identified to confirm this).

The use of Phe was chosen for reaction in mineral slurries because of its high-yield of $^{\cdot}OH$-specific hydroxylation products *ortho*- and *meta*-tyrosine (*o*-Tyr and *m*-Tyr) found in studies of homogeneous solutions (e.g., Fenton reagents (Biondi et al. 2001) and irradiated water through pulse radiolysis (Buxton et al. 1988)) (Figure 1.1). The biologically derived isomer *para*-Tyr is also formed from $^{\cdot}OH$ hydroxylation of Phe, and understanding the ratios formed abiotically could be useful in distinguishing mechanisms between biotic and abiotic Phe loss in experiments involving cells and minerals. A simple and sensitive HPLC-MS method developed for this work can simultaneously monitor Phe loss and Tyr formation, along with additional

reaction products resulting from hydroxylation of the isomers of Tyr (e.g., the six isomers of dihydroxyphenylalanine (DOPA)) (Figure 1.1). Although adenine was already being used as a biologically-relevant probe for ·OH (Cohn et al. 2010), Phe is more soluble and yields three reaction products at ratios that could be used to determine solution versus surface reactions. It is important from a biological perspective to understand how solution chemistry affects the formation of ·OH in mineral slurries, and the formation of the *o*-Tyr and *m*-Tyr has been used in many studies *in vivo* (e.g., in proteins or as free amino acids found in urine (Marvin et al. 2003), eye cataracts (Molnar et al. 2005a), and saliva (Nair et al. 1995)) to identify signs of oxidative stress or redox chemistry related to ·OH.

In the following sections, details are presented regarding: ROS formation in solutions and mineral slurries; redox chemistry of pyrite and MnO_x in aqueous suspensions that may lead to the formation of ROS; and, previous findings related to the use of molecular probes to monitor ·OH in mineral suspensions and how they relate to the use of Phe.

1.2 Reactive oxygen species in mineral slurries

Schoonen et al. (2006) recently published a comprehensive review that shows five general mechanisms for ROS formation in the presence of minerals from the perspective of human exposure. Three of the mechanisms for ROS formation in solution are general and not specific to biological systems; whereas the other two mechanisms require direct cellular interaction to propagate ROS reactivity. Although work in this dissertation focused on monitoring mineral reactivity in the absence of cells, solution conditions were modified in some experiments to simulate specific biological and environmental conditions. Therefore, four of the five mechanisms described by Schoonen et al. (2006), along with several other studies relevant to this dissertation, are summarized below.

1.2.1 Mechanisms for mineral-induced formation of reactive oxygen species

The dissolution of metal ions from the surface of a mineral can induce ROS formation through catalytic reactions in solution, such as the Fenton reaction (Fenton 1894; Walling 1975).

In the Fenton reaction, ferrous iron (in this case released from the mineral in solution) reacts with H_2O_2 to form $^{\cdot}OH$.

$$Fe^{2+} + H_2O_2 \rightarrow Fe^{3+} + {}^{\cdot}OH + OH^- \quad (1.1)$$

The H_2O_2 shown in Equation 1.1 can be introduced to the system either by biological processes (e.g., superoxide dismutase) or through preceding reactions where dissolved oxygen reacts with Fe^{2+} to form superoxide ($O_2^{\cdot -}$), followed by a subsequent reaction with another Fe^{2+} and two protons to form H_2O_2 (Cohn et al. 2008).

$$Fe^{2+} + O_2 \rightarrow Fe^{3+} + O_2^{\cdot -} \quad (1.2)$$

$$Fe^{2+} + O_2^{\cdot -} + 2\ H^+ \rightarrow Fe^{3+} + H_2O_2 \quad (1.3)$$

The reaction in Equation 1.1 has also been shown to occur with a number of other metals (e.g. copper, nickel, and cobalt) in their reduced state that could also dissolve from mineral surfaces and reduce H_2O_2 in solution to form $^{\cdot}OH$ (and are considered to be "Fenton-like" reactions). Other metals, however, are not generally believed to undergo Fenton-like reactions (e.g., manganese) unless in the presence of coordinating compound (e.g., bicarbonate as suggested by Stadtman et al. (1990)).

$$Mn^{2+}\text{–}(HCO_3^-)_3 + H_2O_2 \rightarrow Mn^{3+}\text{–}(HCO_3^-)_3 + {}^{\cdot}OH + OH^- \quad (1.4)$$

The second mechanism for ROS formation in mineral slurries involves dissolved oxygen reduction at the mineral surface. In a number of recent studies with pyrite (discussed in more detail below), the formation of H_2O_2 is hypothesized to be the result of a series of electron-transfer reactions that ultimately leads to a two-electron reduction of oxygen to peroxide (similar to Equations 1.2 and 1.3 but as adsorbed species). The H_2O_2 can then go on to react through the Fenton reaction (Equation 1.1) with reduced iron in solution or on the mineral surface.

Formation of ROS at specific sites on the mineral surface with electron-deficits (or "defect" sites) may be important for a variety of minerals and involves electron transfer at the surface with water, oxygen, or carbon dioxide. These sites can be intrinsic or induced by mechanical processing such as grinding. Borda et al. (2003) speculated that iron(III) defect sites on the surface of pyrite caused the formation of $^{\cdot}OH$ from reaction with water in the absence of

dissolved oxygen. Later studies suggest that defect sites in pyrite slurries likely account for very little of the total ·OH formed in oxygenated slurries (Schoonen et al. 2010).

One of the cell-specific mechanisms for mineral-induced ROS involves formation of a "primary" ROS (such as H_2O_2) as an immune response to the mineral particles. Upon contact with the mineral, the primary ROS reacts to form a "secondary" ROS (i.e., ·OH), which is typically more reactive. The surface of the mineral is continuously exposed to H_2O_2 generated by phagocytes attempting to destroy the particle (Ng et al. 2004), which leads to a continuous flux of ROS that can potentially harm surrounding cells. With particles such as pyrite, inundation of H_2O_2 can effectively by-pass the need for surface or solution catalyzed H_2O_2 formation (Equations 1.2 and 1.3) leading to an increase in the rate of ·OH formation (Equation 1.1). This scenario was examined with Phe in the presence of pyrite and MnO_x by addition of H_2O_2 with results presented later in this dissertation.

One theory that combines several of ROS generation mechanisms is the potential for dissolved metals that do not undergo Fenton-like chemistry in solution to adsorb to the mineral surface and become stronger reductants. For example, Schoonen et al. (2006) hypothesized that adsorbed Mn^{2+} may induce the formation or transformation of ROS (e.g., H_2O_2 and/or ·OH) since the rate of reaction between dissolved Mn^{2+} and oxygen increases significantly following Mn^{2+} adsorption to a metal-oxide surface (Davies and Morgan 1989). Watts et al. (2005a) observed the loss of hexanol by reduced manganese upon addition of H_2O_2 to solution or MnO_x slurries, presumably through H_2O_2 transformation to ·OH via electron transfer (though this appears to contradict other studies previously mentioned that asserts the solution-phase formation of ·OH through Fenton-like chemistry with Mn^{2+} cannot reduce H_2O_2 without a coordinating ligand (Equation 1.4)).

1.2.2 Reactions of hydroxyl radical in mineral slurries

Once ·OH is formed in mineral slurries its fate can be controlled by a number of different pathways depending on the types and concentrations of ROS, dissolved metals and/or ions, and organic compounds present. Reactions with ·OH in solutions are generally rapid and tend to result in formation of other ROS (Walling 1975).

$$2\ {}^{\cdot}OH \rightarrow H_2O_2 \quad (1.5)$$

$${}^{\cdot}OH + H_2O_2 \rightarrow {}^{\cdot}OOH + H_2O \quad (1.6)$$

Dissolved transition metals have varying degrees of reactivity with ROS depending on their oxidation state and coordination with ligands (as shown in Equation 1.4). An example of oxidation-state dependence is with the Fenton reaction, where rates of ·OH formation have been shown to be optimal in the range of pH 3 – 6 because iron can readily cycle between Fe^{2+} and Fe^{3+} as reactions are catalyzed (the dominant iron species is Fe^{2+} at pH < 2 and Fe^{3+} at pH > 6) (Burbano et al. 2005) and H_2O_2 is more stable (at lower pH) (Jung et al. 2009). Additionally, direct oxidation of dissolved metals (M^{n+}) by ·OH can occur if the change in speciation (n) is favorable (e.g., oxidation from Fe^{2+} to Fe^{3+} occurs but not Fe^{3+} to Fe^{4+}).

$$M^{n+}{}_{(aq)} + {}^{\cdot}OH \rightarrow MOH^{n+}{}_{(aq)} \quad (1.7)$$

$$M^{n+}{}_{(aq)} + {}^{\cdot}OH \rightarrow M^{(n+1)+}{}_{(aq)} + OH^{-}{}_{(aq)} \quad (1.8)$$

The degradation pathway for organic compounds in the presence of ·OH has been theorized to be the result of either direct hydroxylation or hydrogen abstraction (Dorfman and Adams 1973). Direct hydroxylation of an organic compound by ·OH can occur with unsaturated or aromatic bonds forming an intermediate radical species on the reactant (e.g., benzene (C_6H_6)) (Walling 1975).

$$C_6H_6 + {}^{\cdot}OH \rightarrow {}^{\cdot}C_6H_6\text{–}(OH) \quad (1.9)$$

Succeeding reactions remove the free electron through an oxidizing agent (e.g., molecular oxygen (Equation 1.10) or M^{n+} (Equation 1.11)) and concurrent loss of a proton, resulting in the overall hydroxylation of the compounds (such as benzene to phenol).

$${}^{\cdot}C_6H_6\text{–}(OH) + O_2 \rightarrow C_6H_5OH + O_2^{\cdot -} + H^{+} \ (\text{or } {}^{\cdot}OOH) \quad (1.10)$$

$${}^{\cdot}C_6H_6\text{–}(OH) + M^{n+}{}_{(aq)} \rightarrow C_6H_5OH + M^{(n-1)+}{}_{(aq)} + H^{+} \quad (1.11)$$

Hydrogen abstraction induced by ·OH can also be important, and is often associated with reactions of saturated bonds, resulting in the formation of water and an unpaired electron on the reactant (RH).

$$RH + {}^{\cdot}OH \rightarrow R^{\cdot} + H_2O \quad (1.12)$$

Subsequent reactions of the resulting radical shown in Equation 1.12 can occur through many different pathway (Burbano et al. 2005; Walling 1975), a few of which are addition of ROS (Equations 1.13 and 1.14), oxidation by metal ion (Equation 1.15), addition of another non-radical compound (R') or ion (X) (Equations 1.16 and 1.17), or coupling of two reaction products (Equation 1.18).

$$R^{\cdot} + {}^{\cdot}OH \rightarrow ROH \quad (1.13)$$

$$R^{\cdot} + H_2O_2 \rightarrow RH + {}^{\cdot}OOH \quad (1.14)$$

$$R^{\cdot} + M^{n+} \rightarrow R^{+} + M^{(n-1)+} \quad (1.15)$$

$$R^{\cdot} + X^{-} \leftrightarrows RX^{\cdot -} \quad (1.16)$$

$$R^{\cdot} + R'H \rightarrow RH + R'^{\cdot} \quad (1.17)$$

$$2\ R^{\cdot} \rightarrow R\text{–}R \quad (1.18)$$

The concentration (both R and ·OH), structure and speciation of reactants, stability of the reactant radical ($R^{\cdot}$), solution chemistry (e.g., pH), and presence of additional compounds or elements ultimately affect which of the reaction pathways (Equation 1.13 – 1.18) will follow the initial ·OH interaction (Equations 1.9 and 1.12). It should be noted that the reaction of $R^{\cdot}$ with another ·OH (Equation 1.13) or formation of dimers (Equation 1.18) in solution without a surface or enzyme to bring two radicals together appear to be less likely than other reactions at low concentrations of reactants ((Walling 1975); e.g., preliminary, unpublished work conducted for this project showed dityrosine formation from tyrosine in the presence of horseradish peroxidase (HRP) but not Fenton reagents).

The intense reactivity of ·OH stems from a combination of high electrophilicity and an incomplete octet of electrons on the oxygen atom. Organic molecules with greater electron availability, such as unsaturated or aromatic compounds, will typically react at a faster rate than saturated compounds (Dorfman and Adams 1973). Similarly, electron-withdrawing functional groups (e.g., nitroso and alcohol groups) often increase the rate of ·OH-reactivity of a compound. Due to the highly reactive nature of ·OH, there can be a variety of degradation products that

form; however, hydroxylation of simple aromatic compounds can be rapid and produce stable, relatively ·OH-specific products.

Molecular probes that rely on phenyl hydroxylation to help quantify ·OH rely on the preferential reaction with the aromatic ring. Substituted aromatic compounds also tend to direct reactions such as ·OH-hydroxylation to specific sites. Phe was chosen for use in mineral slurries was because hydroxylation can be directed to the *ortho* and *meta* positions (as well as the *para* position) of the phenyl ring in significant proportions (with the *ortho* and *para* positions favored slightly). A description of what can be learned from specific reactions with several selected molecular probes, including Phe, is presented later in this chapter.

The multiple compounds and/or components of a slurry will compete for available ·OH at rates relative to their respective second-order rate constant. Most second-order rate constants for reaction of ·OH with organic and inorganic compounds or elements have been determined by pulse radiolysis, where a steady flux of ·OH is generated from the irradiation of water molecules (Buxton et al. 1988). The calculated rates constants for reaction of organic compounds with ·OH can range from non-reactive (e.g., carbon tetrachloride (Smith et al. 2004)) to near diffusion-rate limiting (e.g., tryptophan 1.3×10^{10} M^{-1} s^{-1} (Buxton et al. 1988)).

Reactivity of charged inorganic species with ·OH in solution depends on their ability to be oxidized. For example, reaction with ·OH of cobalt (II) has a low rate constant (8.0×10^{5} M^{-1} s^{-1} (Buxton et al. 1976)) while cobalt (I) has a high rate constant (8.0×10^{9} M^{-1} s^{-1} (Buxton and Sellers 1975)) because oxidation to cobalt (III) is not preferred. Another example is the difference in rate constants for bicarbonate (1.0×10^{7} M^{-1} s^{-1} (Buxton and Elliot 1986)) and dihydrogen phosphate (2.4×10^{4} M^{-1} s^{-1} (Maruthamuthu and Neta 1978)). Reactions of ·OH with halides have been shown to be reversible, with the net-reaction rates dependent on pH (low pH favors forward reaction while high pH favors the reverse reaction) (Jayson et al. 1973).

In complex solutions of biological or environmental matrices, the production of ·OH can be affected by various components of the solution (e.g., iron chelation by citrate (Hamm et al. 1954) or ethylenediaminetetraacetic acid (EDTA) (Cohn et al. 2010) can limit the Fenton reaction) (Equation 1.1). On the contrary, the absence of ancillary components may also limit the formation of ·OH (e.g., manganese-bicarbonate coordination necessary to degrade H_2O_2 by way

of Fenton-like reaction (Equation 1.4)). The various contributions of these and other biologically-relevant components were tested to determine their effect on ·OH formation in pyrite slurries by way of Phe loss and Tyr formation.

1.2.3 Implications of mineral-induced reactive oxygen species formation

The adverse human-health effects caused by internalization of minerals through inhalation or ingestion have been the topic of many studies (Cohn et al. 2006a; Elder et al. 2006; Swaen et al. 1995). Prior work includes characterizing the reactivity of quartz (Albrecht et al. 2002; Cohn et al. 2006b; Kwan and Voelker 2003), goethite (Wu et al. 2006), pyrite (Cohn et al. 2010; Pham et al. 2009; Schoonen et al. 2010), and various forms of manganese oxides (Post 1999; Stone and Morgan 1984a; Wang and Stone 2006) *in vitro*, in simulated fluids, and in pure water. Some minerals, such as quartz in its pure form, have been shown to be relatively inert with respect to the ability to degrade organic compounds in aqueous slurries (Schoonen et al. 2006); but can induce an inflammatory response in cellular matrices, possibly from ROS formation from phagocyte interaction. On the other hand, minerals such as pyrite and MnO_x have been shown to undergo catalytic redox chemistry and can degrade organic compounds by way of ·OH formation (Cohn et al. 2010; Pham et al. 2009; Schoonen et al. 2010) or direct surface reaction (Chien et al. 2009; Stone 1987), respectively, in both abiotic and biotic slurries that simulates epithelial tissue.

The U.S. Environmental Protection Agency set air-quality controls in the late 1980s as part of the Clean Air Act that defines particle diameters of 10 μm or smaller (PM-10) as particularly harmful since they can reach deep into the lungs to the alveolar sacs (Huang and Finkelman 2008). Workers exposed to high levels of PM-10 minerals are particularly vulnerable to respiratory ailments (Dalal et al. 1995; Valavanidis et al. 2009) as they are less likely to expel particles that are bound in the thin layer of intracellular alveolar fluid (which can be up to100 μm thick (Ng et al. 2004)). A recent interpretation of mineral dissolution rates suggests pyrite particles with a diameter of 1 μm could take more than a year to dissolve in lung fluid (Harrington et al. 2011). Prolonged ROS generation by phagocytes exposed to the entrenched minerals increases the risk of developing cancerous cells through oxidation of the nucleobases of

DNA (Moller et al. 2010), which can lead to improper transcription and replication. There are many studies of DNA oxidation that focus on the conversion of guanine to 8-oxoguanine as it appears to be a common marker of oxidative stress that may be overlooked by repair enzymes. In order to better understand the rates and duration of ·OH formation in the presence of components that comprise the alveolar lung fluid, work with Phe in simulated lung fluid (SLF) containing pyrite and pyritic coal has been characterized and presented later in this dissertation.

Exposure to pyrite and pyritic coal has also been tied to a number of respiratory diseases that result from inflammation and ROS formation (Huang et al. 2005; Moller et al. 2010). Burning coal makes up roughly 50% of the U.S. energy usage (Huang et al. 2005), and mining coal requires intense manpower, often in unsafe working conditions. Mine workers that are not properly protected inhale fine, pyrite-containing coal particles, and are at high risk for coal workers' pneumoconiosis (CWP), or "black lung syndrome" (Huang et al. 2005; Huang and Finkelman 2008). Current research also directly correlates the sulfur content of coal (typically on the order of a few percent by mass in pyritic coals) to the number of CWP cases (Huang et al. 2005).

The mining of manganese for the steel industry and synthesis of MnO_x for the production of alkaline batteries make up the bulk of MnO_x applications (Post 1999); thus miners and factory workers exposed in these fields have been studied for the effects of exposure. Most illnesses resulting from inhaled MnO_x dust are due to impaired lung function and increased Mn^{2+} levels in the blood as particles slowly dissolve (Elder et al. 2006; Roels et al. 1992). Dissolved manganese has also been shown to precipitate in the brain, leading to neurological and psychological diseases (Elder et al. 2006). Unlike pyrite and pyritic coal exposure, there is no literature that shows ROS (including ·OH) formation occurs in MnO_x suspensions; though studies have theorized (Schoonen et al. 2006) or implicated (Watts et al. 2005a) ·OH-formation in MnO_x slurries upon addition of Mn^{2+} or Mn^{2+} with H_2O_2 respectively. Recent work with APF in a collaborating lab indicated that some samples of MnO_x (pH 7.4) induce the formation of fluorescein, presumably by formation of ·OH. In experiments conducted for this dissertation, Phe was added to slurries of four different types of MnO_x under various conditions to monitor Tyr formation indicative of ·OH formation.

Mineral-mediated oxidation of organic compounds is of importance in the formation and transformation of organic compounds in complex matrices of aquatic environments. Formation of ·OH by minerals has drawn interest in the field of astrobiology with studies of biomolecules and the evolution of life (Cohn et al. 2004). In engineered systems, Fenton- and mineral-based ROS reactions are also being investigated for use in the environmental remediation of soils (Watts et al. 2005b; Zhang et al. 2008) and waters (Pham et al. 2009) polluted by organic contaminants. Treatments that use dissolved transition metals (e.g., iron, copper, or cobalt) and titration of H_2O_2 (and sometimes UV-irradiation) are capable of generating high levels ·OH, which have been shown to oxidize contaminants that are not otherwise degraded in the environment or in wastewater treatment facilities. To date, experiments utilizing natural pyrite or synthetic minerals of MnO_x to catalytically degrade organic contaminants have been limited to the laboratory; such as degradation of TCE in pyrite slurries made in pure water (Pham et al. 2009). Similarly, although through a different mechanism (i.e., reductive dissolution), a number of environmental contaminants (e.g., carbon tetrachloride (Watts et al. 2005b) and antimicrobials (Zhang et al. 2008)) have been shown to degrade in the presence of MnO_x.

Experiments for this study were designed to incubate pyrite in complex solution matrices (i.e., simulated sea water and Aldrich® humic acid (HA)) that might be representative of conditions where it is naturally abundant (e.g., organic-rich marine sediment) or that of complex wastewater streams high in organic matter.

1.3 Pyrite

Pyrite is an abundant iron sulfide found in sedimentary deposits. The mineral morphology of pyrite can vary depending on the environment in which it is formed, ranging from large, cubic crystals to small framboids. Framboidal pyrite is the common type found embedded into coal matrices ((Cohn et al. 2006a)). Other metals can be incorporated into the crystal structure of pyrite as it forms, which can affect the redox potential and dissolution of the mineral (Schoonen 2004). Natural dissolution of pyrite generates a number of different iron- and sulfur-oxide complexes which are dependent on solution chemistry (e.g., pH and levels of dissolved oxygen) (Descostes et al. 2004; Descostes et al. 2006; Druschel and Borda 2006; Rimstidt and

Vaughan 2003; Schoonen et al. 2010; Usher et al. 2004). Acid-mine drainage is a common consequence of pyrite dissolution in the environment, a result of sulfuric acid formation (Moncur et al. 2009).

Formation of iron hydroxides/oxides reflects the majority of redox chemistry that occurs on the pyrite surface (Descostes et al. 2004; Rimstidt and Vaughan 2003; Schoonen et al. 2010). However, as the pyrite surface oxidizes it also can transfer electrons through the crystal lattice (due to its semiconductor properties) and generate ROS (Schoonen 2004; Schoonen et al. 2010). For the purposes of this dissertation, only the reactions believed to be relevant to ROS formation at the pyrite surface and in solution will be discussed.

Research in the Schoonen lab has led to a number of advancements in explaining the possible mechanisms that lead to the formation of H_2O_2 and $^{\cdot}OH$ in pyrite slurries (Cohn et al. 2006a; Cohn et al. 2009; Harrington et al. 2011; Schoonen et al. 2006; Schoonen et al. 2010). Incubations with LCV as a probe molecule have measured H_2O_2 in the high-nanomoles per gram-pyrite range within seconds of initializing the reaction (Cohn et al. 2005). It should be noted that in order to measure the amount of H_2O_2 produced in a pyrite slurry, an iron chelator (e.g., EDTA) is required to prevent reactions (e.g., Fenton reaction) from degrading H_2O_2 (Cohn et al. 2005). Slurries with APF have indentified $^{\cdot}OH$ in the sub-micromolar range following a 24-hours incubation (at pH 7.4 with phosphate buffer) (Cohn et al. 2009). An understanding of the potential for pyrite-induced ROS formation in environmental and biological settings can be useful in many applications, such as developing new remediation techniques or helping to assess the health-risk following exposure. The following serves to summarize the reactions believed to ultimately lead to the formation of $^{\cdot}OH$ in oxygenated pyrite slurries through a combination of pyrite dissolution, electron transfer, and Fenton chemistry.

1.3.1 Pyrite-induced formation of reactive oxygen species

A study by Usher et al. (2004) showed that most of the dissolved oxygen in pyrite slurries oxidizes iron, while water oxidizes the sulfur. It was suggested that a net reaction which includes both water and oxygen might be misleading when considering the electron-transport mechanism

(Usher et al. 2004). For this reason, the oxidation of pyrite in oxygenated solution is shown in two half-reactions (Equations 1.19a and 1.19b).

Oxidative dissolution generates ferrous iron (which may remain adsorbed or release into solution) as sulfur is oxidized.

$$>FeS_2 + 8\ H_2O \rightarrow Fe(II)_{(ad\ or\ aq)} + 2\ SO_4^{2-}{}_{(aq)} + 16\ H^+ + 14\ e^-_{(pyr)} \quad (1.19a)$$

Concurrent oxidation of iron either at the surface or in solution occurs as sulfuric acid is formed (Equation 1.19a), converting Fe(II) to Fe(III)-oxyhydroxide (Usher et al. 2004).

$$Fe(II)_{(ad\ or\ aq)} + {}^1/_2\ H_2O + {}^3/_4\ O_{2\ (aq)} \rightarrow FeO(OH)_{(ad\ or\ aq)} \quad (1.19b)$$

Note the dramatic effect on the pH of the slurry that results from the release of a greater number of protons (H^+) from oxidative dissolution (Equation 1.19a). Each sulfur oxidized in Equation 1.19a ultimately results in the generation of 7 electrons that are believed to be transported within the pyrite lattice ($e^-_{(pyr)}$) and can induce the formation of H_2O_2 through the reduction of dissolved oxygen (Equations 1.20 and 1.21).

$$e^-_{(pyr)} + O_{2\ (aq)} \rightarrow O_2^{\cdot -}{}_{(ad)} \quad (1.20)$$

A subsequent reduction of adsorbed superoxide ($O_2^{\cdot -}{}_{(ad)}$) forms peroxide (O_2^{2-}), which acquires two protons in solution to form H_2O_2.

$$e^-_{(pyr)} + O_2^{\cdot -}{}_{(ad)} + 2\ H^+_{(aq)} \rightarrow H_2O_{2\ (ad\ or\ aq)} \quad (1.21)$$

It is unclear at this time whether the reduction adsorbed oxygen to H_2O_2 occurs as sequential one-electron reactions (Equations 1.20 and 1.21) or as a single two-electron reaction (Equation 1.22; which also represents the net-reaction of Equations 1.20 and 1.21).

$$2\ e^-_{(pyr)} + O_{2\ (ad)} + 2\ H^+_{(aq)} \rightarrow H_2O_{2\ (ad\ or\ aq)} \quad (1.22)$$

In either mechanism, the H_2O_2 formed can remain adsorbed to the surface or desorb into solution. A recent study by Schoonen et al. (2010) concluded that 5 – 6% of the total dissolved oxygen reacting in pyrite slurries is used to generate H_2O_2 rather than oxidize iron. The fate of H_2O_2 in pyrite slurries depends on the type of reactant in which it comes in contact. Iron oxides will degrade H_2O_2 to water and O_2 (Schoonen et al. 2010); whereas reaction of H_2O_2 with ferrous

iron (either on the surface or in solution) can lead to the formation of ·OH via Fenton chemistry (Equation 1.1).

As previously mentioned, an alternative mechanism for ·OH formation at the pyrite surface has been shown by Borda et al. (2003) which involves the oxidation of water (tested under anoxic conditions) at small "defect sites" where Fe(III) exists without a corresponding oxide/hydroxide.

$$>Fe(III) + H_2O \rightarrow >Fe(II) + {}^{\cdot}OH_{(ad \text{ or } aq)} + H^+ \quad (1.23)$$

Again, the reaction shown in Equation 1.23 is likely less significant in the presence of dissolved oxygen (Schoonen et al. 2010), though it has not been disproven and may contribute a small amount of adsorbed ·OH.

The low pH resulting from pyrite dissolution can allow for the speciation of iron in the system to cycle and remain catalytic. The optimal pH range for the Fenton reaction (Equation 1.1) is pH 3 – 6, which is a function of the ability for ferric iron to reduce back to ferrous iron in order to catalyze H_2O_2 reduction to ·OH (Chang et al. 2008; Jung et al. 2009). In a similar way, slurries containing solutes such as carbonates, phosphates, and citrate (which are abundant in many natural waters and in physiological fluids) can affect iron speciation by way of chelation or ligand formation. Citrate can chelate ferric and ferrous iron species depending on the pH of the solution (Hamm et al. 1954; Konigsberger et al. 2000) and, unlike EDTA, citrate has been shown to enhance H_2O_2 reduction to ·OH in SLF at low levels (Vidrio et al. 2008). On the other hand, iron coordinated with carbonates or phosphates can degrade H_2O_2 to products other than ·OH (King and Farlow 2000; Yoshimura et al. 1992). Experiments conducted for this dissertation and a recent report (Harrington et al. 2011) show that SLF significantly decrease the amount of ·OH formed in pyrite slurries.

Environmental matrices can contain similar levels of salts, buffers, and chelating agents as physiological fluids, and also containing complex organic matter such as humic acids (HA), which can hinder pyrite dissolution (Lalvani and Zhang 1994) and reduction of H_2O_2 to ·OH in solutions containing Fenton reagents (Lindsey and Tarr 2000). HA can act as a sink for ·OH, reducing reaction rates with target molecules. Conversely, HA have been shown to stabilize free radicals either with organic functional groups (i.e., quinones) or complexed metals; the stabilized

radical can potentially be available for reaction with dissolved constituents (Chen and Pignatello 1997; Struyk and Sposito 2001). The effect on formation and fate of pyrite-induced ·OH in slurries of dissolved HA was examined for this study. Organic matter similar to HA comprises the bulk of coal. Depending on its origins, coal can contain various amounts of pyrite in its matrix, and the reactivity of several samples has been shown to induce ROS formation.

1.3.2 Pyrite in coal

Coal is a complex matrix of reduced organic matter that forms deep underground following the decomposition and burial of plant life under anoxic conditions. The amount of sulfur and iron associated with coal can vary based on the environment in which it formed (Altschuler et al. 1983). Although coal is not a mineral, pyrite can incorporate into the bulk solids of the organic coal matrix at mass-fractions as high as 10% (Gluskoter and Simon 1968). Pyrite embedded in coal has been shown to undergo similar dissolution despite the presence of various degrees of reduced organic matter that makes up the bulk of the solid, and the ROS generated in coal slurries has been directly related to the pyritic sulfur composition (Cohn et al. 2006a).

The potential for coals to generate ROS has been correlated to its pyrite content (Cohn et al. 2006a; Dalal et al. 1995). A study by Cohn et al. (2006) has shown that H_2O_2 and ·OH can be quantified (using LCV and APF respectively) in slurries of well-defined pyritic coal from the National Institute of Science and Technology (NIST). The results were in agreement with work by Huang et al. (2005) that related the incidence of CWP to the sulfur content of coal. The same study by Cohn et al. (2006b) also attributed loss of RNA to reaction with ·OH in slurries of NIST pyritic coal over time; whereas NIST coals that had no pyrite content did not form ·OH in solution. The addition of pyrite-free coal to slurries containing samples of pyrite mineral had no effect on the level of ·OH as measured by APF, indicating that particulate organic matter is not an effective competitor for ·OH (Cohn et al. 2006b). The same NIST coals were incubated with Phe to better understand the kinetics of ·OH formation over time and results are presented in this dissertation.

1.4 Manganese oxides

MnO_x formation in the environment can result from biological or geological processes (Greene and Madgwick 1991) and can be found as small, blackish crystals coating soils (Risser and Bailey 1997), as precipitates in fresh water environments, and in ore deposits. Most natural and synthetic MnO_x have manganese oxidation states of +2, +3, and/or +4 depending on the environment in which they were precipitated (of the three oxidation states, only Mn(II) is soluble at any appreciable amounts at pH 7 or less). Natural MnO_x can co-precipitate with various alkali and transition metals and have mixed oxidation states (e.g., Mn(III) and Mn(IV) in the same structure), which can result in an amorphous, poorly-defined crystal structure (Post 1999). Conversely, synthesized MnO_x is precipitated in solutions of pure manganese salts (e.g., manganese sulfate) saturated with dissolved oxygen, typically resulting in a more orderly crystal structure. Bulk-synthesis of MnO_x is mainly used in industrial applications such as the production of cells for batteries (Liu et al. 2012; Post 1999; Xi et al. 2012). The high redox-potential that makes Mn(III)- and Mn(IV)-oxides useful as a battery cathode can also induce the oxidation of organic compounds in solution.

Birnessite (δ-MnO_2) is the most prevalent MnO_x in soils and has long-been studied for its role in forming humic substances (Jokic et al. 2001), as well as for its potential to degrade organic contaminants in soils (Zhang and Huang 2005). Degradation of organic compounds results from the reductive dissolution of the MnO_x surface which releases manganese into solution (as Mn^{2+}). The rates at which reductive dissolution of MnO_x occurs have been shown to depend on pH (Zhang and Huang 2003a), dissolved oxygen (Chien et al. 2009), and oxidation states of manganese and the electron donor (i.e., reductant) (Stone and Morgan 1984ab).

$$>MnOOH + 3\ H^+ + e^- \rightarrow Mn^{2+}{}_{(aq)} + H_2O \quad (1.24)$$

$$>MnO_2 + 4\ H^+ + 2\ e^- \rightarrow Mn^{2+}{}_{(aq)} + H_2O \quad (1.25)$$

The source of electrons in Equation 1.24 and 1.25 can be from reduced transition metals, or inorganic or organic compounds. Dissolution rates are also dependent on the properties and concentration of the reductant as the redox potential must be lower than the MnO_x (Stone and Morgan 1984aa, b). For the purposes of this study, only mechanisms related to oxidation of organic compounds will be discussed.

1.4.1. Oxidation of organic compound at the manganese oxide surface

Reactions of organic compounds in MnO_x slurries have been studied extensively (Ono et al. 1977; Pratt and Vandecasteele 1961; Pratt and Suskind 1963; Pratt and McGovern 1964; Stone and Morgan 1984a; Stone 1987; Ulrich and Stone 1989; Wang and Stone 2006). The mechanisms of substrate degradation in oxygenated MnO_x slurries are fundamentally different than those in pyrite slurries. Although reactions in slurries of pyrite and MnO_x depend on the intrinsic properties (i.e., molecular structure) of the target compound, rate-determining factors in pyrite-induced degradation are net-H_2O_2 flux and subsequent second-order rate constant for reaction with $^{\cdot}OH$. The rate of reaction with organic compounds in MnO_x slurries depends on adsorption rates and a sufficient difference in redox potentials of the mineral and substrate (Stone and Morgan 1984ab).

Initial interaction of an organic compound with the MnO_x surface ($>Mn^n O_x H$) can form by either a "bonded mechanism" with the manganese directly to induce the transfer of electron(s) to the surface directly (Equation 6.3) or a "non-bonded mechanism" where the organic compounds sorbs to the mineral (Equation 1.27), depending on its molecular structure (Stone and Morgan 1984ab).

$$>Mn^n O_x H + RH_{(aq)} \rightarrow >Mn^n O_{x-1} R + H_2O \quad (1.26)$$

$$>Mn^n O_x H + RH_{(aq)} \rightarrow >Mn^n O_x H \text{ -- } RH_{(ad)} \quad (1.27)$$

Note Equations 1.26 and 1.27 do not induce a change in manganese oxidation state. The subsequent oxidation of the bonded substrate (R) (Equation 1.26) then occurs which causes a reduction of the manganese. Reaction via the "non-bonded mechanism" (Equation 1.27) is believed to occur through an intermediate which generates a radical species (Pratt and Vandecasteele 1961; Pratt and Suskind 1963; Stone 1987; Zhang et al. 2008).

$$>Mn^n O_x H \text{ -- } RH_{(ad)} \rightarrow >Mn^{(n-1)} O_x H \text{ -- } R^{\cdot}_{(ad)} + H^+ \quad (1.28)$$

The adsorbed radical species ($R^{\cdot}$) may continue to react at the surface or desorb into solution (Zhang et al. 2008) (Equation 1.29).

$$>Mn^{(n-1)}O_xH\text{ -- }R^{\cdot}_{(ad)} \rightarrow >Mn^{(n-1)}O_xH + R^{\cdot}_{(aq)} \quad (1.29)$$

Subsequent reactions of $R^{\cdot}$ in Equations 1.28 and 1.29 can follow pathways described in the previous section (Equations 1.13 – 1.18), react with dissolved oxygen, or interact at the MnO_x surface. Overall, the reductive dissolution of MnO_x by an organic compound acting as a reducing agent results in the release of Mn^{2+} into solution and the oxidation of the organic substrate.

A higher oxidation state of manganese metals translates into a higher MnO_x oxidation potential in the presence of reactants. However, the reactions among minerals with different manganese oxidation states do not necessarily degrade the same compounds in a similar order (Wang and Stone 2006), even if the reaction site of the mineral is at the same state. This is postulated by Stone and Morgan (1984b) to be due to differences in alignment of functional groups with the MnO_x crystal structure at the surface.

The polarity, net-charge, type and location of functional group(s) all dictate whether an organic compound will interact according to Equation 1.25 or Equation 1.26 (if at all) and subsequently participate in redox chemistry at the mineral surface (Stone and Morgan 1984ab). Many studies with MnO_x have focused on reactions with aromatic compounds with electron-withdrawing groups such as alcohols (Pratt and Vandecasteele 1961; Stone 1987) and hydroxyquinones (Stone and Morgan 1984b) as they are more reactive with the MnO_x surface than saturated compounds (Stone and Morgan 1984a). Furthermore, the same study (along with subsequent studies with different compounds (Wang and Stone 2006)) showed that even different isomers of a compound can yield considerably different rates of MnO_x reduction. The orders of magnitude differences in degradation rates shown in studies with groups of highly-oxidized organic acids (Wang and Stone 2006) and various substituted aromatics (Zhang and Huang 2003a; Zhang and Huang 2005) are good examples of the complexities of MnO_x reaction kinetics.

1.4.2 Potential for manganese-induced hydroxyl radical formation

Studies of reactions of organic compounds in solutions of dissolved Mn^{2+} have indicated that $^{\cdot}OH$ may be formed through Fenton-like reactions in the presence of H_2O_2 (Stadtman et al.

1990; Watts et al. 2005a). Hydroxyl radical was believed to be the main oxidant of hexanol via Fenton-like reactions (solutions of Mn^{2+} or slurries of MnO_x and H_2O_2) with no other influencing compounds or ions (Watts et al. 2005a); however, the results from two other studies contradict this. As previously mentioned, reactions of Mn^{2+} and H_2O_2 were only shown to degrade organic compounds in the presence of a bicarbonate, where $^{\cdot}OH$ was presumably formed as an intermediate during decomposition of H_2O_2 to water at pH 7.4 (Equation 1.4) (Stadtman et al. 1990). Secondly, the adsorption of dissolved Mn^{2+} to the MnO_x surface has been found to be greater than 90% between pH 5 – 7 (Zhang and Huang 2003b). On the other hand, the possible formation of $^{\cdot}OH$ has also been speculated to occur through adsorbed Mn^{2+} (Schoonen et al. 2006).

Experiments in a collaborating lab recently found that APF is degraded to fluorescein in the presence of several different MnO_x minerals without the addition of H_2O_2, which led to speculation that $^{\cdot}OH$ was being formed. Concurrent experiments were also run to assess the reactivity of Phe in MnO_x slurries and confirm $^{\cdot}OH$ formation by monitoring for Tyr formation, and the results are presented in this dissertation.

1.5 Hydroxyl radical probes previously tested in mineral slurries

An array of simple and complex molecules (including Phe) have already been used to probe for $^{\cdot}OH$ in variety of solutions with Fenton and Fenton-like reagents. However, there have only been a small number of analytical methods developed to observe and quantify $^{\cdot}OH$ used in mineral applications. Application of DMPO, TCE, APF, RNA, and adenine as probes for $^{\cdot}OH$ have been reported in slurries containing pyrite, offering some insight into the conditions that promote the formation of $^{\cdot}OH$ and how $^{\cdot}OH$-production varies as a function of time. Incubations with APF and RNA in pyritic coal and APF in MnO_x have also been studied. Results from work with these probes are summarized below; many of which have been tested with pyrite by members of a collaborating lab. Compounds that have been added to slurries of MnO_x have already been discussed in the previous section in the context of reductive dissolution; and since there are currently no published reports implicating formation of ROS in MnO_x without addition of bicarbonate, or H_2O_2 and/or Mn^{2+}, MnO_x will not be discussed in this section.

1.5.1 Spin traps

Molecular spin-traps are a group of compounds that generally contain a nitrogen-oxygen functional group either part of (as nitrone) or adjacent to (as nitroso) a conjugated or unsaturated system that would promote free-radical oxidation. Reactions with ·OH with these probes generally involve breaking a single point of unsaturation on the molecule and forming a covalent bond with the radical compound at the atom bearing the lone electron. Upon hydroxylation, the lone electron is stabilized by the host molecule by shifting the radical between the adjacent tertiary nitrogen and oxygen as a nitroxyl radical (Frejaville et al. 1995) long enough for analysis by ESR.

DMPO is a popular spin trap used in biological and other heterogeneous systems to monitor oxidative stress by ROS (Frejaville et al. 1995) and has been tested in slurries of pyrite to measure ROS formation (Cohn et al. 2006c). The presence of ·OH was confirmed in these slurries by interpreting the differences in ESR spectra to identify the reaction products (Cohn et al. 2006c). One drawback to the use of spin-traps, and ESR in general, is that the data are not readily quantifiable in the presence of dissolved metals like iron (Cohn et al. 2006c); thus it cannot be used for kinetic analyses of ·OH formation through time.

1.5.2 Trichloroethylene

Pyrite has also been tested with the environmental pollutant TCE, which can persist in oxygenated soils (Pham et al. 2008; Pham et al. 2009). TCE is a small, volatile chlorinated compound with a single double-bond and hydrogen that has been shown to readily react with ·OH (Chen et al. 2001). Degradation of TCE in the presence of Fenton reagents have been shown to form dichloroacetic, glyoxylic, and formic acids, eventually leading to complete decomposition to CO_2 and residual chloride ions; the same products found by Pham et al. (2008; 2009) in the presence of pyrite. In their study, formation of ·OH continued for more than 5 days in some incubations, which is consistent with results from this study with Phe and Cohn et al. (2010) with adenine. It was assumed by Pham et al. (2009) that the degradation of TCE and its

subsequent reaction products followed first-order kinetics with respect to reactant concentration (though only one, relatively low initial TCE concentration was tested). Results from experiments with Phe will be shown in later chapters that indicate that reactions in substrate are closer to zero-order in substrate at higher concentrations.

Since TCE is volatile relative to its oxidation products, separate analyses were conducted to track the loss of TCE and formation of degradation products. Gas chromatography was used for TCE, whereas its less volatile degradation products were analyzed by HPLC. Another potential drawback using TCE is that the degradation products are not necessarily specific to ·OH reaction and can be formed through biological processes (Little et al. 1988; Pant and Pant 2010).

1.5.3 3'-(*p*-aminophenyl) fluorescein (APF)

Fluorogenic probes are monitored by fluorescence analysis following a reaction (generally specific) that causes the cleavage or addition of a function group which shifts the electronic configuration of the molecule. A relatively new class of fluorogenic probes, which includes APF, was designed to react specifically with ROS species (Setsukinai et al. 2003) in controlled biological settings. The structure of APF is theorized to have only one "vulnerable" site for ·OH reaction – a phenolic group that prevents the fluorescein molecule from fluorescing (Setsukinai et al. 2003). Hydrogen abstraction by ·OH is believed to induce the cleavage of the aminophenolic group, which results from oxidation and cleavage of the aminophenyl group through the oxygen-carbon. The intensity of the fluorescent signal then indicates the total amount of ·OH that formed over the incubation period (i.e., ·OH flux). Cohn et al. (2008; 2009) adapted APF for use in mineral slurries such as pyrite (Cohn et al. 2008; Cohn et al. 2009). Prior to studies by Cohn et al., APF had only been studied *in vitro* to determine the extent of ·OH produced by oxidative stress induced within cell cultures.

Work with APF in pyrite and other mineral slurries has proven to be useful for quantifying ·OH-flux in the nanomolar range; however, there are several potential drawbacks to its use in mineral slurries. Although APF is sensitive to reaction with ·OH, it can also been used to identify peroxynitrite and hypochlorite anions with similar sensitivity (Setsukinai et al. 2003). The reaction and detection of APF requires buffering at pH 7.4, which is appropriate for most

biological matrices, but only some environmental conditions. Fluorescence monitoring can be complicated by interferences from other dissolved compounds or ions with similar or overlapping excitation/emission spectra. The fate of fluorescein and the resulting phenolic compound has not been studied with regard to continued ·OH reactivity. Without fluorescence of APF, the kinetics of reactant loss and simultaneous reactant formation cannot be monitored. Lastly, the use of APF in MnO_x slurries of pure water suggested formation of ·OH, contrary to mechanisms proposed by a number of other studies (including use of Phe in this study). The question is raised as to whether that reactivity was in-fact due to the high oxidation potentials at the MnO_x surfaces.

1.5.4 Ribonucleic acid

Rapid degradation of RNA in pyrite and pyritic coal slurries has been shown using a fluorescent dye which distinguished nucleic acids based on strand length (Cohn et al. 2004; Cohn et al. 2006b; Cohn et al. 2006c). In these studies, ·OH was implicated as the primary reactant in the slurries, reacting with the sugar and/or nucleobases. Reaction at the pyrite surface was not considered to be an important mechanism since sorption of RNA was not observed (though an earlier study suggests that reversible interaction of phosphate anion with the pyrite surface may be possible despite negative surface charges (Elsetinow et al. 2001)). Interestingly, RNA loss in pyrite was suppressed by coating the pyrite or RNA with high concentrations of lipids, suggesting reduction in the rate of iron dissolution and/or H_2O_2 formation at the pyrite surface (Cohn et al. 2004). Although fluorescent monitoring of RNA strand-lengths is a good probe to monitor the deleterious effects on large biomolecules in the presence of pyrite and potentially other minerals, it is not a probe that yields reaction products unique to ·OH for studies in systems where other reactants may exist.

1.5.5 Adenine

Oxidation products of biologically-relevant aromatic compounds, such as nucleobases, have been implicated in many studies as important markers for oxidative stress *in vivo* (Rao

2009). Unlike oxidations of amino acids or proteins, mutations of the nucleobases (e.g., guanine to 8-oxoguanine and adenine to 8-oxoadenine) within nucleic acids (i.e., DNA and RNA) strands can lead to improper transcription and potentially the formation of cancer if not repair or excised (Rao 2009). Along with amino acids, nucleobases can be useful for detecting ·OH in matrices where minerals may be present as they are often ubiquitous in biological and environmental systems.

A recent study monitored the loss of adenine in pyrite slurries (Cohn et al. 2010), which showed slow but steady loss for up several weeks in low pyrite loadings (1 g L^{-1}). As previously mentioned, initial work on this topic involved examining adenine reaction mixtures in pyrite and Fenton reagents which were filtered and injected onto the HPLC-MS for analysis. Low, but detectable levels, of 2-hydroxyadenine and reasonable levels of 8-oxoadenine were measured simultaneously with adenine at similar levels in pyrite slurries and Fenton reagents, suggesting solution-phase formation of ·OH (Cohn et al. 2010). Although the kinetics of adenine loss and product formation was not fully examined in these studies, the work was significant in determining the extent of pyrite reactivity and confirmed ·OH detections from simultaneous incubations with APF.

The specificity of adenine for ·OH is good; however, the phenyl hydroxylation of Phe in mineral slurries was developed for this dissertation for reasons presented in the following section and throughout the dissertation. The following section outlines several reactions of Phe and *p*-Tyr that can occur *in vivo* and in the presence of ROS, and discusses the reasons for selecting Phe as a probe for mineral-induced ·OH.

1.6 Phenylalanine as a probe for hydroxyl radical

Phenylalanine ($C_9H_{11}NO_2$ | average molar mass of 165.19 g mol^{-1} | Figure 1.1) is one of only three naturally-occurring amino acids with an aromatic functional group; the other two being *p*-Tyr and tryptophan. Despite its nonpolar phenyl moiety, Phe has a solubility of 14 g L^{-1} (Ji and Feng 2008), which is more soluble than adenine at 1.1 g L^{-1} (Devoe and Wasik 1984) and even Tyr at only 0.45 g L^{-1} (at 25°C) (Ji and Feng 2008). The pK_a of the carboxyl group is 1.8 and the amino group is 9.1 with an isoelectric point at pH 5.5, making Phe mostly net-neutral at

biological and environmental pHs (i.e., pH 5 – 8). The dual charge on Phe and solubility should favor Phe staying in the aqueous phase of mineral slurries (thus minimizing sorption to the mineral surfaces).

Structurally, Phe has two chiral isomers, L-Phe and D-Phe. Only the levo-isomers of amino acids are naturally derived and used in biological processes, while most dextro-isomers must be manufactured synthetically. L-Phe is considered an essential amino acid, important for humans and cell functions, but it can only be acquired from food; whereas the role of D-Phe as a supplement for human health appears to still be under investigation (Friedman 2010). Throughout this dissertation, "Phe" is used to denote the L-Phe enantiomer only.

1.6.1 Biological relevance of phenylalanine

The concentration of dissolved Phe in physiological fluids such as blood is on the order of hundreds of micromolar (van Spronsen 2010). There is also Phe found in natural waters at concentrations that can vary significantly based on the environment. Protein and enzyme synthesis are the primary uses for Phe in eukaryotic cells. In addition to protein synthesis, Phe is converted to *p*-Tyr through enzymatic oxidation by phenylalanine hydroxylase (PheH) in the presence of O_2 (van Spronsen 2010). Although *p*-Tyr is an essential amino acid obtained through diet, it can also be produced by Phe-hydroxylation. The rate of Phe-hydroxylation by PheH is slow relative to the incorporation of Phe into proteins. Through similar processes as Phe, *p*-Tyr is converted to 3,4-dihydroxyphenylalanine (3,4-DOPA) by tyrosine hydroxylase as an intermediate for producing the neurotransmitter dopamine (Cohen et al. 1998; Zegota et al. 2005).

Oxidative stress caused by ROS in biological systems can result in formation of *o*-Tyr and *m*-Tyr in proteins or as free amino acids, which are believed to be specific to reaction with $^{\cdot}OH$ (Davies 2005; Molnar et al. 2005a). The same study indicates the co-occurrence of *o*-Tyr in biological fluids with other biomolecules such as lipids that also appear oxidized by ROS-induced stress. Dityrosine has been documented as an oxidative stress marker in proteins (Marvin et al. 2003) and is the result of oxidative coupling between two tyrosine molecules following hydrogen abstraction of the phenol group or adjacent carbon (Equations 1.12 and

1.18). Preliminary experiments conducted prior to selecting Phe as a probe attempted to induce the formation of dityrosine in Fenton reagents with *p*-Tyr. Dityrosine formed in the presence of HRP and H_2O_2 but not Fenton reagents, suggesting that the chances of two Tyr-radical molecules reacting within close proximity of Fe^{2+} and H_2O_2 in solution are less likely at low concentrations (whereas enzymes can align the tyrosine molecules accordingly). No further research was conducted with dityrosine or HRP for this study.

1.6.2 Phenylalanine as a probe for hydroxyl radical in mineral slurries

Conversion of Phe to the three isomers of Tyr (Figure 1.1) by ·OH has already been documented in reactions with Fenton reagents (Biondi et al. 2001), pulse hydrolysis (Buxton et al. 1988), and *in vivo* and *in vitro* studies (Matayatsuk et al. 2007). The mechanism for solution-phase reactions with Fenton reagents are illustrated in Figure 1.2, which shows two potential Phe degradation mechanisms for reaction with ·OH. Hydrogen abstraction in Figure 1.2 path A, involves removal of a hydrogen atom by ·OH (Equation 1.12), leaving behind a free radical to be stabilized by the ring structure which can then react with another ·OH, water, oxygen, or H_2O_2 to form an isomer of Tyr. The reaction in Figure 1.2 path B, involves direct addition of ·OH to the aromatic ring (Equation 1.9), which also causes a free radical to be stabilized by the ring structure. The subsequent removal of an electron from the Phe radical by Fe^{3+}, oxygen, or other oxidant results in the loss of a proton and restoration of aromaticity resulting in the formation of Tyr. Several studies suggest that path B is preferred for ·OH reaction with aromatic compounds, though path A has not been ruled out as a potential mechanism (Dorfman and Adams 1973; Oturan and Pinson 1995).

Basic attributes of Phe that make it a useful probe in mineral slurries include its solubility, stability in the presence of H_2O_2 (determined in preliminary experiments for this study), and selectivity for ·OH reaction via phenyl hydroxylation (Biondi et al. 2001; Kaur et al. 1988). The second-order rate constants for reaction of ·OH with Phe and Tyr are 5.8×10^9 M^{-1} s^{-1} and 1.2×10^{10} M^{-1} s^{-1} respectively (Buxton et al. 1988), which are similar and near diffusion rate limiting, allowing them to outcompete some of the other components that may be present. High yields of Tyr have already been shown for homogeneous solutions with Fenton reagents (Biondi et al. 2001). Furthermore, ·OH interaction with any isomers of Tyr generated can yield the

various isomers of DOPA (Figure 1.1), which may provide additional insight into the fate of Phe in mineral slurries. Analysis of Phe and Tyr isomers (and likely DOPA) can be monitored simultaneously in the same HPLC method (Biondi et al. 2001), and reaction chemistry is not limited to specific pHs requiring buffered solutions. As mentioned previously, Phe is also biologically-relevant, non-toxic (even at millimolar concentrations (Kaur et al. 1988)) and naturally present in physiological and ecological settings, so can be added without poisoning the host system.

1.7 Organization of Thesis

The research conducted for this dissertation sought to further elucidate factors that influence ROS production in pyrite, pyritic coal, and MnO_x slurries. The extent of mineral-induced ROS formation is important when considering the effects on human-health from exposure. The results of experiments conducted for this dissertation are organized into five chapters. The use of Phe as a probe in simulated, abiotic slurries was the first conducted with pyrite, as the mechanism for catalytically derived ·OH had already been well characterized by Schoonen, Cohn, and others from collaborating lab groups.

Reported in Chapter 2 are experiments that show Phe reacts with ·OH in pyrite slurries to form the three isomers of Tyr at proportions consistent with solution-phase chemistry (i.e., Fenton reaction). A sensitive analytical method was developed for the HPLC-Tof-MS, which requires minimal processing to monitor the kinetics of pyrite-induced ·OH in slurries by way concurrent monitoring of Phe loss, Tyr formation and subsequent loss, and in some cases formation of DOPA.

Chapter 3 presents data that helped confirm the bulk of ·OH reacting with Phe occurs in the aqueous-phase of the pyrite slurries by comparing Tyr-isomer ratios. Also tested were the effects of added Fenton reagents and adjusted pH to pyrite slurries by way of changes in the kinetics of Phe degradation. The temporal variations in the formation of ·OH in pyrite slurries was also studied with incubations of "aging" pyrite, to which Phe was spiked at set intervals and measured for loss.

Experiments conducted for Chapter 4 involved the incubation of pyrite in simulated lung fluids and seawater to document the effects of biological and environmental matrices on $^{\cdot}OH$ formation. The individual components that comprise SLF were also added to slurries of pyrite and Phe in separate experiments to determine the extent of competition for $^{\cdot}OH$ and effect on the ability of iron to catalyze ROS formation or transformation (i.e., through iron chelation or coordination in solution or at the surface).

Presented in Chapter 5 are results from incubations of Phe in four bituminous (pyritic) coals (where $^{\cdot}OH$ formation had been reported using APF and RNA by Cohn et al. (2006b; 2006c; 2009)) and two sub-bituminous (non-pyritic) coal slurries. A sample of the most reactive bituminous coal at a constant pH of 4.5 and 7.4 to simulate physiological pHs. Phe results were also compared to the experiments conducted by Cohn et al. (2006), who used the same coals to relate $^{\cdot}OH$ and H_2O_2 in slurries to the sulfur and pyrite content of each sample.

Experiments from Chapter 6 were conducted to compare results of Phe incubations with four synthetic MnO_x of varying manganese oxidation states. Some of these minerals had degraded APF in a study conducted in a collaborating lab, implying formation of $^{\cdot}OH$ without addition of Mn^{2+}, H_2O_2, or bicarbonate. Incubations of Fenton-like reactants with and without added MnO_x were also run to compare differences in Phe loss. Lastly, MnO_x was incubated with Phe in SLF at different pHs to simulate physiological conditions.

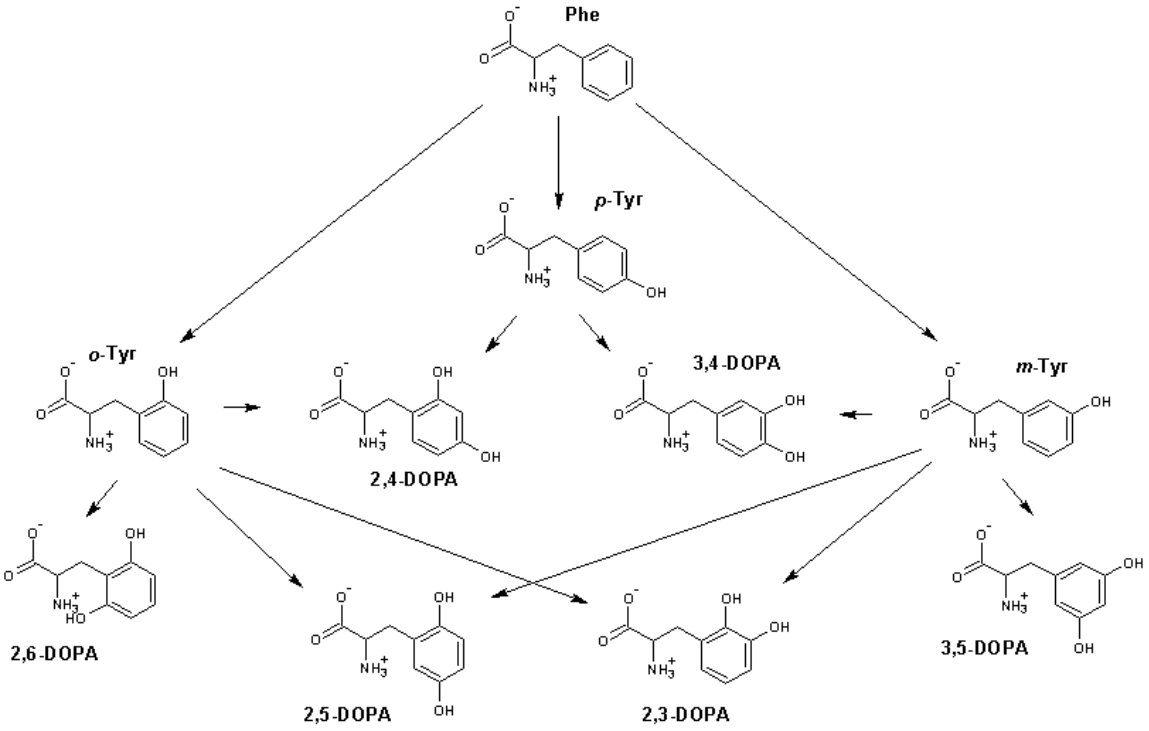

Figure 1.1 Potential ·OH-hydroxylation pathways of Phe and Tyr isomers. In this study, phenyl hydroxylation of Phe by ·OH has been shown to form *o*-, *m*-, and *p*-Tyr. Subsequent degradation of Tyr isomers are the six different isomers of DOPA. Only *p*-Tyr and 3,4-DOPA are produced enzymatically during normal biological processes. (Fisher et al. 2012)

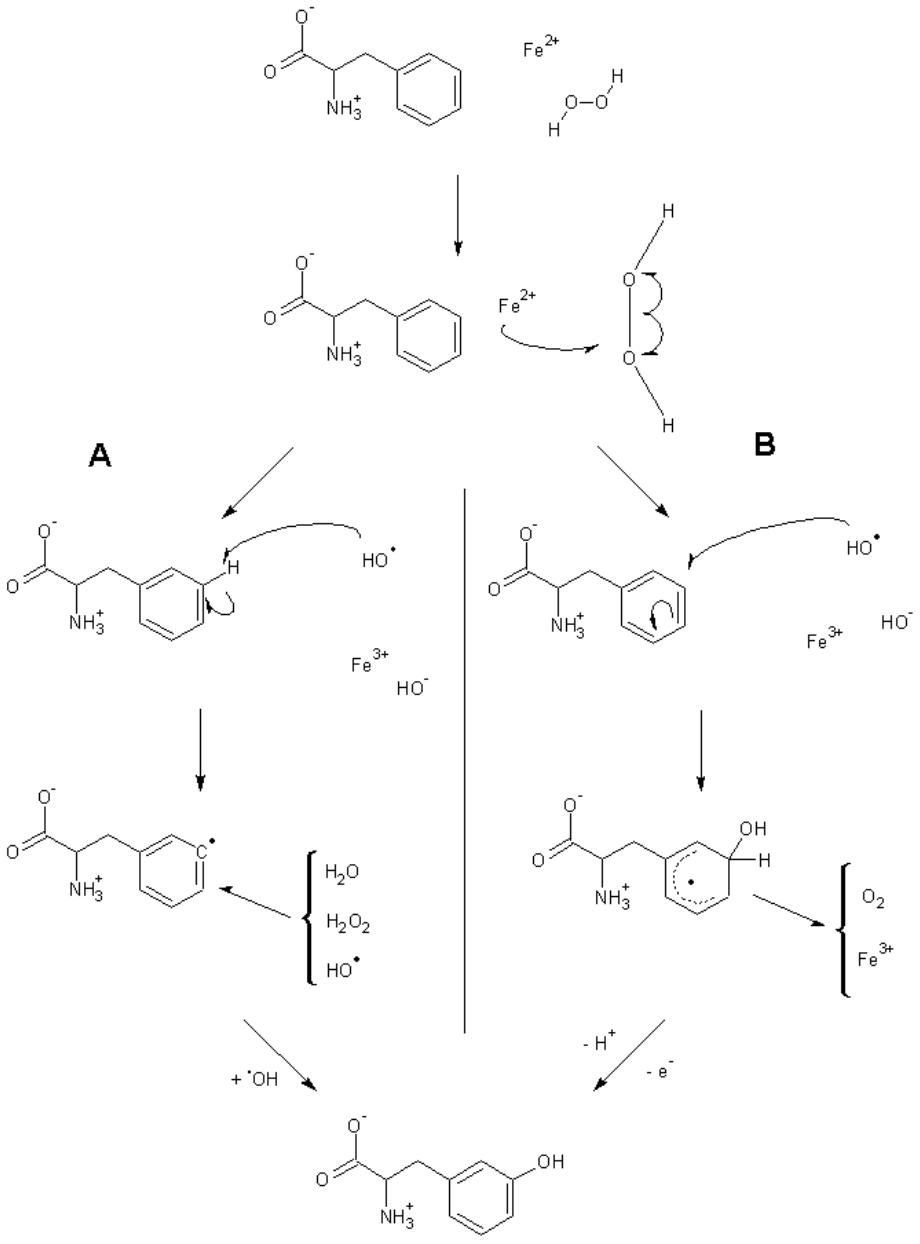

Figure 1.2 Fenton-based phenylalanine hydroxylation schematic. Shown are two possible mechanisms for Phe hydroxylation by ·OH to one of the three isomers of Tyr (formation of *m*-Tyr shown as an example in the above figure). Following the Fenton reaction where ·OH is generated, reaction by the hydrogen abstraction pathway (**A**) removes a hydrogen atom from Phe, which then undergoes a subsequent reaction with water, H_2O_2 or ·OH. The addition pathway (**B**) adds ·OH directly to Phe which is followed by oxidation by an electron donor such as Fe^{3+} or oxygen. It should be noted that the literature favors addition reactions in cases of ·OH hydroxylation of aromatic compounds (Dorfman and Adams 1973). *Bond lengths are not to scale and were stretched in some cases for illustrative purposes.*

Chapter 2

PHENYLALANINE AS A HYDROXYL RADICAL-SPECIFIC PROBE IN PYRITE SLURRIES

*Fisher, S.C., Schoonen M.A.A., Brownawell, B.J. 2012. Geochemical Transactions **13(3)**:18p.*

2.1 Abstract

The abundant iron sulfide mineral pyrite has been shown to catalytically produce hydrogen peroxide (H_2O_2) and hydroxyl radical (˙OH) in slurries of oxygenated water. Understanding the formation and fate of these reactive oxygen species is important to biological and ecological systems as exposure can lead to deleterious health effects, but also environmental engineering during the optimization of remediation approaches for possible treatment of contaminated waste streams. This study presents the use of the amino acid phenylalanine (Phe) to monitor the kinetics of pyrite-induced ˙OH formation through rates of hydroxylation forming three isomers of tyrosine (Tyr) – *ortho*-, *meta*-, and *para*-Tyr. Results indicate that about 50% of the Phe loss results in Tyr formation, and that these products further react with ˙OH at rates comparable to Phe. The overall loss of Phe appeared to be pseudo first-order in [Phe] as a function of time, but for the first time it is shown that initial rates were much less than first-order as a function of initial substrate concentration, $[Phe]_o$. These results can be rationalized by considering that the effective concentration of ˙OH in solution is lower at a higher level of reactant and that an increasing fraction of ˙OH is consumed by Phe-degradation products as a function of time. A simplified first-order model was created to describe Phe loss in pyrite slurries which incorporates the $[Phe]_o$, a first-order dependence on pyrite surface area, the assumption that all Phe degradation products compete equally for the limited supply of highly reactive ˙OH,

and a flux that is related to the release of H_2O_2 from the pyrite surface (a result of the incomplete reduction of oxygen at the pyrite surface). An empirically derived rate constant, $\mathbf{K_{pyr}}$, was introduced to describe a variable ·OH-reactivity for different batches of pyrite. Both the simplified first-order kinetic model, and a more detailed numerical simulation, yielded results that compare well to the observed kinetic data describing the effects of variations in concentrations of both initial Phe and pyrite. This work supports the use of Phe as a useful probe to assess the formation of ·OH in the presence of pyrite, and its possible utility for similar applications with other minerals.

2.2 Background

Reactive oxygen species (ROS) are highly reactive compounds that have been studied extensively in biological and environmental systems and have been linked to numerous human health issues, including Parkinson's disease (Rao 2009) and lung cancer (Houghton et al. 2008). In addition to forming naturally in cells as a function of respiration (Turrens 1997) and in the atmosphere (Monks et al. 2009), recent studies have observed that ROS can form at the surface of some minerals in water (Kwan and Voelker 2003; Schoonen et al. 2006; Schoonen et al. 2010). In particular, pyrite (FeS_2) has been shown to be efficient at forming hydrogen peroxide (H_2O_2) and hydroxyl radical (·OH) in the presence of oxygenated solutions (Borda et al. 2003; Schoonen et al. 2010). Of significant interest in pyrite slurries is ·OH, as it is transient and will rapidly react with any organic compound. The abundance of naturally-occurring pyrite in environments such as coal mines, where fine dust particles are frequently inhaled by workers, introduces the potential risk of human exposure to mineral-induced ROS. As an abundant mineral in many sediments and geological deposits, pyrite may also play a role in transformations of natural organic matter. Finally, the potential usefulness of pyrite as a tool for remediation of wastewater is also being considered as engineers continue to look for new methods of removing anthropogenic compounds before discharging effluent back into the environment.

Several mechanisms for surface-derived ROS in systems containing pyrite have been proposed that include iron-catalyzed, electron-transfer reactions. Schoonen et al. (2010) suggests

molecular oxygen is reduced to form H_2O_2 by reacting with iron-II (Fe(II)) sites at the pyrite surface. H_2O_2 may either remain adsorbed on the surface and be further reduced to ·OH (Equation 2.1), or desorb and undergo Fenton chemistry with dissolved ferrous iron (Fe^{2+}) to form ·OH in solution (Equation 2.2); with pyrite dissolution acting as the source of Fe^{2+}.

$$\mathrm{Fe(II)}_{(s)} + \mathrm{H_2O_{2\,(ad)}} \rightarrow \mathrm{Fe(III)}_{(s)} + \mathrm{OH^-} + \cdot\mathrm{OH}_{(ad)\ \mathrm{or}\ (aq)} \quad (2.1)$$

$$\mathrm{Fe^{2+}}_{(aq)} + \mathrm{H_2O_{2\,(aq)}} \rightarrow \mathrm{Fe^{3+}}_{(aq)} + \mathrm{OH^-} + \cdot\mathrm{OH}_{(aq)} \quad (2.2)$$

The proportion of H_2O_2 that reacts to form ·OH on the pyrite surface versus in solution is not known, although it has been proposed that the production of ·OH and subsequent reactions with organic compounds occur primarily in the aqueous phase (Schoonen et al. 2010). Alternatively, earlier work by Borda et al (2003) hypothesizes that ·OH can be formed directly from the oxidation of water by Fe(III) defect sites on the pyrite surface. Although more recent studies suggest this pathway is much less important in the presence of dissolved oxygen, it remains a potential ·OH source.

There have been a number of studies observing interactions with ·OH and organic reactants in biological and ecological systems. Because direct measurement of ·OH is not possible, a number of probes have been developed. In some studies ·OH-specific phenyl-hydroxylation products of aromatic substrates have been employed (Vione et al. 2010). In the case of pyrite slurries, probes that have been applied to determine ·OH-flux include electron-spin resonance analysis with molecular traps (Cohn et al. 2006c) and fluorogenic probes such as 3'-(*p*-aminophenyl) fluorescein (APF) (Cohn et al. 2008; Cohn et al. 2009). Cohn et al. (2009) recently adapted the *in-vitro* APF method for use in pyrite slurries to quantify ·OH. However, in order to measure ·OH with APF, solution chemistry (e.g., pH) must be strictly controlled to prevent interference in fluorescence monitoring. Pyrite-mediated formation of ·OH has also been implicated in RNA strand shortening (Cohn et al. 2004) and oxidation of the nucleobase adenine to 8-oxoadenine (Cohn et al. 2010). Recent studies have shown that trichloroethylene (TCE) and its reaction products are degraded by pyrite (ultimately producing carbon dioxide (CO_2)), implicating pyrite-derived ·OH as the main oxidant (Pham et al. 2008; Pham et al. 2009). Contributions such as this have led to an interest in the potential use of pyrite in engineered systems to facilitate remediation of organic chemicals in waste stream. However, the TCE

degradation products identified are not necessarily specific to ROS reactions, and alternative pathways (e.g., microbial) may yield similar products in the environment (Little et al. 1988; Pant and Pant 2010). Thus there is a need for a probe to study reactions in unconstrained mineral systems that can be monitored over time with ·OH-specific products, and is relevant to address a range of human health and environmental concerns.

The fate of phenylalanine (Phe) and its degradation products were investigated in this work as a potential probe to examine pyrite-mediated ·OH reactions. As a naturally occurring amino acid, Phe has been shown to undergo ·OH-specific phenyl hydroxylation reactions to form *ortho*-, *meta*-, and *para*-tyrosine (*o*-Tyr, *m*-Tyr, and *p*-Tyr) (Biondi et al. 2001) as depicted in Figure 2.1. The *o*- and *m*-Tyr isomers have been used to monitor oxidative stress both *in-vitro* and *in-vivo* (Davies 2005) as they do not form during normal biological processes. The Tyr isomers are stable enough to be measured in urine and proteins (Matayatsuk et al. 2007; Matta et al. 2007; Molnar et al. 2005a; Molnar et al. 2005b). Analysis of Phe and the Tyr isomers can be observed simultaneously and at low levels (tens of nanomolar) with HPLC-MS methods, providing usefulness as a biologically-relevant probe. Additionally, isomers of Tyr can oxidize in the presence of ·OH to various isomers of dihydroxylphenylalanine (DOPA) (Figure 2.1), which may provide additional insight into the fate of Phe in mineral slurries as only 3,4-DOPA is naturally formed as the primary product through biological transformation of *p*-Tyr (Cohen et al. 1998; Zegota et al. 2005).

This work describes the development of a sensitive HPLC-MS based method to evaluate the use of Phe and its reaction products as a way to probe ·OH-specific reactions involving pyrite in aqueous solution. The method was applied to study the kinetics of observed reactions as a function of both pyrite loading and concentration of Phe in order to gain additional insights into processes that control reaction rates. As had been described in earlier studies with other organic compounds (Pham et al. 2009; Schoonen et al. 2010), the loss of Phe in an individual experiment could be adequately represented as pseudo first-order as a function of time. However, the effect of initial concentration of reactant had not been examined, and an unanticipated dependence on initial concentration of Phe ($[Phe]_o$) was observed. A conceptual model is presented using a number of simplifying assumptions that incorporates the combined effects of pyrite loading and $[Phe]_o$ on ·OH levels in bulk solution (e.g., competition reactions between Phe and its

degradation products), allowing for interpretative comparisons between predicted and observed data for both Phe and Tyr.

2.3 Experimental methods

2.3.1 Materials

Pyrite from Huanzala, Peru (Wards Natural Science, Rochester, NY) was ground and sieved to a range of 38 – 63 μm with a surface area of 1.25 m^2 g^{-1} as per Cohn, et al. (2010). Phenylalanine, *para*-tyrosine, *ortho*-tyrosine, 3,4-dihydroxyphenylalanine, and beta-mercaptoethanol (β-ME), all 99% ACS-grade or better, were obtained from Alfa Aesar (Ward Hill, MA). *meta*-Tyrosine was obtained from TCI America (Portland, OR). Methanol was GC^2-grade from Burdick & Jackson (Morristown, NJ). Formic acid was ACS-grade from EMD Chemicals (Gibbstown, NJ). All water used for cleaning, standards, reactions, dilutions, and chromatography work was purified with a Milli-Q filtration system (Millipore Corporation, Billerica, MA) to a resistivity of 18.3 MΩ cm^{-1}.

2.3.2 Phenylalanine degradation experiments

Fresh samples of crushed pyrite were treated prior to each experiment with a nitrogen-purged solution of hydrochloric acid to remove surface oxidation and rinsed in a glove box with nitrogen-purged water, as per Cohn et al. (2010). The pyrite was kept in a sealed vial and removed from the glove box no-more than several hours prior to the experiment. Aqueous stock solutions of Phe (or Tyr) were prepared under ambient room conditions, diluted to desired initial concentrations, and added to pyrite in 15 or 50 mL disposable centrifuge tubes to initiate the reaction (leaving 25 – 30% of the volume as oxic headspace). Total volume of each reaction mixture was always at least 4-times that of the combined volume of aliquots sequentially removed during kinetic studies. Tubes were then immediately set to rotate end-over-end on a carousel at a constant 24 rotations-per-minute (the minimum rate found to fully suspend the slurry) and covered with aluminum foil to prevent light exposure. All experiments were conducted at room temperature of 25° ± 3° Celsius.

At predetermined time points, tubes were briefly removed from the carrousel, briefly vortexed, and a 300 µL aliquot was removed with a 1 mL Eppendorf® pipette at the same pyrite-to-water ratio as the sample (determined by a mass-balance test of repetitive sampling). Samples, including controls, were then quenched with 5 µL of β-ME (for a concentration of 234 mM) and filtered with 0.22 µm nylon Costar® centrifuge vial filters (Corning Life Sciences, Lowell, MA). Portions of the filtrate were then diluted (to different extents based on their initial concentrations) with water directly in a 2 mL HPLC vial. Methanol (5%) and formic acid (0.5%) were also added to each vial to match initial mobile phase conditions.

Each experiment was conducted independently and consisted of sets of incubations that ran concurrently for a predetermined length of time. Seven individual experiment sets (A – G) were conducted for this study. Table 2.1 lists the conditions for each experiment including incubation time, $[Phe]_o$ levels, and pyrite loadings. For the majority of the experiments conducted, pyrite was added at 100 g L^{-1} levels. The pH was monitored during three sets of experiments (Table 2.1) and was observed to drop rapidly within the first several minutes of incubation, after which it remained in a narrow range over the time-course of the experiment (pH 2.6 – 2.9) when pyrite loading was ≥50 g L^{-1}. When less pyrite was added, the final pH of these unbuffered solutions was higher (pH 4.2 – 5.5; Table 2.1), increasing as pyrite loadings decreased from 25 to 5 g L^{-1}.

2.3.3 Instrumental analysis

Instrumental analyses were conducted on a Waters Corporation (Milford, MA) Alliance® 2695 HPLC coupled to a Waters Corporation Micromass LCT Time-of-Flight Mass Spectrometer (ToF-MS). A Phenomenex (Torrance, CA) Luna® C18(2) HPLC column 3 mm x 250 mm with 5 µm particle size was heated to 40°C and run with a gradient containing methanol (Solvent A) and 10 µM ammonium formate / formic acid in water (pH 3.5) (Solvent B). Total run time was 16 minutes with a gradient of: 10% to 70% Solvent A over 8 minutes; 70% to 10% in 4 minutes; followed by a re-equilibration time of 4 minutes. A solution of Leucine enkephalin (Sigma Aldrich, St. Louis, MO) was injected post-column, generally at 1 – 3 µL min^{-1}, for internal mass calibration. Mass spectrometer parameters were 2800 V for the capillary voltage in

positive-ion, electrospray (ESI+) mode with cone and extraction voltages were set at 20 V and 3 V respectively. Calibration standards containing Phe, *o*-, *m*-, *p*-Tyr, and sometimes DOPA (with concentrations ranging from 100 nM to 5 μM) were run with each sample set with method detection limits for Phe and Tyr of 50 nM (as determined by a signal-to-noise ratio of 3:1). Accurate mass measurements of analytes in both standards and samples were calculated to be within 2 mDa of the actual $M+H^+$ mass with spectral resolutions between 5000 – 6000 for all experiments.

2.3.4 Controls

Excess β-ME was added for controls in several experiments as a quenching reagent; the reported second-order rate constant for β-ME and ·OH is 6.9×10^9 M^{-1} s^{-1} (Jayson et al. 1971), similar to 6.5×10^9 M^{-1} s^{-1} for Phe and ·OH (Buxton et al. 1988). No loss of Phe from solution was observed when 0.1% (14.2 mM) β-ME was added to pyrite slurries (Figure 2.2). This provides evidence that the observed loss of solution-phase Phe was not due to adsorption of Phe to pyrite. Additional control incubations of Phe in water without pyrite accompanied each experiment and always resulted in complete recoveries, indicating that there were no other losses of Phe (including enzymatic reactions in non-sterile media) occurring in this study.

Production of H_2O_2 has been measured in prior studies with similarly prepared pyrite slurries (Cohn et al. 2005). No loss of Phe over 72 hours was observed in pyrite-free solutions of H_2O_2 added at a wide range of concentrations (10 μM, 100 μM, and 1000 μM) (Figure 2.2); nor was Tyr production observed. The H_2O_2 level shown in Figure 2.2 is far greater than the range found to be produced in 160 g L^{-1} pyrite slurries, which varied from undetectable in the absence of the iron chelator ethylenediaminetetraacetate (EDTA) and up to 26 μM in the presence of EDTA (Cohn et al. 2005). These observations indicate that there was no direct reaction between Phe and H_2O_2, no measurable losses to adsorption of Phe to pyrite, and no microbial degradation (which would have resulted in a coincidental loss of Phe and preferential formation of *p*-Tyr).

2.4 Results

2.4.1 Kinetics of phenylalanine loss

The kinetics of Phe degradation in aqueous suspensions of pyrite were highly dependent on the $[Phe]_o$ and the amount of pyrite mineral surface in solution. The observed effects of the $[Phe]_o$ proved to be interesting and were examined in four experiments conducted under different conditions (Exp. A – D; Table 2.1). The results from these studies are illustrated in Figures 2.2 through 2.4. In each experiment the timescale for the disappearance of Phe was seen to increase with increasing $[Phe]_o$. As shown in studies conducted with pyrite and TCE (Pham et al. 2009) or adenine (Schoonen et al. 2010), loss of Phe as a function of time is described well as pseudo first-order (Equation 2.3); however, prior studies did not examine the effect of initial concentrations of Phe and pyrite loadings.

$$-\frac{\mathrm{d[Phe]}}{\mathrm{dt}} = k'\,[\mathrm{Phe}] \tag{2.3}$$

Where ***k'*** is the pseudo first-order rate constant derived through a fit of the data between the start of the reaction and when 90% of the Phe was lost (when reaction times permitted) (see fits in Figures 2.2 and 2.3). Calculated ***k'*** values were inversely related to $[Phe]_o$ as illustrated in Figure 2.2 (Exp. A) with values of 0.45 hr^{-1}, 0.13 hr^{-1}, and 0.04 hr^{-1} for initial concentrations 26.6 µM, 103 µM, and 307 µM, respectively. Observed data was well described by Equation 2.3 (Figure 2.1) with correlation ($R^2 = 0.972 \pm 0.031$) provided in Table 2.2.

Figure 2.2 also illustrates other important observations from this study. Experiment A was one of several experiments where a high mass loading of pyrite was added (100 $g\ L^{-1}$). At the highest $[Phe]_o$, 307 µM, degradation continues for as long as 120 hours, consistent with evidence for long-term production of H_2O_2 and $^{\cdot}OH$ obtained in prior studies with pyrite conducted for up to several weeks under similar conditions (Cohn et al. 2010). Also, initial rates, $\boldsymbol{R_o}$ (µM hr^{-1}), varied non-linearly as a function of $[Phe]_o$. Values of $\boldsymbol{R_o}$ were estimated to be 4.1 µM hr^{-1}, 9.6 µM hr^{-1}, and 10.3 µM hr^{-1} for $[Phe]_o$ of 26.6 µM, 103 µM, and 307 µM respectively (Figure 2.2). $\boldsymbol{R_o}$ was estimated by linear regression of data collected at **t** = 0 through the time at which [Phe] is approximately 80% of initial values.

A similar dependence of $\boldsymbol{R_o}$ on $[Phe]_o$ was also observed in experiments A – D, even at different pyrite loadings (Exp. D) (Table 2.2). In experiment D, incubations on a shorter

timescale (12 hours) were monitored at a greater frequency for better resolution of Phe loss (Figure 2.3). The loss of Phe was determined under conditions where both $[Phe]_o$ (11 – 286 μM) and pyrite loading (25 – 100 g L^{-1}) were varied (the effect of pyrite loading will be addressed later in this section).

Figure 2.4 shows the same relationship between the initial rates for each incubation from experiments A – D as a function of $[Phe]_o$ when normalized to a maximum rate determined for each respective experiment ($\boldsymbol{R_o}$ / $\boldsymbol{R_{max}}$) are combined (all conducted at 100 g L^{-1} pyrite loading). This normalization of $\boldsymbol{R_o}$ accounted for differences between $\boldsymbol{R_{max}}$ values determined in experiments conducted on different days (Table 2.2). While pyrite samples were all derived from the same homogenized batch of ground and sieved mineral, the explanation for variability in the reactivity of pyrite was not determined, but hypothesized to have resulted from subtle differences in acid pretreatment conditions that affected the abundance of Fe(III) surface sites. As further seen below, when results of different experiments with different samples of pyrite were combined, measured observations could be described by the same mechanistically-based kinetic model.

Rates increased proportionally with increasing concentration below 30 μM and clearly plateau at higher $[Phe]_o$. Estimates of $\boldsymbol{R_o}$ at lower $[Phe]_o$ were based on few data points where Phe had already degraded appreciably, and thus estimates of $\boldsymbol{R_o}$ are more uncertain and underestimate the true initial rate to a greater extent. Still, the results in Figure 2.4 follow a hyperbolic relationship, which has often been interpreted using the Langmuir-Hinshelwood (L-H) equation when describing rates of reactant loss with catalysts (e.g., UV-irradiated titanium dioxide (TiO_2)) that generate $^{\cdot}OH$ at the metal surface (Turchi and Ollis 1989; Turchi and Ollis 1990). Alternatively, it is proposed here that observed kinetics of the Phe data are more likely due to changes in $[^{\cdot}OH]_{(aq)}$ controlled simultaneously by the rate of H_2O_2 production at the pyrite surface and $^{\cdot}OH$ interaction with Phe and its products (a detailed explanation can be found in the Discussion section).

The effects of varying pyrite loading and surface area (which affect $^{\cdot}OH$ production) on Phe degradation rates are evident in Figures 2.3, 2.5, and 2.6. Increased pyrite loadings of 25 g L^{-1} up to 100 g L^{-1} resulted in proportional increases in $\boldsymbol{R_o}$ and $\boldsymbol{k'}$ at the same $[Phe]_o$ (Figure 2.3; Table 2.2). Figure 2.5 illustrates that rates (as $\boldsymbol{R_o}$ / $\boldsymbol{R_{max}}$) versus pyrite loading for several

different $[Phe]_o$ have first-order dependence on pyrite loading. Although the effect of pH on Phe degradation was not studied for this work, it is noteworthy to point out that $\boldsymbol{R_o}$ determined at the lowest pyrite loading (pH = 5.5 at 5 g L^{-1}, Table 2.1 (Exp. E)) was easily measured and still linearly correlated with those determined at higher pyrite loadings (pH = 2.9 and 2.6 at 50 and 100 g L^{-1} pyrite, Table 2.1 (Exp. E)). Interestingly, the initial rates of H_2O_2 formation in similar systems have been observed to be relatively unaffected over a range of pHs (Schoonen et al. 2010). Because many steps leading to the formation and fate of H_2O_2, $^{\cdot}OH$, and ferrous iron have the potential to be pH-dependent, more tests are needed to better understand the catalytic properties of pyrite as a function of pH.

Figure 2.6 illustrates the relationship between Phe loss and the surface area of pyrite in solution (Exp. F). At the same pyrite loading of 10 g L^{-1}, $\boldsymbol{R_o}$ increased from 0.88 µM hr^{-1} to 9.4 µM hr^{-1} when the surface area was increased from 1.25 m^2 g^{-1} (38 – 63 µm) to 14 m^2 g^{-1} (< 38 µm fraction) respectively (Table 2.2), using pyrite that passed through the 38-µm sieve following initial particle-size separation. The difference in Phe loss between the two incubations equates to approximately a 10-fold increase in estimated $\boldsymbol{R_o}$ for a corresponding 11-fold increase in pyrite surface area and thus is also consistent with first-order kinetics in pyrite surface area. Additionally, Figure 2.6 shows the Phe loss continuing for 10 days, twice the timescale in experiment A.

2.4.2 Tyrosine production and loss resulting from phenylalanine degradation

The hydroxylation products of Phe were readily measured as *o*-, *m*-, and *p*-Tyr in these pyrite incubation studies (Figure 2.7). The formation of the three isomers of Tyr has been attributed to $^{\cdot}OH$-specific reactions, and was not observed to occur with H_2O_2. The production of the sum of the three Tyr isomers (ΣTyr) initially occurs at rates that correlate with changes in initial rates of loss of Phe. Figure 2.7 illustrates the [ΣTyr] through time in experiment A, corresponding with losses of Phe shown in Figure 2.2. Similar to $\boldsymbol{R_o}$ for Phe results, the initial increase in Tyr levels (from 2.0 to 2.5 µM hr^{-1}) is relatively independent of $[Phe]_o$, contrary to expectations of reactions that are first-order in reactants. As the reactions proceed, ΣTyr levels peak then decrease over time. This would be expected as the production rate of Tyr drops due to

less production from decreasing [Phe], combined with expected concurrent reactions of Phe and Tyr competing for the same available ·OH pool.

The highest levels of [ΣTyr] always peaked at time points occurring near to or just beyond the half-lives of Phe, and within a relatively narrow percentage of [ΣTyr] / $[Phe]_o$, typically between 12% and 18% (Figure 2.8). There is especially good agreement when [ΣTyr] versus Phe half-life is plotted for incubations run of with the same sample of pyrite. Results agree with predictions from the quantitative model developed and presented below.

Ratios of the three Tyr isomers were observed to be the same among all experiments, and thus consistent with a common mechanism for conversion of Phe to Tyr independent of $[Phe]_o$ or pyrite loadings. Random hydroxylation of the five aromatic reaction sites on Phe would result in a ratio of 2:2:1 for *o*-, *m*-, and *p*-Tyr isomers, respectively. Illustrative of other experiments from this study, data normalized to [ΣTyr] shows that *o*-, *m*-, and *p*-Tyr were relatively constant over time in experiments with variable pyrite loading with ratios of 0.40 (± 0.02) : 0.28 (± 0.02) : 0.32 (± 0.02) respectively (see Appendix, Figure A.1). These results show that Tyr products are not formed at equal-molar concentrations as hypothesized elsewhere (Biondi et al. 2001) or at a 2:2:1 ratio. Instead, the electrophilic attack of the ·OH appears directed to the *para* position over the *ortho* and *meta* positions. In experiments where ·OH was produced via pulse-radiolysis, *ortho*- and *para*- directed hydroxylation of toluene resulted in *o*-, *m*-, *p*-cresol ratios of 0.48 : 0.23 : 0.29, respectively (Albarran et al. 2003). More importantly, the Tyr-isomer ratios in pyrite slurries agree with those observed in homogeneous solutions containing variable levels of Fenton reagents (H_2O_2 and Fe^{2+}) (presented in Chapter 3). This finding is consistent with mechanisms where hydroxylation of Phe occurs in the aqueous phase, rather than a surface reaction where molecular orientations of adsorbed species may lead to changes in reaction product yields.

The degradation of individual Tyr isomers was compared to that of Phe in experiment G (Figure 2.9; Table 2.2). Reaction rates for *m*- and *p*-Tyr were very similar to each other with an estimated $\boldsymbol{k'}$ of 0.17 hr^{-1}, which were faster than those determined for *o*-Tyr and Phe (approximately 0.08 hr^{-1}). Estimates for $\boldsymbol{R_o}$ for each reactant were closer; 22 µM hr^{-1} for *m*- and *p*-Tyr and 15 µM hr^{-1} for *o*-Tyr and Phe. These modest differences in rates between Phe and Tyr are consistent with published second-order rate constants with ·OH of 1.3 x 10^{10} M^{-1} s^{-1} for *p*-Tyr

and 6.5 x 10^9 M^{-1} s^{-1} for Phe (solution at pH 2 for each) determined by pulse radiolysis (Buxton et al. 1988). Thus Tyr can be expected to compete effectively with Phe with an average rate (for the 3 isomers) that is approximately 1.3 to 1.7 times faster.

The production of DOPA as a phenyl-hydroxylation product of Tyr was also observed in this study. DOPA was identified by correspondence of HPLC retention with an authentic standard of one of the possible isomers (3,4-DOPA) which eluted before *p*-Tyr, and further confirmed by accurate mass measurements by Tof-MS that were within 2 mDa of the actual mass. This finding is consistent with production of DOPA for reactions of Tyr and ·OH in prior work (Zegota et al. 2005). No other peaks corresponding to the mass of DOPA were identified. Due to the very low concentrations of DOPA (when detected) in Phe experiments at the dilution-levels injected, it was not routinely monitored. It is noteworthy that in an experiment with *p*-Tyr, DOPA was only measured at a maximum concentration around 2% relative to $[p\text{-Tyr}]_o$. Although a comprehensive HPLC-MS method to chromatographically separate, indentify, and quantify the 6 possible isomers of DOPA was not conducted, it appears that Tyr-to-DOPA may not be as sensitive of a probe as Phe-to-Tyr in monitoring ·OH-specific reactions mediated by pyrite.

2.5 Discussion

2.5.1 Phenylalanine as a hydroxyl radical probe

A sensitive method was developed for the quantification of Phe and Tyr at ≥50 nM levels by HPLC-MS methods with direct aqueous injection without the need for pre-concentration or derivatization steps that could lead to more analytical uncertainty. The role of ·OH in the degradation of Phe is confirmed by the production of a characteristic composition of three isomers of Tyr – *ortho*, *meta*, or *para*. The presence of *m*- and *o*-Tyr has been used previously to assess the importance of ·OH in oxidative stress (Davies 2005); whereas observation of primarily *p*-Tyr is normal in biological systems. High yields, characteristic ratios, and persistence of readily-measured Tyr products are other traits that make Phe a good probe to monitor ·OH production in pyrite and other mineral slurries. Yields of Phe to ΣTyr conversion were estimated in this study to be between 30% and 60% by extrapolating initial changes in the $[\Sigma\text{Tyr}]_t$ / $([\text{Phe}]_o$

- $[Phe]_t$) back to time-zero (data not shown). The stability in pyrite slurries of Tyr is similar to that of Phe, allowing it to be monitored at appreciable levels throughout the period of Phe decay.

There are of course other molecular probes that have been developed that rely upon measurement of phenyl hydroxylation products to determine concentration levels of ·OH in aqueous solutions. Two of the more sensitive ones are production of hydroxybenzoic acids from benzoic acid (Vione et al. 2010) and hydroxyterephthalic acid from terephthalic acid (Saran and Summer 1999). In each case, the determination of products by fluorescence or HPLC-fluorescence can be even more sensitive and require less expensive instrumentation than the HPLC-MS based detection of Phe and Tyr described here. However, neither benzoic acid nor terephthalic acid are nearly as fluorescent as their products. Hence, in experiments with those probes only the hydroxylated products are typically measured, while the substrate – often added in excess – is routinely not analyzed for. When detection of these substrates is required, it is usually conducted with far less sensitive UV-based methods (Thiruvenkatachari et al. 2006).

There are other potential advantages of developing Phe as a probe to study ·OH-mediated reactions. The presence of Phe in cells and body fluids allows for meaningful interpretation of the ratios of *o*-, *m*-, *p*-Tyr *in vivo* (Matayatsuk et al. 2007; Molnar et al. 2005a). Similarly, in contrast to other aromatic probes used to date, Phe is naturally present at low levels in all natural waters and biologically active geological matrices, including environments where pyrite is present. With methods available for determining ultra-trace environmentally relevant concentrations of Phe and Tyr isomers (Sommerville and Preston 2001; Wing et al. 1990), it may be possible to conduct field studies that could shed insight into the conditions where ·OH-mediated reactions are occurring in the environment.

The mass spectrometric methods utilized also provide certain advantages. With the full-spectral sensitivity of LC-ToF-MS, direct injection of aqueous samples offers the potential to identify other non-targeted reaction products that may have otherwise been lost in isolation or purification steps. For example, in this work, trace levels of DOPA were identified in some experiments with confirmation using accurate-mass measurement. Finally, in more complex matrices characteristic of biological fluids or organic matter-rich natural waters, the increased specificity of analysis by ToF-MS allows for greater discrimination from matrix that can potentially complicate the use of some UV or fluorescence-based detection methods.

2.5.2 Pyrite-mediated hydroxyl radical formation

The mechanisms of ·OH production in pyrite slurries are not certain, yet appear important for understanding the reaction it undergoes with Phe and other organic compounds. For example, if $\cdot OH_{(ads)}$ is the primary source of ·OH involved in Phe reactions, and Phe reacts at the pyrite surface, then the dependence of $\boldsymbol{R_o}$ on $[Phe]_o$ might be appropriately described by a L-H surface catalysis model. However, if the primary source of ·OH is derived in solution by Fenton-like reactions, then there needs to be a reaction mechanism to describe the nonlinear response of $\boldsymbol{R_o}$ with varying $[Phe]_o$ (Figure 2.4).

Any surface catalyzed reactions would most likely require the production of adsorbed ·OH which may be formed through cathodic reduction of H_2O_2 at the pyrite surface (Equation 2.1) (Schoonen et al. 2010), or through Fe(II) / Fe(III) electron-transfer reactions with water at surface defect-sites (Borda et al. 2003). However, it has been argued recently that surface-defect sites in oxygenated slurries are less likely to form ·OH than the Fenton reaction in solution (Schoonen et al. 2010). Reaction of Phe directly at the pyrite surface with $\cdot OH_{(ads)}$ seems unlikely to be a major contributor to its overall loss as Phe, Tyr, and soluble probes used in prior studies of pyrite mediated reactions (Cohn et al. 2010) do not measurably adsorb to the surface (Figure 2.2). However, desorption of $\cdot OH_{(ads)}$ may occur and resulting reactions (i.e., with Phe) could be limited to diffuse boundary layers when sufficient substrates are present occur within a limited distance from the surface (Turchi and Ollis 1990). Turchi and Ollis (1990) showed that such boundary layer reactions could explain kinetic behavior consistent with the L-H model, providing one possible mechanism for near surface reactions that cannot be completely ruled out.

The possibility that higher Phe levels could affect the catalytic properties of pyrite seems unlikely as in the absence of observed adsorption of Phe, its surface coverage would be very low, and decrease with increasing pyrite loading. Furthermore, there was no observed effect to reaction rates with the addition of excess Fe^{2+} (see below), consistent with Phe not affecting the availability of iron in solution needed for the Fenton reaction.

Support for ·OH formation via the Fenton reaction in the aqueous phase (Equation 2.2) is much stronger for a number of reasons. For example, dissolved H_2O_2 can be observed

accumulating in pyrite slurries at concentrations relevant to this and other studies (micromolar-range) when the Fe^{2+} in solution is chelated by EDTA, inhibiting the Fenton reaction (Cohn et al. 2005; Pham et al. 2009; Schoonen et al. 2010). Ferrous iron in solution also acts as a catalyst in the Fenton reaction and has been measured elsewhere to be in excess of H_2O_2 (Cohn et al. 2005). To confirm that ferrous iron is present in excess, experiments with 50 $g\ L^{-1}$ pyrite slurries containing excess ammonium ferrous sulfate (500 μM) were incubated with 100 μM Phe. Results indicated no difference in initial or overall rates of Phe degradation when compared to a pyrite solution without iron addition (see Appendix, Figure A.2; also, Chapter 3). Therefore, there is sufficient Fe^{2+} in pyrite slurries to suggest the ·OH production is limited to the rate of production and release of H_2O_2, and thus by extension, the production rate of H_2O_2 at the pyrite surface affects the kinetics of Phe loss (and its degradation products).

2.5.3 Kinetics of phenylalanine loss

The reaction of ·OH and Phe is described by the following second-order rate equation:

$$-\frac{\mathrm{d[Phe]}}{\mathrm{dt}} = k_{\mathrm{Phe}}\,[\mathrm{Phe}]\,[\cdot\mathrm{OH}] \tag{2.4}$$

Where $\boldsymbol{k_{Phe}}$ is the second-order rate constant and is equivalent to 6.5 x 10^9 M^{-1} s^{-1} (as mentioned in the Results section). However, it is shown (e.g., in Figures 2.2 – 2.4) that -d[Phe]/d**t** does not vary proportionally with $[Phe]_o$, and plateaus at higher concentrations. We suggest that the most likely mechanism for these observations is that as $[Phe]_o$ increases, there is a near-proportional decrease in [·OH] in the aqueous phase. This situation contrasts with more typical experiments monitoring the production of ·OH or its reaction products, where either excess reactant is used and product determined, or in cases where the reactant is added at low levels in comparison to other species in solution that are sinks for ·OH. This balance is constrained by the limited production rate (or flux) of ·OH at any given time. To support this hypothesis we present a conceptual model that can explain most of the results from this study using three primary assumptions.

Assumption 1 asserts that the *·OH flux is constant over the time course of the experiment*. This is supported by evidence that H_2O_2 production has been shown to be proportional to pyrite

loading (Cohn et al. 2005), and does not react with substrates such as adenine (Cohn et al. 2010) and Phe. If the rate of ·OH formation is assumed to be constant and proportional to pyrite loading, it can be assigned a reaction coefficient that represents the pyrite reactivity (Equation 2.5), incorporating all factors related to formation of ·OH for a particular sample of pyrite.

$$R_{\cdot OH\ \text{formation}} = \mathrm{K_{pyr}}\,[\mathrm{pyr}] \tag{2.5}$$

Where $\mathbf{K_{pyr}}$ has units of mol g^{-1} hr^{-1} (and also corresponds to the maximum rate at which Phe can be degraded). $\mathbf{K_{pyr}}$ is determined for each pyrite sample to account for aforementioned variability in reaction rates (i.e., rate of ·OH-formation) that was observed between different experiment sets and hypothesized to be related to conditioning of the pyrite prior to incubation.

Assumption 2 states that *·OH is in approximate steady-state* with a loss dominated by reaction with Phe (and its degradation products) and the rate of formation related to the loading and surface area of pyrite. The rate of decay for each reactant product through time is related to its individual rate constant and concentration, and with ·OH formation assumed constant in Equation 2.5, steady-state requires the loss of ·OH be constant. Thus the combined loss of total reactants must also remain constant.

$$\frac{\mathrm{d}[\cdot\mathrm{OH}]}{\mathrm{dt}} = \mathrm{K}_{pyr}\,[\mathrm{pyr}] - [\cdot\mathrm{OH}](k_{\mathrm{Phe}}[\mathrm{Phe}] + k_{\mathrm{Tyr}}[\mathrm{Tyr}] + \Sigma(k_{\mathrm{i}}[\mathrm{i}])) = 0 \tag{2.6}$$

Where $\boldsymbol{k_{Tyr}}$ and $\boldsymbol{k_i}$ are the second-order rate constants for the reaction of ·OH with Tyr and other degradation intermediates, collectively Σ *i*, respectively.

Equation 2.6 represents a balance of production and loss of ·OH, but also underscores that many degradation products of Phe that are likely important for describing the kinetics are unaccounted for. The degradation intermediates compete with Phe, Tyr, and each other for reaction with the limited ·OH until completely oxidized to carbon dioxide (CO_2). Therefore, the third simplifying assumption states that *the sum of all oxidizable reactants is equal to* $[Phe]_o$ (i.e., $[Phe]_t + [Tyr]_t + \Sigma[i]_t \approx [Phe]_o$) for most of the time course of the experiments (i.e., where Phe was still readily detectable (≥10% Phe remaining)). In addition, it is also assumed that the second-order rate constants of those products with ·OH are all relatively high and similar to each other (i.e., $\boldsymbol{k_{Phe}} \approx \boldsymbol{k_{Tyr}} \approx \boldsymbol{k_i}$). Similar approaches have been used to simplify complex competitive

rate equations in other studies involving surface-catalyzed ·OH-mediated reactions (Turchi and Ollis 1989). Therefore, a simplified approximation of Equation 2.6 is represented in Equation 2.7.

$$\frac{\mathrm{d}[\cdot\mathrm{OH}]}{\mathrm{dt}} = \mathrm{K}_{pyr}\,[\mathrm{pyr}] - k_{\mathrm{Phe}}\,[\mathrm{Phe}]_{\mathrm{o}}\,[\cdot\mathrm{OH}] = 0 \tag{2.7}$$

Which can also be rewritten in terms of [·OH]

$$[\cdot\mathrm{OH}] = \frac{\mathrm{K}_{\mathrm{pyr}}\,[\mathrm{pyr}]}{k_{\mathrm{Phe}}\,[\mathrm{Phe}]_{\mathrm{o}}} \tag{2.8}$$

With substitution of Equation 2.8 into Equation 2.4, Phe loss can now be described with a rate expression that is a function of both pyrite loading and $[Phe]_o$.

$$-\frac{\mathrm{d}[\mathrm{Phe}]}{\mathrm{dt}} = \frac{\mathrm{K}_{\mathrm{pyr}}\,[\mathrm{pyr}]}{[\mathrm{Phe}]_{\mathrm{o}}}\,[\mathrm{Phe}] \tag{2.9}$$

Note that in Equation 2.9, $\mathbf{K_{pyr}}$ [pyr] / $[Phe]_o$ is analogous to the experimentally determined pseudo first-order rate constant ***k'*** defined in Equation 2.3, where ***k'*** was found to be proportional to pyrite loading and inversely related to $[Phe]_o$ (at $[Phe]_o \geq 30$ μM at 100 $\mathrm{g\ L^{-1}}$).

$$k' = \frac{\mathrm{K}_{\mathrm{pyr}}\,[\mathrm{pyr}]}{[\mathrm{Phe}]_{\mathrm{o}}} \tag{2.10}$$

Therefore, $\mathbf{K_{pyr}}$ can be derived experimentally for a given pyrite sample and allows for the modeling of Phe and Tyr concentrations through time.

2.5.4 Modeling phenylalanine and tyrosine concentrations through time

2.5.4.1 Determination of K_{pyr}

To account for the differences in reactivity among pyrite samples, a unique value for $\mathbf{K_{pyr}}$ was determined for experiments A, B, D, and E using all kinetic data collected. As described in the Results section, the temporal loss of Phe generally fits an exponential function well where ***k'*** is the slope of ln[Phe] versus **t**. As per Equation 2.10, $\mathbf{K_{pyr}}$ is then derived from the slope of ***k'*** versus $[pyr]/[Phe]_o$. The measured data were described by linear correlations between ***k'*** and

$[pyr]/[Phe]_o$ (see Appendix, Figure A.3), and an averaged $\mathbf{K_{pyr}}$ was estimated for each experiment (A, B, D, and E) by setting the y-intercepts to zero.

2.5.4.2 Phenylalanine loss

Integration of Equation 2.9 allows for the modeling of Phe loss through time.

$$[\mathrm{Phe}]_t = [\mathrm{Phe}]_o \left(e^{-\frac{K_{pyr}[pyr]}{[Phe]_o} t} \right) \tag{2.11}$$

Observed Phe data from Experiments A, B, D and E along with predicted values (modeled with Equation 2.11) are plotted in Figure 2.10. Comparisons of predicted versus observed $[Phe]_t$ was fit by a linear regression model with a slope of 0.985 with an R^2 of 0.996.

2.5.4.3 Tyrosine production and loss

The kinetics of Tyr formation and loss are governed by consecutive reactions, and using the assumptions described above, the rate of change can be represented in Equation 2.12.

$$\frac{d[\mathrm{Tyr}]}{dt} = K_{pyr}[pyr] \left(\frac{\alpha\, k_{Phe}[\mathrm{Phe}] - k_{Tyr}[\mathrm{Tyr}]}{k_{Phe}[\mathrm{Phe}] + k_{Tyr}[\mathrm{Tyr}] + \Sigma(k_i[i])} \right) \tag{2.12}$$

Where **α** is the fraction of the Phe reaction products corresponding to Tyr. For modeling purposes, **α** was estimated to be 0.5, which was within the range of yields determined from initial rate data. Again, assumptions made in this model consolidate the competitive factor that affect Phe and other products that react with ·OH in the slurry. Thus Equation 2.12 can be simplified to:

$$\frac{d[\mathrm{Tyr}]}{dt} = \frac{K_{pyr}[pyr]}{[Phe]_o} (\alpha[\mathrm{Phe}] - [\mathrm{Tyr}]) \tag{2.13}$$

Integration of Equation 2.13 yields:

$$[\mathrm{Tyr}]_t = \alpha\, K_{pyr}[pyr]\, t \left(e^{-\frac{K_{pyr}[pyr]}{[Phe]_o} t} \right) \tag{2.14}$$

Equation 2.14, based on data for Phe loss, provided predictions of $[Tyr]_t$ that agreed with measured values from experiments A, B, D, and E reasonably well (Figure 2.11). A linear regression fit of points in Figure 2.11 has a slope of 1.18 with an R^2 of 0.888.

This simplified model is able to predict much of the change in Phe and Tyr through time when the specific $\mathbf{K_{pyr}}$ for a pyrite sample is determined. Importantly, it allows for most of the observed dependence of $[Phe]_o$ and pyrite loading to be accounted for while describing the apparent first-order dependence of Phe loss through time. Based on this analysis, there is no need to consider potential surface reactions between ·OH and Phe to model the hyperbolic function of $\boldsymbol{R_o}$ at higher $[Phe]_o$ (Figure 2.4), normally ascribed to surface catalytic reactions. However, it should be pointed out that this simple model does not describe the decrease in $\boldsymbol{R_o}$ observed at lower $[Phe]_o$ as well. Although this may be related to the paucity of initial measurements when Phe degrades rapidly at lower $[Phe]_o$, it does seem likely that initial rates are lower when $[Phe]_o$ is low (<30 μM). We hypothesize that at low $[Phe]_o$, there are other reactions that compete for ·OH with Phe and other products. Whether or not such reactions occur at the pyrite surface or with trace inorganic reactants in solution is uncertain and beyond the scope of this work.

A more detailed numerical simulation was also developed to compare to results from the simplified model presented above (Equations 2.11 and 2.14), and to provide greater flexibility for testing the effect of assumptions concerning reaction pathways and relative rates of multiple products with ·OH (see Appendix, *Numerical simulation* section). Values of second-order rate constants for different reaction products (i.e., Tyr and DOPA) and the fraction of Phe-to-ΣTyr conversions (reaction yield, or $\boldsymbol{\alpha}$) were adjusted to test basic assumptions made above. The assumption of constant ·OH-flux was not changed. Figures A.6 and A.7 in the Appendix show that calculations made with $\boldsymbol{k_{Phe}} = \boldsymbol{k_{Tyr}} = \boldsymbol{k_{DOPA}}$ and $\boldsymbol{\alpha} = 0.5$ (50% conversion of Phe-to-ΣTyr) offer the closest match to observed and modeled data for most incubations.

2.6 Conclusion

Loss of Phe varied in pyrite slurries at rates that were first-order in pyrite loading and pseudo first-order dependent on Phe as a function of time; whereas the rate of Phe loss was much less-than first-order in $[Phe]_o$. The data for the loss of Phe as well as the production and loss of

Tyr products could be described well by a mechanistically-based kinetic model that reconciles the observations concerning the initial concentration dependence of Phe. The competitive effects of degradation products on reactions of molecular probe have been included in kinetic descriptions; as such products become important when substrate is not added in great excess. Not limited to experiments with pyrite, there have been few studies that have considered that observed exponential decay of reactants may be due to increased competition for available ·OH (Turchi and Ollis 1989), rather than due to true first-order behavior. In systems where the flux of ·OH is likely the rate limiting step, observed kinetics will depend on whether the relative amounts of competing reactants change as a function of time. The [ΣTyr] / $[Phe]_o$ and [Tyr-isomer] / [ΣTyr] ratios were consistent throughout experiments, with total-Tyr formation estimated to be about 50% of the Phe conversion via ·OH. The use of Phe and its ·OH-specific products is argued to be a useful probe that should be further developed for the study of the mechanisms of pyrite and other mineral-mediated reactions, and has the potential to be a valuable tool for the study of ·OH reactions in a range of other systems with more complex matrices.

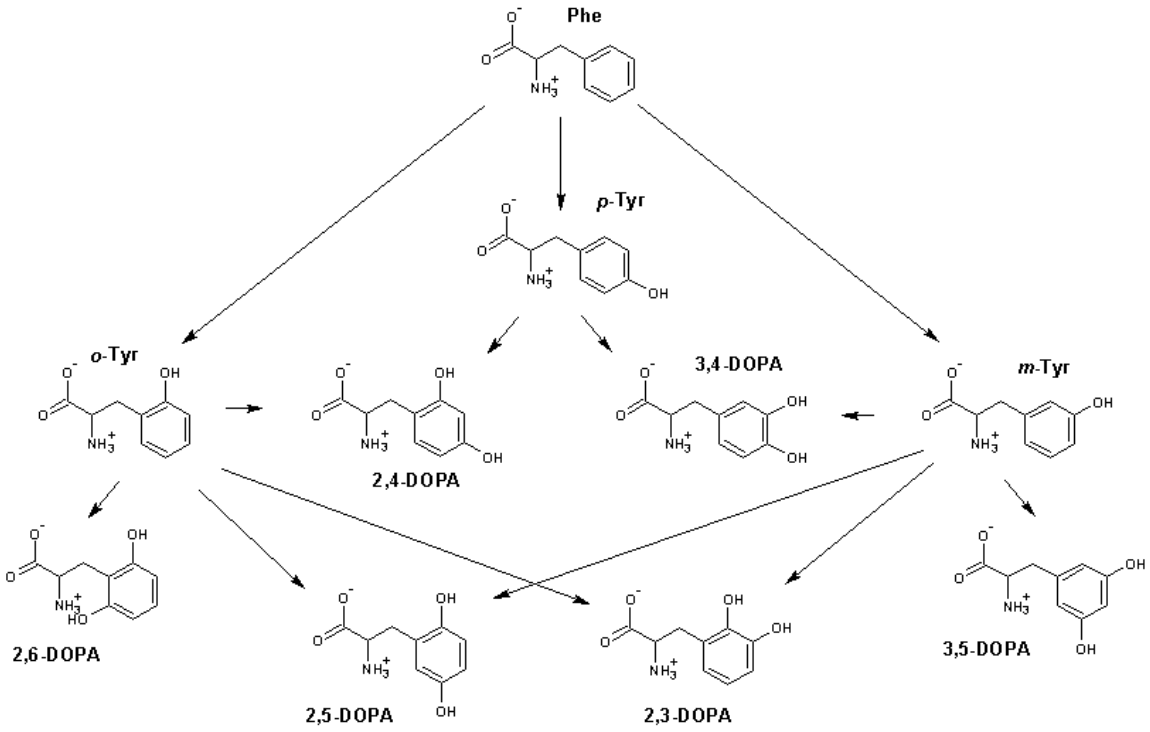

Figure 2.1. Potential oxidation pathways of Phe and Tyr isomers. In this study, phenyl hydroxylation of Phe by ·OH has been shown to form *o*-, *m*-, and *p*-Tyr. Subsequent degradation of Tyr isomers are the six different isomers of DOPA.

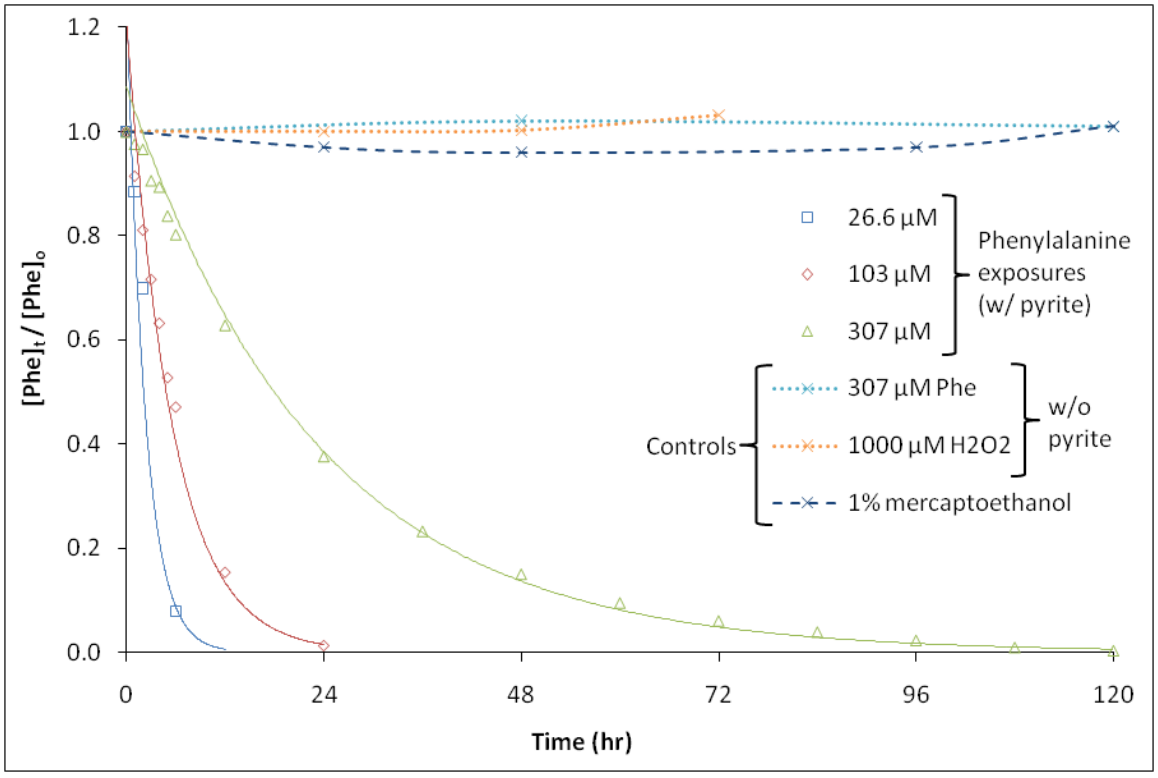

Figure 2.2. Degradation of various Phe concentrations in the presence of 100 g L^{-1} pyrite (Exp. A). Phe concentrations through time are fit well with exponential regressions. Controls of 307 µM Phe are also shown without pyrite in pure water and 112 µM Phe in 1000 µM H_2O_2; as well as with pyrite quenched with 0.1% (14.2 mM) β-ME.

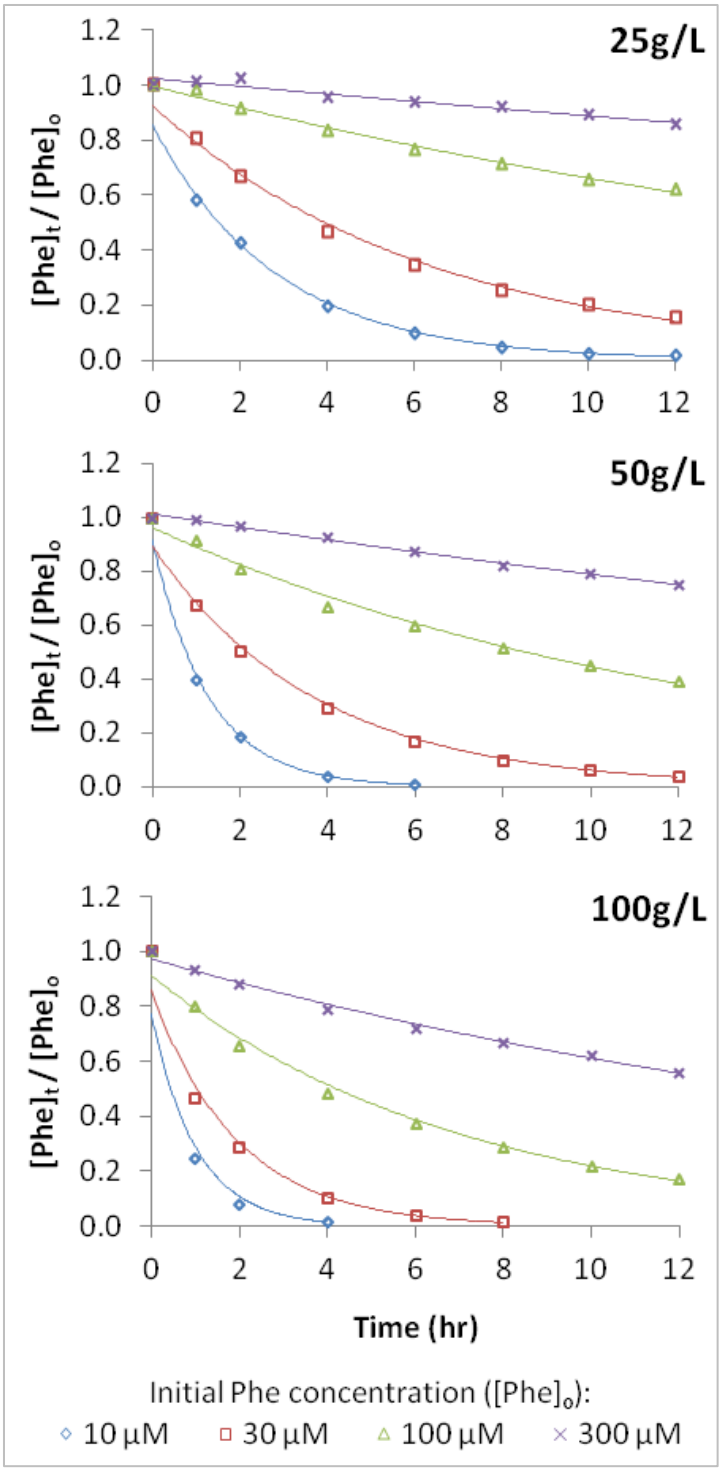

Figure 2.3. Concentration of Phe over time as a function of pyrite loadings (Exp. D). Data is normalized to $[Phe]_o$. For each pyrite loading, incubations of $[Phe]_o$ from 10 µM to 300 µM were monitored for 12 hours. Data points for Phe are compared with fits to exponential regressions corresponding to a first-order model.

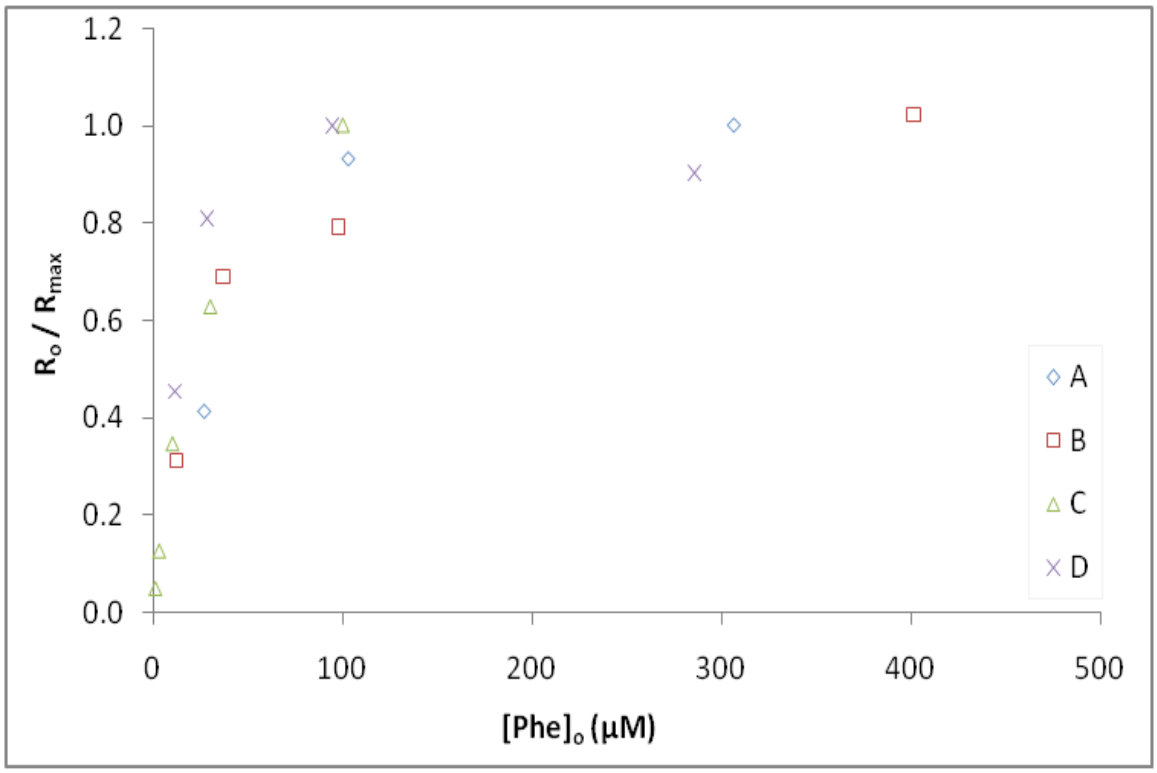

Figure 2.4. Initial degradation rates of Phe as a function of [Phe]$_o$. Shown is R_o normalized to maximum initial degradation rates (R_{max}) for each experiment set (hypothesized to vary due to subtle differences in pretreatment of pyrite). Pyrite loadings of 100 g L^{-1} were used in all experiments. R_{max} for each experiment set: **A** is 10.3 µM hr^{-1}, **B** is 4.69 µM hr^{-1}, **C** is 16.3 µM hr^{-1}, **D** is 18.9 µM hr^{-1}. Results illustrate the lack of first-order dependence of degradation as a function on the disappearance of Phe.

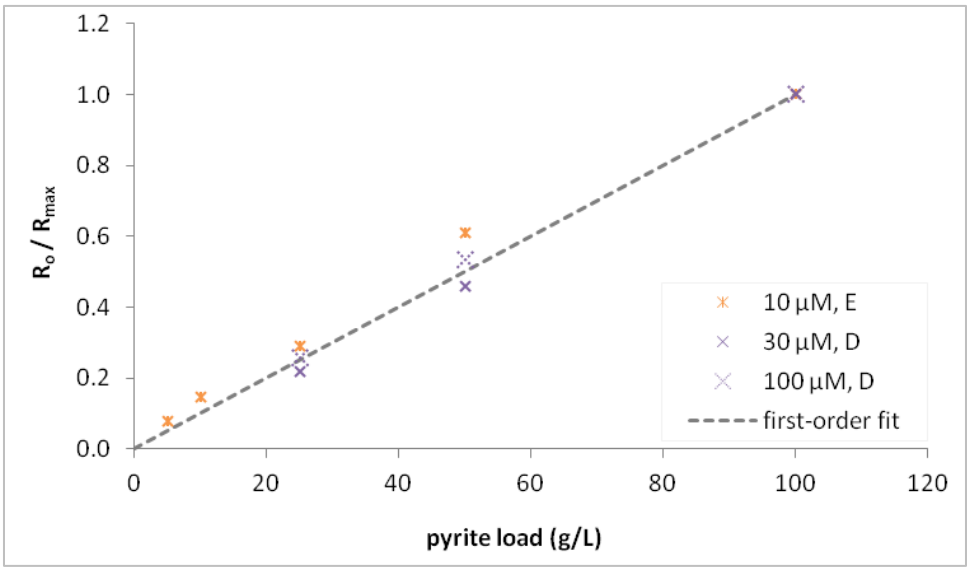

Figure 2.5. The effect of pyrite loading on relative rates. Shown is $\boldsymbol{R_o}$ normalized to maximum initial degradation rates ($\boldsymbol{R_{max}}$) combining data where pyrite loading was varied for three $[Phe]_o$: 10 µM (Exp. E); and 30 µM and 100 µM (Exp. D). $\boldsymbol{R_{max}}$ was greatest at highest pyrite loading but varied among the three experiments due to the effect of $[Phe]_o$ on $\boldsymbol{R_o}$ (Figure 2.4) and differences in pyrite reactivity between experiments D and E (see Table 2.2).

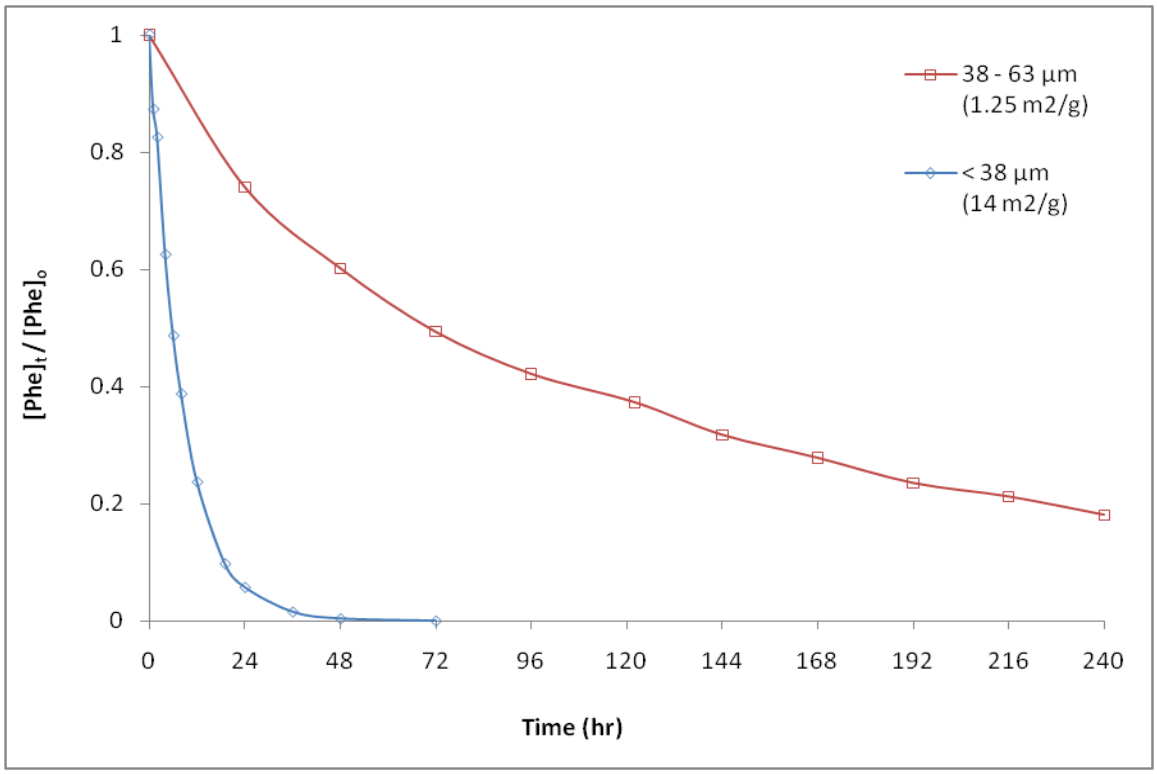

Figure 2.6. Effect of surface area on the rate of Phe degradation. Loss of 100 µM $[Phe]_o$ in 10 g L^{-1} pyrite with surface areas were 1.25 m^2 g^{-1} for 38 – 63 µm (size used in all other experiments) and 14 m^2 g^{-1} for < 38 µm particle sizes.

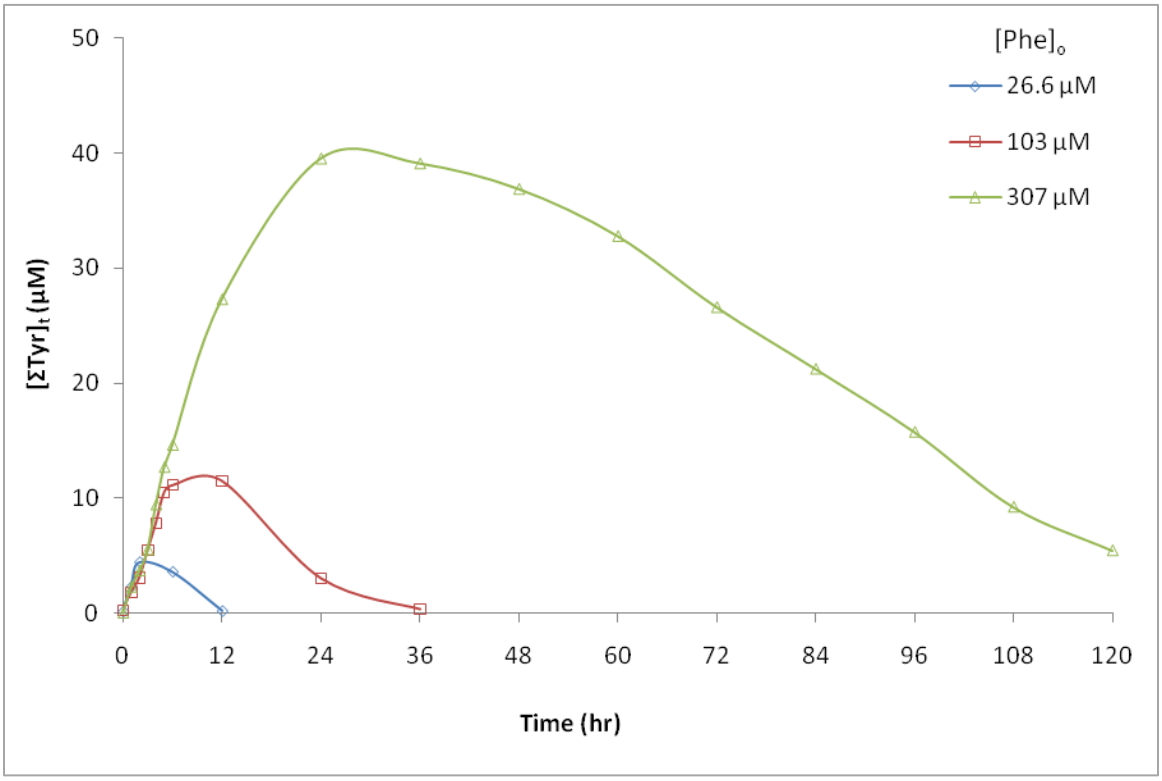

Figure 2.7. Concentration of ΣTyr relative to $[Phe]_o$. The time-course of Tyr in experiment A, corresponding to the loss of Phe, illustrated in Figure 2.2. Accumulation reaches a maximum of 15% ± 3% of the initial Phe concentration at time points immediately following the half-life of Phe, after which degradation of Tyr exceeds its production.

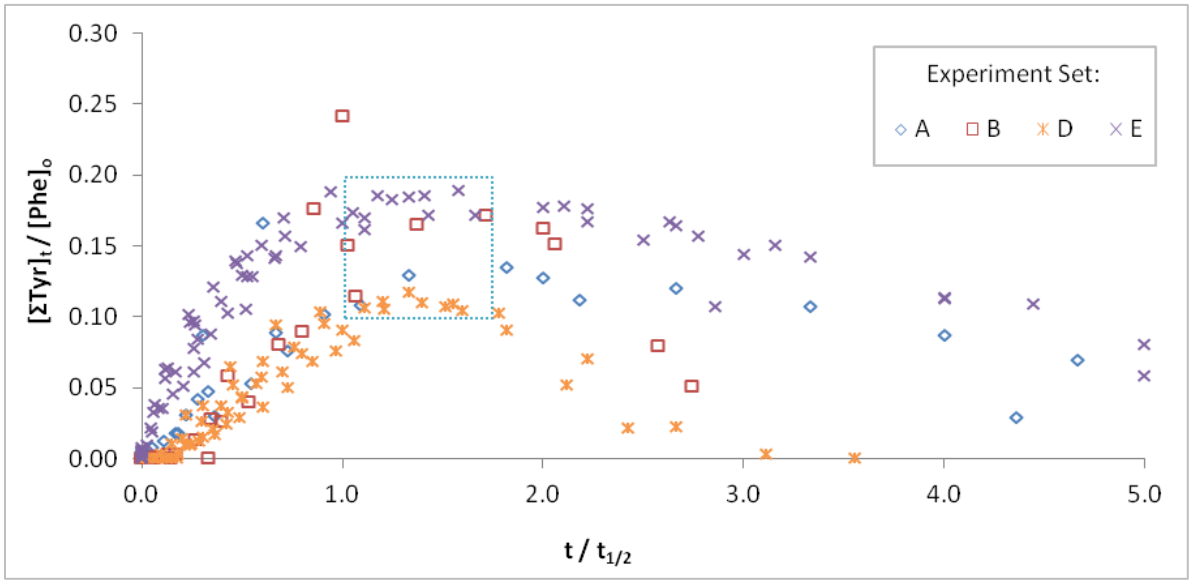

Figure 2.8. Time-dependence of ΣTyr relative to $[Phe]_o$ across all conditions of variable Phe and pyrite levels. The [ΣTyr] through time relative to the $[Phe]_o$ peaks within a narrow range (shown in the boxed area) corresponding to similar timescales relative to Phe loss. The differences that are apparent in the kinetics of Tyr decay between experiments are due to variations in pyrite reactivity, but predicted by model calculations show below.

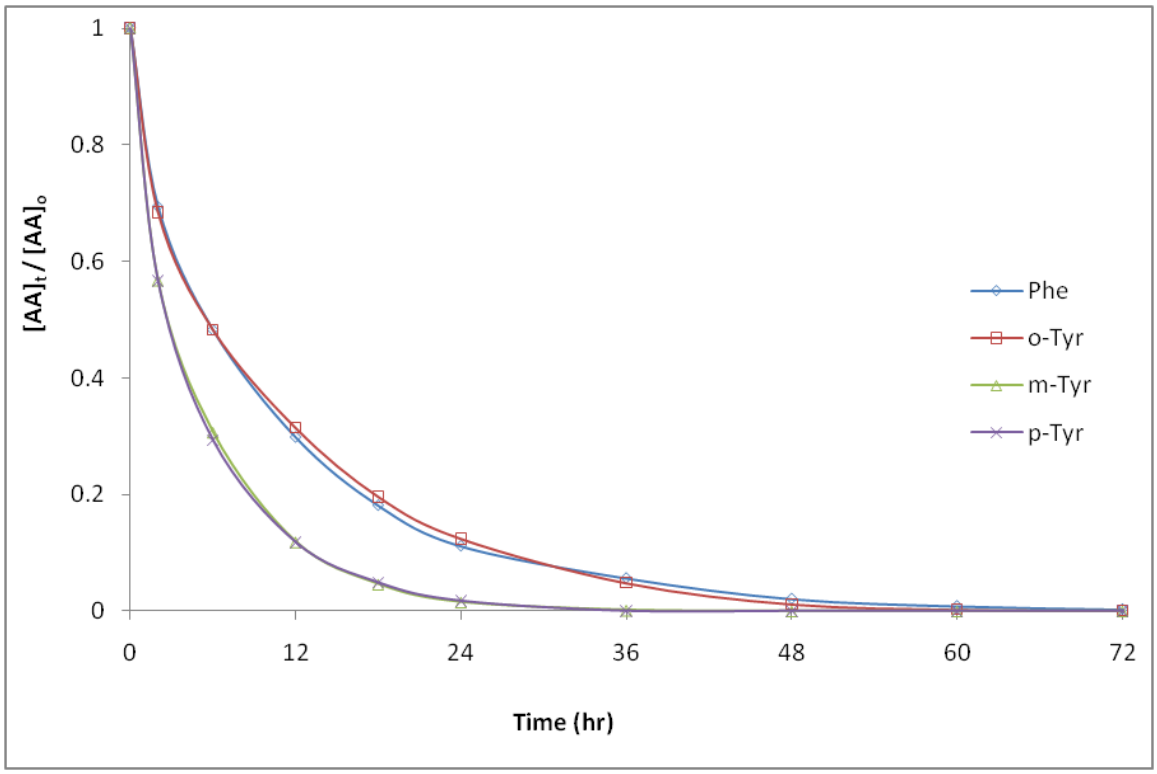

Figure 2.9. Degradation of 100 µM initial concentrations of Phe, *o*-, *m*-, and *p*-Tyr in 50 g L^{-1} pyrite (Exp. G). The initial rate of *m*- and *p*-Tyr loss is 1.4 ± 0.1 times faster than that of Phe and *o*-Tyr, likely due to differences in the distribution of electron-density in the phenyl group.

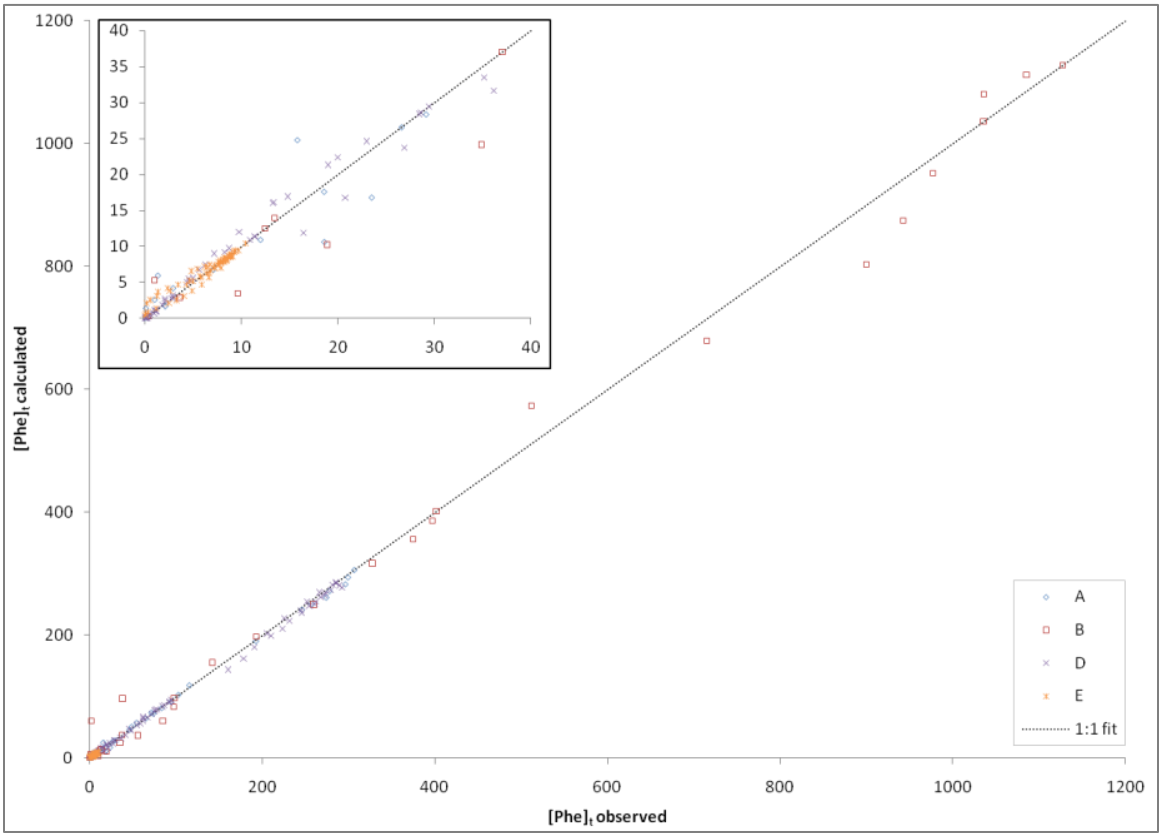

Figure 2.10. Modeled versus observed Phe concentrations for 4 different sets of experiments. Calculated concentrations of Phe were derived from Equation 2.10 using the $\mathbf{K_{pyr}}$ calculated for experiment sets A, B, D, and E. The model values fit the observed data well despite the observed variability in $\mathbf{K_{pyr}}$ among batches of pyrite.

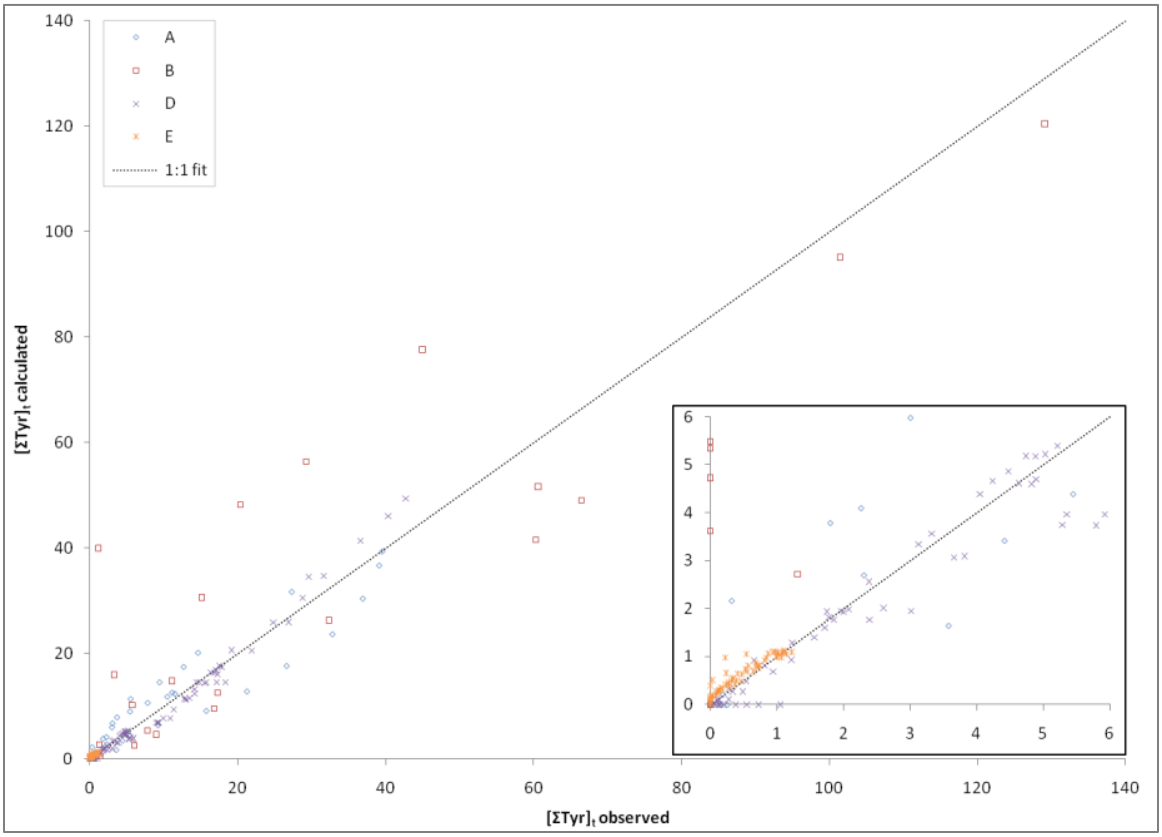

Figure 2.11. Modeled versus observed ΣTyr concentrations for 4 different sets of experiments. Corresponding to the data for Phe shown in Figure 2.10, concentrations of ΣTyr were derived using Equation 2.14, the $\mathbf{K_{pyr}}$ calculated for each experimental set, and a value of 0.5 for α. Note that for points where values are predicted but not measured for Tyr, there was an apparent lag in Phe degradation at the first time point (see inset). Similarly, several instances when no Tyr is predicted to be present, low-levels were observed corresponding to later time points in the incubation where the vast majority of Tyr had been degraded.

Table 2.1. Experimental Design.

Experiment Set	$[Phe]_o$ (µM)	[pyr] ($g\ L^{-1}$)	Incubation time (hr)	pH
A	26.6	100		2.5
	102.8	100	72	2.6
	306.7	100		2.5
B	**12.5**	**100**		
	37.1	**100**		
	97.8	**100**	**120**	
	401.5	**100**		
	1127	**100**		
C	1	100		
	3	100	6-hour pyrite incubations + 1 hr pyrite and Phe	
	10	100		
	30	100		
	100	100		
D	**10.9**	**25**		
	11.4	**50**		
	11.4	**100**		
	28.5	**25**		
	29.5	**50**		
	28.6	**100**	**12**	
	93.9	**25**		
	91.9	**50**		
	94.5	**100**		
	285.2	**25**		
	281.4	**50**		
	285.6	**100**		
E	8.7	5		5.5
	9.4	10		5.1
	9.3	25	16	4.2
	10.4	50		2.9
	10.4	100		2.6
F	**81.68**	**10**	**72**	
	107.2	**10 ($14\ m^2/g$)**	**240**	
G	98.8	50		2.8
	$[o\text{-Tyr}]_o$ 94.0	50	72	
	$[m\text{-Tyr}]_o$ 97.6	50		
	$[p\text{-Tyr}]_o$ 97.7	50		

Table 2.1. Experimental Design. Experiments A – G listed above with corresponding $[Phe]_o$, initial pyrite loading, incubation time of the experiment, and pH data. The pH was not monitored in every reaction vessel for each experiment as it was not a variable as all (Exp. B, C, F, and G) or multiple vials (Exp. D) had the same pyrite loadings. Reaction vessels in experiment G contained only one reactant each – Phe, *o*-Tyr, *m*-Tyr, or *p*-Tyr. Pyrite was added to the respective dilutions of Phe (or Tyr) to initiate the reaction.

Table 2.2. Kinetic values for experimental sets of data for this study.

Experiment Set	$[Phe]_o$ (μM)	[pyr] (g L^{-1})	R_o (μM hr^{-1})	k' (hr^{-1})	Obs. half-life (hr)	Calc. half-life (hr)	half-life ratio	ln[Phe]/t R^2 - correl.
A	26.6	100	4.01	0.447	3.3	1.6	0.47	0.9627
K_{pyr} = 0.122 μmol g^{-1} hr^{-1}	103	100	9.32	0.157	5.5	4.4	0.80	0.9849
	307	100	10.3	0.040	18.0	17.3	0.96	0.9994
B	**12.5**	**100**	**1.43**	**0.642**	**3.5**	**1.1**	**0.31**	**0.9293**
K_{pyr} = 0.079 μmol g^{-1} hr^{-1}	**37.1**	**100**	**3.17**	**0.199**	**6.0**	**3.5**	**0.58**	**0.9498**
	97.8	**100**	**3.63**	**0.093**	**14.0**	**7.5**	**0.53**	**0.9717**
	402	**100**	**4.69**	**0.025**	**35.0**	**27.7**	**0.79**	**0.9768**
	1130	**100**	**4.57**	**0.008**	**90.0**	**86.6**	**0.96**	**0.9422**
C	1	100	0.79	--	--	--	--	--
	3	100	2.05	--	--	--	--	--
	10	100	5.65	--	--	--	--	--
	30	100	10.2	--	--	--	--	--
	100	100	16.3	--	--	--	--	--
D	**10.9**	**25**	**+ 4.59**	**0.400**	**1.5**	**1.7**	**1.16**	**0.9917**
K_{pyr} = 0.165 μmol g^{-1} hr^{-1}	**11.4**	**50**	**+ 6.86**	**0.844**	**0.8**	**0.8**	**1.03**	**0.9969**
	11.4	**100**	**+ 8.57**	**1.39**	**0.7**	**0.5**	**0.71**	**--**
	28.5	**25**	**4.74**	**0.156**	**3.6**	**4.4**	**1.23**	**0.9935**
	29.5	**50**	**9.53**	**0.283**	**2.0**	**2.4**	**1.22**	**0.9975**
	28.6	**100**	**+ 15.3**	**0.559**	**0.9**	**1.2**	**1.38**	**0.9915**
	93.9	**25**	**4.15**	**0.041**	**16.8**	**16.9**	**1.01**	**0.9907**
	91.9	**50**	**8.65**	**0.077**	**8.5**	**9.0**	**1.06**	**0.9909**
	94.5	**100**	**18.9**	**0.143**	**3.8**	**4.8**	**1.28**	**0.9932**
	286	**25**	**3.83**	**0.014**	**38.6**	**49.5**	**1.28**	**0.9426**
	282	**50**	**6.45**	**0.025**	**23.2**	**27.7**	**1.19**	**0.9942**
	286	**100**	**17.1**	**0.047**	**15.1**	**14.7**	**0.98**	**0.9916**
E	8.7	5	0.11	0.017	28.0	40.8	1.46	0.8834
K_{pyr} = 0.021 μmol g^{-1} hr^{-1}	9.4	10	0.2	0.042	16.5	16.5	1.00	0.9611
	9.3	25	0.40	0.092	10.0	7.5	0.75	0.9000
	10.4	50	0.84	0.130	6.6	5.3	0.81	0.9529
	10.4	100	1.38	0.174	4.5	4.0	0.89	0.9880
F	**81.7**	**10**	**0.88**	**0.007**	**70**	**99.0**	**1.41**	**0.9863**
	107	**10 (14 m^2/g)**	**9.38**	**0.116**	**6**	**6.0**	**1.00**	**0.9993**
G	98.8	50	15.1	0.079	5.5	8.8	1.59	0.9854
	$[o\text{-Tyr}]_o$ 94.0	50	14.9	0.081	5.5	8.6	1.56	0.9941
	$[m\text{-Tyr}]_o$ 97.6	50	21.1	0.166	3	4.2	1.39	0.9945
	$[p\text{-Tyr}]_o$ 97.7	50	21.2	0.163	3	4.3	1.42	0.9922
					Average R^2 (sets A, B, D, E, F)			**0.97 ± 0.03**

Table 2.2. Kinetic values for experimental sets of data for this study. Data for $\boldsymbol{R_o}$ determined where approximately 20% of initial Phe was degraded. ***k'*** was estimated from time points up to 90% of Phe loss when possible, and varies between experiment sets due to variability in pyrite activity relative to ·OH production. Set **C** was a single-time point experiment and thus the data do not yield relevant ***k'*** values or half-lives.

$^{+}$ = $\boldsymbol{R_o}$ was estimated as Phe loss was greater than 30% by the first time point.

Chapter 3

INTRINSIC CONDITIONS AFFECTING HYDROXYL RADICAL FORMATION IN PYRITE SLURRIES

3.1 Introduction

The kinetics of reactive oxygen species (ROS) formation in pyrite slurries are governed by the intrinsic properties associated the pyrite mineral and its resulting slurry components. Surface condition (e.g., iron speciation), solution composition related to pyrite dissolution, and duration of exposure to oxygenated water (i.e., pyrite "age"), are all factors that ultimately affect the formation of hydrogen peroxide (H_2O_2) and subsequently hydroxyl radical ($^{\cdot}OH$) production. The model developed in Chapter 2 incorporates these variables into the calculations as they pertain to the pyrite-induced hydroxylation of phenylalanine (Phe), and are collectively represented by the constant $\mathbf{K_{pyr}}$ for a given sample of pyrite. Application of the model generally corroborated with the data; however, anomalies in some samples arose that prompted further investigation into the role of dissolved ferrous iron (Fe^{2+}), H_2O_2, pH, and pyrite aging effect in the overall kinetics of $^{\cdot}OH$ formation and Phe degradation.

The oxidation state of iron on the surface of a freshly-prepared sample of pyrite (treated with a hydrochloric acid (HCl) solution as per (Cohn et al. 2004)) is mostly in the reduced form (Fe(II)). When prepared pyrite is introduced to pure-water or water containing weak electrolytes, the main solution chemistry components of the resulting slurry are derived from a combination of redox reactions at the surface with water and oxygen, and the dissolution of iron and sulfur (as

sulfate) (Moncur et al. 2009). Pyrite samples that have been conditioned with HCl also decrease the redox potential of the system upon addition to water (Descostes et al. 2004) as the reduced iron dissolves from the surface and oxygenated water begins to react with the surface and form patches of Fe(III) (i.e., iron(III) hydroxides). Concurrently, the pH of the slurry decreases as a result of the sulfur oxidation represented the net equation:

$$>FeS_2 + {}^{7}/_{2}\ H_2O + {}^{15}/_{4}\ O_2 \rightarrow Fe(OH)_{3\ (ad\ \text{or}\ aq)} + 2\ SO_4^{2-} + 4\ H^+ \qquad (3.1)$$

A majority of the dissolved oxygen that reacts in pyrite slurries has been shown to form complexes with iron (Usher et al. 2004); however, a recent study estimated that roughly 5-6% is reduced to generate H_2O_2 via the electron transport across the surface and/or within the pyrite (Schoonen et al. 2010). The overall net equation for H_2O_2 formation at the surface (Equation 3.2) reveals that along with the reduction of oxygen with two electrons, the addition of two protons (generated in excess as the pyrite oxidizes (Equation 3.1)) is also required:

$$2\ Fe(II) + O_2 + 2\ H^+ \rightarrow\rightarrow 2\ Fe(III) + H_2O_2 \qquad (3.2)$$

Once formed, the H_2O_2 may either remain adsorbed to the surface or desorb into solution. It has been shown in other studies that H_2O_2 can react rapidly with patches of oxidized iron on the pyrite surface – in which case products formed include water and oxygen, but not $^{\cdot}OH$ (De Laat and Gallard 1999). Some of the H_2O_2 can also be reduced by ferrous iron to form $^{\cdot}OH$ (either in solution or potentially on the surface) through the Fenton reaction (Equation 3.3).

$$Fe^{2+} + H_2O_{2\ (ad\ \text{or}\ aq)} \rightarrow Fe^{3+} + OH^- + {}^{\cdot}OH_{\ (ad\ \text{or}\ aq)} \qquad (3.3)$$

Note that the reaction between Fe^{2+} and H_2O_2 shown in Equation 3.3 occurs independently of pH (unlike the reaction in Equation 3.2) and thus is not specifically favored by the increased formation of sulfuric acid in order to form $^{\cdot}OH$. On the other hand, studies have shown that reactions of organic compounds with $^{\cdot}OH$ in solutions containing Fenton reagents do have a pH dependence with respect to the rate of degradation (Chen et al. 2009) and differences in reaction products (Chang et al. 2008). The observed pH dependence for degradation, which has been shown to range from 2 and 5 pH units in above-mentioned studies, is likely a result of iron catalysis (as iron speciation favors Fe^{2+} over Fe^{3+} at lower pH and reduced environments) allowing Fe^{3+} to cycle back to Fe^{2+} following reduction of H_2O_2. Additionally, variations in

reaction products (including isomer ratios) in the some studies were observed, though no reason or interpretation was given or referenced (Chang et al. 2008). Lower pH can also help maintain a greater amount of Fe(II) on the pyrite surface after extensive oxidation in the presence of dissolve oxygen, thus preventing it from completely oxidizing to Fe(III) and affecting H_2O_2 production (Equation 3.2).

The effect of altered solution chemistry in pyrite slurries has not been examined with respect to variations of additional iron and H_2O_2. Some studies have reported concentrations of Fe^{2+} and Fe^{3+} along with H_2O_2 fluxes (separately) taken at several time points as a sample of pyrite incubated (Cohn et al. 2006c). Data from that work provided a starting point for pyrite experiments with increased levels of Fe^{2+} and H_2O_2. Changes in rates of Phe degradation when excess Fe^{2+}, H_2O_2, and/or H^+ (lower pH using sulfuric acid) are present in the initial solution of the pyrite slurries are examined in this chapter to identify potential component(s) that limit the redox chemistry involved in the formation of H_2O_2 and $^{\cdot}OH$ formation, as well as Phe loss.

Direct comparison of the kinetics of Phe loss through time between solution-phase Fenton reagents or pyrite slurries would be difficult to replicate given the non-steady-state reactants in the Fenton experiment and low-levels of H_2O_2 observed in pyrite slurries. Simultaneous titrations of Fe^{2+}, low levels of H_2O_2, and sulfuric acid without significantly changing the volume to mimic solution chemistry in the slurries would be required. Alternatively, it was hypothesized that any differences in Tyr-isomer and $[\Sigma Tyr] / [Phe]_o$ ratios observed when reactions of Phe in homogeneous Fenton solutions and pyrite slurries were compared (at the same pH) would suggest that at-least some direct surface interactions with Phe and pyrite were involved (Chapter 2).

Evidence from control experiments in Chapter 2 show that Phe does not adsorb measurably to the pyrite surface (Figure 2.2), and thus the conversion of Phe to Tyr is speculated to occur exclusively in the aqueous phase. Furthermore, recent studies have suggested that the formation of $^{\cdot}OH$ occurs mainly in the solution phase, based on leuco crystal violet (LCV) fluorescent probes that measure H_2O_2 (Cohn et al. 2005). However, it is not clear though if the LCV is reacting with any adsorbed H_2O_2 as well. Similarly, it cannot be completely ruled out that measurements of $^{\cdot}OH$ with probes such as 3'-(p-aminophenyl) fluorescein (APF) (Cohn et al. 2009) in pyrite slurries could also be reacting with adsorbed $^{\cdot}OH$ or through direct oxidation (via

electron transfer) at the surface. Therefore, experiments designed to distinguish reactions in the aqueous-phase would be useful in understanding the ·OH-reaction mechanism – some of which were conducted in this chapter.

In several incubations described in Chapter 2 (experiments A and B), loss of Phe appeared to lag, or degrade less rapidly, initially (Figure 3.1). The example in Figure 3.1 shows an exponential curve that has been fit to all the data points up to and including approximately 90% Phe loss (as per Chapter 2, Figure 2.2) and shows that the first few points have a shallower slope that is inconsistent with the rest of the degradation pattern. It was suspected that the condition of the pyrite surface was causing this apparent lag, and that it was directly related to the rate of H_2O_2 production following initial exposure. As pyrite incubations progress and the sample ages in solution, the continuous exposure to oxygenated water changes the pyrite surface, and thus the ability to generate H_2O_2 (Schoonen et al. 2010). Therefore, additional experiments were conducted with the same batch of pyrite to better understand the effect prolonged exposure to water on the ability for the slurry to produce ·OH at a consistent rate.

The effects of variable iron and H_2O_2 concentrations in solution, as well as pH, are important as they are also relevant in biological and environmental systems where pyrite can be introduced and interact. Inhalation of pyrite dust can induce an immune system response causing phagocytes to react and enzymatically generate H_2O_2 formation within the cell. In the gut, pyrite can experience pH as low as 2 (Campbell et al. 1999) as it passes through the stomach before passing into the small intestines where enzymes and other chemicals can bring the pH up to around 7 (de la Cruz Moreno et al. 2006). Additionally, residence time for pyrite in either of these systems can be prolonged, depending on particle size, and thus the long-term potential for ·OH production is important to understand.

The focus of the experiments in this chapter was: 1) to provide additional evidence related to whether the reactions of Phe with ·OH were occurring in the aqueous phase or on the surface of pyrite; 2) develop a better understanding of the influences several major components (i.e., Fe^{2+}, H_2O_2, and pH) in pyrite slurries have on formation of ·OH; and 3) to test the affect of pyrite "aging" on production of ·OH and determine whether the apparent lag in Phe degradation that is observed in some experiments could be verified. To address these issues, incubations of Phe, similar to those conducted in Chapter 2, were run with and without pyrite.

3.2 Methods

Pyrite from Huanzala, Peru (Wards Natural Science, Rochester, NY) was ground and sieved to a range of 38 – 63 μm. Samples were treated prior to each experiment with a nitrogen-purged solution of 0.1 M HCl to remove surface oxidation (Fe(III)) and rinsed in a glove box with nitrogen-purged water. Phenylalanine, *para*-tyrosine, *ortho*-tyrosine, beta-mercaptoethanol, and ammonium ferrous sulfate (Mohr's salt) – all 99% ACS-grade or better – were obtained from Alfa Aesar (Ward Hill, MA). *meta*-Tyrosine was obtained from TCI America (Portland, OR). Hydrogen peroxide (30% w/w) was acquired from Sigma Aldrich (St. Louis, MO). Reagent grade sulfuric acid was obtained from JT Baker (Phillipsburg, NJ). Methanol was GC^2-grade from Burdick & Jackson (Morristown, NJ). Formic acid was ACS-grade from EMD Chemicals (Gibbstown, NJ). All water used for cleaning, standards, reactions, dilutions, and chromatography work was purified with a Milli-Q filtration system (Millipore Corporation, Billerica, MA) to a resistivity of 18.3 MΩ cm^{-1}.

3.2.1 Phenylalanine reactions with added Fenton reagents

Solutions prepared for pyrite incubations contained supplemental Fe^{2+} (in the form of Mohr's salt) or H_2O_2 to compare the loss of Phe and net production of Tyr isomers in aqueous solutions (containing dissolved Fenton reagents) to those in pyrite slurries (both with and without added Fe^{2+} or H_2O_2). Reactions of Phe in solution and pyrite slurries were also conducted to test the affect of adjusting the solution to pH 2.5, which is more acidic than derived from pyrite slurries monitored in this study. Several incubations with pyrite loadings of 50 g L^{-1} were run for 6 hours, with five time points taken throughout the run to observe differences in initial rates ($\boldsymbol{R_o}$) and kinetics that result from the addition of 500 μM Fe^{2+} or 500 μM H_2O_2.

Incubations of Phe in solutions without pyrite were run with concentrations of 100 – 400 μM Mohr's salt added to pure water to replicate and exceed iron levels that would be present at the pyrite loadings used most often in this dissertation, 50 g L^{-1} and 100 g L^{-1}. These levels are based on results obtained by Cohn et al (2006) where $[Fe^{2+}]$ = 1.6 μM upon addition of 1 g L^{-1} of

pyrite to water – a linear increase in concentration versus loading was then assumed for this work. H_2O_2 was added at 100 – 400 μM (400 μM H_2O_2 was only used with 200 μM Mohr's salt), far in excess of concentrations of 2.2 – 26 μM observed by Cohn et al (2006) after a brief exposure to oxygenated water of pyrite loadings of 20 – 160 g L^{-1} (in slurries containing ethylenediaminetetraacetic acid (EDTA) which chelated Fe^{2+} in solution to limit or prevent the Fenton reaction from occurring). Preliminary experiments of 6-hour incubations revealed that the [Phe] and [ΣTyr] remaining in solution following exposure to Fenton reagents was the same for each subsequent sample beyond **t** = 1 hr for all the samples. This indicated the reaction occurred rapidly and had fully exhausted the H_2O_2 initially spiked by the first hour. Therefore, experiments conducted in solutions without pyrite only had an initial (**t** = 0 hr) and a 1-hour time point.

For each experiment, aqueous stock solutions were first prepared. A concentrated solution of 2 mM Mohr's salt was diluted to 1 mM stocks with and without added sulfuric acid to adjust the pH. The 1 mM stocks were then combined and diluted to the desired concentrations with stocks of 1 mM Phe in either pure or pH-adjusted (to a pH of 2.5) water for the desired pH and iron concentrations. The pH of the unadjusted solutions varied between 4.3 and 3.1 pH units as the concentration of Mohr's salt and H_2O_2 (both of which are generally acidic). To initiate the reaction, H_2O_2 was spiked or pyrite was added (or both) to the reaction solution. The $[Phe]_o$ was 100 μM for all incubations in this section and reactions were conducted in 15 mL disposable centrifuge tubes with volumes of at-least four times the volume of the total volume of aliquots taken as samples for time points. Tubes were simultaneously set to rotate end-over-end on a carousel at a constant 24 rotations-per-minute after water had been added to all vials. Samples were at room temperature of 25° ± 2° Celsius and covered with aluminum foil to prevent light exposure. Tubes were briefly vortexed and aliquots of 300 μL were removed, quenched with 5 μL of β-ME, then pyrite-containing samples were filtered using 0.22 μm nylon Costar® centrifuge vial filters (Corning Life Sciences, Lowell, MA). Methanol (50 μL) and formic acid (5 μL) were added to 20 μL of aqueous sample or filtrate and diluted to a total volume of 1 mL with water in an HPLC vial for analysis.

3.2.2 Pyrite aging experiment

To better understand the ability of pyrite to continuously produce ·OH as a function of time, parallel incubations of Phe were compared. Thirty-two individual 2-mL disposable centrifuge vials were weighed out with 100 mg of pyrite to represent the number of incubation points (or pyrite age) ($\mathbf{t_i}$). To each vial was added 990 µL of water with a 1 mL Eppendorf® pipette, starting with the longest incubation time to minimize error of the independent variable (time). A stock solution of 1 mM Phe was used to spike 10 µL (for a final concentration of 10 µM) into each vial at predetermined $\mathbf{t_i}$ and allowed to continue incubating for 2 additional hours (see Figure 3.2 for visual representation of experimental design). Vials were simultaneously set to rotate end-over-end on a carousel at a constant 24 rotations-per-minute after water had been added to all vials. Samples were at room temperature of 25° ± 2° Celsius and covered with aluminum foil to prevent light exposure. Vials were only removed briefly for spiking purposes and to quench and filter after the 2-hour Phe incubation. Samples were briefly vortexed, quenched with 15 µL of β-ME (for a concentration of 260 mM), then filtered with 0.22 µm nylon centrifuge vial filters. Triplicate samples were collected for pyrite incubating from 0 to 2 hours and 12 to 14 hours. Methanol (25 µL) and formic acid (2.5 µL) were added directly to 500 µL filtrate in an HPLC vial for analysis.

3.2.3 Analyses

All experiments were analyzed using a Waters Corporation (Milford, MA) Alliance® 2695 HPLC coupled to a Waters Corporation Micromass LCT Time-of-Flight Mass Spectrometer (ToF-MS) as described in the Methods section of Chapter 2.

3.3 Results and Discussion

3.3.1 Effects of iron, hydrogen peroxide, and pH on degradation of phenylalanine in solution and pyrite slurries

Experiments were conducted with and without pyrite to gain more insight into whether the reactions with Phe in pyrite slurries are a result of ·OH generated and reacted at the pyrite surface or in solution. The concentration of Fe^{2+} (through the addition of Mohr's salt) and H_2O_2

were varied and the pH was adjusted to compare degradation rates of Phe, along with formation of Tyr and isomer-ratios, in both solutions and pyrite slurries. For all experiments in this section, 100 μM Phe was used. The Tyr-isomer formation and ratios of $[\Sigma Tyr] / [Phe]_o$ were monitored as variations in either may result from differences in reaction mechanisms (i.e., solution versus surface reaction of adsorbed Phe or ·OH that might impact Phe reactivity or degrees-of-freedom).

3.3.1.1 Aqueous-phase degradation of phenylalanine in the presence of Fenton reagents

Loss of Phe and formation of Tyr was observed in aqueous incubations containing varying concentrations of ammonium ferrous sulfate (Mohr's salt), H_2O_2, and at both adjusted and unadjusted pH (Figures 3.3 and 3.4). The addition of sulfuric acid to pH-adjusted solutions resulted in a decrease in pH that did not vary over time. Variations in H_2O_2 were more significant than the effects of Fe^{2+} and pH with respect to differences in remaining [Phe] after each 1-hour incubation. No H_2O_2 was added to control samples (Figures 3.3 and 3.4), which were used to represent $[Phe]_o$ for mass-balance purposes. Approximately 40% of the Phe remained following incubations of 100 μM H_2O_2 compared to only 10% Phe with 200 μM H_2O_2. No Phe remained in pH-unadjusted solution of 400 μM H_2O_2 and 200 μM Fe^{2+}, and only 0.33 μM (i.e., less than 0.5%) Phe remained of a similar solution with the pH was adjusted to 2.5 (Figure 3.3).

Variations in Fe^{2+} were less significant than H_2O_2 in the degradation of Phe, with an average of 34.2 ± 5.9 μM Phe remaining for all 100 μM H_2O_2 and 9.7 ± 2.2 μM Phe for 200 μM H_2O_2 (with one outlier at 200 μM H_2O_2 and 100 μM Fe^{2+}) (Figure 3.3). The remaining Phe in pH-unadjusted solutions of 200 μM and 400 μM Fe^{2+} were similar and less than the Phe remaining in 100 μM Fe^{2+}, indicating that the $[Fe^{2+}]$ likely had met and exceeded necessary levels for the Fenton reaction to rapidly consume H_2O_2 at 100 μM. Previous studies have also indicated that optimal ratios of $[H_2O_2]$-to-$[Fe^{2+}]$ in Fenton reactions degrading organic compounds is much greater than 1:1 (Chang et al. 2008; Chen et al. 2009).

There was slightly more Phe loss in reaction solutions with a pH of 2.5 (except for with 100 μM Fe^{2+}) than the pH-unadjusted solutions with a pH range of 4.3 to 3.1. This agrees with some studies that found an optimal range of 2 – 5 pH units yielded the greatest degradation of compounds containing aromatic moieties in solutions of Fenton reagents (Kos et al. 2010).

Interestingly, the addition of 400 μM H_2O_2 to 200 μM Fe^{2+} did not completely degrade all the Phe when the pH was adjusted to 2.5 as it did in the pH-unadjusted reaction (Figure 3.3). Although the remaining [Phe] was low, it seems unusual because it is not consistent with results of the other incubations or the above mentioned studies (i.e., the extent of the pH-adjusted reaction of Phe would have been expected for the pH-unadjusted incubation). One possible explanation for this is that the degradation pathways of Phe, Tyr, and other reaction products are slightly different at lower pH, similar to what was observed when the pH was varied in reactions of Fenton reagents and salicylic acid (Chang et al. 2008). Consequently, some reaction products of Phe, Tyr, and other degradates in solutions of pH 2.5 may have slightly higher rate constants than those products formed in the pH-unadjusted incubations, resulting in loss of less Phe in the pH-adjusted solution due to greater competition for ·OH. To confirm this theory, more experiments are required to determine the pH-dependent pathways of Phe degradation.

3.3.1.1.1 Tyrosine concentrations and isomer comparisons

Relative ratios of $[\Sigma Tyr] / [Phe]_o$ and composition of Tyr-isomers are presented in Figures 3.4 and 3.5 (respectively) and are consistent with the patterns observed for Phe incubations in pyrite slurries – supporting the assumption that the reaction of ·OH and Phe occurs in the aqueous phase. The remaining levels of Tyr in all incubations represent reactions that extended beyond the Phe half-life and thus had reached or exceeded the $[\Sigma Tyr] / [Phe]_o$ peak observed in time-series degradation experiments (as depicted in Figure 2.8). Indication that the mechanism of solution-phase Phe hydroxylation is similar to that in pyrite slurries is supported by the observed $[\Sigma Tyr] / [Phe]_o$ ratio, which were between 10% and 22% for each incubation (where Phe was still observed at appreciable concentrations (100 μM and 200 μM H_2O_2 exposures)). These percentages are consistent with those observed in incubations containing pyrite at time points with a comparable $[Phe] / [Phe]_o$ (Chapter 2).

The variations in levels of H_2O_2 among incubations had the most significant effect on remaining [ΣTyr] while variations in $[Fe^{2+}]$ had the least effect (Figure 3.4). Unlike with remaining Phe, there was noticeably more Tyr remaining when the pH was adjusted down to 2.5 than the pH-unadjusted reactions. This could also be explained with similar reasoning as stated

above regarding remaining Phe at 400 μM H_2O_2 and pH 2.5 – low pH may have formed other reaction products from Phe that compete better for ·OH than Tyr.

Isomer-ratios of Tyr were similar within incubations of the same [H_2O_2] and were in the same proportions to those in pyrite incubations from Chapter 2 – [*o*-Tyr] > [*p*-Tyr] > [*m*-Tyr] (Figure 3.5). Of the three variables, only variations in H_2O_2 affected the Tyr-isomer ratios observed. Average ratios of Tyr-isomers were 0.39 ± 0.02, 0.31 ± 0.03, and 0.30 ± 0.01 (respectively) for solutions with 100 μM H_2O_2 and 0.43 ± 0.05, 0.29 ± 0.06, and 0.28 ± 0.02 (respectively) for solutions with 200 μM H_2O_2. This compares well with the Tyr-isomer ratios of 0.40 ± 0.02, 0.32 ± 0.02, and 0.28 ± 0.02 (respectively) for slurries of 100 μM $[Phe]_o$ (nominally) reported in Chapter 2 for experiment D, which was stable throughout the duration of the 12-hour incubation (see Appendix, Figure A.1) at the end of which Phe reached about 20% of $[Phe]_o$.

Figure 3.5 also shows that in incubations with 200 and 400 μM H_2O_2, there tends to be more *o*-Tyr remaining than *p*-Tyr relative to the [ΣTyr]. This subtle difference is likely a result of the differences in second-order rate constants affecting loss of each Tyr isomer (as mentioned in Chapter 2, Figure 2.9) that became more important as the reaction proceeds and production of Tyr decreased (i.e., in exposures where [Phe] approaches 90%-loss and [ΣTyr] is also dropping). This pattern has also been observed in previous experiments with pyrite where remaining [Phe] was near total depletion and *o*-Tyr appeared to degrade slower than *m*- and *p*-Tyr – providing even more evidence that the mechanism for the conversion of Phe, as well as Tyr, in pyrite slurries occurs in the aqueous phase.

3.3.1.1.2 Fate of hydroxyl radical produced by added hydrogen peroxide

An increase in [H_2O_2] from 100 μM to 200 μM did not result in a 2-fold decrease in remaining Phe or Tyr. This is due to the increase in the levels of other reaction products (related to the loss of Phe) that are competing for the same ·OH pool and important in defining the kinetic model for the overall reaction as described in Chapter 2. The fraction of H_2O_2 added that led to direct loss of Phe in this experiment decreased with increasing H_2O_2 (Figure 3.3). Mass-balance calculations allowed for the estimation of the relative fraction of ·OH that reacted with Phe, Tyr, or other and/or subsequent reactive products (collectively denoted in this section as "other").

Estimates of the relative sinks for ·OH using the observed data assumed that all the H_2O_2 added is quantitatively transformed to ·OH via the Fenton reaction. Values for these calculations are given in Table 3.1 (and graphically represented in Figure 3.6) for three different scenarios:

100% Phe-to-Tyr conversion represents full conversion of Phe to Tyr with no other product formed, which corresponds to $\boldsymbol{\alpha} = 1$ in the kinetic model and simulation developed in Chapter 2. Calculations for Phe, Tyr, and "other" (·OH sinks) were derived by the following equations:

[Phe]-reacted: Δ[Phe]

[ΣTyr]-reacted: Δ[Phe] – [ΣTyr]-remaining

["other"]-reacted: $[H_2O_2]_o - (\Delta[\text{Phe}] + (\Delta[\text{Phe}] - [\Sigma\text{Tyr}]\text{-remaining}))$

50% Phe-to-Tyr conversion represents only half of the Phe is converted to Tyr, with the remaining half forming products other than Tyr. This corresponds to $\boldsymbol{\alpha} = 0.5$. This particular model was found to be the best fit for the experimental data presented in Chapter 2. Calculations for Phe, Tyr, and "other" (·OH sinks) were derived by the following equations:

[Phe]-reacted: Δ[Phe]

[ΣTyr]-reacted: $(0.5 \times \Delta[\text{Phe}]) - [\Sigma\text{Tyr}]\text{-remaining}$

["other"]-reacted: $[H_2O_2]_o - (\Delta[\text{Phe}] + ((0.5 \times \Delta[\text{Phe}]) - [\Sigma\text{Tyr}]\text{-remaining}))$

"Tyr formed does not react" conversion represents the least amount of Phe converted to Tyr and assumes that no-further degradation of Tyr occurs. Thus, the [ΣTyr] observed after the 1-hour incubation was the only Tyr formed during that time, none of which had degraded. Calculations for Phe, Tyr, and "other" (·OH sinks) were derived by the following equations:

[Phe]-reacted: Δ[Phe]

[ΣTyr]-reacted: 0

["other"]-reacted: $[H_2O_2]_o - \Delta[\text{Phe}]$

Although neither Case 1 or 3 are likely (due to reasons given in Chapter 2), the mass-balance calculations constrain the amount of ·OH consumed by other species. For example, if Case 1 is assumed, the relative amount of 100 μM H_2O_2 that formed ·OH and reacted with "other" degradation products of Phe were sometimes negative (Table 3.1), which is very unlikely since it implies that more H_2O_2 reacted than was available. Similarly, in Case 3, even though no

negative values were calculated, reactions with only Phe and its degradation products other than Tyr has also been shown in Chapter 2 to be theoretically and practically unlikely.

The conversion of 50% Phe-to-Tyr (Case 2) is analogous to $\boldsymbol{\alpha} = 0.5$ in the model and simulation developed in Chapter 2; thus is the most reasonable assumption for estimating the fate of ·OH derived from the $[H_2O_2]_o$ (Figure 3.6). To confirm, results from this experiment were compared by running the simulation developed in Chapter 2 for pyrite incubations. For the simulation, values of ·OH-flux, rate constants, and fraction-converted variables (i.e., **β**, **γ**, etc) were all set to "1" as in Chapter 2. This was done to determine specific changes as individual variables are adjusted. Then, using the a nominal 100 μM $[Phe]_o$, $\boldsymbol{\alpha} = 0.5$, and $\boldsymbol{k_{Phe}} = \boldsymbol{k_{Tyr}}$ (i.e., both set to 1 as well), the observed [ΣTyr]-remaining values were compared to those of observed and calculated [Phe]-remaining. The same was done for mass-balance calculations from Case 1 and 3 as well; however, there was only good correlation between the simulation and values determined for Case 2 (correlation was very good in the incubations that the pH was unadjusted).

Figure 3.6 also shows a clear pattern of a 20%-decrease in the proportion of total-H_2O_2 that leads to loss of Phe per doubling of $[H_2O_2]$. This is also consistent with modeled results when the flux of ·OH was doubled in the simulation. As the $[H_2O_2]_o$ increased, the percentage of Phe that reacted with the ·OH generated was smaller as more competitors ("other" reactants) were formed. Therefore, these results of aqueous-phase reactions of H_2O_2 and Fe^{2+} are consistent with both simulated and observed pyrite-generated reactions and the simulation provides more evidence for solution phase ·OH reactions.

Experiments in the following section were conducted to provide further insight into the limiting kinetics of each component (Fe^{2+}, H_2O_2, and pH) concerning the formation of ·OH in pyrite slurries (with respect to the degradation of Phe).

3.3.1.2 Pyrite slurries with added ferrous iron or hydrogen peroxide

The rate of degradation of 100 μM Phe in 50 g L^{-1} pyrite slurries with solutions altered prior to incubations was found to be significantly affected by a lower pH and addition of 500 μM

of H_2O_2; whereas the addition of 500 μM of Fe^{2+} did not affect the rate (Figure 3.7). Control samples of Phe were also run without pyrite at 500 μM Mohr's salt or H_2O_2 (separately) in pH-adjusted and pH-unadjusted solution – no Phe loss was observed over the 6-hour incubations (Figure 3.7). A concentration of 500 μM for each component (Fe^{2+} and H_2O_2) was chosen to saturate the solution with levels higher than what have been shown to be dissolved or formed (respectively) during the initial time points in slurries of pyrite alone (Cohn et al. 2006c). The pH-unadjusted pyrite incubation served as a baseline for reactivity with respect to Phe loss, and the observed rate was relatively constant over the 6-hour timescale, with an $\boldsymbol{R_o}$ of 11.7 μM hr^{-1}. Without acid addition, the pH decreased from roughly neutral (pure water) to 3.4 by the end of the incubation. Addition of 500 μM Mohr's salt to a comparable pyrite slurry had no significant effect on the kinetics of Phe loss (similar to results in the Fenton experiments in the previous section), suggesting that the amount of ferrous iron released through the dissolution of pyrite was sufficient for the continued catalytic reduction of all H_2O_2 generated at the pyrite surface.

When the pH of the solution was adjusted to 2.5 prior to addition of pyrite, Phe degradation rates were significantly slower ($\boldsymbol{R_o}$ = 2.6 μM hr^{-1}) than the pH-unadjusted solutions (Figure 3.7). The pH dropped negligibly in the acidified slurry (0.05 pH units) by the end of the experiment. Again, reaction rates with and without 500 μM Mohr's salt exhibited little difference which indicates that dissolved [Fe^{2+}] is not a rate-limiting component in production of $^{\cdot}OH$ under acidic (pH 2.5 – 3.4) conditions. The effect of pH on the reaction rates in the pyrite slurries was contrary to observations made in the solution-only experiments from the previous section (with respect to the extent of remaining Phe in pH-adjusted and pH-unadjusted solutions comparatively), which suggests the conditions influencing the pyrite surface factor into the rate of H_2O_2 generation. One potential explanation is that the lower initial pH of the slurry may not have allowed for sufficient Fe(III) patches to form at the pyrite surface, which is believed to be important in initiating the electron-transfers required for the reduction of oxygen to form H_2O_2 at the pyrite surface (Rosso et al. 1999; Schoonen et al. 2010).

As expected, the addition of 500 μM H_2O_2 degraded most of the 100 μM initial Phe by the first time point (**t** = 0.5 hrs) in both pH-adjusted and pH-unadjusted slurries (Figure 3.7). While this level of H_2O_2 is in great excess of that determined in pyrite-only slurries (Cohn et al. 2005), it further supports the notion that the production of H_2O_2 is the rate-limiting factor in

pyrite-induced ·OH production. Degradation occurred so rapidly in these two samples that within the 15 to 30 seconds between initiation (i.e., addition of pyrite followed by H_2O_2) and the time it took to take the first aliquot (**t** = 0 hr), a significant portion of Phe had already been lost and Tyr formation was easily detectable (Figure 3.8; though not apparent in Figure 3.7 due to the normalization of data to $[Phe]_o$).

Based on the [ΣTyr] formed, the initial rates of Phe loss would be on the order of 35 to 720-times faster with the addition of 500 μM H_2O_2 to the pyrite slurry than in pyrite alone. Assuming that in 30 seconds, and 50% of Phe lost converted to Tyr ($\boldsymbol{\alpha}$ = 0.5), $[Phe]_o$ would have been 13.6 μM and 5.8 μM higher than observed at **t** = 0 hr based on the respective [ΣTyr] observed (in pH-unadjusted and pH-adjusted, respectively). Estimating $\boldsymbol{R_o}$ with the higher $[Phe]_o$ and comparing the overall loss over to the pyrite-only incubations reveals a crude estimate of $\boldsymbol{R_o}$ for Phe degradation of 700 μM hr^{-1} for the pH-unadjusted sample and 1600 μM hr^{-1} for the pH-adjusted incubations. Note that the calculated rate of Phe loss for the pH-adjusted incubation is estimated to be greater than in the pH-unadjusted slurries, which is more representative of the solution-phase reactions from the previous section (Figure 3.3) than the pH affect on pyrite-only slurry reactions (Figure 3.7). Following the initial decay (to **t** = 0.5 hr), only 2% of $[Phe]_o$ was still detectable. The remaining Phe continued to decay over the next 5.5 hours of the experiment at a very slow rate of 0.15 μM hr^{-1} (Figure 3.7). In fact, a similar rate was recorded near the end of an incubation in Experiment G ($[Phe]_o$ = 98.8 μM, 50 g L^{-1} pyrite loading) where Phe reacted more than 95% and the reaction products act as the primary sink for ·OH (Chapter 2). These observations, as previously discussed, are likely the result of the numerous Phe degradates competing for the limited ·OH formed as H_2O_2 production continues at the pyrite surface. Interestingly, the extent of iron oxidation on a fresh pyrite surface exposed to H_2O_2 may be similar to a sample of pyrite that has been incubating in oxygenated water for some-time, as H_2O_2 is a strong oxidant. More experiments on the oxidation state of pyrite surfaces would be required to explore this notion.

Concentrations of ΣTyr in the experiments with and without additional Fe^{2+} were consistent with previous pyrite incubations described in Chapter 2 reaching about 14% of $[Phe]_o$ for the pH-unadjusted pyrite incubations and about 8% of $[Phe]_o$ for the pH-adjusted (Figure 3.8). Ratios of Tyr-isomers were again consistent in experiments with and without pyrite, where

[*o*-Tyr] > [*p*-Tyr] > [*m*-Tyr], with ratios averaging 0.39 ± 0.04, 0.32 ± 0.05, and 0.29 ± 0.05 respectively. However, identification of similar products and ratios is only one part of establishing a mechanism for the overall fate and reactivity of $^{\cdot}OH$ in pyrite slurries through time. As aforementioned, the formation of H_2O_2 at the surface of pyrite is the limiting factor in the overall formation of reactive $^{\cdot}OH$. Two likely factors that affect the ability of the pyrite surface to generate H_2O_2 in oxygenated slurries include the extent of conditioning with HCl prior to incubation and the age or length of time pyrite is in aqueous suspension. These factors were evaluated in the following section.

3.3.2 Effect of pyrite incubation time on phenylalanine loss

Rates of Phe loss were determined by calculating loss during two-hour incubations, which revealed changes in reaction rates as the pyrite aged in solution (Figure 3.9, Table 3.2). The final [Phe] measured in each incubation was compared to a nominal $[Phe]_o$ of 10 μM based on a control incubation without pyrite. Illustrated in Figure 3.9 are degradation rates of Phe as pyrite aged in water, which reached a maximum of 4.8 μM hr^{-1} (from $\mathbf{t_i}$ = 6 – 8 hours) and a low of 1.6 μM hr^{-1} (from $\mathbf{t_i}$ = 72 – 74 hours). Precision of analysis was good with two sets of triplicates, with estimated rates of 5.18 ± 0.19 μM ($\mathbf{t_i}$ = 0 – 2 hours) and 1.08 ± 0.11 μM ($\mathbf{t_i}$ = 12 – 14 hours). For each sample, the formation of the three isomers of Tyr confirmed the conversion of Phe was a result of $^{\cdot}OH$ reaction; however, quantification of Tyr was not an objective of this experiment.

Initially, the rate of Phe degradation during pyrite incubations from $\mathbf{t_i}$ = 0 – 2 to 2.5 – 4.5 hours increased from 2.4 μM hr^{-1} to 4.8 μM hr^{-1} (Figure 3.9). This observation confirmed the presence of a lag in pyrite reactivity as observed in experiment A (Figure 3.2), where the rate of degradation was noticeably slower at the beginning of the reaction and deviated from an exponential fit of all data points. A similar lag was also observed to a lesser extent in experiment B, but not in any other experiment. Data from these initial time points did not conform as well to the exponential fits obtained for most of the experiments with pyrite (Chapter 2) or in other studies of reactions of pyrite and organic reactants, such as adenine (Cohn et al. 2010) and trichloroethylene (TCE) (Pham et al. 2009).

Since levels of Fe^{2+} have already been shown to be in excess in the previous sections, the likely explanation for the initial lag is that H_2O_2 formation at the pyrite surface is hindered. Pyrite samples from this section were prepared in a similar manner to those used in experiments A and B – that is, they were soaked in the conditioning-solution of HCl overnight rather than for a few hours as were the pyrite samples from other experiments conducted later. Pyrite from the experiments with overnight acid washes lowered the pH to less than 3 (Table 2.1) within 15 minutes of initiation and maintained it to the end of the incubations, which was faster than other experiments that initially only decreased the pH to about 3.4 (also with a loading of 100 g L^{-1}), then slowly decreased the pH by the end of the incubation. The additional time spent in strong acid likely caused a greater amount of the surface Fe(III)-oxide patches to reduce (which as mentioned in the previous section has been hypothesized to contribute to optimal electron-cycling at the surface required to form H_2O_2) and thus the lag was time it took to oxidize the surface again. This notion is consistent with the explanation of the results from the previous section, where the degradation of Phe in the pH-adjusted pyrite slurry was slower than in the pH-unadjusted slurry over the short timescale of the experiment.

Beyond the initial increase in rates of Phe degradation, the ·OH flux in the system does not change very dramatically for several hours ($\mathbf{t_i}$ = 4 – 12 hours). Rates of Phe loss stabilize around 4.7 μM hr^{-1}, or 94% loss, over the 2-hour Phe incubation. This plateau where the change in [·OH] through time is zero represents steady-state for ·OH production that was assumed for the all experiments in the simplified model derived in Chapter 2.

As the pyrite aged beyond 12 hours ($\mathbf{t_i}$ > 12 hours), the rate of Phe loss decreased slowly over the remaining 2 days from 4.7 μM hr^{-1} to 1.6 μM hr^{-1} at an average of 0.05 μM hr^{-2}. The rates, however, appear to begin leveling-off as $\mathbf{t_i}$ reached 74 hours (illustrated with linear fits of changes in rate through time in Figure 3.9). It has been shown in prior experiments from this work (Chapter 2, experiment F) and others (Cohn et al. 2010) that ·OH-specific degradation of target compounds (Phe and adenine, respectively), even at relatively low pyrite loadings (10 g L^{-1}), continues for a much longer incubation time (240 hours and 21 days, respectively). This suggests that the rates determined beyond $\mathbf{t_i}$ = 74 hours would have likely continue to stabilize, perhaps reaching a steady-state of ·OH production around 1 to 1.6 μM hr^{-1} (based on the trend of decreasing slopes (Figure 3.9)).

One explanation for the diminished Phe degradation rates at $\mathbf{t_i}$ > 12 hours in this experiment is that the smaller reaction vessels may have caused the slurries of later time points to become anoxic, effectively halting the oxidation of the pyrite surface and the formation of H_2O_2. Recent work by Schoonen et al (2010) sought to quantify oxygen uptake in pyrite slurries and found that about 1 μM min^{-1} was removed from a system of comparable loading and headspace (which in this experiment was only 0.5 mL). Low dissolved oxygen would theoretically lead to the observed drop-off in the rate of Phe loss as the catalytic cycle of H_2O_2 formation would only recommence following an introduction of more oxygen (via opening the vessel and addition of oxygenated solution during the Phe spike). Therefore, it may be possible that had each vessel been opened periodically (e.g., for removal of aliquots (similar to how the other experiments were conducted in this study)), the maximum rates in Phe degradation that was reached by $\mathbf{t_i}$ = 2.5 hours (Figure 3.9) may have continued at that rate rather than fall – exemplifying the steady-state production of ·OH assumed in Chapter 2 for the model. Further investigation into this would be required to prove this assumption.

3.4 Summary

Several major pyrite-induced components related to the formation of ·OH in slurries (Fe^{2+}, H_2O_2, pH, and duration pyrite is in solution (pyrite age)) were examined to determine their contributions to the kinetics Phe hydroxylation. Results from Phe degradation experiments with Fenton reagents conducted without pyrite provided evidence that ·OH reactions occurring in the solution phase are similar in several respects to those in pyrite slurries. Results supporting this assertion include the low adsorption of the polar Phe (Chapter 2), comparable levels of ΣTyr as a function of $[Phe]_o$, and similar ratios of Tyr isomers relative to [ΣTyr] solutions of Fenton reagents, which were in agreement with those observed in pyrite slurries. Variations in $[Fe^{2+}]$ added to solution had little effect on the loss of Phe following the 1-hour incubations, and degradation was only slightly greater with lower pH. The greatest effect on Phe loss came with variable H_2O_2, where the differences in [Phe] remaining after the 1-hour incubations were significant as $[H_2O_2]_o$ increased.

Reactions of Phe in pyrite slurries of 50 g L^{-1} with additional Fe^{2+} and H_2O_2 revealed that iron-dissolution from the pyrite surface (upon introduction to water) is at sufficient levels for the Fenton reaction to form ·OH from any available H_2O_2 generated by the pyrite. Degradation of Phe proceeded rapidly with increased levels of H_2O_2 in the slurry, making H_2O_2 the limiting reagent in the reaction mixture. These two observations are in agreement with the flux of H_2O_2 from the pyrite surface representing the rate-limiting step in ·OH production as assumed in Chapter 2. Altering the pH with sulfuric acid prior to incubation slowed the generation of H_2O_2 at the surface of pyrite, which may be due to the resulting differences in the fraction of Fe(III) on the surface, and in turn produced less ·OH to react with Phe.

Examples from other studies have measured optimal ratios of Fenton reagents to be 5:1 [H_2O_2]-to-[Fe^{2+}] for the degradation of an aromatic organic dye at pH 3 (Chen et al. 2009) and 6.8:1 [H_2O_2]-to-[Fe^{2+}] for the degradation of salicylic acid at pH 4 (Chang et al. 2008). The catalytic nature of iron in acidic solutions allows for these ratios to be greater than 1. Although these two compounds also have similar second-order rate constants to Phe, solution chemistry differed from this experiment slightly. For example, in the Chen et al (2009) study, high levels of chloride ions were measured, which can compete for ·OH at rates comparable to those of aromatic compounds (4.3×10^9 M^{-1} s^{-1}) (Grigorev et al. 1987), and therefore increase the amount of H_2O_2 required to degrade the same quantity of the dye in solutions without chloride. On the other hand, in pyrite slurries, [Fe^{2+}] is in great excess compared to the apparent flux of H_2O_2 with an estimated ratio of about 0.1:1 (as per other studies where the [Fe^{2+}] that initially dissolves from the pyrite surface is roughly 1.6 μmol g^{-1} (extrapolated from Cohn et al (2006)) in solution, along with initial [H_2O_2] formed in the presence of EDTA was 0.16 μmol g^{-1}-pyrite). However, the addition of 500 μM H_2O_2 to 50 g L^{-1} pyrite theoretically increased the ratio to 6.4:1, which is comparable to the studies mentioned for optimal degradation of similar organic compounds where over 95%-loss was observed in the Fenton solution alone. This estimate of H_2O_2 and Fe^{2+} (via pyrite) ratios could be used as a foundation for the use of pyrite in environmental engineering of remediation techniques (discussed later in the section).

Results of the pyrite aging and the pH-adjusted pyrite experiments showed that the condition of the pyrite surface and the pH of the solution prior to pyrite addition can affect the initial ·OH formation rate. As mentioned, a pyrite surface devoid of Fe(III) patches may not

afford the ideal conditions to induce electron transfer along the pyrite surface to reduce dissolved oxygen ultimately to H_2O_2. Similarly, a low initial pH (less than 3) has been shown here to decrease the degradation, which is hypothesized to be due to reduced formation of H_2O_2 in pyrite slurries.

The chemical and physiological environments where pyrite-mediated reactions occur can be highly variable. Pyrite-induced ·OH formation can to occur over the wide pH-range of these systems, and the range of dissolved iron levels in the matrices is vast. Although iron levels generated by pyrite alone in solutions have been shown to be sufficient to facilitate the Fenton reaction, results from this chapter strongly suggest that the rate of H_2O_2 generation at the surface is the limiting factor and subject to conditions such as pH and Fe(II) / Fe(III) ratios. Furthermore, the reduction of H_2O_2 to ·OH via the Fenton reaction is affected by pH in solution with respect to Fe^{2+} / Fe^{3+} ratios (but not the direct conversion of H_2O_2 to ·OH) (Equation 3.3), which decreases at higher pH.

The human health implications determined by other studies with minerals containing pyrite (mainly coal) (Cohn et al. 2006a; Harrison et al. 1993; Huang and Finkelman 2008; Swaen et al. 1995) can also be considered an exposure risk to pyrite. Some potential examples of the impact on human health from pyrite-induced ·OH and variations in conditions are analogous to a studies showing elevated risks of gastric and lung cancers in coal-miners (Harrison et al. 1993). The low pH of the stomach, which with a pH that can range from around 2 to 3 (Freire et al. 2011), could initially suppress H_2O_2 formation at the surface of ingested pyrite (similar to what was observed in this chapter). Then, as the pyrite passes through the intestines, the pH increases, interacts with cellular fluids in the villi linings, and could promote an increase in H_2O_2 and ·OH production.

Phagocytes present in lung tissue not only decrease the pH in the immediate area of foreign particles to as low as 4.6 (Nyberg et al. 1992), they inundate the particles (such as pyrite) with H_2O_2, which is similar to experiment in Section 3.3.2 where large quantities of ·OH are produced by association with the reduced iron supplied by the pyrite. This essentially allows pyrite to form ·OH without the need for producing H_2O_2. Similarly, there is also potential for physiological interactions with pyrite and enhancement of ·OH-formation from the treatment of a dirty flesh wound with H_2O_2 (generally a 3% dilution is used as a disinfectant), which could

form ·OH in the immediate area and cause cell damage should the dirt contain various forms of iron minerals. This is supported by a recent study that found some samples of mineral clays, which are known to kill flesh-eating bacteria when used to coat the infected dermal tissue over an extended period, contain up to 8% pyrite – leading to the theory that the bactericidal properties may be the in-part due to pyrite-induced ·OH formation (Williams et al. 2011).

In ecological systems, one example of direct-exposure to pyrite are waters contaminated by the spoils of coal mining which typically contains some amount of pyrite (Moncur et al. 2009). Runoff of very acidic water in the vicinity of mines have been well studied (Moncur et al. 2009), and can potentially containing high dissolved-iron content (mostly as Fe^{2+}) as polluted water travels downstream and slowly reaches a higher pH as it becomes diluted and dispersed. These conditions may be very conducive to the generation of H_2O_2 and ·OH; however, other water-quality parameters (e.g., salt content and buffering capacities), would likely affect production and fate of ROS in natural waters.

Besides some of the deleterious effects of ROS generation, environmental engineers have been looking to redox and Fenton chemistry as an efficient alternative and/or supplement to biological treatment methods in wastewater treatment facilities (Deegan et al. 2011) and other contamination sources such as landfill leachate (Umar et al. 2010). Recently, pyrite has been assessed (in the laboratory setting) for its usefulness in the removal of a known wastewater and environmental contaminants, such as TCE (Pham et al. 2009) and trinitrotoluene (Matta et al. 2007). Understanding the factors that affect the ability of pyrite to continuously generate ·OH is the first step towards industrial use of the mineral as a remediation tool. Speciation of iron, solution pH, addition of H_2O_2, and the duration of time the pyrite is suspended have all been shown in this chapter to affect the ·OH flux. The pretreatment of pyrite has also been shown to be a factor, which with more research, could assist in the practical application of pyrite use in wastewater systems (e.g., development of a cycling schedule for the conditioning of "used" pyrite and how long to "recondition" in HCl for reuse).

The more that is known about how external variables affect the formation of ·OH in a pyrite slurry, the more complex the simulation in Chapter 2 can become to better predict the reactants (e.g., Phe) and subsequent products (e.g., Tyr, dihydroxyphenylalanine, etc.) through time, even in multiple-component systems. Concentration and speciation of iron or influences of

other dissolved constituents that affect parameters such as pH and ionic strength can vary drastically in the environment depending on conditions (i.e., oxic or anoxic, seawater or fresh water, groundwater or surface water, etc). Moreover, the presence of any-number of organic and inorganic compounds can compete with Phe for ·OH produced in pyrite systems to various degrees. Some of these basic conditions act as potential competitors and are examined in Chapter 4, where the degradation of Phe in observed in pyrite slurries containing simulated biological and environmental media.

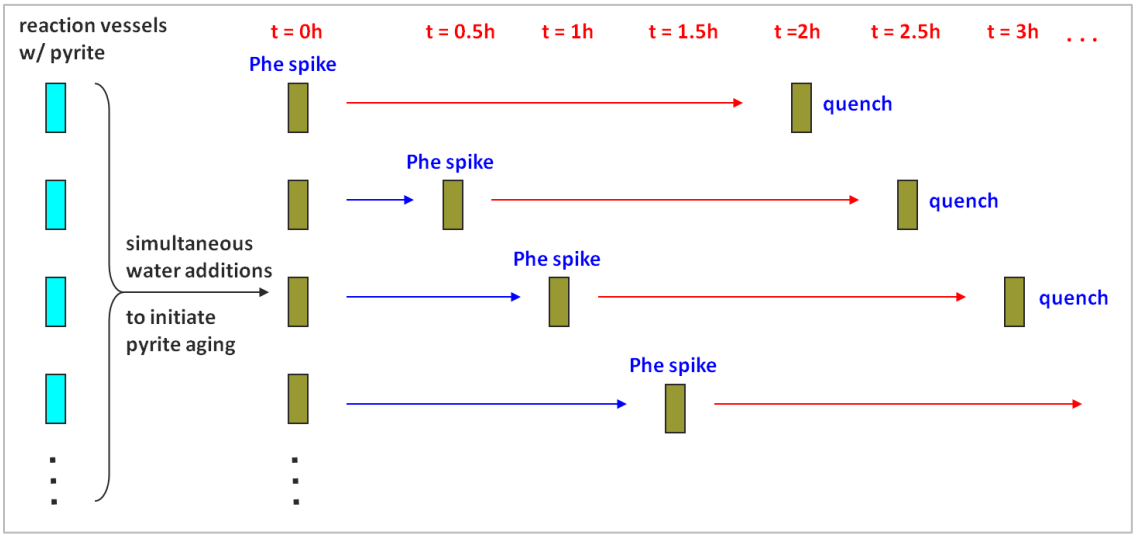

Figure 3.1. Pyrite aging experimental design. Individual vials of pyrite slurries were incubated without Phe for various lengths of time ($\mathbf{t_i}$), then spiked with Phe and allowed to incubate 2 additional hours before being quenched and filtered for analysis.

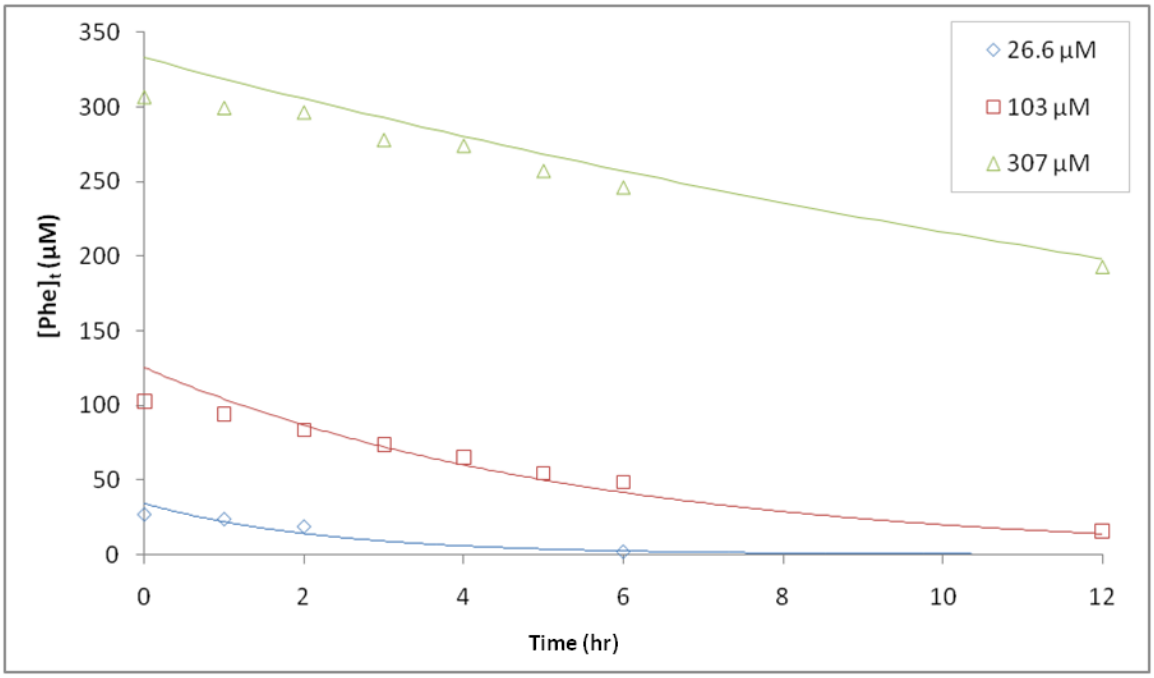

Figure 3.2. Phe degradation over the first 12 hours of Experiment A. Data points fitted with exponential curves for the three incubations of Phe (26.6 µM, 103 µM, and 307 µM) Experiment A. The modeled first-order curves are identical to those in Figure 2.2; though for clarity, the $[Phe]_t$ is not normalized to $[Phe]_o$ and the plot is zoomed to focus on the first 12 hours of the incubations. Note the apparent change after the first 2 hours where kinetics better fit the first-order model. These results prompted the pyrite aging experiment.

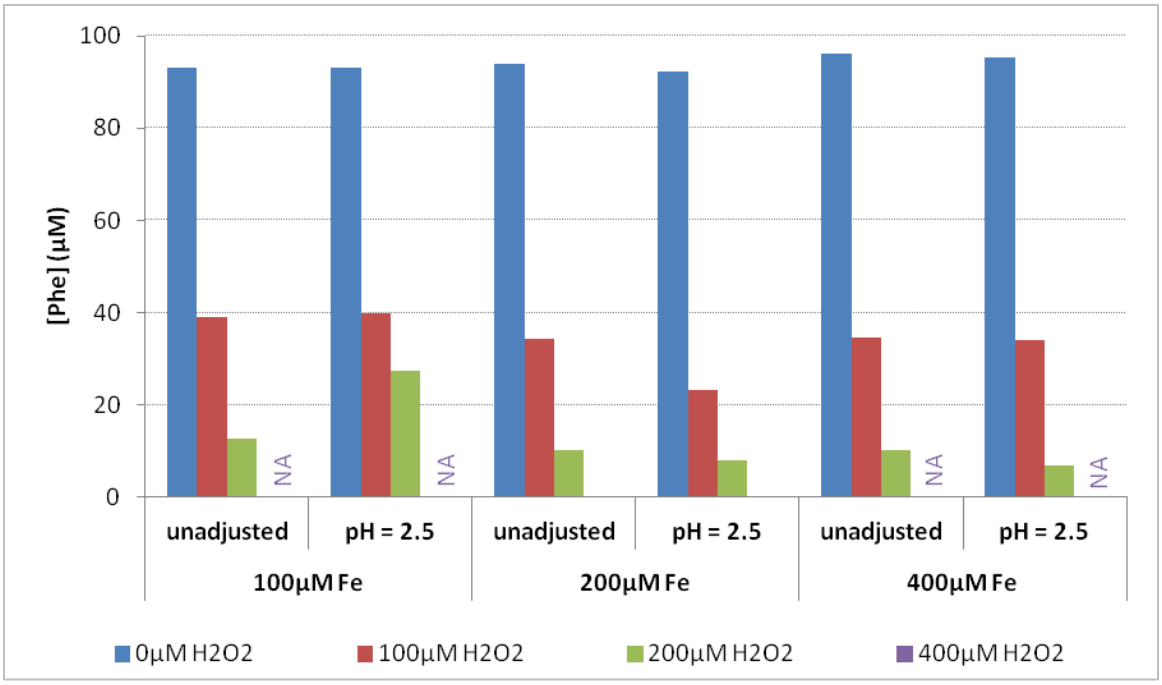

Figure 3.3. Solution-based degradation of Phe in variable concentrations of Fenton reagents. Levels of Phe following reactions with H_2O_2 are compared across different [Fe^{2+}] (added as Mohr's salt). The pH was also adjusted to 2.5 or left unadjusted. Differences in degradation of Phe over the 1-hour incubations are most notable when comparing the H_2O_2 levels. Control samples were also incubated for 1 hour with respective Fe^{2+} levels and pH adjustments, but without H_2O_2, and served as the $[Phe]_o$ for mass-balance calculations in this experiment. NA represents "not applicable" for incubations of 400 µM H_2O_2 in 100 µM and 400 µM Fe^{2+} since 400 µM H_2O_2 was only reacted with 200 µM Fe^{2+} samples, where values of remaining Phe were 0 µM and 0.33 µM in pH-unadjusted and pH 2.5 solutions, respectively.

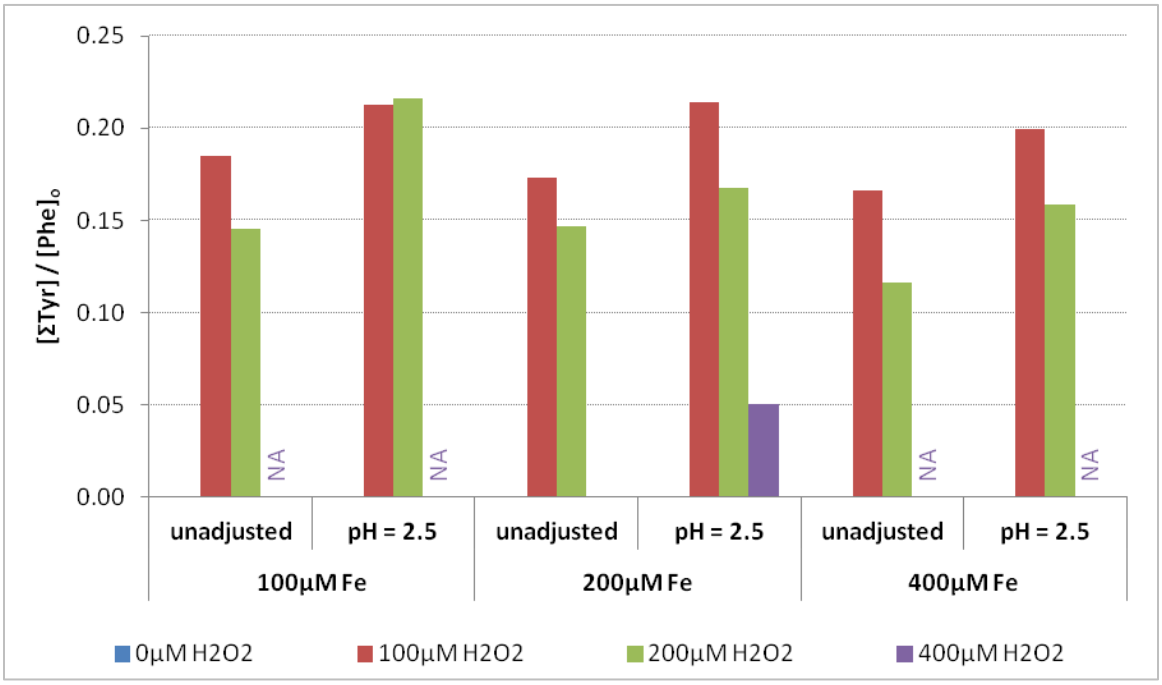

Figure 3.4. Concentrations of remaining total-Tyr relative to the initial Phe in solution-based Phe degradation. The [ΣTyr] remaining after Phe has reacted in various incubations of Fenton reagents is similar to those observed in pyrite slurries at times corresponding to 1 – 3 half-lives. Results also show little influence on ratios from changing [Fe^{2+}], and significant influence from different [H_2O_2] resulting from extent of Phe loss and number of other degradation products competing for $^{\cdot}OH$. The pH-adjusted samples had more Tyr remaining compared to the unadjusted incubations, despite slightly greater Phe loss, perhaps a result of differential product formation at different pHs. NA represents "not applicable" for incubations of 400 µM H_2O_2 in 100 µM and 400 µM Fe^{2+} since 400 µM H_2O_2 was only reacted with 200 µM Fe^{2+} samples.

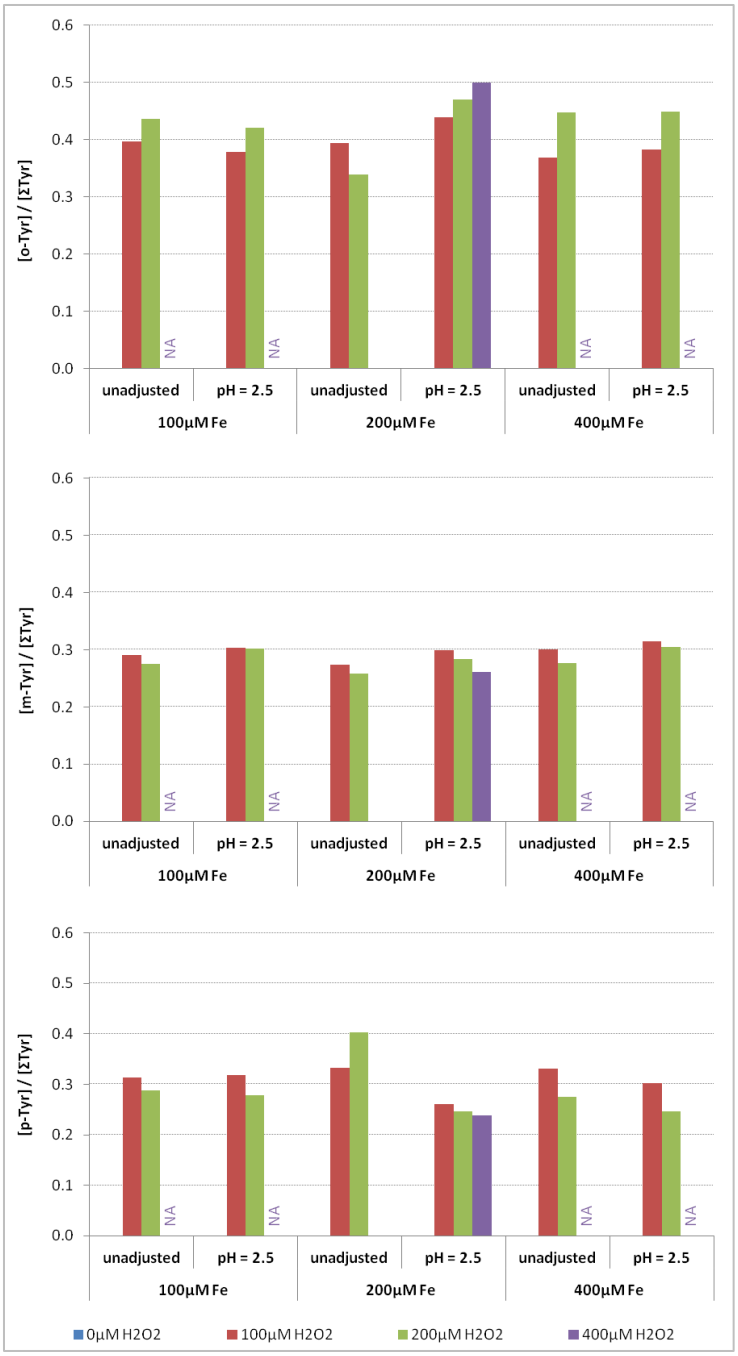

Figure 3.5. Isomer ratios of Tyr relative to total-Tyr in solution-based Phe degradation. Comparisons of *o*-, *m*-, and *p*-Tyr reveal only minor variations among the different treatments; most notably *o*-Tyr appears slightly favored as [H_2O_2] increases. This is likely due to it lower second-order reactivity compared to *m*- and *p*-Tyr. The effect of pH and Fe^{2+} does appear to be significant. NA represents "not applicable" for incubations of 400 µM H_2O_2 in 100 µM and 400 µM Fe^{2+} since 400 µM H_2O_2 was only reacted with 200 µM Fe^{2+} samples.

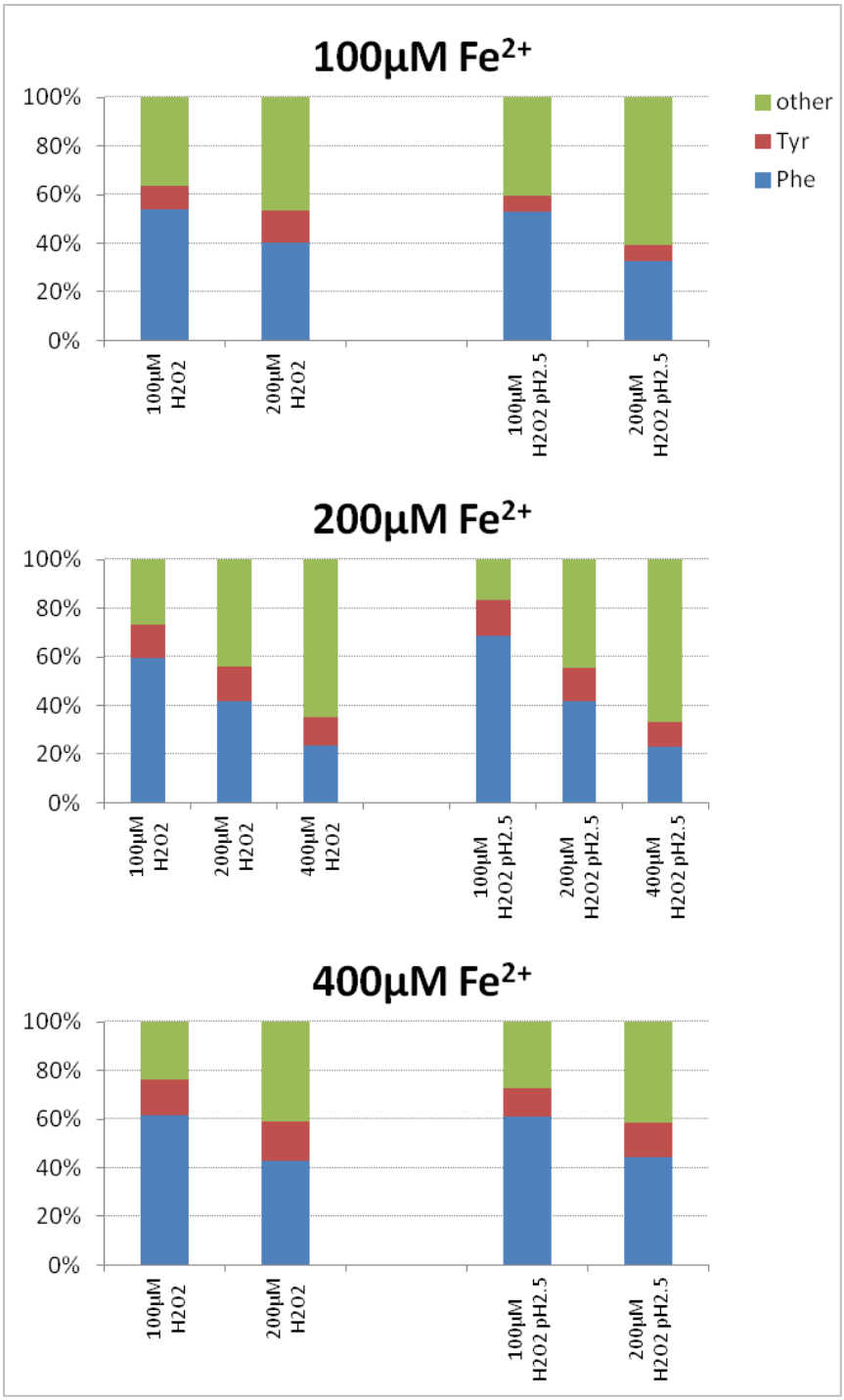

Figure 3.6. Percentage of Phe, Tyr, and "other" Phe-degradation products lost relative to total H_2O_2 spiked assuming 50% (α = 0.5) Phe-to-Tyr conversion. Loss of Phe makes up a lower percentage of total H_2O_2 as [H_2O_2] increases; however, Tyr loss appears to be more consistent with 9.8 – 16% of the reacted H_2O_2 regardless of [Fe^{2+}].

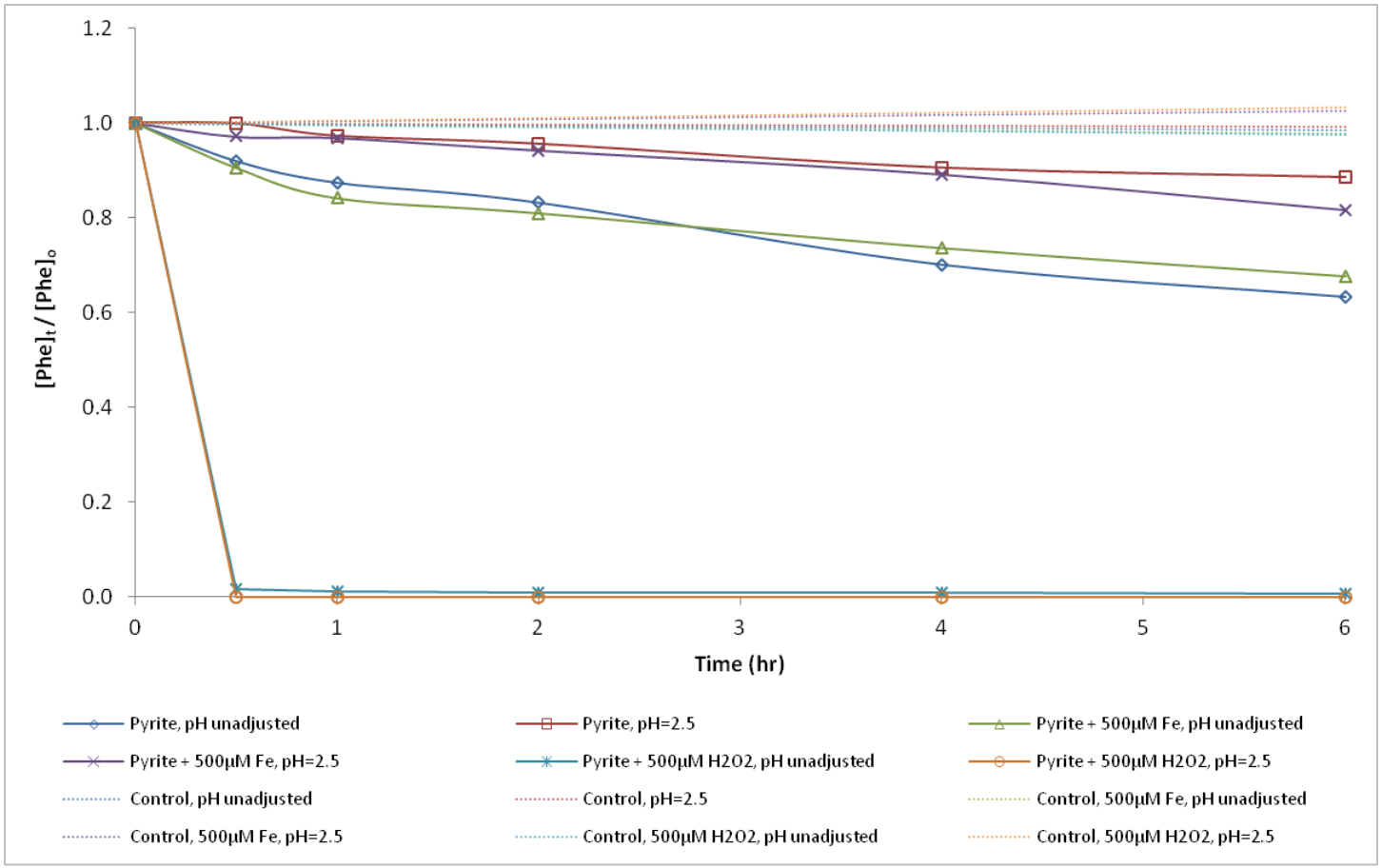

Figure 3.7. Incubations of Phe in pyrite slurries with added Fe^{2+} and H_2O_2. Degradation of 100 µM Phe was monitored over 6 hours in slurries with and without adjusted pH. Also, 500 µM Fe^{2+} or 500 µM H_2O_2 was added to similar incubations to determine the extent of influence of each component on Phe degradation is shown. H_2O_2 clearly had the greatest effect on the rate of Phe loss. Decrease in initial pH to 2.5 had an adverse affect on the rate of Phe loss, suggesting the surface related decrease in H_2O_2 formation. Controls were also incubated without pyrite, analyzed at **t** = 0 hr and **t** = 6 hr. No loss of Phe or formation of Tyr was observed in controls.

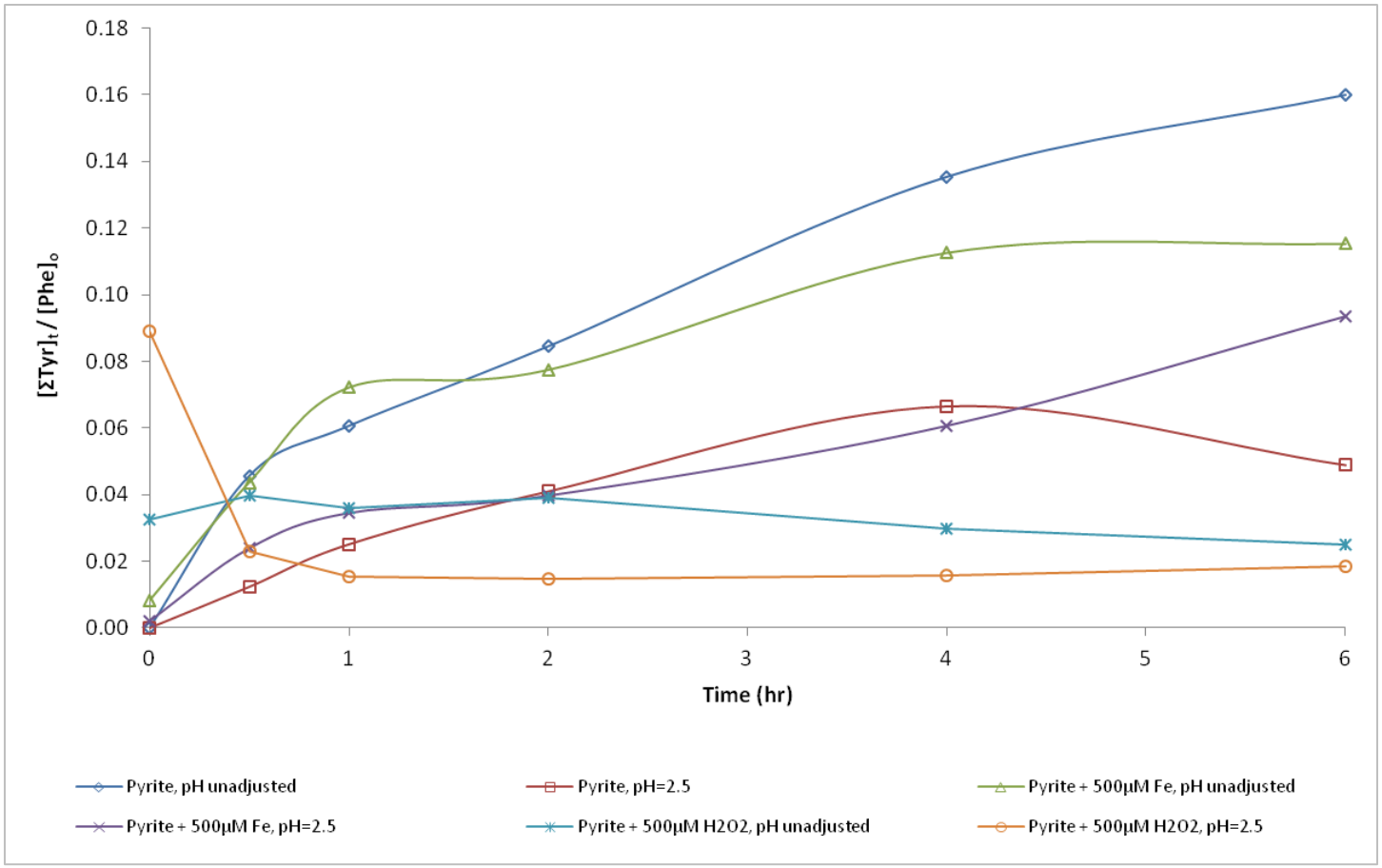

Figure 3.8. Total-Tyr formation through time in incubations of altered pyrite slurries. Ratios of $[\Sigma Tyr] / [Phe]_o$ for incubations of 100 µM Phe in 50 g L^{-1} pyrite with and without the addition of 500 µM Mohr's salt (Fe^{2+}), 500 µM H_2O_2, and sulfuric acid to a pH of 2.5. Tyr ratios in slurries of pyrite-only and additional Fe^{2+} were comparable to those in experiments shown in Chapter 2. Incubations with additional H_2O_2 had little Tyr remaining as most had degraded following near-complete loss of Phe by the first time point (**t** = 0.5 hr).

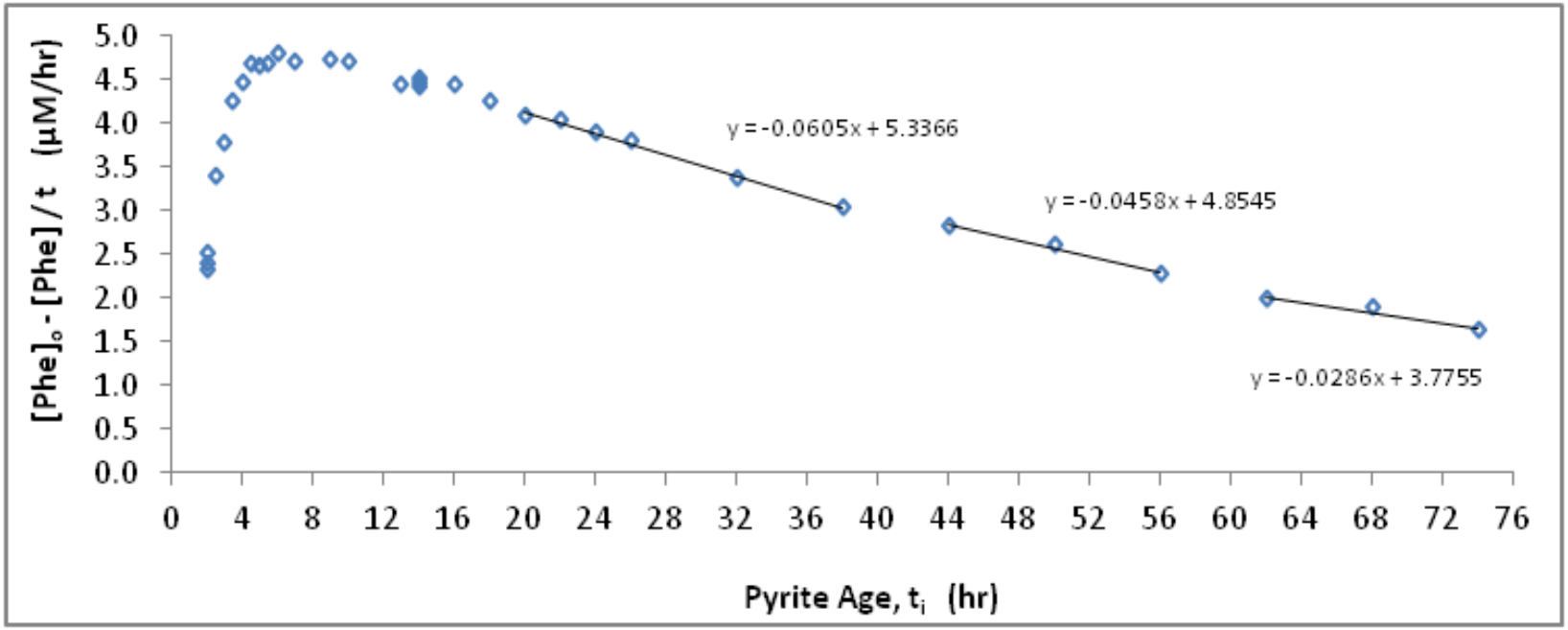

Figure 3.9. Pyrite incubation aging experiment – Phe degradation rates. Incubations of 10 µM Phe were spiked into individual 100 g L^{-1} pyrite slurries at the time points shown above. Data points represent change in Phe (relative to an $[Phe]_o$ = 10 µM) over the 2-hour incubation following Phe spike (note **t** is a constant for each time point (**t** = 2 hours)). Pyrite age ($\mathbf{t_i}$) represents the duration of time the pyrite has been in water. Plotting the data reveals an apparent lag in ·OH formation, followed by a plateau of rates at around 4.7 µM hr^{-1}, then a decrease that appears to stabilize (denoted by shallower slopes) for the remainder of the 74-hour experiment.

		[H_2O_2] associated with the degradation of each compound assuming:								
		Case 1: 100% Phe to Tyr			Case 2: 50% Phe to Tyr			Case 3: Tyr formed does not react		
		Phe	ΣTyr	other	Phe	ΣTyr	other	Phe	ΣTyr	other
100µM Fe^{2+}	100µM H_2O_2	54.0	36.8	9.2	54.0	9.8	36.2	54.0	0.0	46.0
	200µM H_2O_2	80.4	66.9	52.7	80.4	26.7	92.9	80.4	0.0	119.6
	100µM H_2O_2 pH2.5	53.0	33.2	13.8	53.0	6.7	40.3	53.0	0.0	47.0
	200µM H_2O_2 pH2.5	65.5	45.5	89.0	65.5	12.7	121.8	65.5	0.0	134.5
200µM Fe^{2+}	100µM H_2O_2	59.6	43.4	-3.0	59.6	13.5	26.8	59.6	0.0	40.4
	200µM H_2O_2	83.7	69.9	46.4	83.7	28.0	88.3	83.7	0.0	116.3
	400µM H_2O_2	93.9	93.9	212.1	93.9	47.0	259.1	93.9	0.0	306.1
	100µM H_2O_2 pH2.5	68.8	49.1	-17.9	68.8	14.7	16.5	68.8	0.0	31.2
	200µM H_2O_2 pH2.5	84.0	68.6	47.4	84.0	26.5	89.4	84.0	0.0	116.0
	400µM H_2O_2 pH2.5	91.8	87.2	221.0	91.8	41.2	266.9	91.8	0.0	308.2
400µM Fe^{2+}	100µM H_2O_2	61.6	45.6	-7.2	61.6	14.8	23.6	61.6	0.0	38.4
	200µM H_2O_2	86.0	74.8	39.2	86.0	31.8	82.2	86.0	0.0	114.0
	100µM H_2O_2 pH2.5	61.2	42.2	-3.5	61.2	11.6	27.1	61.2	0.0	38.8
	200µM H_2O_2 pH2.5	88.2	73.1	38.7	88.2	29.0	82.8	88.2	0.0	111.8

Table 3.1. Hypothetical relative amounts of ·OH (as initial H_2O_2) that reacted with Phe, Tyr, and other reactants. Values represent the theoretical portion of $[H_2O_2]_o$ that reduced to ·OH and reacted with each compound (assuming total H_2O_2 to ·OH conversion) in three different scenarios. Loss of Phe is actual values since the controls (variable Fe^{2+}, 0 µM H_2O_2) showed no decrease over time compared to the incubation without Fe^{2+} or H_2O_2. Mass-balance calculations were based on equations listed in Section 3.3.1.1.2. Of the three assumptions, only the Case 2 (illustrated in Figure 3.6 as ratios) compares well to predictions of fate of ·OH based on the simulation used (Chapter 2) to describe results in the presence of pyrite.

Pyrite Age	Remaining Phe	Rate of Phe loss
t_i	$[Phe]_2$	$\frac{10\ \mu M - [Phe]_2}{2\ hr}$
(hr)	(μM)	($\mu M\ hr^{-1}$)
2.0	5.22	2.39
2.0	4.98	2.51
2.0	5.35	2.33
2.5	3.24	3.38
3.0	2.46	3.77
3.5	1.52	4.24
4.0	1.08	4.46
4.5	0.65	4.68
5.0	0.69	4.66
5.5	0.64	4.68
6.0	0.41	4.79
7.0	0.59	4.71
9.0	0.57	4.71
10	0.59	4.71
13	1.12	4.44
14	1.06	4.47
14	0.98	4.51
14	1.20	4.40
16	1.13	4.43
18	1.51	4.24
20	1.83	4.09
22	1.93	4.04
24	2.24	3.88
26	2.40	3.80
32	3.25	3.37
38	3.92	3.04
44	4.38	2.81
50	4.78	2.61
56	5.48	2.26
62	6.04	1.98
68	6.24	1.88
74	6.73	1.64

Table 3.2. Data points for pyrite aging experiment. Results corresponding to Figure 3.9, tabulated for reference.

Chapter 4

PYRITE-INDUCED DEGRADATION OF PHENYLALANINE IN THE PRESENCE OF SIMULATED BIOLOGICAL AND ENVIRONMENTAL MEDIA

4.1 Introduction

Research involving pyrite-induced hydroxyl radical (·OH) formation and subsequent reactivity has mainly been limited to the use of molecular probes such as adenine (Cohn et al. 2010) and phenylalanine (Phe) in systems of pure water with little or no competition (Chapter 2; (Cohn et al. 2010; Pham et al. 2008). However, the adverse effects attributed to pyrite reactivity in oxygenated waters occur in the presence of environmental and biological compounds that can affect the rate of reactive oxygen species (ROS) production and compete for ·OH. As shown in previous chapters, rates of pyrite-induced ROS formation and reactivity are influenced by many factors, such as pyrite surface oxidation (Chapter 2) and pyrite aging in solution (Chapter 3). Experiments in this chapter expose pyrite to abiotic simulated fluids as a proxy for natural matrices that may enhance or interfere with the formation of ·OH in solution influenced by dissolution and redox chemistry.

There are many studies that focus on the affects of ROS-activity in cells conducted under physiological conditions of the lungs (Dalal et al. 1995; Houghton et al. 2008; Valavanidis et al. 2009; van Maanen et al. 1999). Exposure to foreign particles such as soot, coal and pyrite dust (from mining operations, for example) via inhalation can impair respiratory function (e.g., irritated lungs and trouble breathing (Dalal et al. 1995; Valavanidis et al. 2009)) and lead to

adverse physiological or biochemical effects (e.g., tissue and DNA damage (Houghton et al. 2008)) as micron-sized particles become lodged in the alveoli of the lungs (Huang and Finkelman 2008). To better understand the potential for pyrite reactivity (with respect to hydrogen peroxide (H_2O_2) and $^{\cdot}OH$ formation) at the alveolar interface, the effect of solution matrix and its components should be studied.

Simulated lung fluid (SLF) is a mixture of several basic inorganic salts and small organic compounds (Eastes et al. 1995) to which pyrite and probes for $^{\cdot}OH$ can be added for *in vitro* experiments. One simple recipe for SLF was chosen as a starting point to test the effectiveness of Phe as a probe for $^{\cdot}OH$ in complex mixtures. These mixtures are buffered at biologically-relevant pH – higher than those previous characterized in experiments from this study. A recent study with the $^{\cdot}OH$-specific probe 3´-(*p*-aminophenyl) fluorescein (APF) and pyrite has shown that $^{\cdot}OH$ can form in pyrite slurries containing SLF, but to a lesser extent than in solutions of pure water (Harrington et al. 2011).

The redox reactions in pyrite that lead to the eventual formation of $^{\cdot}OH$ (Schoonen et al. 2010) are expected to be dependent on iron speciation (both in solution for the Fenton reaction and on the pyrite surface), which in-turn is dependent on the pH of the solution and its composition. As seen in Chapter 3, the surface of pyrite can be sensitive to initial pH, which directly affected the H_2O_2 formation, and although SLF has a pH of 7.4 (much higher than in experiments from the previous chapters) and iron speciation is expected to favor Fe^{3+}, the dissolution of pyrite would supply a continuous source of dissolved ferrous iron (Fe^{2+}) (over the course of the experiments). Furthermore, the Fenton reaction has been shown to occur over a much wider pH-range (2 – 7) in water with low levels of electrolytes (Chang et al. 2008; Jung et al. 2009). However, the addition of components such as buffers of carbonate and phosphate, as well as citrate, present in SLF and many other natural systems have been shown to form ligands or chelate iron which can limit or prevent the reduction of H_2O_2 to $^{\cdot}OH$ (King and Farlow 2000; Yoshimura et al. 1992).

Citrate is normally present in human cells at levels between 100 and 400 μM (Konigsberger et al. 2000) and is an effective chelator of Fe^{2+} at circum-neutral pHs (Graham et al. 1998), which prevents it from precipitating as iron oxide in biological fluids. Modeled predictions of Fe^{2+} speciation in SLF suggest Fe^{2+}-citrate complexes are dominant (Harrington et

al. 2011). The formal charge of citrate is pH-dependent (i.e., less protonated at higher pH and vice versa), which allows it to form complexes with both Fe^{2+} and Fe^{3+} in solution (Hamm et al. 1954; Konigsberger et al. 2000). However, complexation of ferrous iron by citrate and other ions may also prevent Fe^{2+} from participating in the Fenton reaction. In fact, the iron chelator ethylenediaminetetraacetic acid (EDTA) is used to intentionally prevent the Fenton reaction from reducing H_2O_2 in order to measure H_2O_2 in slurries of pyrite via the leuco crystal violet (LCV) method (Cohn et al. 2005).

Phosphate can also be a significant component of biological fluids that can affect iron chemistry through buffering the pH and complexation. The [Fe^{2+}] decreases significantly as the pH increases in solutions with phosphate added as a buffer due to oxidation to Fe^{3+}. Iron-phosphate complexes have been calculated to account for 12% of the total Fe^{2+} in based on the component concentrations of SLF (Harrington et al. 2011). Adsorption of phosphate ions to the pyrite surface in anoxic or oxic slurries has been shown to affect the oxidation potential of the pyrite surface (Bebie and Schoonen 1999; Elsetinow et al. 2001), and may interfere with the formation or flux of H_2O_2. One study found that RNA is particularly vulnerable to degradation in the presence of pyrite (Cohn et al. 2004), perhaps due to a strong attraction of the phosphate backbone to the pyrite surface.

Perhaps the most complicating component of SLF is carbonate, as it has the potential to buffer the pH, complex iron, and compete for $^{\cdot}OH$ at significant rates. Dissolved Fe^{2+} in solutions of carbonate ions forms iron-carbonate complexes that readily undergo redox reactions with H_2O_2 at reaction rates greater than the Fenton reaction, but do not yield $^{\cdot}OH$ (King and Farlow 2000). Carbonate-containing solutions have also been shown to oxidize iron on the pyrite surface (Evangelou et al. 1998), though it is not known if iron carbonates at the surface can affect the formation and fate of H_2O_2 and $^{\cdot}OH$ in a similar way as with iron(III) oxides patches (Schoonen et al. 2010). Further complicating the interpretations related to formation and fate of $^{\cdot}OH$ in pyrite slurries with complex ions is that bicarbonate and citrate also happen to be highly reactive with $^{\cdot}OH$ (Zepp et al. 1992), making them an active competitors for $^{\cdot}OH$.

Competition for reaction with the limited $^{\cdot}OH$ produced in pyrite slurries depends on concentration and second-order rate constant of the reactive chemical species. A good molecular probe (such as Phe) should have a high second-order rate constant for reaction with $^{\cdot}OH$ (i.e.,

$>10^9$ M^{-1} s^{-1}) to be effective at identifying sub-micromolar levels of ·OH generated by pyrite slurries in the presence of other reactive components. Since ·OH is so reactive, most components of SLF are subject to reaction to various extents (except sodium, calcium, or any other Group I and II elements of the periodic table as oxidation is not energetically favorable), and thus have the potential to decrease the rate of Phe hydroxylation relative to slurries containing only pyrite (i.e., experiments in Chapter 2). For example, SLF contains the amino acid glycine (Gly), which is present at much higher concentrations (6 mM) than levels of Phe added in this study; however, due to its molecular structure (i.e., lack of reactive moieties such as a phenyl or alcohol group), it is far less competitive then Phe for ·OH (Scholes et al. 1965).

In this chapter, differences in Phe-degradation rates are used to determine the extent of decreased ·OH formation in pyrite slurries suspended in SLF and also in simulated solutions representative of matrices present in natural waters. Simulated seawater (SSW) and solutions of Aldrich® humic acid (HA) each represent different environmental conditions where pyrite is naturally present under conditions where redox chemistry can vary. Pyrite forms under anoxic conditions in the sediment of marshes and estuaries where it occasionally becomes disturbed and exposed to oxygen in sediments or surface waters. In the marine environment where the pH is generally circum-neutral, the [Fe^{2+}] is available at nanomolar levels (Gonzalez-Davila et al. 2005) due to natural oxidation of iron resulting in the formation of less-soluble Fe^{3+} and complexation with abundant anions that leads to precipitation. In fresh water, where humic substances are abundant, the pH is typically lower (pH < 7) and has a lower buffering capacity; thus dissolved iron may be more abundant.

The dissolved organic matter that is HA or can be found in SSW is poorly characterized but known to be comprised primarily of very complex mixtures of small geopolymers containing acid functional groups that result in iron complexing characteristics. Levels of dissolved organic nitrogen (2.9 μmol kg^{-1}) and organic phosphate (0.1 μmol kg^{-1}), as well as total organic carbon (29 μmol kg^{-1}), are reported for solutions made with Instant Ocean® SSW (Atkinson and Bingman 1998). Levels of total carbon (49% by weight), hydrogen (4.7% by weight), and nitrogen (0.6% by weight) have been reported for HA by the manufacturer (Sigma Aldrich 2008a). All organic molecules have the potential to react with ·OH, and there are some reports of second-order rate constants for other model humic substances for reaction with ·OH based on

reaction with Fenton reagents (Goldstone et al. 2002; Lindsey and Tarr 2000), which can be useful when comparing reaction with Phe. The reaction of ·OH and aromatic probes was slower than in pure water when Fenton reagents were added to soil slurries and humic substances (Lindsey and Tarr 2000) – though not quenched. Aldrich HA and other HA derived from terrestrial soil can be highly aromatic and contain quinone functional groups that, along with complexed iron, are especially important in the stabilization of free radicals or transport of electrons to other compounds (Chen and Pignatello 1997; Lindsey and Tarr 2000; Petigara et al. 2002; Struyk and Sposito 2001). Quinones in particular also appear to enhance the Fenton reaction by stabilizing and transferring free electrons which can reduce Fe^{3+} in solution back to Fe^{2+} (Chen and Pignatello 1997; Struyk and Sposito 2001).

Halides such as chloride and bromide are abundant not only in seawater, but in many biological and environmental systems where pyrite may be present. Chloride and bromide are highly reactive with ·OH with reported second-order rate constants nearly as high as those for aromatic organic compounds such as Phe (Jayson et al. 1973; Zehavi and Rabani 1972). There is wide range of chloride concentrations in natural solutions that can reach the high-millimolar range, and at these levels, chloride would be expected to quench reactions of ·OH with molecular probes. However, products formed through halide reactions with ·OH have been shown to dissociate back to the original ion and ·OH rapidly at rates that are most rapid at pH > 6 (Liao et al. 2001; Zehavi and Rabani 1972).

In this chapter, experiments were devised to better understand the formation and fate of ·OH in pyrite slurries by comparing the rates of Phe degradation in controlled solutions that are basic proxies for physiological and environmental conditions. Degradation experiments are presented where Phe was added to pyrite suspended in solutions of SLF, SSW, and HA containing basic salts, complex ions, and various amounts of organic compounds to which pyrite may be exposed in the environment or in the lungs. Pyrite slurries were monitored for kinetic trends in Phe loss and formation of the three isomers of tyrosine (Tyr) (*ortho*-, *meta*-, and *para*-Tyr) for that provide additional confirmation of ·OH. Results indicate that pyrite is capable of producing ·OH available for reaction with Phe under a range of different solution conditions (i.e., high pH, high ionic strength, high organic content, etc.), but its formation and/or reactivity is highly controlled by solution chemistry.

4.2 Methods

Pyrite from Huanzala, Peru (Wards Natural Science, Rochester, NY) was ground and sieved to a range of 38 – 63 μm. Samples were treated prior to each experiment with a nitrogen-purged solution of hydrochloric acid (HCl) to remove surface oxidation and rinsed in a glove box with nitrogen-purged water as per Cohn et al. (2010). Phenylalanine, *para*-tyrosine, *ortho*-tyrosine, and beta-mercaptoethanol – all 99% ACS-grade or better – were obtained from Alfa Aesar (Ward Hill, MA). *meta*-Tyrosine was obtained from TCI America (Portland, OR). Glycine, sodium chloride, sodium citrate, sodium bicarbonate, sodium carbonate, sodium dihydrogen phosphate, ammonium chloride, and calcium chloride were all 99% ACS-grade from Sigma Aldrich® (St. Louis, MO). Formalin (37% formaldehyde and 5% methanol by volume) was obtained from Fisher Scientific (Pittsburgh, PA). Reagent grade sulfuric acid was obtained from JT Baker (Phillipsburg, NJ). Methanol was GC^2-grade from Burdick & Jackson (Morristown, NJ). Formic acid was ACS-grade from EMD Chemicals (Gibbstown, NJ). All water used for cleaning, standards, reactions, dilutions, and chromatography work was purified with a Milli-Q filtration system (Millipore Corporation, Billerica, MA) to a resistivity of 18.3 $M\Omega\ cm^{-1}$.

4.2.1 Simulated lung fluid

Three variations of the SLF recipe from Eastes et al. (1995) were prepared (Table 4.1): 1) solution complete with all components ("with organic acids and formalin"); 2) solution that contained everything but formalin ("with organic acids"); and, 3) solution that contained only inorganic components (i.e., no glycine, citrate, or formalin ("without organic acids")). A stock solution of 2 mM Phe was added directly to SLF solutions (without further dilution) in 15-mL centrifuge tubes to the desired initial Phe concentration ($[Phe]_o$). Pyrite was added at 100 $g\ L^{-1}$ to each reaction vessel to start the reaction. Samples were collected every 24 hours over 240 hours. An incubation of Phe and pyrite in pure water was also run for comparison.

Individual components that comprise the SLF were also tested in separate experiments. A stock solution of 1 mM Phe was prepared for dilution to an $[Phe]_o$ of 10 μM in matrices of pure water and 120 mM sodium chloride solution. Glycine and sodium citrate crystals were dissolved in each matrix (individually) to final concentrations of 6 mM and 200 μM (respectively). Pyrite was added at 10 $g\ L^{-1}$ to initiate the reaction and incubations were run in 15-mL disposable centrifuge tubes for 96 hours with 9 aliquots collected (except for the set of incubations in pure water). Duplicates were collected from each vial at two time points.

The effects of phosphate and carbonate buffers in pyrite slurries were evaluated as a function of pH (4, 5, 6, 7, and 8). Solutions were prepared with either sodium bicarbonate (10 mM) or sodium dihydrogen phosphate (10 mM) and adjusted with HCl or sodium hydroxide (carbonate buffer only) to the appropriate pH. All buffer solutions were then adjusted with sodium chloride for a final chloride concentration of 30 mM to rule out potential differences in variable in chloride levels on Phe degradation kinetics. The amount of sodium chloride added ranged from 80 – 1750 $\mu g\ mL^{-1}$. A stock solution of 1 mM Phe was diluted with the buffer solutions to 10 μM in 15 mL disposable centrifuge tubes. A pyrite loading of 10 $g\ L^{-1}$ was spiked to start each reaction.

Experiments with whole SLF were conducted on a different day than those with individual components; thus the pyrite samples used were treated with HCl separately. Incubation conditions, aliquot handling, and preparation for HPLC analysis were conducted as outlined in Chapter 2 Methods section.

4.2.2 Simulated environmental matrices

A stock solution of 53 parts-per-thousand (ppt) Spectrum Brands Instant Ocean® (Madison, WI) was prepared in purified water (stock pH = 8.4) and diluted to the desired concentrations. Salinities of 8, 16, and 32 ppt were created to emulate a range of estuarine conditions and were confirmed using an Atago S/Mill hand refractometer. Experiments were run with a pyrite loading of 100 $g\ L^{-1}$, and a stock solution of 1 mM Phe was diluted to an $[Phe]_o$ of around 300 μM for all incubations. An incubation of pyrite and Phe was also run with pure water at the same $[Phe]_o$ to compare differences in rates.

An 800 mg L^{-1} stock solution of the protonated form of Aldrich® HA was created with purified water and sonicated in a sonic-bath for several minutes until the solution was homogenized. Content analysis provided by the manufacturer puts the amount of organic matter within a range of molecular masses from 2,000 to 500,000 g mol^{-1} – though a majority of the compounds lie in the range of 20,000 to 50,000 g mol^{-1} (Sigma Aldrich 2010). Although the protonated form of HA was used, ICP analysis was only available for HA as the sodium salt (reported by the manufacturer to be analogous to the protonated form with respect to transition metal content) and showed that the only metals of potential interest for reactivity with ·OH were aluminum at 1.2% and iron at 0.60% by weight (Sigma Aldrich 2008b).

Dilutions of 200 mg L^{-1} and 400 mg L^{-1} HA were made in 15 mL centrifuge tubes. A stock solution of 1 mM Phe was added to each set of HA solution to make an $[Phe]_o$ of 30 μM, 100 μM, and 300 μM. Pyrite (100 g L^{-1}) was then added to initiate the reaction. A 300 μM Phe control was also run without HA.

Experiments with SSW were conducted on a different day than those with HA; thus the pyrite samples used were treated with HCl separately. For all experiments described in this section, data was collected at 24-hour intervals over 120 hours. Reactions were conducted in 50 mL disposable centrifuge tubes with volumes of at-least four times the volume of the total volume of aliquots taken as samples for time points. Incubation conditions, aliquot handling, and preparation for HPLC analysis were conducted as outlined in Chapter 2 Methods section.

4.2.3 Analyses

All experiments were analyzed using a Waters Corporation (Milford, MA) Alliance® 2695 HPLC coupled to a Waters Corporation Micromass LCT Time-of-Flight Mass Spectrometer (ToF-MS) as described in the Methods section of Chapter 2.

4.3 Results and Discussion

4.3.1 Effect of simulated lung fluid and its components on pyrite-induced hydroxyl radical formation

Simulated lung fluid was used as a proxy for alveolar fluid for testing the ability of pyrite to form ·OH via Phe hydroxylation. As described in Chapter 3, the rate of ·OH formation depends on the intrinsic properties of the pyrite surface and the solution chemistry (e.g., pH) as they directly relate to formation of H_2O_2 and modify iron speciation (both dissolved and at the surface). Components that comprise the matrix of SLF include salts (both organic and inorganic) and organic compounds, which can directly affect the pH and pyrite surface. Some of these also act as sinks for the ·OH, and the extent of competition with Phe for the limited ·OH depends on the relative second-order rate constant of each component. The experiments in this section were conducted to better understand the kinetic effects of SLF and several of its individual components on the degradation of Phe in the presence of pyrite.

4.3.1.1 Simulated lung fluids

The observed loss of 10 μM Phe in 100 g L^{-1} pyrite slurries was very slow in each of the three different formulations of SLF relative to pyrite in pure water (Figure 4.1). Reactions were fast in the absence of SLF such that no Phe or Tyr was detected by the first time point (**t** = 24 hours), which is consistent with results from Chapter 2 for low-Phe in a high-pyrite loading incubation. A linear fit of the data yields a very slow initial rate ($\boldsymbol{R_o}$) of 10.5 nM hr^{-1}, 11.5 nM hr^{-1}, and 21.4 nM hr^{-1} for reactions of Phe in pyrite in SLF with organic acids and formalin, SLF with organic acids, and SLF without organic acids (inorganic salts only) respectively (Figure 4.1). Only trace levels (at or below the 50 nM detection limit) of *o*-Tyr and *m*-Tyr were observed at several time points in SLF with and without organic acids, despite losses of 60% and 40% (respectively) of $[Phe]_o$ following 240 hours of incubation (Figure 4.1). There was no loss of Phe or Tyr formation in control samples without pyrite. These results indicate the presence of greatly reduced but still detectable levels of ·OH in the presence of SLF.

Although the effect was not as large as that seen in this study, a decrease in the amount of ·OH formed (roughly 78%) was also observed in SLF slurries containing 10 μM APF compared to pyrite suspensions in phosphate buffer (Harrington et al. 2011). The low levels of Tyr

observed suggests that in addition to reaction with ·OH, a different mechanism was also responsible for the degradation of a majority of Phe in SLF. Contributing factors to the significantly slower loss of Phe (and APF) observed in SLF slurries likely include a combination of four types of effects: 1) increased pH from addition of carbonate and phosphate buffers affect iron speciation and mineralogy at the pyrite surface; 2) complexation with dissolved iron which affects reactions with H_2O_2 and iron speciation in solution; 3) adsorption of species that affect the redox reactions at the pyrite surface that control the formation and subsequent reactions of ROS; and, 4) the ability of many of the observed components of SLF to compete with Phe for the ·OH that is formed. Therefore, separate experiments were conducted with the two organic acids (Gly and citrate), as well as with sodium chloride, sodium carbonate, and sodium phosphate to determine whether the observed effects of each component could be understood through competition reactions, or whether additional effects on pH or iron speciation are needed to describe the observations.

4.3.1.2 Simulated lung fluids components

4.3.1.2.1 Calculating competition factors

The extent to which each component competes with Phe for ·OH can be estimated based on its concentration and second-order rate constant for reaction with ·OH. Table 4.2 lists the individual components (**x**) of SLF, their concentrations, and their second-order rate constants for reaction with ·OH ($\boldsymbol{k_x}$). The simplified model developed in Chapter 2 can be used to compare observed rates of Phe loss to calculated rates in the presence of a competitor by introducing a competition factor described below.

Phe competes for ·OH not only with components of SLF, but also with a range of Phe degradation products (**i**), including Tyr (Chapter 2). Using the assumption that $\boldsymbol{k_{Phe}} = \boldsymbol{k_{Tyr}} = \boldsymbol{k_i}$ made in Chapter 2, $\boldsymbol{k_x}$ can be more directly compared to $\boldsymbol{k_{Phe}}$ (Equation 4.1).

$$f_x = \frac{k_x}{k_{Phe}} \tag{4.1}$$

Where f_x represents the relative competition rate constant of a component that is then related to it concentration in the matrix to determine a relative competition concentration ($\mathbf{K_x}$).

$$K_x = f_x [x]_o \quad (4.2)$$

Table 4.2 lists the values for f_x and $\mathbf{K_x}$ which are independent of the [Phe] and can be used with any pyrite loading or $[Phe]_o$, and in the numerical simulation developed in Chapter 2. When $\mathbf{K_x}$ is equal to $[Phe]_o$, then that component is expected to compete at a 1:1 ratio with Phe and its reaction products for ·OH. Note that in Equation 4.2, the same assumption used to set $[Phe]_o = [Phe]_t + [\Sigma Tyr]_t + \Sigma[i]_t$ was also used to account for all unknown degradation products of competitors (i.e., $[\mathbf{x}]_o$), which is reasonable considering most competitors present in solutions for this study have concentrations comparable-to or greater-than that of Phe. The $[Phe]_o$ for a given experiment will then determine the competition factor (Equation 4.3) that can be used with the simplified model described in Chapter 2 to predict the change in pseudo first-order rate constant of Phe loss (***k'***) resulting from the presence of a competing compound or element and compare it to the observed differences in ***k'*** that are measured.

$$competition\ factor = \frac{1}{1 + \frac{K_x}{[Phe]_o}} \quad (4.3)$$

As described in Chapter 2, the [Phe] through time can be modeled using a simplified consecutive competitive equation (Equation 2.11). Multiplying the competition factor by the ***k'*** observed for incubation of pyrite suspended in pure water at the same $[Phe]_o$ yields the calculated ***k'*** for reaction with the given competitor. A competition factors equal to 1 would represent no competition, while lower values equate to greater competition with Phe and its reaction products for ·OH. A calculated ***k'*** that is appreciably greater than the observed ***k'*** for reaction of Phe in a slurry with a competitor implies that other factors are affecting the competition and/or the rate of formation of available ·OH is lower.

4.3.1.2.2 Incubations of SLF components with pyrite and phenylalanine

Glycine

Degradation of 10 μM Phe in 10 g L^{-1} pyrite suspended in pure water ("Phe-only") yielded an exponential curve with a ***k'*** of 0.139 hr^{-1} (Figure 4.3A; Table 4.3). A $\mathbf{K_{pyr}}$ was calculated to be 0.134 μmol g^{-1} hr^{-1} (as defined in Chapter 2, Equation 2.10) for the samples of pyrite used in the competition experiments presented in this section.

The addition of 6 mM Gly to a pyrite slurry only slowed the rate of Phe loss by about 2-times, despite a ratio of $[Gly]_o$ to $[Phe]_o$ of 600:1. The data was still fit by an exponential regression with a ***k'*** of 0.063 hr^{-1}, and the competition factor predicted a calculated ***k'*** of 0.053 hr^{-1} (Table 4.3), indicating that the effect of Gly on the lower degradation rate of Phe was due to competition. The relatively small amount of competition was the result of the difference in second-order rate constants for reaction with ·OH, where $\boldsymbol{k_{Gly}}$ = 1.7 x 10^7 M^{-1} s^{-1} (Table 4.2; (Scholes et al. 1965)) and $\boldsymbol{k_{Phe}}$ = 6.5 x 10^9 M^{-1} s^{-1} (Buxton et al. 1988).

The three isomers of Tyr were observed in incubations of Phe with and without Gly (Figures 4.2B). As predicted, the rate of net-production of Tyr was also slowed when Gly was added. Ratios of [ΣTyr] / $[Phe]_o$ peaked at roughly 11%, similar to when the same batch of pyrite was incubated in pure water (Figure 4.2B). The Tyr-isomer ratios were also comparable and consistent with those expected with Fenton reagents in unbuffered solutions ([*o*-Tyr] > [*p*-Tyr] > [*m*-Tyr] (Chapters 2 and 3)). Therefore, the addition of Gly to pyrite slurries does not appear to impact ROS production at the surface of pyrite or in solution and competes for ·OH as predicted from its second-order rate constant.

Citrate

The rate of Phe degradation in the pyrite slurry containing sodium citrate was significantly lower than in the slurry containing Phe only, with an observed ***k'*** of 0.008 hr^{-1} (Figure 4.3A). Using a competition factor of 0.57 (6.5 μM $[Phe]_o$) resulted in calculated ***k'*** of 0.082 hr^{-1} based on a 200 μM citrate concentration and $\boldsymbol{k_{citrate}}$ of 1.5 x 10^8 M^{-1} s^{-1} (Zepp et al. 1992). This large disparity in degradation rates of Phe with and without citrate added to the pyrite slurry suggests that the role of citrate is both as a modest competitor and an iron chelator, thereby limiting the rate of the Fenton reaction by either binding some of the dissolved Fe^{2+} (which would slow the rate of H_2O_2 reduction to ·OH) or Fe^{3+} (which could limit the catalytic

cycle of conversion back to Fe^{2+}). The proposed chelation effect of citrate would be analogous to that of EDTA (which is a stronger iron chelator than citrate at the given pH) in work by Cohn et al. (2005), which was used to determine the amount of H_2O_2 formed in pyrite slurries.

Utilizing published complexation stability constants, citrate chelation was also theorized to be a major contributor to the decrease in fluorescein formation in SLF slurries with APF (Harrington et al. 2011). Although the iron concentration in unbuffered pyrite slurries was shown in Chapter 3 to be sufficiently in excess for the Fenton reaction to convert the limited H_2O_2 that is generated at the pyrite surface to $^{\cdot}OH$ (with an amount of Fe^{2+} dissolution of about 1.6 μmol g^{-1}-pyrite shown in a study using a sample of the same crushed stock of pyrite (Cohn et al. 2006c)), the addition of 200 μM of citrate appears to have chelated most of Fe^{2+} and thus slowed the rate of Fenton chemistry. Furthermore, citrate may have also interacted with the iron on the surface, affecting the formation of H_2O_2. In either case, the overall effect on the kinetics of Phe loss could be simulated by decreasing the steady-state $[^{\cdot}OH]_t$ from 1.34 μM hr^{-1} (Table 4.3) to 0.11 μM hr^{-1} (Table 4.3) in addition to a competitive effect predicted to have reduced the rate of Phe loss by approximately a factor of two. A more detailed study characterizing the concentrations and effects of dissolved iron, H_2O_2, pyrite, and citrate as a function of pH would be required to determine the full extent of the effect of citrate chelation on flux of ROS in the system.

Formation of the three isomers of Tyr confirmed hydroxylation of Phe by $^{\cdot}OH$ in the presence of citrate (Figure 4.3B). The ratio of $[\Sigma Tyr] / [Phe]_o$ for the incubation containing citrate did not reach its peak as Phe had not degraded past the half-life by 48 hours. Only a small amount (< 50 nM) of *o*-Tyr was detected in the first 24 hours, after which low levels of *m*-Tyr and *p*-Tyr were also observed as Phe continued to degrade. There was also some loss of Phe observed in the control sample that did not contain pyrite (though no Tyr formation was observed). The loss of Phe in the control sample was not factored into the calculation but doing so would have lowered the calculated ***k'*** by one-quarter. However, it is not clear how much Phe loss would have occurred if the pH of the control was as low as the pH of the pyrite slurry.

Chloride

Degradation of Phe in pyrite slurries containing 120 mM sodium chloride was slower than the pure-water incubations with Phe. The pyrite incubation containing only Phe and chloride yielded an observed $\boldsymbol{k'}$ of 0.039 hr^{-1} (Figure 4.4A; Table 4.3), which can be compared to the $\boldsymbol{k'}$ of 0.139 hr^{-1} measured without chloride added (Figure 4.2A). With such a high chloride level relative to $[Phe]_o$ and a $\boldsymbol{k_{Cl^-}}$ of 4.3 x 10^9 M^{-1} s^{-1}, the competition factor suggests that the rate should have been much lower ($\boldsymbol{k'}$ of only 1.0 x 10^{-4} hr^{-1}). The reason that chloride did not completely quench the hydroxylation of Phe is due to complex reaction paths of chloride and ·OH, which has been shown to be significantly affected by pH (Liao et al. 2001).

Studies have shown that the reaction of chloride ions with ·OH forms hypochlorous acid radical; however, this reaction is highly reversible with a rate constant ($\boldsymbol{k_{ClOH\cdot^-}}$) of 6.1 x 10^9 s^{-1} for the dissociation back to chloride and ·OH (Jayson et al. 1973).

$$Cl^- + \cdot OH \underset{k_{ClOH\cdot^-}}{\overset{k_{Cl^-}}{\rightleftharpoons}} ClOH\cdot^- \qquad (4.4)$$

Although the pH does not appear to directly affect the equilibrium in Equation 4.4, there are other reactions with hypochlorous acid radical that are dependent on the available proton concentration (Liao et al. 2001). Based on experiments using butyl chloride as an ·OH probe, Liao et al. (2001) suggest that in the presence of high chloride concentration (2.5 M) there is a 100-fold decrease in the available ·OH at pH 2 versus pH 6 due to greater loss of hypochlorous acid ion to chlorine radical through reaction with protons. Thus, chloride may be a better competitor under the low pH conditions of the experiments with sodium chloride than it would be in SLF that was buffered at pH 7.4. Interestingly, the same study (Liao et al. 2001) showed that carbonate is a better competitor than chloride for ·OH when pH increases because carbonate has a higher $\mathbf{K_x}$ than bicarbonate and carbonic acid. Based on results from that study, at the pH (7.4) and relative anion composition of SLF, carbonate would have been a better competitor for ·OH than chloride.

Additional incubations of pyrite in sodium chloride and Phe with Gly or citrate were added to observe the combined effects of competitors. Degradation of Phe in a pyrite slurry with containing both chloride and Gly (with an observed $\boldsymbol{k'}$ of 0.021 hr^{-1} ($\mathbf{t}$ = 0 – 48 hours)) (Figure 4.4A) was 67% less than in incubations with only Gly (with an observed $\boldsymbol{k'}$ of 0.063 hr^{-1}) (Figure

4.2A). This reduction was nearly the identical to the observed 72% drop in the rate of Phe loss between incubations with and without chloride and Phe only, which means the competitive effect of the two components are additive as expected. The results of the pyrite incubation of chloride containing Phe with citrate were also consistent with an additive effect of the two competitors, but interpretation was somewhat complicated by a control sample which exhibited some loss by the 96-hour time point (Figure 4.4A). Although the reason for this loss was not determined, no Tyr formation was observed in either control. Data points for the reaction in pyrite with chloride and citrate fell along the projected line for the loss of Phe in the control sample (Figure 4.4A); however, formation of *o*-Tyr at **t** = 18 hours (with *m*-Tyr and *p*-Tyr appearing at the 72-hour time point) proves some ·OH was formed and reacted with Phe.

The $[\Sigma Tyr] / [Phe]_o$ ratios observed in sodium chloride slurries (Figure 4.4B) were modestly higher than in pyrite incubations prepared with pure water for both Phe-only and Phe with Gly (Figure 4.2B), reaching maximum values of 19% and 15% (respectively) at **t** = 48 hours (Figure 4.4B). Similar to pyrite slurries with Phe with citrate (Figure 4.3B), the *m*-Tyr and *p*-Tyr formation lagged behind *o*-Tyr in the pyrite incubation of Phe with citrate prepared in sodium chloride solution. It should be noted that the potential for Phe degradation products resulting from reactions with chlorine-containing radicals were investigated, but no evidence of such products were found in the MS spectra.

Carbonate and phosphate

Addition of carbonate and phosphate buffers greatly reduced degradation of Phe and the formation of ·OH-specific isomers of Tyr could not be detected over a range of pHs tested (Figure 4.5). Even in solutions with a lower initial pH, the loss of Phe in carbonate at pH 4, 6, and 7 was limited to reactions other than hydroxylation to Tyr (Figure 4.5A). The speciation of carbonate varies between carbonic acid (more prevalent at lower pH) and bicarbonate (more abundant as pH increases). Bicarbonate has a second-order rate constant of 1.0×10^7 M^{-1} s^{-1} (Buxton et al. 1988) and had maximum potential concentration of 10 mM. The maximum competition factor was calculated to be 0.4, with a predicted ***k'*** for Phe loss of 0.06 hr^{-1} at pH 7. The effect of carbonate must have been more than competition alone as there was no measurable

Phe loss observed at pH 7, and the maximum observed rate of loss (***k'*** = 0.02 hr^{-1}) was measured at pH 4, when carbonate is no longer an effective competitor. Note that the 30 mM chloride present was not sufficiently high to be responsible for the large drop in rates of Phe loss observed in the carbonate solutions, let alone the lack of observed Tyr formation. Therefore, Phe degradation may have been hindered by carbonate limiting Fe^{2+} in a pH-dependent manner (complexation and indirect effects of pH on Fe^{2+}), affecting the Fenton reaction (especially at high pH). It is also possible that Fe^{2+} complexes formed with carbonate at higher pH that led to dissociation of H_2O_2 to products other than $^{\cdot}OH$ (King and Farlow 2000). Potentially more important, is that carbonate can oxidize iron at the pyrite surface (Evangelou et al. 1998), a process that may greatly affect both the formation and fate of H_2O_2 and is supported by a slower Phe loss at pH 4.

Complete loss of Phe was observed in phosphate-buffered slurries between pH of 5 – 8 and no loss indicated at pH 4 (Figure 4.5B); however, only *p*-Tyr was present in experiments where Phe was lost. This clearly indicates microbial contamination and growth that increased with time, consistent also with the lag in Phe loss and *p*-Tyr build-up. At pH 4, which may be less favorable for microbial communities, no Phe degradation was observed. The speciation of phosphate at pH 4 is almost entirely dihydrogen phosphate, which has a low second-order rate constant for reaction with $^{\cdot}OH$ (2.4 x 10^4 M^{-1} s^{-1} (Table 4.2); (Maruthamuthu and Neta 1978)). There would have been little competition for $^{\cdot}OH$ at the given phosphate concentration (10 mM, competition factor of 0.97), thus a halt to $^{\cdot}OH$ formation was likely the cause for lack of *o*-Tyr and *m*-Tyr formation at all pH and absence of Phe degradation observed at pH 4. The strong binding potential of phosphate with pyrite likely hindered the redox chemistry at the pyrite surface (Elsetinow et al. 2001), thus limiting the H_2O_2 formation.

4.3.2 Effect of simulated environmental matrices on pyrite-induced hydroxyl radical formation

Experiments with Instant Ocean® SSW and Aldrich® HA were conducted to determine the influence of environmental matrices on pyrite-induced $^{\cdot}OH$ by way of Phe hydroxylation. Various dilutions of SSW and loadings of HA were incubated to emulate different environmental

conditions where pyrite is found naturally. Although hindered, the degradation rates of Phe were quantifiable for comparison to reactions of pyrite suspended in pure water.

4.3.2.1 Phenylalanine loss in the presence of pyrite and simulated seawater

The degradation rates of 300 μM Phe in 100 g L^{-1} pyrite slurries containing SSW decreased as the concentration of sea salts increased from 8 ppt to 32 ppt (Figure 4.6A). Initial pH of solutions prior to addition of pyrite was 6.5, 7.8, and 8.2 for sea salt concentrations of 8, 16, and 32 ppt (respectively). Despite the high concentrations of bicarbonate (Table 4.4), the SSW had limited buffering capacity in the presence of 100 g L^{-1} pyrite as pH decreased by the end of the incubations to 4.5, 6.2, and 7.6 (respectively). The degradation rate of Phe in pyrite suspensions of pure water could be described well by a pseudo first-order rate constant (***k'***) of 0.026 hr^{-1} (Figure 4.6A). This compared to exponential fits of Phe loss in SSW where values of ***k'*** were estimated (with a y-intercept forced to $[Phe]_o$) to be 0.009 hr^{-1}, 0.006 hr^{-1}, and 0.005 hr^{-1} for solutions of 8, 16 and 32 ppt, respectively (Figure 4.6A); however the data for incubations with SSW conformed less well due to the observed lag in Phe degradation.

Lag in Phe degradation was observed over the first 24 hours in all three incubations containing SSW (Figure 4.6A). This lag in the rate was likely due to greater iron oxidation resulting in slower H_2O_2 formation at the surface and/or less Fenton reactivity in solution. The lag in Phe degradation was similar to, but more pronounced than, the lags observed in some incubations from experiments A and B of Chapter 2 and the follow-up pyrite aging experiment in Chapter 3 (attributed to low initial pH and/or extensive HCl pretreatment), though in this case it is likely the pyrite surface is more affected by the buffering salts and high pH. By the 48-hour time point, the data fit the more typical exponential curve observed in experiments with pyrite suspended in pure water as the pH decreased to their final values.

The components of the salt mixture, along with their abundance at each dilution and published second-order rate constants for reaction with ·OH are outlined in Table 4.4. Note that only species with favorable reactivity with ·OH have been listed (i.e., Group I and II elements are not listed). Some transition metals that are present at lower concentrations (Table 4.4) may be at higher concentrations in the SSW than natural seawater (Atkinson and Bingman 1998). The

effect of dissolved organic matter present in SSW (about 0.6 mg/L in the most concentrated SSW) can likely be ignored given the range of competitive effects seen below for much higher additions of dissolved HA (200 – 400 mg/L). The most abundant anion in SSW is chloride (concentrations ranging from 140 mM to 560 mM for incubations prepared in this study) (Table 4.4) and as mentioned in the previous section, the competitive effect is complicated and possibly less important at higher pH. Bromide is also present in SSW at appreciable concentrations (350 μM to 1400 μM) for potential competition with Phe (Table 4.4). As with chloride ions, bromide has a high second-order rate constant (1.1×10^{10} M^{-1} s^{-1} (Zehavi and Rabani 1972)) for reaction with ·OH (forming hypobromous acid radical). Similar to interactions with chloride, one study has shown that hypobromous acid radical can also dissociate back to bromide and ·OH as in Equation 4.4 (although at a slower rate of 3.3×10^{7} s^{-1} at pH > 7) (Zehavi and Rabani 1972). Despite being present at much lower concentrations than chloride, bromide may actually be a better competitor than chloride, as suggested by studies of advanced oxidation of organic contaminants (Grebel et al. 2010).

Making estimates of the competitive effects expected from the SSW mixture are complicated because of the uncertainties involved in reversible reactions with halides, and the variations in pH observed as they effect competition with both different forms of carbonate and the halides. Determining competition factors for this complex solution of SSW would require additional information about how well bromide competes for ·OH. Unlike the incubations with SLF where multiple components were predicted to be effective competitors for ·OH, the higher $[Phe]_o$ limited the competitive effect of most components in SSW slurries. For example, at the highest concentration of sea salts (32 ppt), the $\mathbf{K_x}$ for carbonate is 32 μM, or about 10% of the 300 μM $[Phe]_o$ (Table 4.4). Similarly, despite the higher concentration of chloride in 32 ppt SSW, the competitive effect would also be much lower than in the SLF experiment.

All Tyr levels in SSW incubations reached a plateau following an initial lag in formation of 24 hours for 8 and 16 ppt, and 48 hours for 32 ppt sea salt (Figure 4.6B). Formation of the three isomers of Tyr was observed in all incubations, and $[\Sigma Tyr] / [Phe]_o$ ratios for slurries containing SSW were 9.6%, 6.5% and 3.9% for salt concentrations of 8, 16, and 32 ppt respectively (Figure 4.6B); slightly lower than those observed in Chapter 2 relative to the amount of Phe loss through time. Experiments conducted over a longer time-course would be needed to

determine whether the loss of Phe and apparent production of ·OH had declined greatly, thereby limiting formation and further loss of Tyr. In the pyrite suspension of pure water (no SSW), the $[\Sigma Tyr] / [Phe]_o$ ratio reached a maximum of about 13% at the 48-hour time point (where loss of Phe exceeded its first half-life), which is within the expected range of 12 – 20% established in Chapter 2.

Concentrations of *o*-, *m*-, and *p*-Tyr were observed at different proportions than in previous experiments, and differences were more pronounced at higher salt concentrations (Table 4.5). Table 4.5 reveals a shift towards greater production of *o*-Tyr at the expense of *p*-Tyr, while *m*-Tyr remains constant. The observed differences in Tyr-isomer distribution in pyrite slurries with SSW were likely due to changes in product distribution at higher pH (both initially and throughout the run) as discussed in Chapter 2 and shown by Chang et al. (2008) with reactions of Fenton reagents and salicylic acid.

4.3.2.2 Phenylalanine loss in the presence of pyrite and humic acid

Significant degradation of Phe was observed in pyrite slurries containing 200 mg L^{-1} (Figure 4.7A) and 400 mg L^{-1} (Figure 4.8A) HA, despite the complex mixture of organic compounds (including aromatic quinones) that comprises HA. The rate of Phe loss in 200 mg L^{-1} HA slurries appeared to increase between 24 and 48 hours all three incubations (Figure 4.7A) following a slight lag in reactivity similar to that observed in some incubations shown in Chapter 2 and SSW (the latter presumed to be an effect of initial pH). However, the HA did not appear to buffer the slurry upon the addition of pyrite as the pH dropped similar to pyrite suspended in pure water. Following the initial 24-hour lag, the Phe loss fit a slightly exponential decay curve through time. Despite the lag, linear fits of the data were obtained, and observed $\boldsymbol{R_0}$ were 0.44 μM hr^{-1}, 1.01 μM hr^{-1}, and 1.38 μM hr^{-1} for reactions of 32.3 μM, 121 μM and 370 μM $[Phe]_o$ (respectively) in 200 mg L^{-1} HA (Figure 4.7A). A lag was less apparent in incubations with 400 mg L^{-1} HA as degradation rates were overall slower and more linear. Degradation patterns remained linear throughout the time course for all three incubations (Figure 4.8A). Observed $\boldsymbol{R_0}$ were 0.26 μM hr^{-1}, 0.71 μM hr^{-1}, and 1.12 μM hr^{-1} for reactions of 29.3 μM, 102 μM and 303 μM

$[Phe]_o$ in 400 mg L^{-1} HA (respectively) (Figure 4.8A) – slightly less than 2-times slower than incubations in 200 mg L^{-1} HA (when normalized to $[Phe]_o$).

Formation of the three isomers of Tyr in both 200 mg L^{-1} and 400 mg L^{-1} HA slurries confirmed the degradation of Phe by $^{\cdot}OH$ (Figures 4.7B and 4.8B). The slight lag in production of Tyr was observed and consistent with the lag in Phe loss. The ratio of $[\Sigma Tyr] / [Phe]_o$ reached the same 16% maximum for the two highest $[Phe]_o$ in incubations with 200 mg L^{-1} HA (Figure 4.7B). The lower maximum measured $[\Sigma Tyr] / [Phe]_o$ for the incubation with 32 μM Phe is likely the result of insufficient sampling resolution as it corresponded to a sampling time well past the half-life of Phe when Tyr production is lower and its rate of loss faster owing to less competition with Phe. Therefore, it is likely that if samples were taken at time points between 24 and 48 hours, the $[\Sigma Tyr] / [Phe]_o$ would resemble the dashed-line in Figure 4.7B. Reactions with 400 mg L^{-1} HA reached a maximum $[\Sigma Tyr] / [Phe]_o$ ratio of 12%, and was the same for all three $[Phe]_o$ (Figure 4.8B); consistent but somewhat lower than in 200 mg L^{-1} HA loadings. One explanation for a lower $[\Sigma Tyr] / [Phe]_o$ ratio may be due to the naturally occurring quinone complexes of the HA organic matter competing for $^{\cdot}OH$ while stabilizing free radicals (Chen and Pignatello 1997; Struyk and Sposito 2001), which in turn may interact and oxidize Phe to other products. On the other hand, the higher HA loading may have caused some Phe to bind with the dissolved organic matter.

An incubation of pyrite and 316 μM Phe without HA was run to provide a baseline for comparison of reactions as a function of added HA (Figure 4.9). The $\mathbf{K_{pyr}}$ for this experiment with HA was calculated to be 0.10 μmol g^{-1} hr^{-1} using the observed $\boldsymbol{k'}$ of 0.032 hr^{-1}. Although an $\boldsymbol{R_o}$ could not be determined because of insufficient initial sampling frequency, calculations based on $\boldsymbol{k'}$ yielded an $\boldsymbol{R_o}$ of 8.6 μM hr^{-1} for 20% loss after 7.3 hours. This is about 6.2-times faster than reactions in 200 mg L^{-1} and 7.7-times faster than reactions in 400 mg L^{-1} HA. Figures 4.9A and 4.9B also show the results from the incubations from reactions containing HA and the highest $[Phe]_o$ for comparison. A control incubation run without pyrite and 200 mg L^{-1} HA experienced 15% loss of Phe over the time course of the experiment (Figure 4.9A). This may have been due to slow adsorption to the HA matrix; however, there appeared to be some biological activity as a small amount of *p*-Tyr (about 1 μM) that had formed by the 72-hour time point and persisted through the rest of the experiment (Figure 4.9B).

Since a second-order rate constant was not available for reaction of Aldrich® HA with ·OH ($\boldsymbol{k_{HA}}$), an average value for samples of aquatic humic substances reported in the literature 3.4×10^4 (L mg^{-1} HA) s^{-1} (Goldstone et al. 2002; Lindsey and Tarr 2000) was used to estimate an amount of competition that would be expected in these experiments with Phe. This value is likely a good approximation since a study with several types of both humic and fulvic acid substances (both naturally organic-rich materials) spiked with Fenton reagents and pyrene found that these organic complexes have a similar effect on the kinetics of ·OH reaction (Lindsey and Tarr 2000). The competition factors were calculated to be 0.26 and 0.13 for the highest $[Phe]_o$ using $\boldsymbol{k_{HA}}$ and the HA loading of either 200 mg L^{-1} or 400 mg L^{-1}, respectively (Equation 4.3); thus the calculated ***k'*** is 0.008 hr^{-1} and 0.004 hr^{-1} respectively. An exponential fit to the data for the highest $[Phe]_o$ of both HA loadings was complicated by the lag; however, estimates for the observed ***k'*** were 0.015 and 0.011 in 200 mg L^{-1} and 400 mg L^{-1} HA, respectively (Figure 4.9A). Thus, the measured effects of HA on observed ***k'*** were within a factor of 2 to 3 of that predicted from data with other humic substances. Although precise comparisons of the ***k'*** are complicated by the initial lag in Phe loss, the effects of HA on the rates are consistent with competition for ·OH.

4.4 Summary

Experiments in this chapter have shown Phe hydroxylation in pyrite slurries is hindered to various extents when added to simulated matrices that mimic basic physiological (SLF) and environmental (SSW and HA) solutions. The extent to which the amount of ·OH available for reaction with Phe was limited by individual or complex mixtures of matrix components was measured by the differences in Phe degradation kinetics relative to incubations in which pyrite was suspended in pure water. Individual components of SLF affected the loss of Phe via different mechanisms, such as competition (e.g., glycine, chloride, etc.), iron chelation (e.g., citrate), and decrease in H_2O_2 formation at the pyrite surface due to higher pH (buffers). Pyrite slurries containing simulated matrices representative of those found in the environment also slowed the loss of Phe; however, hydroxylation of Phe still occurred to form the three isomers of Tyr – even in the presence of high salt content at relatively high pH (SSW) and a concentrated complex mixture of dissolved organic matter (HA).

As seen in another recent study with the fluorescent probe APF (Harrington et al. 2011), addition of SLF decreased the apparent amount of ·OH generated in pyrite slurries. However the magnitude of the effect was seen to a much greater extent with Phe loss and particularly in the case of formation of ·OH-specific Tyr. There were, however, trace levels of *m*- and *o*-Tyr (less than 50 nM) present in solutions of SLF with and without organic acids. A third SLF formulation containing both organic acids and formalin yielded no Tyr. Although most of the Phe was apparently lost by means other than hydroxylation in SLF, other reaction products were not readily identified by the current ESI+ MS method (perhaps due to a loss of the amino functional group of Phe which is the main site of protonation allowing for detection in positive ionization mode). It is suggested that further experiments be conducted at higher levels of Phe to minimize the effects of competitors and favor accumulation of Tyr. It is clear from results with SLF and other studies (MnO_x presented in Chapter 6) that more detailed experiments are required to understand the difference between the APF and Phe probes.

Several components of SLF are present in high enough concentration to compete for available ·OH when Phe was added at 10 μM. Each component was assumed to react competitively with Phe for available ·OH according to the product of their concentrations and and second-order rate constants. Only Gly exhibited the expected competitive effect on the Phe kinetics (according to competition factor based on its $\boldsymbol{k_{Gly}}$ and concentration). Reactions with added citrate were more interesting as competition for ·OH alone, likely the result of citrate acting as a chelator at limiting the Fe^{2+} necessary for Fenton reaction. Calculated differences in the rates of Phe loss at pH 4 based solely on concentration and second-order rate constants for carbonate (as mostly bicarbonate at the tested pHs) and phosphate (as a mix of dihydrogen and hydrogen phosphate) suggest that adsorption to the pyrite surface decreased the potential for H_2O_2 and/or ·OH formation. The effect of carbonate on the degradation of Phe was attributed to several factors including competition, as well as some combination of limiting the Fenton reaction by reducing the available Fe^{2+} in solution, inhibiting H_2O_2 formation at the surface (Evangelou et al. 1998), or as a result of decomposition of H_2O_2 by Fe^{2+}-carbonate complexes at higher pH. The fact that both phosphate and carbonate have pronounced effects on Phe degradation even in incubations with lower pH is of interest and points to mechanisms operating at the pyrite surface.

The three isomers of Tyr were observed in slurries of Phe containing Gly, chloride, and citrate. A lag in *m*- or *p*-Tyr was observed in slurries containing citrate, though Phe degradation was slow and the presences of all Tyr isomers indicating involvement of ·OH. No hydroxylation of Phe to was observed in slurries containing carbonate or phosphate buffers when incubated independently, even when the initial pH was below 7. Only *p*-Tyr was measured in some pyrite slurries that contained phosphate buffer, likely due to growth of microbial populations that are nitrogen-fixing and limited otherwise by phosphate (despite efforts to maintain clean environment (e.g., muffled glassware)).

Results generated from experiments with SLF and its components allowed for the expansion of equations used in Chapter 2 to include individual components of simulated solutions that could be evaluated for their presumed effect on the fate and formation of ·OH in pyrite slurries versus the observed effect. Calculations of competition factors for each component of SLF or SSW can be useful when determining the potential effects on ·OH reactivity in complex physiological systems. However, interpretation of the effects of halides (especially chloride) were complicated by the fact that the there are reversible reactions that mitigates the competitive effects predicted from second-order rate constants with ·OH. The net effect of adding sodium chloride to the pyrite slurry reduced the rate of Phe loss by about 70% (at the lower pH induced by pyrite). It would appear that chloride does not have an effect on the pyrite surface or its ability to generate ROS. Predicted competitive effects also do not account for effects of complexing agents on iron speciation or the effects of buffers on pH. The effects of solution chemistry that are not direct results of competition are more difficult to determine, but general comparisons between expected and observed ·OH reactions with Phe can quantify which other mechanisms are likely to involved in affecting the loss of Phe.

Unlike true lung fluid, the SLF used in this experiment did not contain enzymes and many other biological components that would normally be present. Since Phe is a naturally occurring amino acid, it is subject to natural degradation by cellular processes. However, the stereoisomer D-Phe has been used in *in vitro* experiments to monitor response to ROS in cells (Biondi et al. 2001) as it does not get incorporated during protein synthesis or transformed to *p*-Tyr enzymatically. Additionally, it has been shown that the abiotic hydroxylation by Fenton reagents of D-Phe produces the same degradation pattern and Tyr-isomer ratio (as D-Tyr) (Biondi

et al. 2001). Therefore, the same likely applies for reactions of D-Phe in pyrite slurries, and thus may be more useful than L-Phe in pyrite incubation in potential future studies conducted with cells, Phe-specific enzymes, or limit the potential for biological contamination. The use of D-Phe may have circumvented the problems encountered in incubations with phosphate buffers where microbial growth was indicated.

Degradation rates of Phe in pyrite slurries with various dilutions of SSW showed the effects of both decreased reactivity from higher initial pH and competition for ·OH from its various components, including chloride and bromide anions (though to a lesser extent than would be predicted based solely on the second-order rate constants). The only significant ·OH competitors in the incubations are believed to be bromide, chloride, and to a lesser extent carbonate. The maximum value for ratios of $[\Sigma Tyr] / [Phe]_o$ decreased as a function of sea salt concentration, and plateaued despite continued Phe degradation. The ratios of Tyr isomers were slightly different as a function of SSW concentration, likely due to a shift in hydroxylation pathway of Phe at higher pH, as observed in other studies with reactions of salicylic acid and Fenton reagents (Chang et al. 2008). More experiments are needed to better understand effects of both pH and the presence of chloride and bromide in pyrite slurries and how they relate to the Phe degradation pathways.

As suggested in studies with humic and fulvic substances in aqueous Fenton systems (Lindsey and Tarr 2000), the complex organic matter that makes up the HA used in this study did not prevent ·OH from forming and reacting with Phe. What had not been shown is that the high levels of dissolved organic matter do not prevent the formation of ROS at the pyrite surface. It appears that degradation of Phe in slurries containing pyrite was slowed mainly by competition effects, generally consistent with predictions based on the averaged second-order rate constant obtained with other dissolved humic substances. Overall, the fact that pyrite-induced ·OH is formed and can hydroxylate Phe in sufficient amounts in the presence of a high levels of dissolved organic matter is impressive, especially considering that the concentration of HA was higher than many natural waters.

Interestingly, the HA used in this study was derived from natural, highly-oxidized lignite coal (Sigma Aldrich 2010). Pyrite is present in mines where coal is extracted, and has been one reason for continued work on the effect of coal inhalation by mine workers. The percentage and

crystal structure of pyrite found in coal varies by type and formation conditions. The following chapter presents results from experiments with several types of pyritic and non-pyritic coal incubated with Phe.

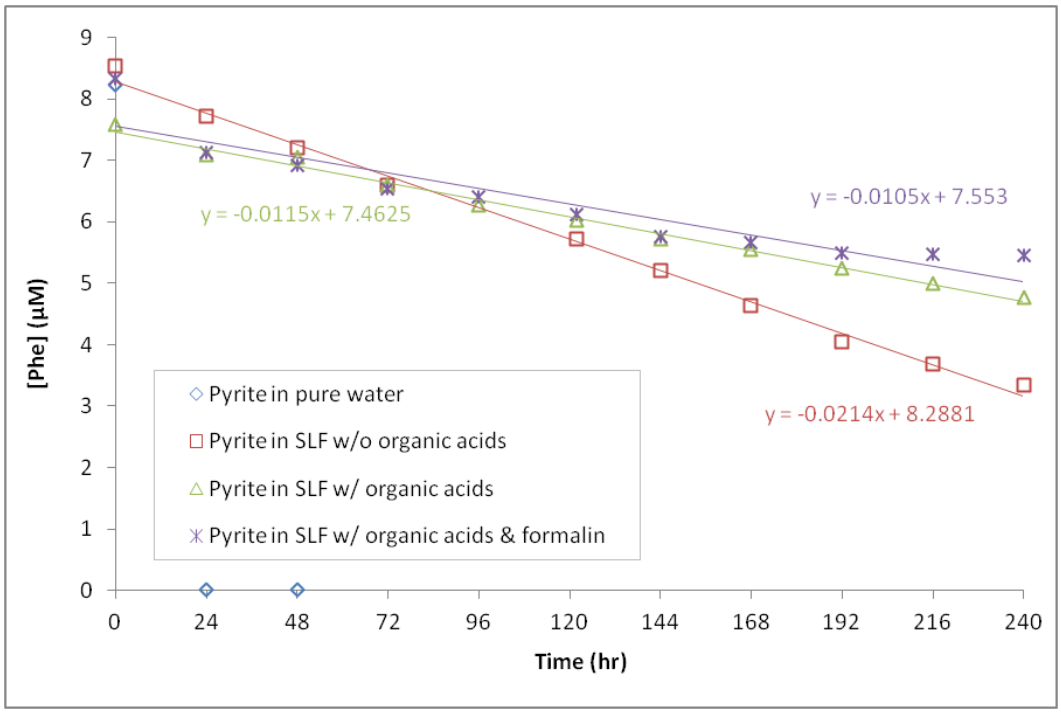

Figure 4.1. Loss of Phenylalanine in the presence of pyrite and simulated lung fluid. Three formulations of SLF were used to determine the combined effects of the organic constituents and formalin on Phe loss in the presence of pyrite. Linear fits of the data reveal a very slow (10 – 20 nM hr^{-1}) degradation rate of Phe of over the 240 hours. The greatest loss of Phe was observed in pyrites suspended in SLF without organic acids. Trace amounts (< 50 nM) of *o*-Tyr and *m*-Tyr were observed at some time point (not shown) indicating some ·OH activity.

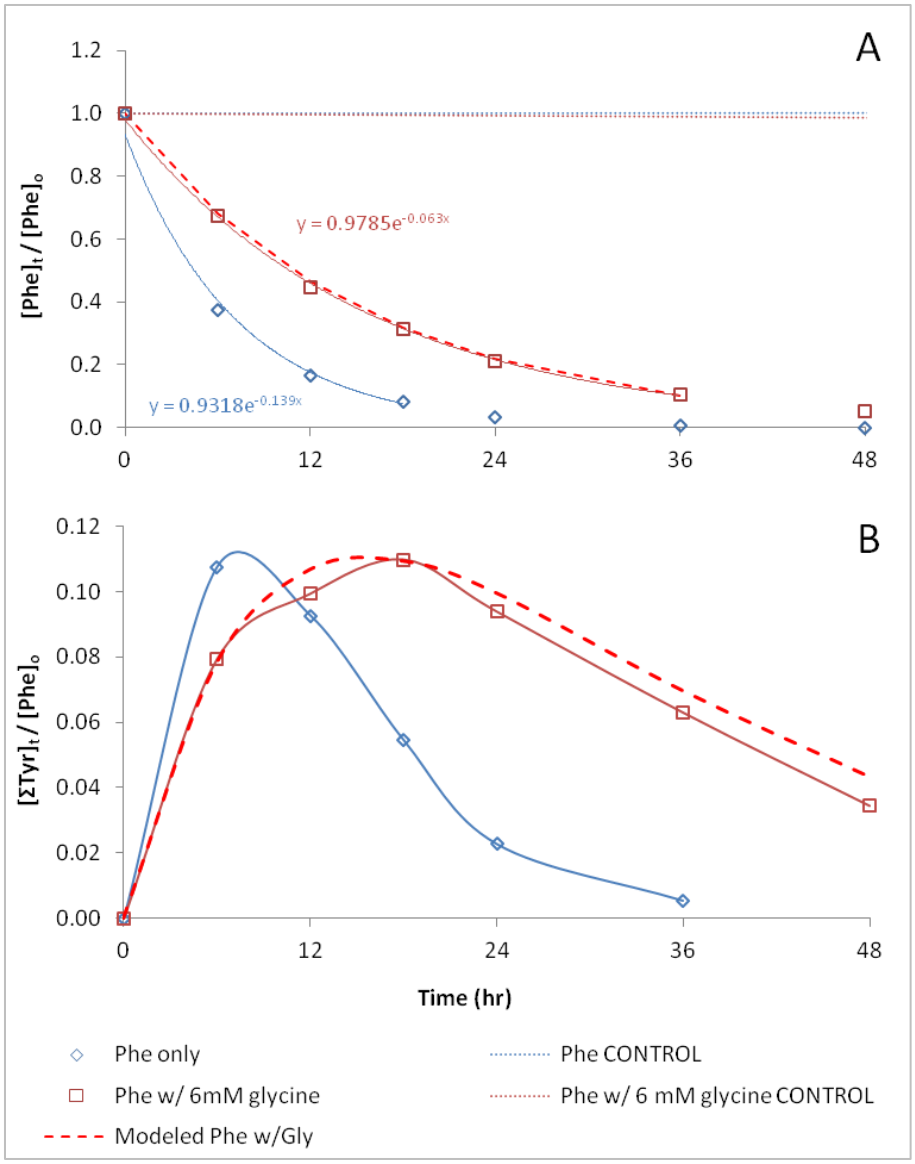

Figure 4.2. Incubations of Phe in pyrite with and without added Gly. (A) Loss of Phe fit an exponential curve in both reactions, but degradation was slowed by competition with 6 mM Gly as predicted by the model. Control samples without pyrite did not reveal any loss of Phe. **(B)** The pattern of ΣTyr formation and loss was the same for incubations of Phe only as with Phe with Gly, and the rate of Tyr formation reflected the slower Phe degradation in slurries containing Gly.

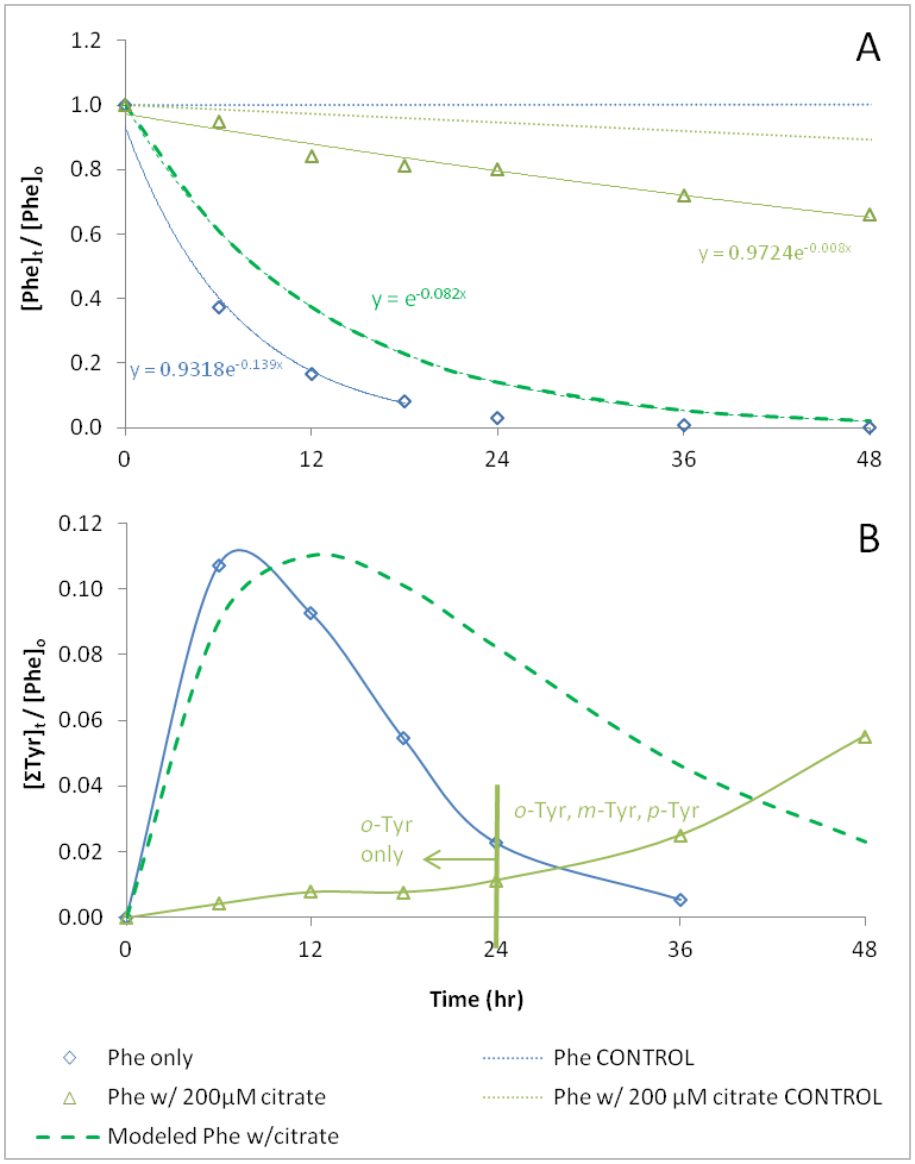

Figure 4.3. Incubations of Phe in pyrite with and without added citrate. (A) Phe degradation was slowed considerably by the addition of 200 µM citrate to suspension of pyrite due to a combination of complexation of dissolved (and possibly surface) iron and competition for the limited ·OH. Control samples without pyrite revealed some Phe loss solutions of citrate without pyrite, but no Tyr was observed. **(B)** The ΣTyr formation was slow in incubations with added citrate, reflecting the slow loss of Phe. Note, only *o*-Tyr was observed for from 0 – 24 hours in incubations with citrate only.

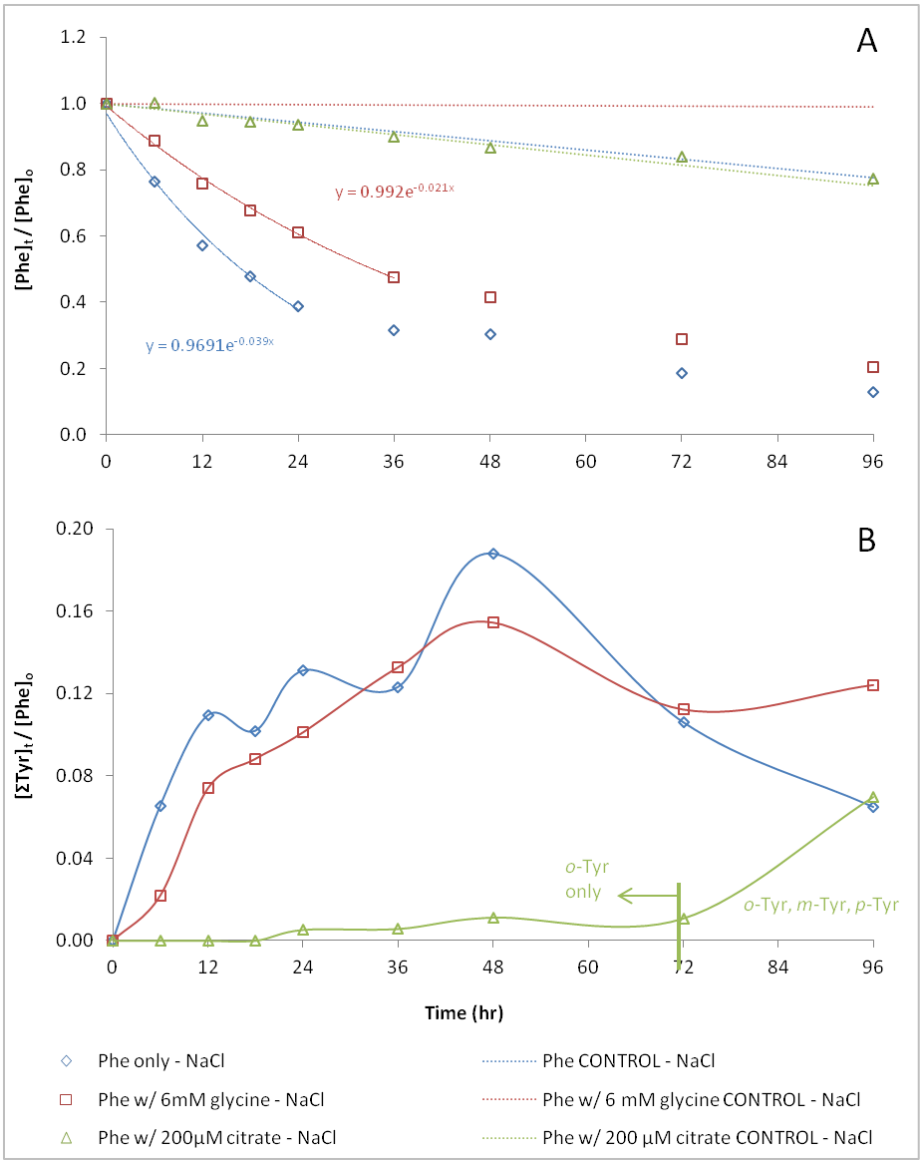

Figure 4.4. Incubations of Gly and citrate in water with 120mM sodium chloride with pyrite and Phe. (A) The degradation of Phe was slower in pyrite slurries containing 120 mM sodium chloride relative to reactions of pyrite suspended in pure water. Phe in the pyrite slurry with citrate did not degrade much and could only be confirmed by the formation of some of the three isomers of Tyr. Control samples without pyrite show that some degradation of Phe occurred in solutions of Phe salt water and citrate without pyrite, though no Tyr was observed. **(B)** Interestingly, the ratio of $[\Sigma Tyr] / [Phe]_o$ appeared to be greater sodium chloride solution than in pure water – though it is still within the expected range. Note, only *o*-Tyr was observed for from 24 – 72 hours in incubations with citrate only.

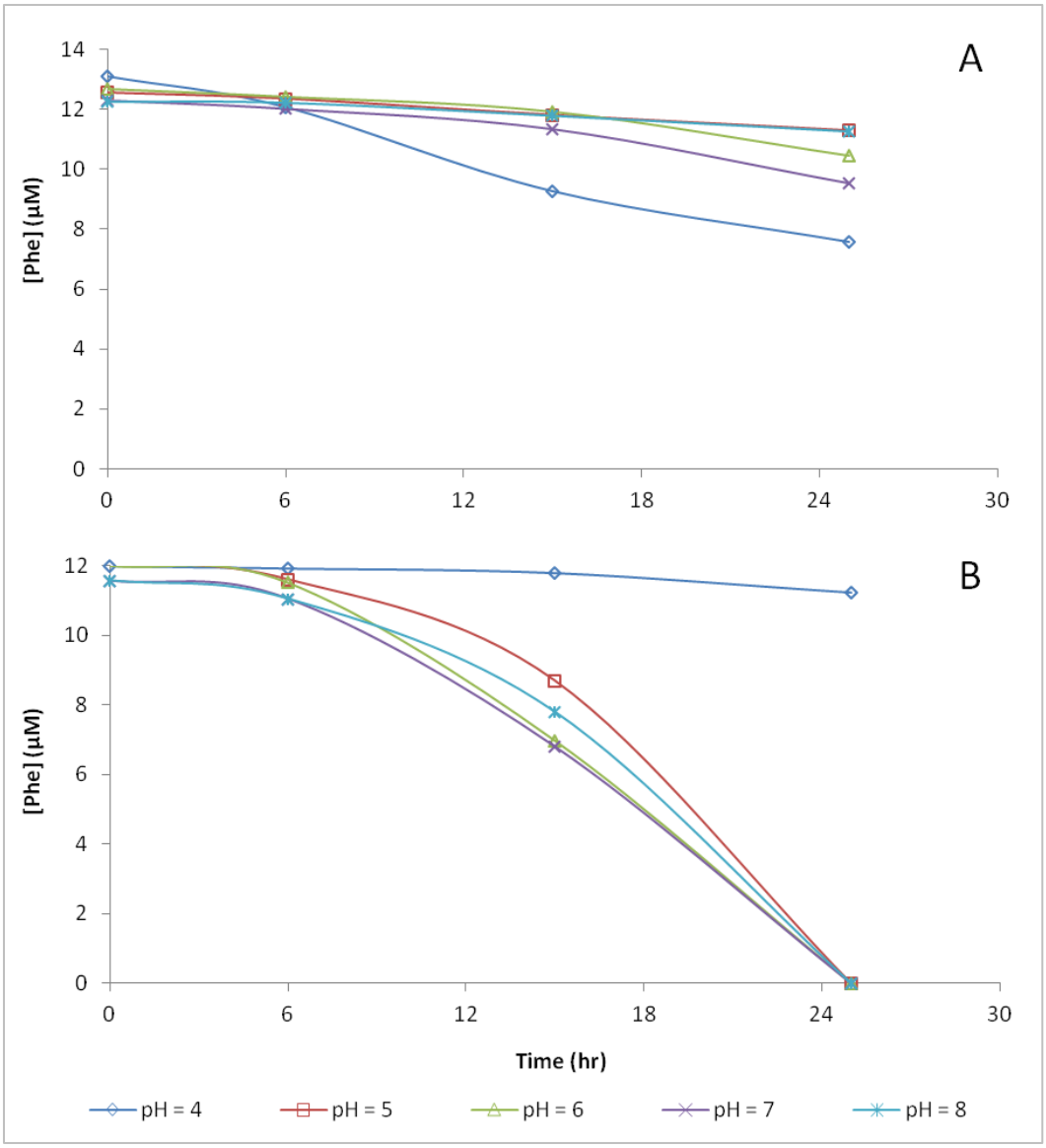

Figure 4.5. Degradation of Phe in pyrite slurries containing carbonate and phosphate buffers over a range of pHs. (A) Minimal loss of Phe was observed at all pHs in carbonate buffered solutions with no Tyr formation observed. **(B)** Loss of Phe in phosphate buffers were mainly the result of microbial degradation at pHs 5 – 8 (as indicated by formation of *p*-Tyr (not shown). Each incubation contained 10 g L^{-1} pyrite to minimize the pyrite-induced pH effect.

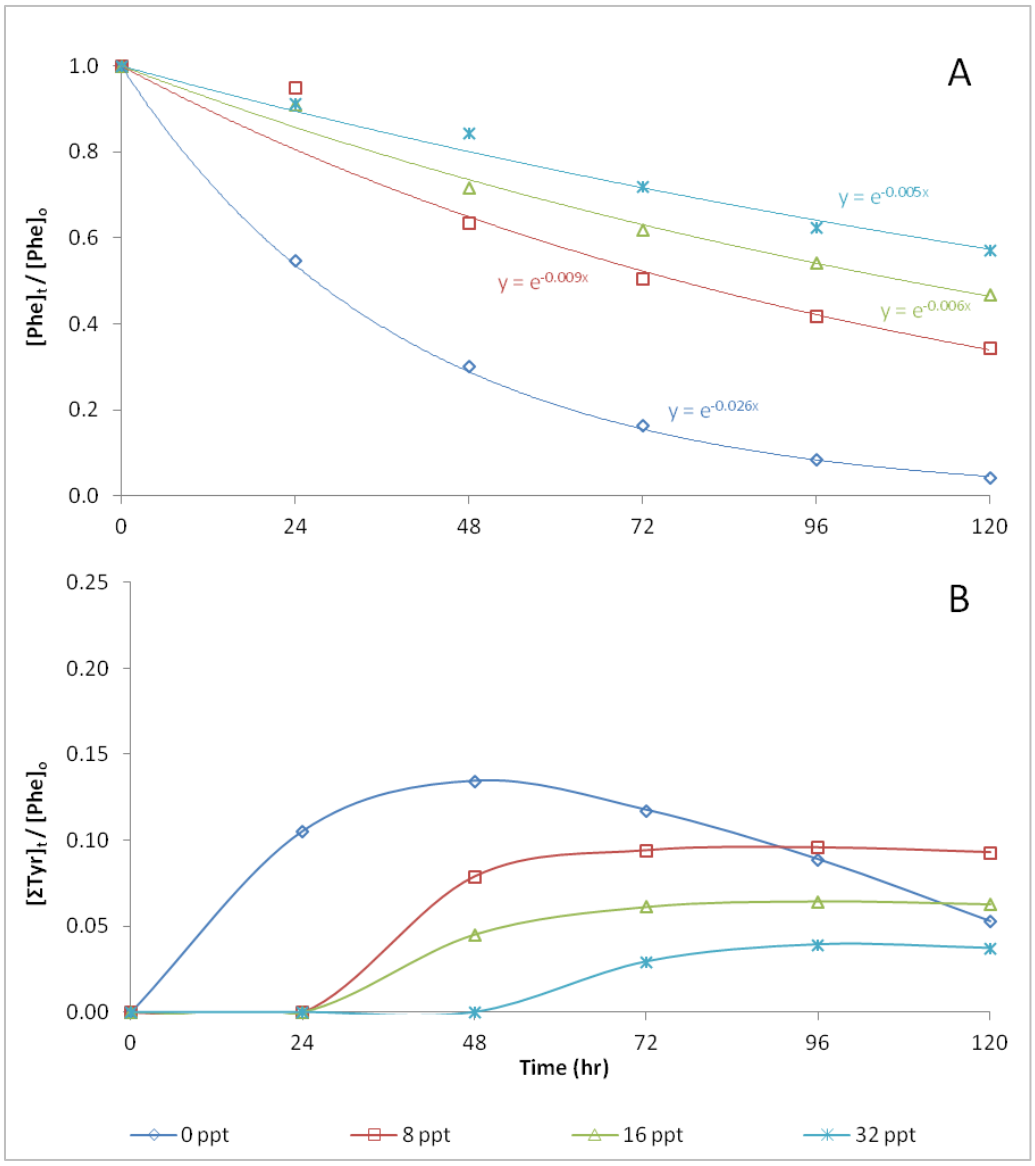

Figure 4.6. Phenylalanine degradation and total-Tyr formations in various dilutions of SSW. (A) Loss of 300 µM Phe was slowed by addition of SSW to extents that related to the concentration of salts. **(B)** Tyr formation was delayed then plateaued, suggesting production and decay were at equilibrium as Phe was still observed to degrade at later time points, though at a slower rate.

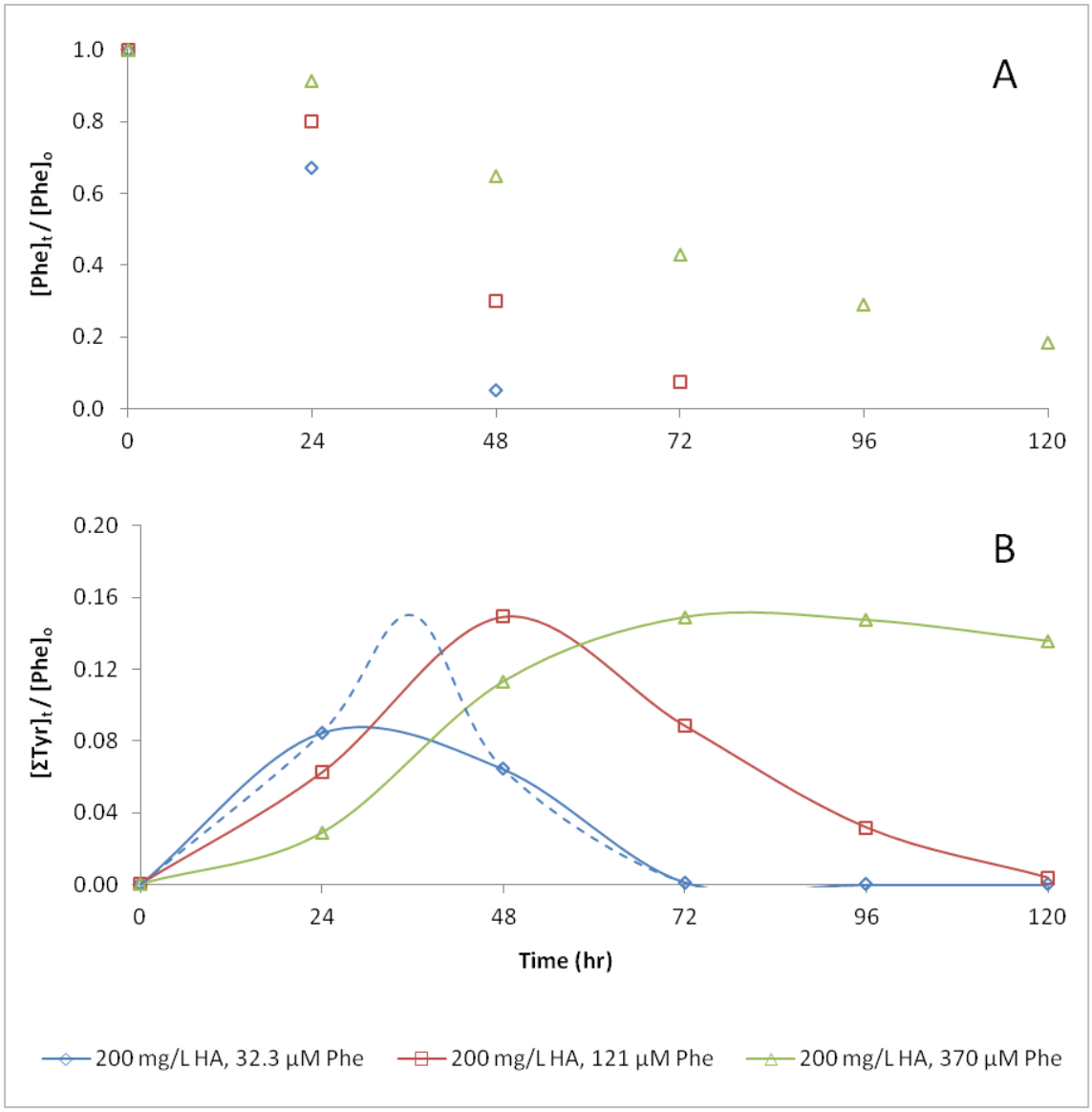

Figure 4.7. Concentrations of Phe and total-Tyr through time in pyrite slurries containing 200 mg L^{-1} HA. (A) Rates of Phe loss were hindered by the complex mixture of organic compounds of HA. **(B)** Formation and decay of Tyr reached the ratio of [ΣTyr] / $[Phe]_o$ expect from pyrite-induced ·OH formation that is not impeded by surface reactions or pH effect. The dashed line represents the likely [ΣTyr] through time for loss of 32.3 µM Phe had a sample been taken between 24-hour and 48-hour time points.

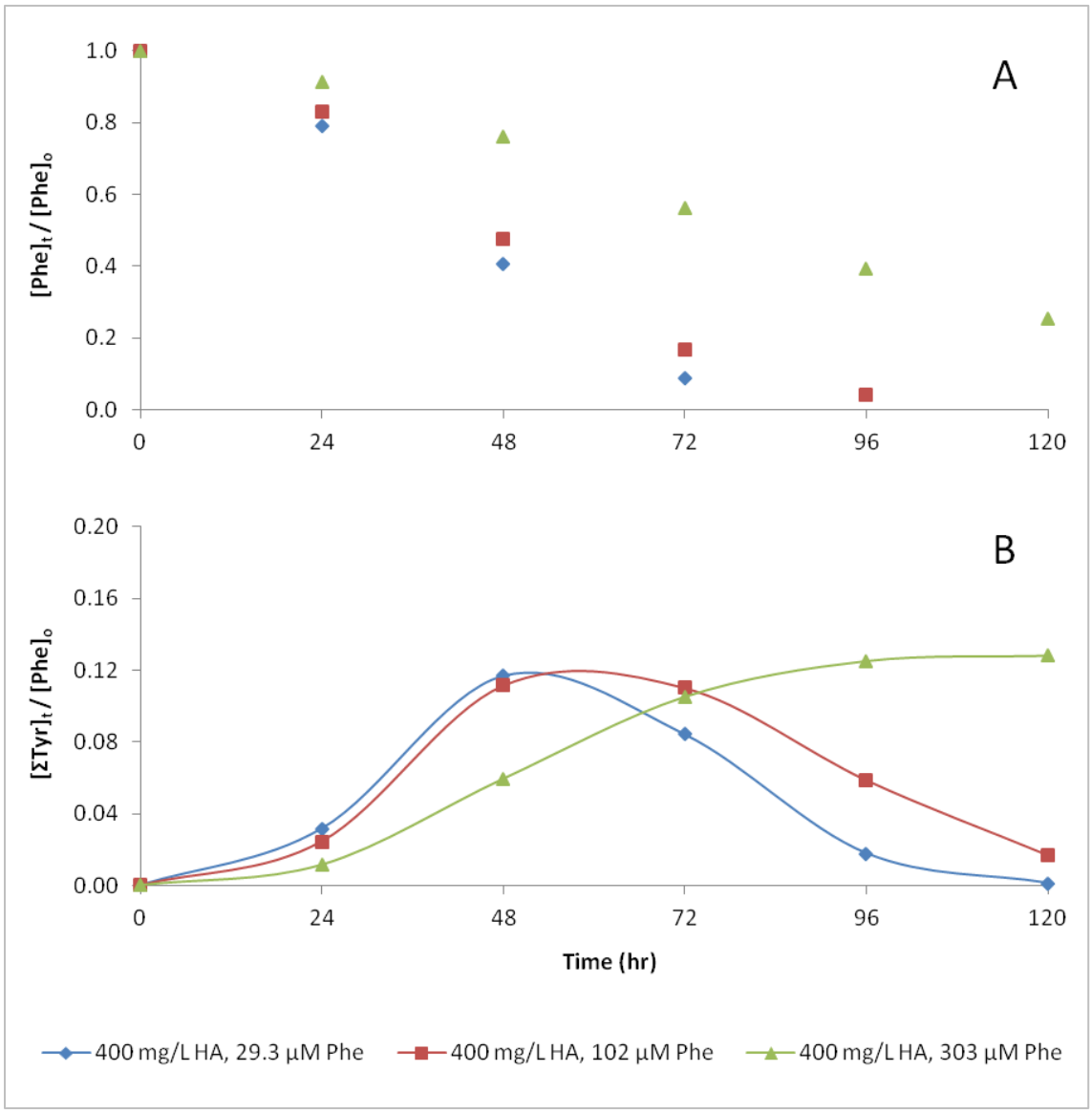

Figure 4.8. Concentrations of Phe and total-Tyr through time in pyrite slurries containing 400 mg L^{-1} HA. (A) Rates of Phe loss were slower than in the 200 mg L^{-1} HA loading by about half. **(B)** Formation and decay of Tyr reached the ratio of [ΣTyr] / $[Phe]_o$ expect from pyrite-induced ·OH formation that is not impeded by surface reactions or pH effect; although the ratios are slightly lower than observed in the 200 mg L^{-1} HA loading.

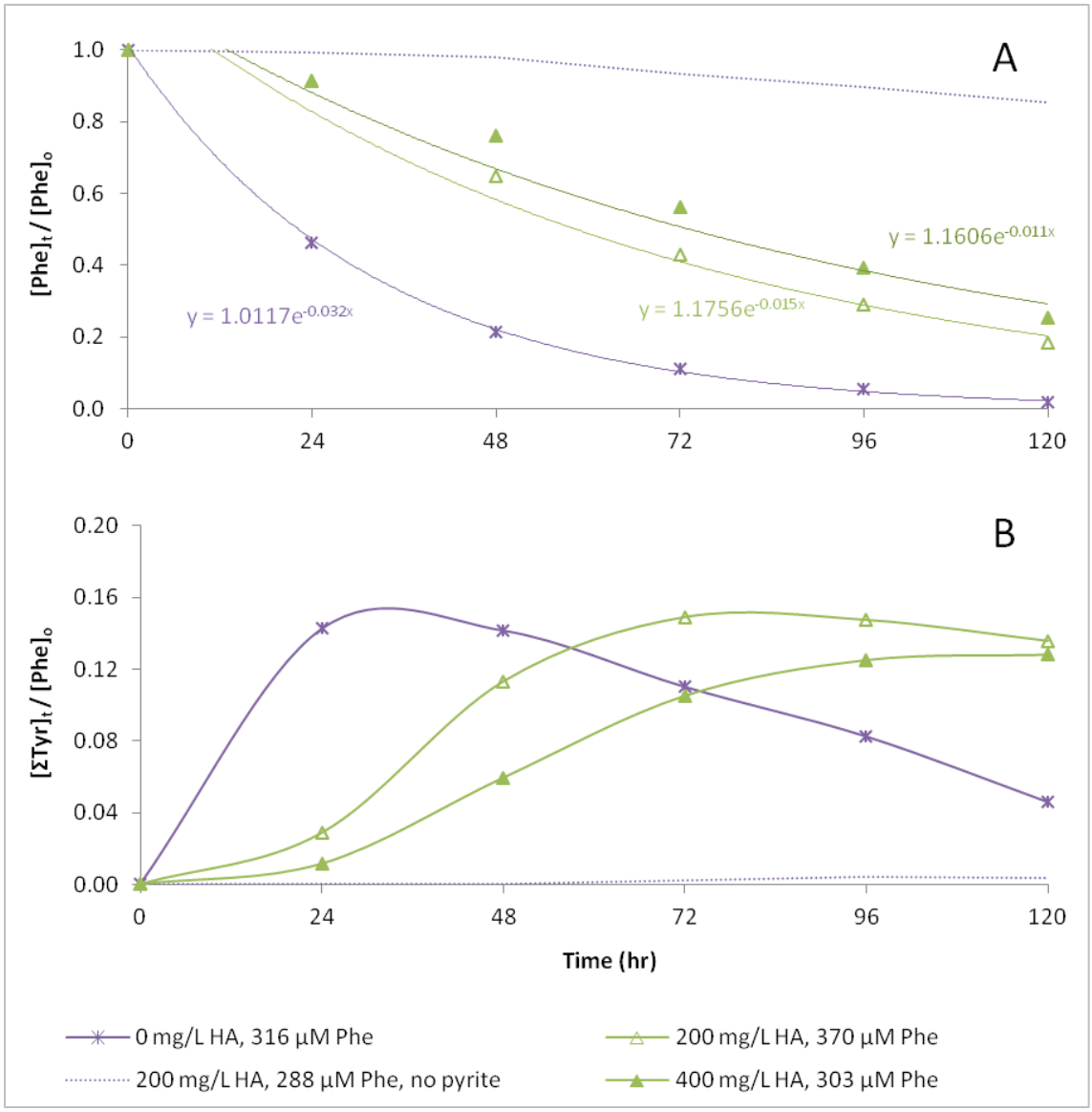

Figure 4.9. Comparison of Phe loss and Tyr formation in various HA loadings at similar initial Phe concentrations. (A) Degradation of Phe at the highest initial-concentrations in 200 mg L^{-1} and 400 mg L^{-1} were compared to 0 mg L^{-1} (pyrite only), which fit an exponential curve well. An initial lag in degradation can be observed in reactions containing HA, followed by a more characteristic exponential fit. A control containing 200 mg L^{-1} HA, Phe, and no pyrite was also run and was slightly lower by the end of the run. **(B)** The $[\Sigma Tyr] / [Phe]_o$ ratio was similar in incubation with HA as in pyrite-only. Note a trivial amount of Tyr formed (all *p*-Tyr) in the control sample containing HA and Phe without pyrite, indicating a small amount of microbial degradation of Phe.

	Concentration (mM)	without organic acids	with organic acids	with organic acids and formalin
ammonium chloride	10	X	X	X
sodium chloride	116	X	X	X
sodium bicarbonate	21	X	X	X
sodium carbonate	5.9	X	X	X
sodium dihydrogen phosphate	1.2	X	X	X
sodium citrate	0.20		X	X
glycine	6.0		X	X
sulfuric acid	1.0	X	X	X
calcium chloride	0.26	X	X	X
formaldehyde (as formalin)	0.33			X
methanol (in formalin)	0.04			X
hydrochloric acid	not recorded	X	X	X

Table 4.1. Composition of SLF formulations. List of individual components added to pure water to make the three different formulations for incubations with pyrite and Phe. Recipe for SLF prepared as per Eastes et al. (1995).

SLF component (**x**)	Conc. (μM)	k_x (M^{-1} s^{-1})	k_x ref.	f_x (k_x / k_{Phe})	K_x (μM)	Note
chloride	127000	4.3×10^9	(Jayson et al. 1973)	0.66	$*8.4 \times 10^4$	Minimum (the relatively small amount of HCl added to adjust the pH was not recorded)
bicarbonate	25200	1.0×10^7	(Buxton and Elliot 1986)	1.5×10^{-3}	38	90% of total carbonate at pH 7.4 (remaining 10% as carbonic acid)
glycine	6000	1.7×10^7	(Scholes et al. 1965)	2.6×10^{-3}	15	
citrate	200	1.5×10^8	(Zepp et al. 1992)	2.3×10^{-2}	4.6	
hydrogen phosphate	800	1.5×10^5	(Maruthamuthu and Neta 1978)	2.3×10^{-5}	1.9×10^{-3}	70% of total phosphate at pH 7.4
dihydrogen phosphate	350	2.4×10^4		3.7×10^{-6}	1.3×10^{-4}	30% of total phosphate at pH 7.4
methanol	42.2	8.3×10^8	(Motohashi and Saito 1993)	0.13	5.4	Methanol only present in "SLF with organic acids and formalin"

Table 4.2. Simulated lung fluid components with known second-order rate constants for reactivity with ·OH. Concentrations and second-order rate constants (k_x) for compounds capable of competing with Phe for ·OH are listed. Rate constants relative to that of Phe as defined in Chapter 2 (f_x) and the relative competition concentration (K_x) calculated for use in the numerical simulation to compare theoretical to observed kinetics of Phe loss. Note that a second-order rate constant for formaldehyde could not be found. * = K_x was calculated for chloride based on published values does not account for the effects reversible reactions that may vary as a function of pH.

	·OH-flux (μM hr^{-1})	$[Phe]_o$ (μM)	$\mathbf{K_x}$ (μM)	Calculated ***k'*** (hr^{-1})	Observed ***k'*** (hr^{-1})
Phe only	1.34	9.1	0.0001	0.139	0.139
Phe with Gly	1.34	8.0	15	0.053	0.063
Phe with citrate	1.34	6.5	4.6	0.082	0.008
Phe with chloride	1.34	9.3	*8.4×10^4	1×10^{-4}	0.039

Table 4.3. Observed and calculated values of *k'* for Phe loss. Numerical simulation values obtained from pyrite incubations of "Phe only" and others were compared. Calculated values of ***k'*** were comparable to the observed kinetics for Gly competition; however, the calculated ***k'*** did not reflect the observed kinetics in the case of citrate or chloride addition (similar to the carbonate and phosphate data). These disparities underscore the complex mechanisms that affect the formation and fate of ROS in more way than just competition for ·OH. ***** = $\mathbf{K_x}$ was calculated for chloride based on published values does not account for the effects reversible reactions that may vary as a function of pH.

SSW component (**x**)	Composition (μmol g^{-1}_{salt})	k_x (M^{-1} s^{-1})	k_x reference	f_x (k_x / k_{Phe})	K_x (μM) 8 ppt	16 ppt	32 ppt
chloride	17500	4.3×10^{9}	(Jayson et al. 1973)	0.66	*9.2×10^{4}	*1.8×10^{5}	*3.7×10^{5}
bicarbonate	640	1.0×10^{7}	(Buxton and Elliot 1986)	1.5×10^{-3}	8.0	16	32
bromide	44	1.1×10^{10}	(Zepp et al. 1992)	17	*594	*1190	*2370
copper (I)	6.1×10^{-2}	3.0×10^{9}	(Goldstein et al. 1992)	0.46	0.22	0.45	0.90
copper (II)		3.5×10^{8}	(Buxton et al. 1988)	5.4×10^{-2}	0.03	0.05	0.10
zinc (I)	1.7×10^{-2}	2.0×10^{10}	(Buxton and Sellers 1975)	31	0.42	0.83	1.66
manganese (II)	4.1×10^{-2}	2.9×10^{7}	(Baral et al. 1986)	4.5×10^{-3}	0.00	0.00	0.01
iron (II)	8.1×10^{-3}	3.2×10^{8}	(Stuglik and Zagorski 1981)	4.9×10^{-2}	0.00	0.01	0.01
lead (II)	7.1×10^{-2}	2.0×10^{8}	(Sukhov and Ershov 1982)	3.1×10^{-2}	0.02	0.03	0.07
silver (I)	7.8×10^{-2}	9.7×10^{9}	(Bonifacic et al. 1991)	15	0.93	1.85	3.70
cobalt (I)	4.4×10^{-2}	8.9×10^{9}	(Buxton and Sellers 1975)	14	0.48	0.96	1.92
cobalt (II)		8.0×10^{5}	(Buxton et al. 1976)	1.2×10^{-4}	0.00	0.00	0.00
titanium (III)	2.3×10^{-2}	1.2×10^{9}	(Samuni et al. 1972)	0.18	0.03	0.07	0.13

Table 4.4. Simulated seawater components with known second-order rate constants for reactivity with ·OH. Concentrations and rate constants (k_x) for compounds capable of competing with Phe for ·OH are listed. Rate constants relative to that of Phe as defined in Chapter 2 for the numerical simulation (f_x) and the relative competition concentration (K_x) calculated for use in the numerical simulation to compare theoretical to observed kinetics of Phe loss. Reports with values for copper and cobalt were not specific with respect to speciation; therefore, each f_x was determined assuming 100% of the given concentration – values of K_x still proved relatively insignificant. * = K_x was calculated for chloride and bromide based on published values does not account for the effects reversible reactions that may vary as a function of pH.

	[*o*-Tyr] / [ΣTyr]	[*m*-Tyr] / [ΣTyr]	[*p*-Tyr] / [ΣTyr]
Pyrite w/ no SSW	0.42	0.26	0.32
Pyrite w/ 8 ppt SSW	0.45	0.29	0.26
Pyrite w/ 16 ppt SSW	0.48	0.26	0.26
Pyrite w/ 32 ppt SSW	0.57	0.26	0.17

Table 4.5. Tyrosine isomers observed at various simulated seawater concentrations. Relative ratios of *o*-, *m*-, and *p*-Tyr formed appear to shift away from *p*-Tyr in favor of *o*-Tyr as the salt content (and pH) increase.

Chapter 5

PHENYLALANINE LOSS IN THE PRESENCE OF PYRITIC COAL

5.1 Introduction

Recent studies have shown that coals containing pyrite (i.e., pyritic coals) can form reactive oxygen species (ROS) in oxygenated solutions (Cohn et al. 2006a; Dalal et al. 1995) similar to samples of pure pyrite. Exposure to coal dust has also been tied to a number of respiratory diseases that result from inflammation and cell-induced ROS formation (Dalal et al. 1995; Demers and Kuhn 1994; Schoonen et al. 2006). In particular, coal miners are at significantly greater risk for developing pulmonary diseases, theorized to be directly related to their exposure to pyritic coal (Huang et al. 2005). One study by Cohn et al. (2006) has already shown that formation of hydrogen peroxide (H_2O_2) and hydroxyl radical ($^{\cdot}OH$) is detectable in select pyritic coal slurries. However, more work is needed to better characterize the factors that affect $^{\cdot}OH$ formation and availability for reaction with different biologically-relevant molecules specific hydroxylation products, such as phenylalanine (Phe), through time.

Coal is a complex matrix of reduced organic matter that forms from the decomposition of plant life under anoxic conditions. The amount of pyrite found embedded in a coal deposit depends on the amount of sulfur present and the environment in which it formed (Altschuler et al. 1983). The pyrite crystals in coal tend to be small framboids only a few microns in size, but can comprise as much as 10% of the total coal mass in some regions (Gluskoter and Simon

1968). Mining operations introduce buried coal to the environment by means of dust that can be inhaled by workers and spoils that can weather into nearby ecosystems affecting the pH of exposed waters through formation of sulfuric acid. Sulfur dissolution from the pyrite surfaces of coal contributes a significant portion of the acid that affects the pH, but can also induce the electron-transfer process that leads to the formation of H_2O_2 (Schoonen et al. 2010). Dissolution also supplies the reduced iron (Fe^{2+}) necessary for Fenton chemistry to generate ·OH in solution through the reduction of H_2O_2 (Fenton 1894). As shown in Chapters 2 through 4, the rate of pyrite-induced ·OH formation and extent by which ·OH is available for reaction with organic compounds like Phe depends on solution chemistry (e.g., pH), presence of components that can interact with iron at the surface or in solution (e.g., chelators), and competing compounds. Interestingly, the Aldrich® humic acid (HA) used to assess pyrite reactivity in the presence of complex dissolved organic matter (Chapter 4) is derived from highly-oxidized lignite, a form of immature coal (written communication, Sigma Aldrich 2011).

The health implications for inhalation of coal have been studied extensively, though only recently has the connection between the pyrite-fraction of the coal and increased ROS production been made. Previous *in vitro* studies have implicated evolution of acid and ROS formation as likely causes of inflammatory response by cells exposed to coal dust (Demers and Kuhn 1994; Vallyathan 1994), which was linked to DNA mutation and lung cancer (Moller et al. 2010). A recent study by Huang et al. (2005) has shown that miners exposed to pyritic coal dust are at a greater risk for coal-workers' pneumoconiosis (CWP) at rates of incidents proportional to the iron and sulfur content of the coal that they are mining.

There have only been a few studies to-date conducted with pyritic coals that monitored ROS formation and reactivity, and the potential for extended ·OH formation had not been evaluated. Therefore, to better understand the fate and formation of coal-induced ·OH through time, Phe was incubated with six different coal samples in suspensions of oxygenated water to assess the rates of Phe degradation and the formation of the three isomers of tyrosine (Tyr), *ortho*-, *meta*-, and *para*-Tyr. Since the composition of coal can vary based on location, samples of well-characterized bituminous and sub-bituminous coals from the National Institute of Standards and Technology (NIST) and the U.S. Geological Survey (USGS) with a pyritic-sulfur content that ranging from 0% to 1.2% were selected for analysis. Samples of these coals were

previously used by Cohn et al. (2006) in experiments that showed the three bituminous NIST coals generate levels of H_2O_2 and ·OH (as measured by leuco crystal violet and 3´-(*p*-aminophenyl) fluorescein (APF) respectively) proportional to their sulfur and pyritic-sulfur content; ROS was not detected in two samples of sub-bituminous coal that did not contain pyrite. Degradation of RNA in pyritic coal samples was also observed in the same study and attributed reaction with ·OH (Cohn et al. 2006b).

Research conducted for this chapter sought to evaluate the extent of ·OH formation in pyritic coal through time while simultaneously testing Phe as a probe in a system with more complex surfaces. The experimental design for incubations of coal was the same as those described in previous chapters for samples of pure pyrite, which also allowed for rates of Phe loss and Tyr formation to be compared to previous experiments. In addition to incubations where the pH was allowed to drift, Phe was added to slurries in which a physiologically-relevant pH of 4.5 or 7.4 was maintained throughout the incubation – representing the pH induced by phagocyte cells as part of an immune system response (Nyberg et al. 1992) and the pH of alveolar lung fluid (Eastes and Hadley 1995) respectively. Control samples were also run with reagents previously used to quench the reaction of ·OH with organic compounds (including Phe), which yielded some interesting results. Some results from this chapter were also compared to the coal experiments conducted by Cohn et al. (2006).

5.2 Methods

Five different coal reference materials were obtained from NIST (standards 1635, 2682b, 2684b, 2685b, 2692b) and were used without additional grinding or preparatory treatment (i.e., coal samples were not soaked in hydrochloric acid (HCl) as done in prior studies with pure pyrite). A sample of CLB-1 coal was also obtained from the USGS and also used without further processing. Phenylalanine, *para*-tyrosine, *ortho*-tyrosine, and beta-mercaptoethanol (β-ME) – all 99% ACS-grade or better – were obtained from Alfa Aesar (Ward Hill, MA). *meta*-Tyrosine was obtained from TCI America (Portland, OR). Ethanol (99.5%) was acquired from Fisher Scientific (Pittsburgh, PA). Methanol was GC^2-grade from Burdick & Jackson (Morristown, NJ). Formic acid was ACS-grade from EMD Chemicals (Gibbstown, NJ). All water used for

cleaning, standards, reactions, dilutions, and chromatography work was purified with a Milli-Q filtration system (Millipore Corporation, Billerica, MA) to a resistivity of 18.3 MΩ cm^{-1}.

5.2.1 Phenylalanine incubations with coal

Composition data for each coal are available from the NIST certificates of analyses (http://www.nist.gov/mml/analy-tical/inorganic/fossfuels.cfm -- accessed January 2012) and a USGS report on the CLB-1 coal (Lyons et al. 1989); information relevant to this study is listed in Table 5.1.

Incubations of the six coals were conducted at 100 g L^{-1} loading and roughly 100 μM Phe, similar to experiments with pyrite in previous chapters. The pH of the bituminous coal slurries immediately decreased from around pH 5.6 to pH 3.8, 4.1, 3.7, and 2.8 upon addition of coals 2684b, 2685b, 2692b, and USGS, respectively. The pH was consistent throughout the first 24 hours of the incubations then slowly decreased to a final pH of about 2.7 in all three NIST coals after 336 hours. The sub-bituminous coals did not contain pyrite, and the pH of the slurries did not decrease significantly upon addition of the coals 1635 or 2682b and reached pH of 5.1 and 4.2 (respectively) by the 336-hour time point. Incubations of 10 g L^{-1} of coals 1635 and 2682b were also run with 100 μM Phe and 100 μM *p*-Tyr (individually).

Disposable centrifuge vials (50 mL) were used in all coal incubations where the pH was allowed to drift, with slurry volumes for all six coals at least 4-times greater than the total volume of all aliquots to be removed. In experiments with quenching reagents, 1% by-volume of either β-ME (140 mM) or ethanol (170 mM) was added prior to spiking coal. In all experiments, 300 μL was extracted at predetermined time points from the reaction vials and immediately transferred to a nylon Costar® 0.22 μm centrifuge vial filter (Corning Life Sciences, Lowell, MA) and 5 μL of β-ME was then added, followed by a brief centrifugation. Preparation of samples for HPLC analyses were conducted as outlined in Chapter 2 Methods section.

5.2.2 Constant-pH incubations

Incubations at pH 4.5 and 7.4 were conducted individually in a jacketed-beaker reaction vessel initially containing 75 mL of 100 g L^{-1} 2684b coal and 100 μM Phe. The pH was set to 4.5 or 7.4 and maintained by the addition of 0.1 M sodium hydroxide (NaOH) to within a tolerance of 0.1 pH-units by a Schott Titroline® alpha titrator (Germany). The top of the reaction vessel was loosely covered with holes for the titrant dispenser and pH probe. A magnetic stir bar kept the coal suspended in solution, and temperature was maintained at 25 °C by warm-water circulation through the jacketed-beaker. Once the coal was fully suspended and homogenized, the pH of the slurry decreased rapidly, and 0.5 M NaOH was used to adjust to the initial pH desired. After the pH was stabilized, the titrator was started. Total volume increased over the course of the experiments, thus diluting the coal loading and concentration of Phe through time (dilution factors are shown in Table 5.2 and were applied post-quantification of chromatographic areas in order to normalize the data for comparison purposes). Aliquots of roughly 300 μL were taken at predetermined time points via disposable syringe through the top cover then filtered with 0.2 μm Millipore® plastic syringe filter. The aliquot was processed as stated above and preparation of samples for HPLC analyses were conducted as outlined in Chapter 2 Methods section.

5.2.3 Analyses

All experiments were analyzed using a Waters Corporation (Milford, MA) Alliance® 2695 HPLC coupled to a Waters Corporation Micromass LCT Time-of-Flight Mass Spectrometer (ToF-MS) as described in the Methods section of Chapter 2.

5.3 Results and Discussion

5.3.1 Coal-induced phenylalanine loss

5.3.1.1 General observations

Loss of Phe was observed over 336 hours in incubations of all six coal samples (Figure 5.1A). The loss of Phe in the two coals classified as sub-bituminous (1635 and 2682b; Table 5.1)

was initially much faster and ultimately more extensive (35% and 65% loss of initial Phe concentration ($[Phe]_o$) by the 1-hour time point respectively) than in the four bituminous coal samples. Among the bituminous coals, degradation of Phe in the USGS coal slurry was the slowest, with an initial rate ($\boldsymbol{R_o}$) of 0.10 μM hr^{-1} that remained constant throughout the entire 336-hour incubation. The degradation of Phe in the 2692b coal slurry had an $\boldsymbol{R_o}$ of 0.40 μM hr^{-1}, then began to slow following the 144-hour time point and degraded linearly throughout the remainder of the experiment. In contrast, the Phe degradation pattern for coal samples 2684b and 2685b fit a shallow exponential curve for roughly 96 hours (with higher $\boldsymbol{R_o}$ of about 2.0 μM hr^{-1} and 1.3 μM hr^{-1} respectively), followed by a period where degradation was minimal (Figure 5.1A).

Formation of ·OH was confirmed by the detection of the three isomers of Tyr and was only observed in incubations of the four bituminous coals 2684b, 2685b, 2692b, and USGS (Figure 5.1B). No Tyr was detected in the two sub-bituminous samples (Figure 5.1B), suggesting a different mechanism had caused the observed Phe loss. These results are consistent with work by Cohn et al. (2006) that showed no H_2O_2 (using LCV) or ·OH (using APF) formation in 1635 and 2682b coals due to their lack of pyritic sulfur (Table 5.1). The same study also showed degradation of RNA in bituminous coals, but not in the sub-bituminous coals (Cohn et al. 2006a). The extent of Phe loss in the sub-bituminous coals is hypothesized to be the result of sorption to the surface or into the pores of the coal (discussed in detail in the next section). It is also speculated that adsorption might be less important in the denser bituminous samples.

The observed total-Tyr (ΣTyr) rates through time mirror the Phe loss. In slurries with the three NIST coals, [ΣTyr] increased at linear rates of roughly 0.2 μM hr^{-1} for the first 24 hours, then reached a plateau by the 96-hour (2684b and 2685b) and 144-hour (2692b) time point (Figure 5.1B) similar to the observed [Phe] over the same time frame. This suggests that the mechanism for producing H_2O_2 and/or ·OH had slowed or ceased by these times, perhaps due to extensive oxidation of the pyrite surfaces (Schoonen et al. 2010).

A steady increase in the [ΣTyr] over the entire experiment was observed in the incubation with USGS coal (Figure 5.1B), which reflected the slow loss of Phe over the course of the experiment (Figure 5.1A). This reveals that the USGS coal was capable of maintaining the

catalytic process of generating pyrite-induced ·OH for 336 hours (or 14 days). A detailed analysis of the kinetics of Phe loss based on the pyrite content of coal is presented later in the section.

5.3.1.2 Phenylalanine loss in sub-bituminous coals

To test the hypothesis that Phe loss in slurries of 1635 and 2682b coals was due to adsorption, incubations were run to determine the rates of Phe loss relative to coal loading (Figure 5.2A). Figure 5.2A shows that loss of 100 μM Phe in each 10 $g\ L^{-1}$ slurry of coal 1635 or 2682b was roughly 25% of $[Phe]_o$ after 48 hours. A concentration distribution coefficient (K_d) was determined and compared to loss of Phe in the 100 $g\ L^{-1}$ incubations over the first 48-hours (75% and 80% of $[Phe]_o$ for coals 1635 and 2682b respectively (Figure 5.1A)).

$$K_d = \frac{1 - f_d}{f_d \cdot TSS} \tag{5.1}$$

Where f_d represents the fraction of Phe dissolved (i.e., [Phe] / $[Phe]_o$ remaining at the given time point) and TSS is the total suspended solid (i.e., 10 $g\ L^{-1}$ or 100 $g\ L^{-1}$ coal) in the slurry. Calculations of K_d values using Equation 5.1 for each coal at both loadings are all between the narrow range of 30 L kg^{-1} and 40 L kg^{-1}, which is consistent with adsorption as the dominant removal mechanism.

To ensure Tyr was not being formed and rapidly adsorbed to the coal surface in coals 1635 and 2682b, *p*-Tyr was also incubated in slurries of 10 $g\ L^{-1}$ (Figure 5.2B). Figure 5.2B shows loss of the more-polar *p*-Tyr was slower and appeared to adsorb to a lesser extent; thus confirming no preferential adsorption of Tyr over Phe. Control incubations of both Phe and *p*-Tyr were run without coal and exhibited no loss over the 168-hour time course. Determination of a full adsorption isotherm for Phe through incubations with a range of concentrations would be interesting, but was outside the scope of this study.

5.3.1.3 Phenylalanine degradation in bituminous coals

Differences in the amount of degradation of Phe in slurries of the four coals containing pyrite was compared to estimates of ·OH production by Cohn et al. (2006) to determine if Phe hydroxylation would produce similar results as the APF probe. The change in the [Phe] after 24 hours was compared to both the percentage of sulfur and pyritic sulfur (Figure 5.3). Unlike in the slurries with APF, there was little correlation between the amount of ·OH that reacted with Phe and sulfur content (Figure 5.3). Similarly, there was no correlation between the changes in [Phe] with respect to pyritic sulfur content. Levels of sulfur were greatest in coal 2685b (4.7% by mass; Table 5.1) but did not induce the highest flux of ·OH for degradation of Phe (Figure 5.1A) as was seen with APF (Cohn et al. 2006a). Rather, coal 2684b with a sulfur content of 3.1% (by mass) generated more ·OH in 24 hours to account for 36 μM of Phe loss. The 2692b coal sample contained the least amount of sulfur and also induced the slowest rate of Phe degradation among the NIST coals. The USGS coal did not have sufficient levels of Phe loss by the 24-hour time point to make a reasonable comparison (Figure 5.1A).

In order to compare results from experiments of pyritic coal to pure pyrite from previous chapters, the pyrite content was estimated by multiplying the pyritic-sulfur content of each coal (Table 5.1) by the mass-fraction of pyrite to sulfur (i.e., 120 g mol^{-1} pyrite / 64.1 g mol^{-1} pyritic sulfur = 1.9). The resulting pyrite content in incubations of 100 g L^{-1} of coals 2684b, 2685b, 2692b, and USGS was 0.99 g L^{-1}, 2.3 g L^{-1}, 0.93 g L^{-1}, and 1.3 g L^{-1}, respectively. As performed in Chapter 2, a rate of ·OH formation relative to Phe loss (i.e., $\mathbf{K_{pyr}}$) was calculated based on a ***k'*** calculated from **t** = 0 – 48 hours for the three NIST coals (shorter period was used because the reactivity of both Phe and Tyr slowed significantly after 48 hours) and over the entire 336 hours for the USGS coal. Values of $\mathbf{K_{pyr}}$ for the pyritic coals presented in Table 5.1 are similar-to (USGS) or greater-than (NIST coals) $\mathbf{K_{pyr}}$ values determined for pure-pyrite samples in Chapter 2 (the highest $\mathbf{K_{pyr}}$ in Chapter 2 was 0.165 μmol g^{-1} hr^{-1}(Table 2.2)), suggesting a greater potential for ·OH production by the NIST coals than the pure-pyrite samples over the first 48 hours in solution.

In addition to high $\mathbf{K_{pyr}}$ values, the small amount of pyrite in the bituminous coal samples had a dramatic effect on the solution chemistry as the pH decreased significantly (from pH 5.5 to pH 2.8 – 4.1) within minutes of spiking, suggesting there may have been oxidation of pyrite surfaces in the coal prior to the experiment, which released acid into the aqueous phase.

However, the surface iron phases must not be so oxidized that ROS formation is inhibited as seen for samples of pure pyrite (Schoonen et al., 2010). Associated with production of hydroxyl radical over time, further oxidation of the pyrite was evidenced by progressive decreases in pH to levels between 2.6 and 2.9 at 336 hr. The apparent faster rates of ·OH formation and the greater decreases in pH relative to pyrite content may be due to a greater surface area of the framboial pyrite in the bituminous coals used in these experiments than the cubic pyrite used in experiments from Chapters 2 – 4. As shown in Chapter 2, the reactivity of pyrite is first-order with respect to surface area, which is likely true regardless of mineral morphology (though more tests would need to be conducted to confirm this).

The ratio of total-Tyr to initial Phe concentrations ($[\Sigma Tyr] / [Phe]_o$) peaked in the range of 8 – 12% in the four bituminous coal slurries (Figure 5.1B) – at or just-below levels attained in reactions in pyrite slurries (Chapter 2). One possible reason for a lower fractional amount of Tyr formation would be if some of the measured loss of Phe was attributable to sorption to coal. The amount of Tyr formed in these incubations were compared to the amount of fluorescein produced by the same coals in the study by Cohn et al. (2006). The amount of fluorescein generated after 24-hour incubations with APF indicated that: 19 g L^{-1} of coal 2684b produced 1.0 μM ·OH; 23 g L^{-1} of coal 2685b produced 1.6 μM ·OH; and, 30 g L^{-1} of coal 2692b produced 0.3 μM ·OH – which normalizes to roughly 5.3 μM, 6.9 μM, and1.0 μM ·OH in 100 g L^{-1} of each coal used in this work, respectively. Figure 5.1B shows that the [ΣTyr] at the 24-hour time point for coals 2684b, 2685b, and 2692b was 4.9 μM, 4.6 μM, and 3.9 μM respectively. It is interesting that despite likely differences in reaction yields and persistence of these products that these measures of ·OH are so similar. More surprising is that the APF experiments were conducted in phosphate buffer, which was seen to negatively affect ·OH formation in Chapter 4, and at a pH of 7.4, where a change in the time course of ·OH formation is noted below.

5.3.2 Effect of quenching agents

Results from experiments with β-ME or ethanol added to bituminous coal slurries of Phe are shown in Figures 5.4 and 5.5 (respectively). Surprisingly, even at a very high concentration of β-ME (1% by volume or 140 mM) loss of Phe was observed, though at a slower rate and to a

lesser extent (roughly 20% Phe loss in each coal slurry; Figure 5.4A). The formation of the three isomers of Tyr confirmed the loss of Phe was due to ·OH reaction (Figure 5.4B). The ratio of $[\Sigma Tyr] / [Phe]_o$ was 75% lower in the samples of 2684b and 2685b coals with β-ME added than without; whereas coals 2692b and USGS appeared less affected by β-ME with Tyr about 40% lower over the same 168-hour time frame (Figure 5.4B). The rate of Tyr formation in the 2692b coal slurry with β-ME was observed to be the same as the incubation without β-ME over the first 12 hours (Figure 5.1B). On the other hand, ethanol was much better at quenching the reaction. Only incubations containing 2684b and 2685b coals exhibited very small Phe loss with added ethanol (Figure 5.5A). Further evidence of ·OH activity was still observed in those two sample as the $[\Sigma Tyr] / [Phe]_o$ ratio slowly increased over the 168-hours, but only reached a high of less-than 1% (Figure 5.5B).

These are interesting results considering the limited amount of pyrite exposed in these coal samples relative to the pure-pyrite used in Chapter 2, where 0.1% of β-ME had prevented Phe degradation at the same $[Phe]_o$. Furthermore, the second-order rate constant for reaction with ·OH is 6.9×10^9 M^{-1} s^{-1} for β-ME (Jayson et al. 1971) and 2.0×10^9 M^{-1} s^{-1} for ethanol (Buxton et al. 1988) compared to 6.5×10^9 M^{-1} s^{-1} for Phe (Buxton et al. 1988). Based on the concentrations and rate constants of reagents, both β-ME and ethanol should have reduced the reactions between ·OH and Phe by more than 99%. It is not known why β-ME does not effectively quench these reactions, but in comparison to ethanol there are many reactions of thiol functional groups that may be important in coal matrices: 1) they undergo Michael additions with unsaturated bonds and have been shown to react with natural organic matrices (Zhang et al. 2004; Zheng et al. 2012); 2) coal matrices contain free radicals (e.g., stabilized by quinones), which may be transferred to thiols and can act as radical-transfer agents in solution (Struyk and Sposito 2001); and, 3) the thiol functional group preferentially interacts with exposed mercury in coal (which is present at mass-fractions in the 100 parts-per-million range (http://www.nist.gov/mml/analytical/inorganic/fossfuels.cfm -- accessed January 2012)). However, the inability of high concentrations of oxidizable organic compounds to quench reactions between ·OH and Phe also leads to the question about whether those reactions occur in the aqueous phase, which has been argued in Chapters 2 and 3. If on the other hand, more ·OH is formed and/or adsorbed at the pyrite surface than previously assumed (Chapter 2), one could

postulate a surface adsorption/complexation mechanism in which Phe reactions was more favored than reaction with ethanol and especially β-ME. The question would then need to be posed as to the reason coal matrix, with organic matter associated in direct contact with pyrite, leads to such differences in surface chemistry and preference for reaction with Phe. Ultimately, more experiments need to be conducted to better characterize competitive effects between different classes of organic compounds in coals, especially related to the reactivity of sulfur-containing organic compounds and their interactions in pyritic coals.

5.3.3 Effect of higher, stabilized pH on phenylalanine degradation kinetics

Slurries of coal 2684b were incubated with Phe at physiologically-relevant pHs of 4.5 and 7.4 that were held constant (via automated titration of NaOH) to compare rates of Phe loss to unadjusted slurries (Figure 5.6). Coal 2684b was chosen because it had the greatest rate of ·OH-formation (i.e., $\mathbf{K_{pyr}}$) relative to the other coals. The [Phe] was adjusted for addition of base at each time point according to a dilution factor shown in Table 5.2 and the calculated values are plotted in Figure 5.6A along with results with this coal (Figure 5.1A) from the first 48 hours of the unbuffered experiment where the pH dropped to 3.8 after a couple minutes and continued to decrease to levels below 3 over time. Loss of Phe was greatest when pH was held at constant 4.5 with an $\boldsymbol{R_o}$ of 3.98 μM hr^{-1} and had almost completely degraded by the 48-hour time point (Figure 5.6A). This $\boldsymbol{R_o}$ was double the rate of Phe degradation in the incubation of 2684b coal where pH was not maintained (Figure 5.1A). On the contrary, a slow, linear decay with an $\boldsymbol{R_o}$ of 0.60 μM hr^{-1} and a loss of about 40% was observed for Phe when pH was constant at 7.4 after 48 hours. Relative to the incubation in the reaction vial that drifted to pH < 3, it appears that ·OH-formation was favored at pH 4.5. This may be due to more optimal iron speciation that was reached at the pyrite surface affecting the H_2O_2 or ·OH production; more tests are needed to confirm this. It was similarly observed in Chapter 2 that a lowering of pH below 3 decreased the ·OH activity. Control samples at pH 4.5 and 7.4 (adjusted with HCl or NaOH respectively) with no pyrite were also run and experienced no loss in Phe or formation of Tyr over the 48-hour incubations (Figure 5.6).

The significantly higher rate of Phe degradation in the slurry at a constant pH of 4.5 was reflected by the formation and subsequent degradation of Tyr (Figure 5.6B). The observed $[\Sigma Tyr] / [Phe]_o$ pattern for the incubation at pH 4.5 was typical of pyrite-induced hydroxylation, where Tyr accumulation peaked at the time point just beyond the half-life of Phe (**t** = 24 hours), followed by loss of Tyr as the [Phe] continued to decrease through to 48 hours (Figure 5.6B). In the incubation of coal 2684b where the pH was not maintained, the [ΣTyr] increased more slowly than was observed in the pH 4.5 incubation, and then stabilized at later times consistent with patterns of [Phe], suggesting a decrease in ·OH activity in those incubations (Figure 5.1A and 5.6).

Incubation at a constant pH of 7.4 led to the greater production of Tyr after 1 – 2 hours than in experiments conducted at lower pH. However, the production peaked at the 2-hour time point with a Tyr-accumulation of roughly 3.3% of $[Phe]_o$ before tapering off (Figure 5.6B). This was unusual considering the [Phe] had not reached the half-life (only 25%-loss of $[Phe]_o$) by the 48-hour time point. The higher pH may have hindered the formation of H_2O_2 and/or ·OH, likely due to the greater oxidation potential creating more Fe(III) oxide patches on the pyrite surfaces (Schoonen et al. 2010), though the fate of Phe and Tyr as they continued to degrade is not clear. Unlike pyrite reactions in solutions of carbonate and other buffers that maintained pH in Chapter 4, formation of the three isomers of Tyr was observed, indicating that circum-neutral pH alone is not enough to stop ·OH from forming and reacting with Phe.

5.4 Summary

The rates of Phe degradation were successfully monitored in four samples of bituminous pyritic coal. Confirmation of ·OH reactivity was provided by formation of the three isomers of Tyr, and no Tyr was detected in slurries of the two sub-bituminous coals that had no pyrite content. Continued hydroxylation of Phe was observed for up to 14 days in coal samples with as little as 0.5% pyritic sulfur (or about 1% pyrite) by-mass. Although the observed rates of Phe degradation were slow, the initial rates of ·OH formation in the bituminous coals normalized to pyrite mass appear to be greater than in pure-pyrite used in all previous experiments from this study; perhaps partly due to greater surface area of framboidal pyrite in coal. Interestingly, the

coal samples used in these experiments were not treated with HCl prior as pyrite was in previous chapters, which means patches of Fe(III) oxides or other potentially interfering organic or inorganic coatings were not removed from the exposed pyrite surfaces. Given the acid released by the coals when mixed with water, the pyrite surfaces had presumably been partially pre-oxidized and continued oxidation was evident based on continued drop in pH. It is known that highly oxidized pure pyrite samples rapidly destroy H_2O_2 and are not effective at generating $^{\cdot}OH$ or other ROS (Schoonen et al. 2010). This suggests that the pyrite-fraction of coal (which had repeated contact with moist air), retained a sufficiently-reduced surface to form ROS, and as suggested by pH experiments, some oxidized iron patches on the surface may in fact promote ROS formation leading to $^{\cdot}OH$.

The rapid loss of Phe and *p*-Tyr observed in slurries of sub-bituminous coals 1635 and 2682b has been attributed to adsorption to the coal surfaces and not $^{\cdot}OH$, since Tyr formation was not observed in incubations with Phe. The lack of $^{\cdot}OH$ reactivity was not unexpected considering the lack of pyritic sulfur and results from the APF study by Cohn et al. (2006) (though adsorption of APF could not be determined due to its lack of fluorescence). The sorption of Phe and *p*-Tyr may be due to greater porosity in the relatively less-mature sub-bituminous coals, which are less dense than bituminous coals and have a different surface composition.

Ratios $[\Sigma Tyr] / [Phe]_o$ measured in incubations of bituminous coals 2684b and 2685b, with pyrite contents of 0.99% and 2.3% respectively, was not quite as high as measured (12 – 20%) in studies conducted with pyrite suspensions in pure water (Chapter 2) or dissolved HA (Chapter 4). This might be attributed, in part, to a modest amount of sorption contributing to the disappearance of Phe (well less than half) such that it was unavailable to be hydroxylated, possible differentness in mechanisms of reaction, or that the production of $^{\cdot}OH$ decreased before Tyr levels were able to peak. On the contrary, coal 2692b reached a $[\Sigma Tyr] / [Phe]_o$ ratio of 12% before $^{\cdot}OH$ formation appeared to decrease significantly and $[\Sigma Tyr]$ plateaued. Degradation of Phe in the USGS coal did not exceed 50% of $[Phe]_o$, though $[\Sigma Tyr]$ formation appeared to be trending towards a ratio higher than 2684b and 2685b (based on the amount of Phe lost and $[\Sigma Tyr]$ at the 336-hour time point). The low $[\Sigma Tyr] / [Phe]_o$ ratios observed in slurries of 2684b and 2685b coals may have been the result of other Phe interactions with the coal surface.

An analysis of Phe degradation rates relative to the sulfur and pyritic-sulfur content revealed that coal 2684b generated the greatest flux of ·OH, despite having a lower sulfur and pyrite content than coal 2685b. These findings are not entirely consistent with APF results of Cohn et al. (2006); however, the experimental conditions were not the same (i.e., APF experiments use phosphate buffer to achieve a pH of 7.4). Assuming that pyrite is the only source of ROS in these slurries, it is possible to compare pyrite mass normalized rates of hydroxyl radical production between coals and pure pyrite samples characterized in Chapters 2 – 4. Despite the fact that some fraction of the pyrite is embedded in the coal matrix and not in contact with water, the results from the three NIST-bituminous coal samples yielded higher $\mathbf{K_{pyr}}$ values than obtained for any of the pure pyrite samples characterized in Chapter 2. Future work to reconcile the differences in relative rates of Phe loss may benefit from estimating pyrite surface area at the coal surface using theoretical calculations based on scanning electron microscopy. It may also be useful to examine the elemental composition of these naturally occurring pyrites to determine the importance of other trace metals that may be present.

Continued Phe hydroxylation in pyritic coal slurries despite the addition of high concentrations of β-ME was quite interesting. Addition of ethanol was much more effective at quenching the reactions, although formation of Tyr appeared after several hours in two of the coal samples, and at levels much-lower than in incubations with β-ME or without quenching agent added. Although the Fenton reaction has been quenched by these solvents in previous chapters, the properties of the coal surface and/or dissolved organics has significantly hindered their ability to compete with Phe for ·OH. There is a potential for β-ME to react in many ways and its actual concentration in coal slurries should be monitored and reactivity better characterized. The inability of high concentrations of quenching agents (in particular β-ME) to completely halt the hydroxylation reactions attributed to ·OH was an unexpected result that opens up the possibility that there may be important alternative reaction mechanisms that need investigation (e.g., there may be more surface-bound ·OH formed and available for reaction than previously thought).

Results obtained from incubating pyritic coal with Phe at constant pH are significant to human-health studies related to respiratory illnesses resulting from the inhalation of coal dust (Demers and Kuhn 1994; Moller et al. 2010; Vallyathan 1994). Formation of ·OH was observed

at physiologically-relevant pH of 4.5 and 7.4, as evidenced by the three isomers of Tyr. The fact that the Phe degradation rate was highest at pH 4.5 is important from a health perspective as this pH was chosen to represent a phagocytic response in the presence of foreign matter (Demers and Kuhn 1994), which also includes the production of H_2O_2 that can increase reactivity of the pyrite component of coal even more (Chapter 3). Incubation at constant pH 7.4 compliments past research at the same pH that show significant amounts of ·OH may result from particles that have the potential of lodging deep in the alveoli of the lungs. The total amount of Phe degradation after the first few hours appeared equivalent to the amount of Tyr formed and was close to the 3 μM of ·OH observed in with APF (Cohn et al. 2006a), and the initial burst of ·OH is consistent with work recently published by Harrington et al. (2011) that showed a similar spike in H_2O_2 formation in simulated lung fluid. This suggests that the redox potential between the reduced iron at the surface and the high pH of the solution may be more of an initial health threat than suggested by results presented in Chapter 4.

This work has shown that pyritic coal particles exposed to oxygenated solutions can generate ·OH for days at under acidic pH conditions, despite a diminished amount of reduced pyrite at the surface (Zhu et al. 2002). Previous studies have implicated ROS in coals slurries (Cohn et al. 2006a) and *in vitro* (Demers and Kuhn 1994); but for the first time, the kinetics of ·OH formation and fate were monitored over an extended time frame, using Phe as a probe. Importantly, the results that show Phe hydroxylation for 14 days in USGS coal and the increased ·OH formation at constant pH 4.5 together indicate a serious potential for long-term exposure issue in cellular matrices. Continued research into the mechanisms of reactivity with respect to coal surface structure, pyritic-sulfur and iron compositions, and properties of the organic matter fraction are certainly warranted and can help advance the understanding of stressors on human physiology.

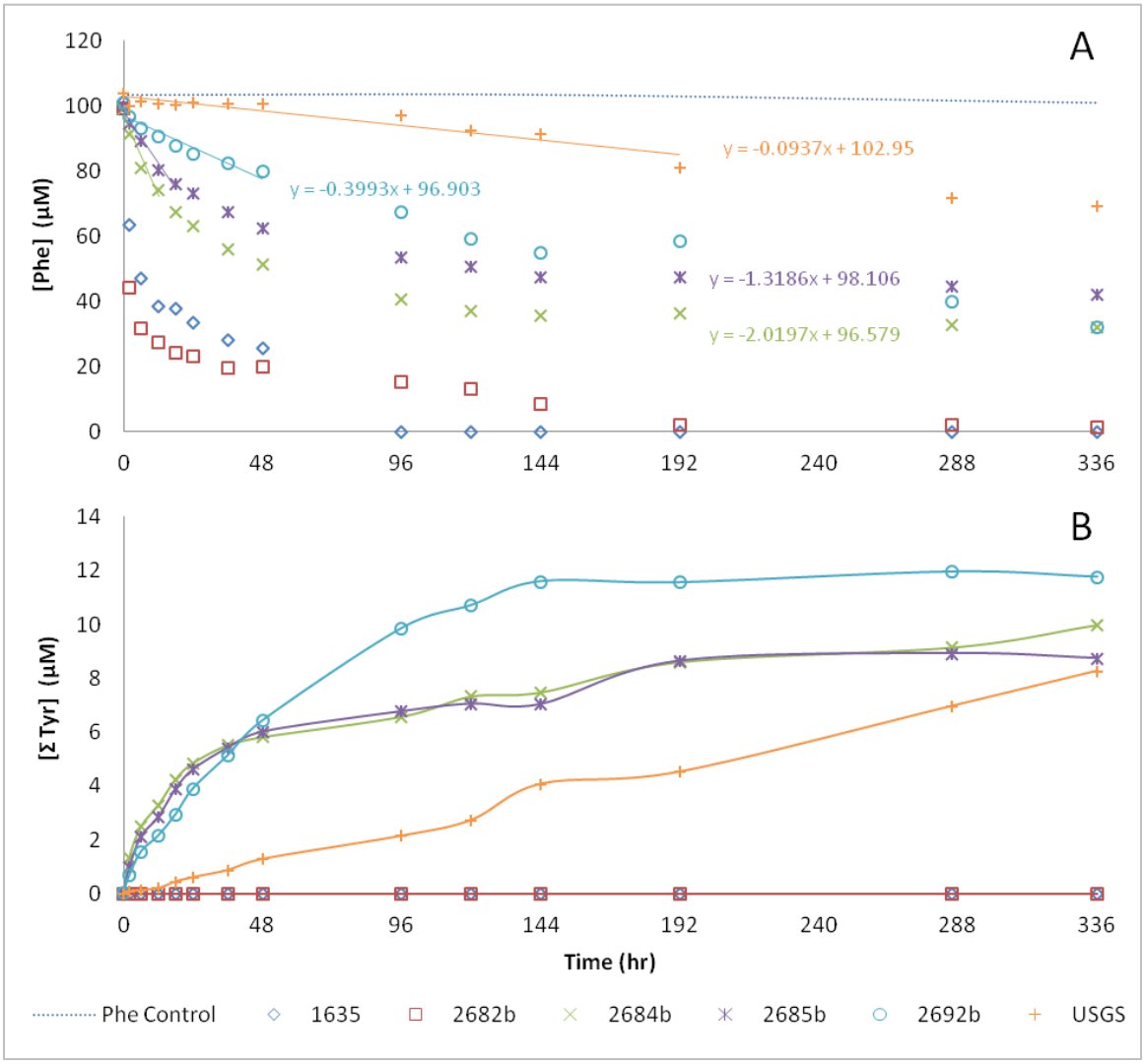

Figure 5.1. Concentrations of Phe and Tyr in coal slurries through time. (**A**) Loss of Phe was greatest in sub-bituminous coals 1635 and 2682b (likely due to adsorption). Degradation of Phe in slurries of bituminous coals 2684b, 2685b, and 2692b was initially rapid, followed by a period of inactivity starting around 96 hours. USGS coal continued to degrade Phe throughout the 336 hours of the experiment. (**B**) Formation of the three isomers of Tyr confirms ·OH presence in the bituminous coal slurries, and the Tyr pattern through time follows the Phe loss closely, as seen in previous experiments.

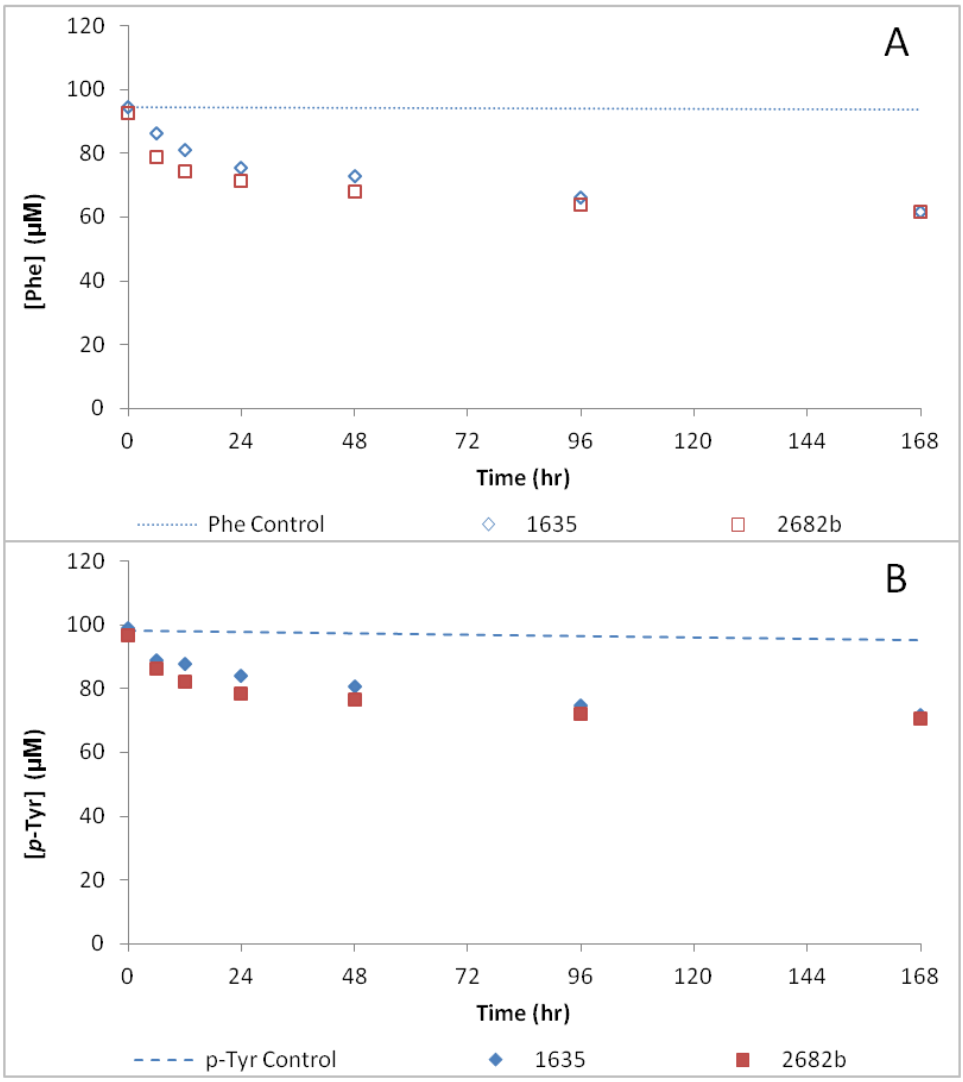

Figure 5.2. Phe and *p*-Tyr in sub-bituminous coal slurries. Loss of 100 µM (**A**) Phe and (**B**) *p*-Tyr in 10 g L^{-1} slurries of sub-bituminous coal samples were roughly the same. The concentration of each amino acid decreased over the first 24 hours, then remained constant through to the end of the experiment. The initial rate, relative to those at higher coal loadings, along with lack of reaction products, support the theory that Phe is adsorbing rather than reacting in slurries of 1635 and 2682b coals.

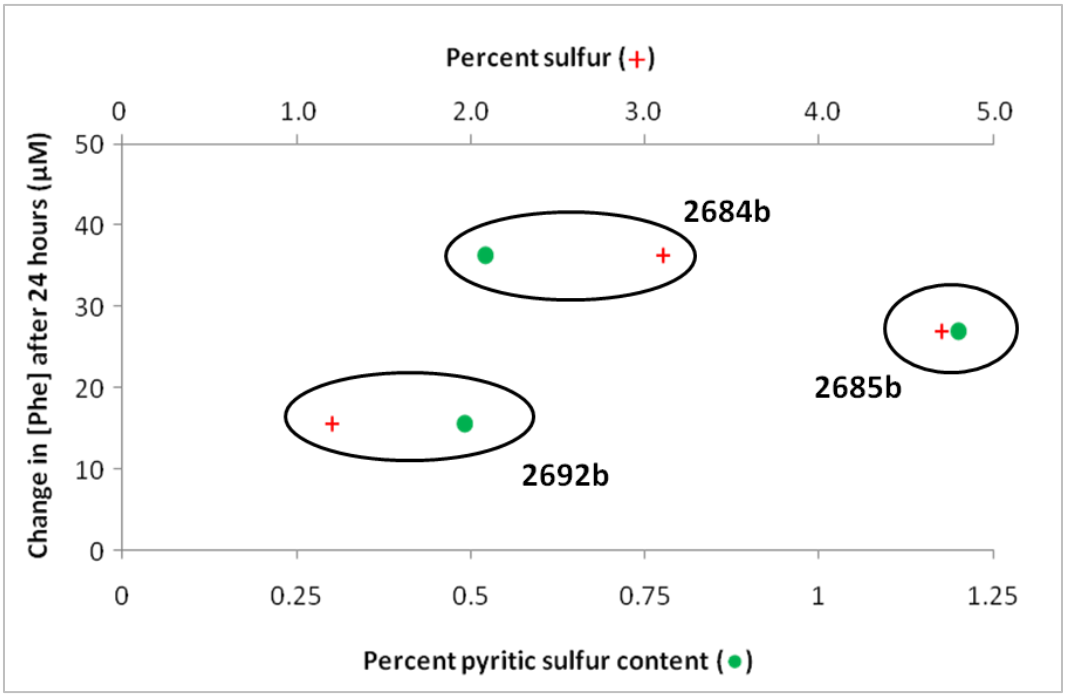

Figure 5.3. Change in Phe concentration relative to pyritic sulfur and sulfur content of the bituminous NIST coals. The change in [Phe] after the first 24 hours are plotted with respect to both pyritic sulfur and sulfur content for coals 2684b, 2685b, and 2692b (Table 5.1). The slurry of 2684b coal induced the greatest change in Phe despite having less than coal 2685b.

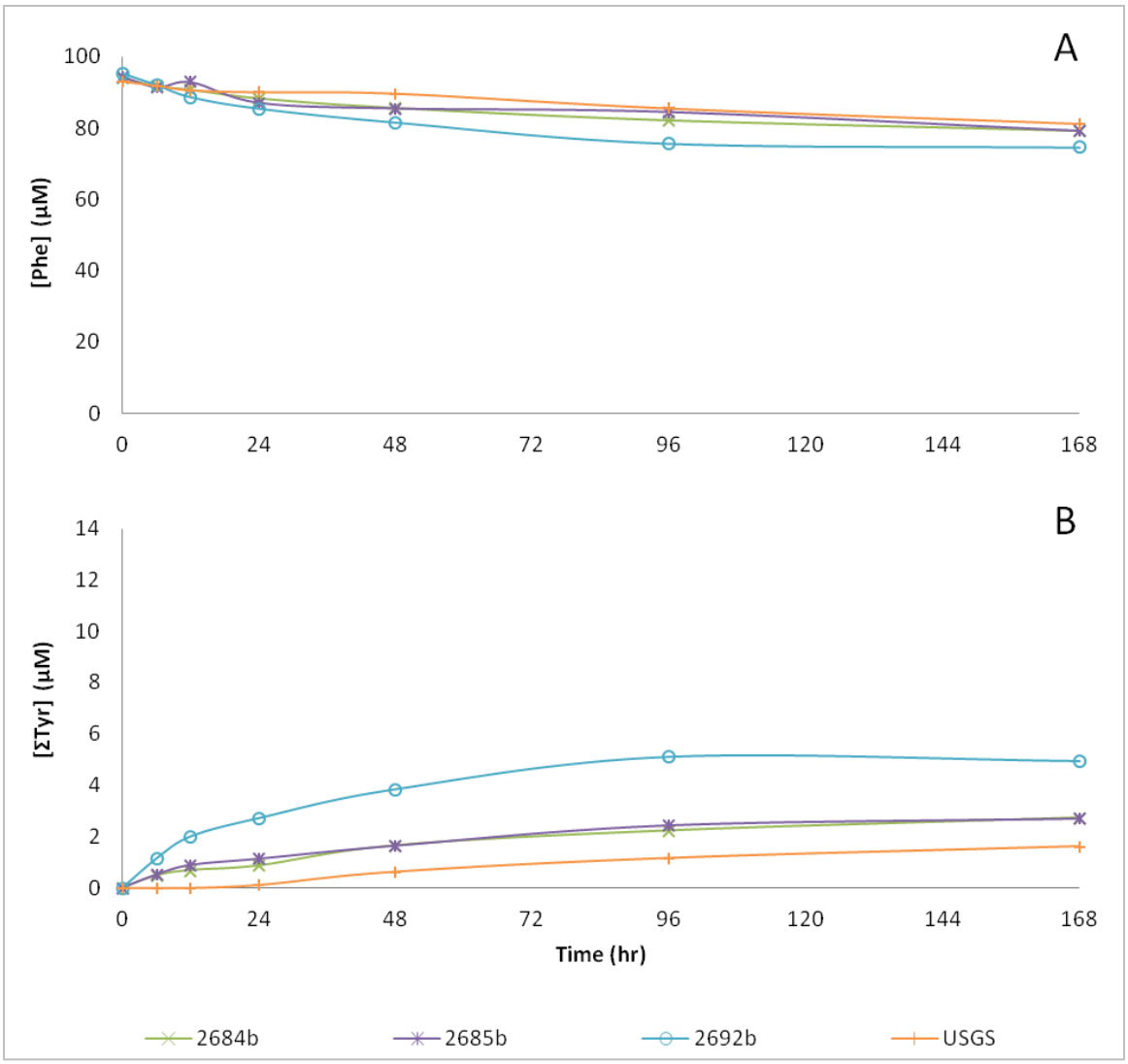

Figure 5.4. Phe loss and Tyr formation in coal slurries containing β-ME. (**A**) Minimal degradation of Phe (≤ 20%) was observed in each of the four bituminous coal slurries when 1% β-ME by-volume was added. (**B**) Surprisingly, a significant level of Tyr was still observed in all incubations.

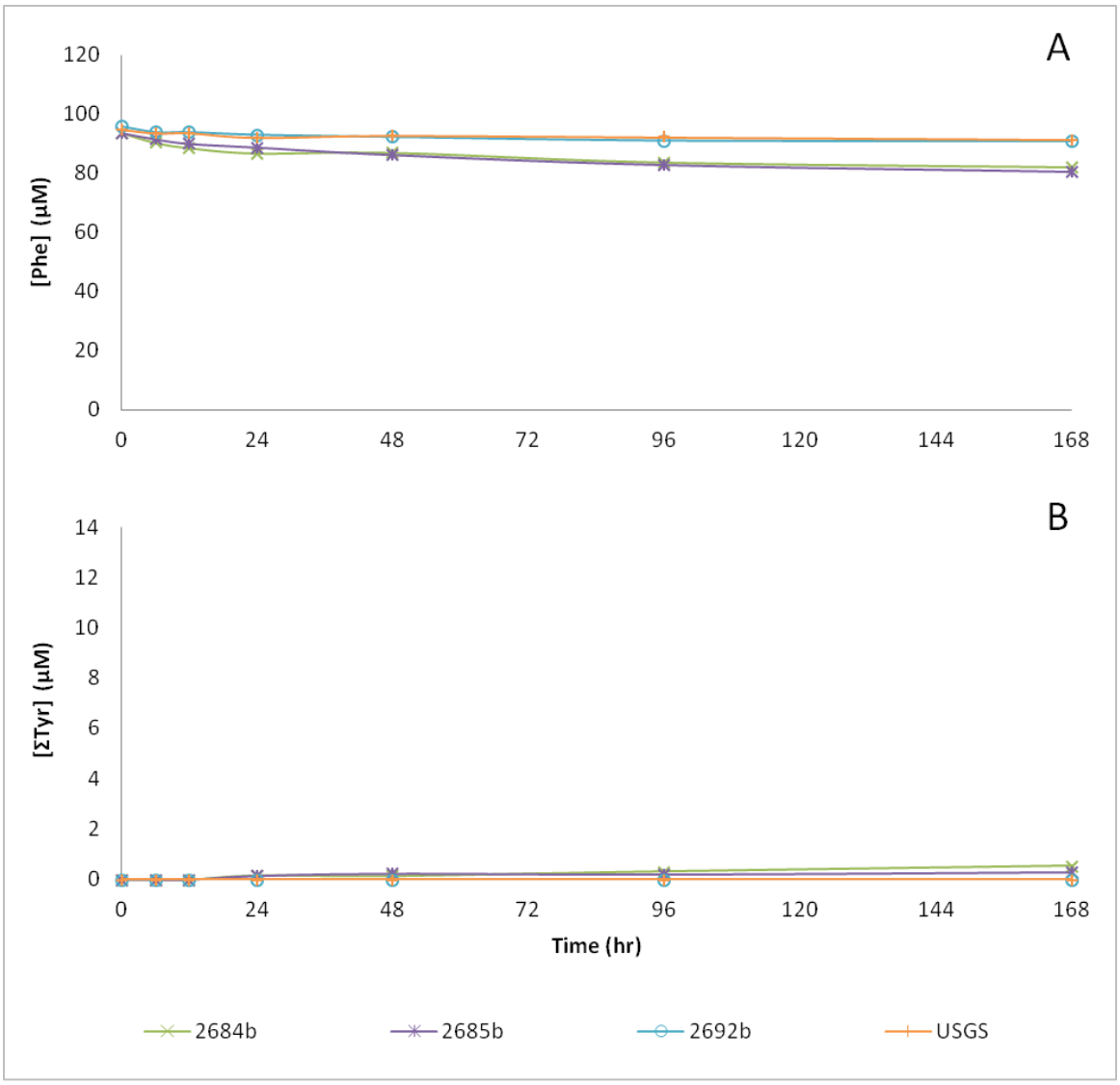

Figure 5.5. Phe loss and Tyr formation in coal slurries containing ethanol. (**A**) Roughly 20% loss of Phe was observed when 1% ethanol by-volume was added to slurries of 2684b and 2685b coals. (**B**) A low, but quantifiable amount of ΣTyr (≤ 1 µM) was observed in slurries of 2684b and 2685b despite the presence of ethanol as a quenching agent.

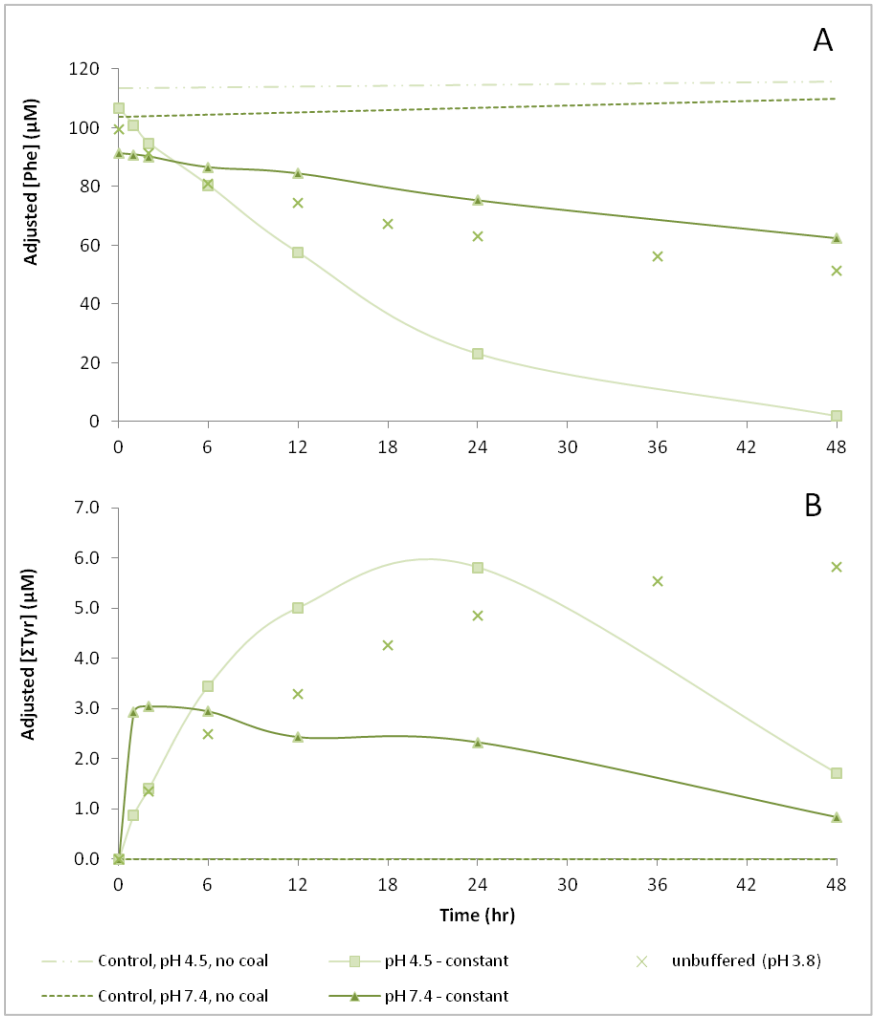

Figure 5.6. Loss of Phe and formation of Tyr in coal slurries at constant pH. Reactions at a constant pH of 4.5 and 7.4 were diluted to different extents at different time points by the addition of NaOH; therefore, the concentrations of Phe and ΣTyr at each time point have been adjusted according to the corresponding dilution factor shown in Table 5.2. (**A**) Rates of Phe loss was greatest with a slurry pH of 4.5, suggesting that the low pH generated when pH is not stable hinders ROS production to some degree at high coal loadings (100 g L^{-1}). (**B**) The [ΣTyr] in the pH 4.5 slurry reached the same level as the unbuffered reaction. Formation of [ΣTyr] in the slurry at pH 7.4 only reached half the levels in the pH 4.5 slurry and did not follow the typical pattern of peaking around the half-life of Phe.

	%-pyritic sulfur (by mass) †, ††	%-sulfur (by mass) †	%-iron (by mass)†	Surface Area ‡ (m^2 g^{-1})	Coal Classification †	Type of Phe loss	Tyr formation	relative R_o	K_{pyr} (µmol g^{-1} hr^{-1})
NIST 1635	0	0.36	0.24	1.79	Sub-Bituminous	adsorption likely	no	very fast	--
NIST 2682b	0.01	0.49	0.24	4.92	Sub-Bituminous	adsorption likely	no	very fast	0
NIST 2684b	0.52	3.1	1.5	2.11	Bituminous	hydroxylation, maybe some adsorption	yes	fast	1.3
NIST 2685b	1.2	4.7	3.9	1.72	Bituminous	hydroxylation, maybe some adsorption	yes	fast	0.39
NIST 2692b	0.49	1.2	--	1.35	Bituminous	hydroxylation	yes	fast	0.43
USGS CLB-1	0.67	1.5	0.9	--	Bituminous	hydroxylation	yes	slow	0.08

† - Certificate of Analysis (http://www.nist.gov/mml/analytical/inorganic/fossfuels.cfm -- accessed January 2012)

‡ - Cohn et al. 2006 (NIST)

†† - Lyons et al. 1989 (USGS)

Table 5.1. Coal attributes and incubation results. The available pyritic sulfur, sulfur, and iron content – all percent (%) by mass – as well as the classification are listed for each coal. The surface areas were determined by Cohn et al (2006). The mechanism for Phe loss was mixed as hydroxylation to the three isomers of Tyr was only observed in slurries of the bituminous coals. Initial rates of Phe loss ($\boldsymbol{R_o}$) were greatest in sub-bituminous coals, hypothesized to be a result of adsorption to the coal surface; whereas the $\boldsymbol{R_o}$ in the NIST bituminous coals were fast relative to reaction in the USGS coal. The $\mathbf{K_{pyr}}$ was estimated for each of the bituminous coals based on their pyritic sulfur multiplied by the mass-fraction of sulfur-to-pyrite.

Time (hr)	dilution factor	
	pH 4.5	pH 7.4
0	0.997	0.668
1	0.993	0.660
2	0.991	0.660
6	0.979	0.660
12	0.951	0.660
24	0.893	0.660
48	0.836	0.660

Table 5.2. Dilution factors in constant-pH experiment. The calculations for [Phe] and pyrite loading at each time point were adjusted according to the dilution factor, which was based on the total volume of 0.1 M NaOH added to the reaction vessel to that time point.

Chapter 6

PHENYLALANINE LOSS IN THE PRESENCE OF MANGANESE OXIDES

6.1. Introduction

Manganese oxide minerals (MnO_x) have been the focus of many studies related to the oxidation of organic compounds in aqueous suspensions (Chien et al. 2009; Stone and Morgan 1984b; Wang and Stone 2006; Watts et al. 2005a; Zhang and Huang 2005). The oxidation of organic compounds occurs in conjunction with reductive dissolution of the mineral, releasing dissolved manganese (Mn^{2+}) following the transfer of one or two electrons depending on the oxidation state of manganese (Mn(III) or Mn(IV) (Equations 6.1 and 6.2)).

$$>MnOOH + 3\ H^+ + e^- \rightarrow Mn^{2+}{}_{(aq)} + H_2O \quad (6.1)$$

$$>MnO_2 + 4\ H^+ + 2\ e^- \rightarrow Mn^{2+}{}_{(aq)} + H_2O \quad (6.2)$$

Rates of reductive dissolution have been shown to depend on pH (Zhang and Huang 2003a), dissolved manganese concentration (Zhang and Huang 2005), and redox potential of the organic compound (Stone and Morgan 1984a). Furthermore, transfer of electrons (Equations 6.1 and 6.2) from the compound to the manganese occurs at the surface, and intermediates that are thought to include radical species have been postulated (Pratt and Suskind 1963; Wang and

Stone 2006). Of relevance to this dissertation, several recent studies have implicated hydroxyl radical ($^{\cdot}OH$) formation in MnO_x slurries (when mixed with hydrogen peroxide (H_2O_2) creating Fenton-like conditions) as a possible mechanism for oxidation of compounds (Tizaoui et al. 2010; Watts et al. 2005a), though degradation products were not necessarily specific to reaction with $^{\cdot}OH$. Therefore, phenylalanine (Phe) was employed to assess the potential for $^{\cdot}OH$ formation in MnO_x slurries.

Minerals of manganese oxides MnO_x are prevalent as amorphous soil coatings (Risser and Bailey 1997) and in deposits formed by biological and geological processes (Greene and Madgwick 1991), and are mostly found in the +2, +3, and +4 manganese oxidation states (Post 1999). Manganese-oxide ores are mined from mineral deposits for use in high-strength steel (Post 1999). MnO_x are synthesized for industrial applications that require precise control over crystal structure and metal content, such as for production of batteries (Liu et al. 2012; Xi et al. 2012). Inhalation of fine MnO_x particles by factory workers and miners has been linked to a number of respiratory and neurological (such as Parkinson's disease) impacts stemming from irritation of the lungs and increased levels of Mn^{2+} in the body (Elder et al. 2006; Roels et al. 1992). Furthermore, the immune response to MnO_x dust triggers formation and release of H_2O_2 by phagocytes (Moller et al. 2010), which can cause additional damage to lung tissue.

The strong oxidizing potential of MnO_x has been studied for use as a remediation tool for environmental contamination such as industrial waste (e.g., carbon tetrachloride and chlorinated phenols (Ulrich and Stone 1989; Watts et al. 2005a)) and antimicrobial agents (e.g., triclosan and fluoroquinolones (Zhang and Huang 2003a; Zhang and Huang 2005)). Proposed systems involve natural and synthetic MnO_x alone, or in conjunction with added Fenton and Fenton-like reagents (Watts et al. 2005b), which might involve approaches similar to those that could be employed with pyrite (as discussed in previous chapters). However, unlike pyrite, MnO_x have not been shown to spontaneously generate H_2O_2 (a precursor to the Fenton reaction).

The degree of reactivity of various compounds in MnO_x slurries depends on their molecular structure. The reactivity is attributed to the differences in redox potential between the compound and the MnO_x, and it has been shown that transfer of electrons from the organic

compound is catalyzed by surface interactions and requires some extent of adsorption to the mineral (Stone and Morgan 1984a). Initial interaction of an organic compound with the MnO_x surface ($>Mn^n O_x H$) can form by either a "bonded mechanism" with the manganese directly to induce the transfer of electron(s) to the surface directly (Equation 6.3) or a "non-bonded mechanism" where the organic compounds essentially sorbs to the mineral (Equation 6.4), depending on its molecular structure (Stone and Morgan 1984a).

$$>Mn^n O_x H + RH_{(aq)} \rightarrow >Mn^n O_{x-1} R + H_2O \quad (6.3)$$

$$>Mn^n O_x H + RH_{(aq)} \rightarrow >Mn^n O_x H \text{ -- } RH_{(ad)} \quad (6.4)$$

Note equations 6.3 and 6.4 do not induce a change in manganese oxidation state. Subsequent oxidation of the bonded substrate (R) (Equation 6.3) then occurs, leading to the reduction of manganese. Reaction of the sorbed complex (Equation 6.4) is believed to occur through an intermediate which generates a radical species (Pratt and Vandecasteele 1961; Pratt and Suskind 1963; Stone 1987; Zhang et al. 2008).

$$>Mn^n O_x H \text{ -- } RH_{(ad)} \rightarrow >Mn^{(n-1)} O_x H \text{ -- } R^{\cdot}_{(ad)} + H^+ \quad (6.5)$$

The adsorbed radical species ($R^{\cdot}$) may continue to react at the surface or desorb into solution (Zhang et al. 2008) (Equation 6.5).

$$>Mn^{(n-1)} O_x H \text{ -- } R^{\cdot}_{(ad)} \rightarrow >Mn^{(n-1)} O_x H + R^{\cdot}_{(aq)} \quad (6.6)$$

Subsequent reactions of $R^{\cdot}$ in Equations 6.5 and 6.6 ultimately leads to the oxidation of the reactant and release of Mn^{2+} into solution, where there is speculation Mn^{2+} could participate in Fenton-like reactions.

Some studies suggest that Fenton-like reactions with Mn^{2+} and H_2O_2 are not favorable, indicating that there is a far greater potential to reduce H_2O_2 to water and molecular oxygen then to generate $^{\cdot}OH$ (Kumara et al. 2011; Stadtman et al. 1990). Another study attributed loss of 1-hexanol, and concurrent evolution of carbon dioxide (CO_2), to the formation of $^{\cdot}OH$ during incubations of MnO_2 or Mn^{2+} (each with added H_2O_2). However, oxidation of aliphatic alcohols

at the surface of MnO_2 have been shown to form aldehydes or ketones (Pratt and Vandecasteele 1961), which could subsequently be further oxidized to CO_2 (Cheney et al. 1996). It has also been hypothesized by Schoonen et al. (2006) that dissolved Mn^{2+} adsorbs to the MnO_x and may induce ROS formation by shifting the oxidation potential at the surface.

The compounds shown to oxidize in the presence of MnO_x in previous studies do not appear to have specific products that could implicate ·OH over other oxidation mechanisms. Therefore, experiments were conducted with Phe in suspensions of MnO_x to determine if the characteristic hydroxylation products – *ortho*-, *meta*-, and *para*-tyrosine (Tyr) are produced. Four synthetic MnO_x with various oxidation states were incubated with Phe to assess their potential for ·OH formation: manganese(II) oxide (MnO), manganese(III) oxide (Mn_2O_3), lithium manganese(III, IV) oxide ($LiMn_2O_4$), and MnO_2. Suspensions of MnO_x were tested in pure water as well as in simulated lung fluid (SLF) at biologically-relevant pH 4.6 and 7.4. Fenton-like conditions were also simulated in slurries and solution through addition of Mn^{2+} and/or H_2O_2 at low pH.

Concurrent experiments in a collaborating lab with samples of these four MnO_x were also run with the fluorogenic probe 3´-(*p*-aminophenyl) fluorescein (APF) (developed to quantify ·OH formation *in vivo* and *in vitro* during cell studies and adapted by Cohn, et al. (2009) to specifically detect ·OH in pyrite and coal slurries) to compare results and quantify potential ·OH formation (Hylton et al. unpublished). Preliminary results from the work with APF suggest that MnO_x slurries produce high levels of ·OH at circum-neutral pH without the addition of H_2O_2. These were promising results for work with Phe to confirm the presence of ·OH formation and determine reaction kinetics in various MnO_x slurries. However, the use of Phe did not suggest the same ·OH-mechanism in MnO_x slurries as did APF, and the differences in results are interpreted in this chapter.

6.2. Methods

All four batches of synthetic MnO_x were acquired from Alfa Aesar (Ward Hill, MA) and used as is without chemical pretreatment (i.e., no acid wash as was done with pyrite (Chapters 2 – 4)). Surface areas of Mn_2O_3 and MnO_2 were measured by BET analysis to be 2.1 $m^2\ g^{-1}$ and 0.81 $m^2\ g^{-1}$ respectively. Samples of Mn_2O_3 and MnO_2 were also ground with a mortar and pestle to increase the surface areas to 2.6 $m^2\ g^{-1}$ and 1.7 $m^2\ g^{-1}$ (respectively). Phenylalanine, *para*-tyrosine, *ortho*-tyrosine, beta-mercaptoethanol (β-ME) were obtained from Alfa Aesar. *meta*-Tyrosine was obtained from TCI America (Portland, OR). Hydrogen peroxide (30% w/w) and manganese fluoride (MnF_2) was acquired from Sigma Aldrich (St. Louis, MO). Components for the simulated lung fluid (SLF) were all 99% ACS-grade from Sigma Aldrich: glycine, sodium chloride, sodium citrate, sodium bicarbonate, sodium carbonate, sodium dihydrogen phosphate, ammonium chloride, and calcium chloride. Formalin (37% formaldehyde and 5% methanol by volume) and trace-metal grade hydrochloric acid (HCl) was obtained from Fisher Scientific (Pittsburgh, PA). Uniformly-labeled ^{14}C-Phe and Ultima Gold™ M liquid scintillation cocktail was obtained from Perkin Elmer (Waltham, MA). Methanol was GC^2-grade from Burdick & Jackson (Morristown, NJ). Formic acid was ACS-grade from EMD Chemicals (Gibbstown, NJ). All water used for cleaning, standards, reactions, dilutions, and chromatography work was purified with a Milli-Q filtration system (Millipore Corporation, Billerica, MA) to a resistivity of 18.3 $M\Omega\ cm^{-1}$.

6.2.1. Phenylalanine in manganese oxide slurries

Incubations of Phe in MnO_x slurries were conducted in a similar manner as with pyrite from previous chapters. Stock solutions of 2 mM Phe were created prior to the experiment and diluted to an initial Phe concentration ($[Phe]_o$) of 100 μM. In incubations where multiple time points were collected, 100 $g\ L^{-1}$ MnO_x was added to 15 mL disposable centrifuge tubes to start the reaction. The initial pH of 5.5 did not change upon addition of any MnO_x, and initial stock solutions of Phe were adjusted in some experiments using HCl to decrease the pH. Incubations of MnO_x with 0.1% β-ME (by volume) added, which increased the pH to around 10 in all four slurries, were also run.

Volumes in reaction vessels were at-least four times that of the total volume of aliquots taken as samples for all time points combined. Tubes were simultaneously set to rotate end-over-end on a carousel at a constant 24 rotations-per-minute after solutions had been added to all vials. Samples were kept at room temperature of 25° ± 2° Celsius and covered with aluminum foil to prevent light exposure. In all experiments, 300 µL was extracted at predetermined time points from the reaction vials and immediately transferred to a nylon Costar® 0.22 µm centrifuge vial filter (Corning Life Sciences, Lowell, MA) and 5 µL of β-ME was then added, followed by a brief centrifugation. Preparation of samples for HPLC analyses were conducted as outlined in Chapter 2 Methods section.

6.2.2. Phenylalanine in dissolved manganese solutions

Stock solutions of Phe, 2 mM MnF_2, and 10 mM H_2O_2 were diluted to a final concentration of 100 µM Phe, 200 µM Mn^{2+} and 100 µM H_2O_2. The pH was adjusted to 3.2 with HCl in some incubations to improve the potential for Fenton-like reactions (as per Watts et al. (2005a)). Reactions were started by the addition of H_2O_2 to sets of 2 mL micro-centrifuge vials (each set comprised of six vials of the same conditions) and were simultaneously set to rotate end-over-end on a carousel at a constant 24 rotations-per-minute. Samples were at room temperature of 25° ± 2° Celsius and covered with aluminum foil to prevent light exposure. At time points of 0, 1, and 4 hours, two reaction vials from each set were quenched with β-ME. Duplicate reaction vessels were run for each set of conditions, and controls without MnF_2 were run with Phe in water and with H_2O_2, both adjusted to a pH 3.2. Tubes were briefly vortexed and aliquots of 50 µL were removed and added to a solution of methanol (50 µL), formic acid (5 µL), and water for a total volume of 1 mL an HPLC vial for analysis.

6.2.3. Radio-labeled phenylalanine incubations

A stock solution was prepared with 19 µL of 0.1 µCi μL^{-1} ^{14}C-Phe (450 µCi $mmol^{-1}$) for a count of 192 dpm μL^{-1}, or 89.6 µCi L^{-1}. Incubations were run in 2 mL micro-centrifuge tubes with 100 g L^{-1} Mn_2O_3 or MnO_2 and a final Phe count of 96 dpm μL^{-1}, or 44.8 µCi L^{-1} (or a $[Phe]_o$ of roughly 100 µM). A total of 6 vials were incubated for each MnO_x for time points up to 48 hours. Incubation conditions and sample preparation for HPLC analyses were conducted as outlined above.

6.2.4. Simulated lung fluid

The recipe for SLF was taken from Eastes and Hadley (1995) and is the equivalent to the solution used in Chapter 4 that contained formalin. Some of the stock SLF (pH 7.4) was split and the pH lowered to 4.6 using HCl to represent the pH within a lysosome of phagocytes (Nyberg et al. 1992). A stock solution of 2 mM Phe was added directly to SLF solutions in 15-mL centrifuge tubes for a final $[Phe]_o$ of 100 µM. Samples of the ground Mn_2O_3 and MnO_2 were added at 100 g L^{-1} to each reaction vessel to start the reaction. Incubations of Phe with added H_2O_2 (simulating phagocytic response to foreign particles) were also run. A total of 11 aliquots were collected over 168 hours. None of the reaction vessels with SLF solutions and MnO_x exhibited a change in pH during the experiments. Incubation conditions and sample preparation for HPLC analyses were conducted as outlined above.

6.2.5. Analyses

Analyses of non radio-labeled Phe in MnO_x slurries and MnF_2 solutions were conducted using a Waters Corporation (Milford, MA) Alliance® 2695 HPLC coupled to a Waters Corporation Micromass LCT Time-of-Flight Mass Spectrometer (ToF-MS) as described in the Methods section of Chapter 2. An extended-HPLC method was also run using the same Phenomenex (Torrance, CA) Luna® C18(2) HPLC column and column temperature (40°C), though the gradient containing methanol (Solvent A) and 10 µM ammonium formate/formic acid

in water (pH = 3.5) (Solvent B) was modified. Total run time was 22 minutes with a gradient of: 10% to 70% Solvent A over 8 minutes; isocratic at 70% Solvent A for 6 minutes; 70% to 10% in 4 minutes; followed by a re-equilibration time of 4 minutes.

The ^{14}C-Phe samples were analyzed with a Packard Flo-One®/Beta in-line Radioisotope detector model 515A which was coupled to a Hewlett-Packard 1050 HPLC (Agilent Technologies, Santa Clara, CA). The same extended HPLC method was run to detect additional degradation products not ionizable by the mass spectrometer under the positive electrospray (ESI+) method. The beta-detector flow cell had a capacity of 500 µL and was run at a flow rate of 1:3 HPLC (mobile phase) to scintillation fluid. The detection limit of the beta-detector was 3 dpm μL^{-1}, or 1.4 µCi L^{-1}, with of sample 50 µL injected. Standard calibration curve ranged from 3 dpm μL^{-1} to 192 dpm μL^{-1} (150 dpm to 9600 dpm total on-column injection).

6.3. Results and Discussion

6.3.1. Phenylalanine in manganese oxide slurries

6.3.1.1. Manganese oxides in pure water and mercaptoethanol solution

The concentration of Phe decreased through time in two of the four MnO_x slurries in pure water (Figure 6.1). In each of these experiments the pH remained close to 5.5 over the time course of the incubations. Linear degradation of Phe in the reaction mixture containing Mn_2O_3 (Mn(III)) was observed over the course of the experiments with an initial rate ($\boldsymbol{R_o}$) (defined in Chapter 2 as the zero-order rate determined to 20% of initial Phe loss) of 0.38 µM hr^{-1}. The overall loss of Phe with time could be described with a pseudo first-order rate constant (***k'***) (exponential fit through to 90% of Phe loss when possible) of 0.004 hr^{-1} (Figure 6.1A). Loss of Phe was greater in MnO_2 (Mn(IV)) slurries with a $\boldsymbol{R_o}$ of 1.5 µM hr^{-1} and a ***k'*** of 0.011 hr^{-1} (Figure 6.1A). There was no loss of Phe observed in slurries containing MnO (Mn(II)) or $LiMn_2O_4$ (Figure 6.1A). Thus, degradation of Phe was only observed when added to pure MnO_x phase containing oxidized forms of manganese that have the potential to be reduced by organic

compounds like Phe. Control vials containing Phe without MnO_x also exhibited no loss over the incubation period of the experiment. No Tyr formation was observed in slurries of MnO_x where Phe loss occurred, suggesting that the loss from Phe was not due to reaction with ·OH.

Reactions of Phe were not observed in the incubations of Mn_2O_3, MnO_2, or $LiMn_2O_4$ with added β-ME (Figure 6.1B). It should be noted, however, that the addition of β-ME caused an increase of the pH to around 10 by the first time point (2 hours) and may be the reason for decreased Phe activity in slurries of Mn_2O_3 and MnO_2 (the affect of pH will be discussed later in the section). There was considerable loss of Phe in the reaction vial containing MnO and β-ME (Figure 6.1B), although any interpretation of this loss is questionable because of profound changes in mineral surface phases that were indicated by formation of opaque, milky-pink solutions. It is noted however, that no Tyr formation was observed. Clearly, the role that β-ME in these incubations with MnO is much more than as a quenching agent for ·OH. It is unclear at this time if the apparent loss of Phe in the slurry of MnO and β-ME was the result of redox chemistry and/or adsorption to the surface of the MnO or precipitates. Further work would be needed to determine the reactions occurring in solutions of Phe, MnO, and β-ME. It is recommended that other compounds, such as ethanol, be used as ·OH quenchers in any future studies aimed at understanding the production of ROS in experiments with MnO_x.

It could not be confirmed by incubations of MnO_x in pure water whether degradation was occurring in the aqueous phase or at the MnO_x surface (although hydroxylation via aqueous-phase ·OH was ruled out as no Tyr was formed). Most reports indicate that MnO_x reactions occur at the surface, and that the rate of reactivity can change based on pH (Huang et al. 2005; Rubert and Pedersen 2006). One study states that ·OH is only formed through the Fenton-like reaction (in MnO_x or in solution) at pH < 5.5 (Watts et al. 2005a). If this is true, hydroxylation of Phe to Tyr would occur if the pH was lowered and H_2O_2 added to the MnO_x slurry.

6.3.1.2. Effect of added hydrogen peroxide and a lower pH

The addition of 100 μM H_2O_2 and a decrease in pH to 3.2 (via addition of HCl) was tested in slurries of Mn_2O_3, MnO_2, and $LiMn_2O_4$ to determine if H_2O_2 can enhance the degradation of Phe beyond what was observed in the previous experiment. Figure 6.2 shows the same steady loss of Phe in slurries of Mn_2O_3 and MnO_2 over the 24-hour period regardless of the added H_2O_2. Loss of Phe was not observed in $LiMn_2O_4$ slurries or in the control samples without MnO_x.

The rates of Phe loss were virtually the same in this experiment as in those without H_2O_2 added or pH-adjustment. The $\boldsymbol{R_0}$ of Phe loss was 0.48 μM hr^{-1} and 1.5 μM hr^{-1} in slurries of Mn_2O_3 and MnO_2 (respectively) without H_2O_2, very similar to the rate parameters determined at pH 5.5 (Figure6.1A). Furthermore, when H_2O_2 was added, $\boldsymbol{R_0}$ of Phe loss was again similar at 0.42 μM hr^{-1} and 1.5 μM hr^{-1} for these two minerals, respectively. This reveals that the mechanism for Phe loss is not affected by pH in the range of 3.2 to 5.5 pH units, nor is it limited by formation of H_2O_2 (as is the case in pyrite slurries (Chapter 3) or observed with MnO_x in another study with different compounds (Watts et al. 2005a)). Therefore, as alterations to the aqueous phase of MnO_x slurries did not induce greater reactivity, it seems likely that the reactions of Phe are occurring at the surface of the MnO_x through redox reactions. To test this theory, the surface areas of Mn_2O_3 and MnO_2 were increased to see if the rate of Phe loss increased proportionally.

6.3.1.3. Effect of increased manganese oxide surface area

Incubations of 100 μM Phe in ground samples of Mn_2O_3 and MnO_2 were run in pure water (pH 5.5), with added HCl (pH 4.6), and with addition of both HCl and H_2O_2 (Figure 6.3). Samples of ground MnO_2 in pure water yielded Phe loss with an $\boldsymbol{R_0}$ of 3.8 μM hr^{-1} and $\boldsymbol{k'}$ of 0.022 hr^{-1} (Figure 6.3A), which is approximately double the rates observed in slurries where MnO_2 was not ground, consistent with the increase in surface area from 0.81 $m^2\ g^{-1}$ to 1.7 $m^2\ g^{-1}$. The loss of Phe in incubations of ground MnO_2 run at a lower pH of 4.6 were consistently slightly greater than those observed at pH 5.5 (Figure 6.3A), while there was no effect of pH

seen in a similar comparison with Mn_2O_3 (Figure 6.3A). The measured rate parameter for ground (2.6 m^2 g^{-1}) and unground (2.1 m^2 g^{-1}) were the same ($\boldsymbol{R_0}$ of 0.28 μM hr^{-1} and $\boldsymbol{k'}$ of 0.004 hr^{-1}), as the effect of grinding did not affect surface area greatly for this mineral.

The kinetics of Phe loss were not affected by added H_2O_2 at either pH (Figure 6.3B), as observed in samples of MnO_x that were not ground (Figure 6.2). Likewise, no Tyr formation in these or any of the reactions with increased MnO_x surface area. However, the rate of Phe loss was also observed to increase proportionally in slurries of pyrite (where degradation is attributed to the Fenton reaction in solution) with increased surface area. Thus, even with added H_2O_2 and a lower pH, the presence of minerals in the previous experiments could not discount the potential for solution-phase reactions with dissolved manganese.

6.3.2. Phenylalanine in Fenton-like reagents

Solutions containing 200 μM Mn^{2+} (as MnF_2) with and without 100 μM H_2O_2 were incubated with 100 μM Phe to determine the potential for aqueous-phase Fenton-like reactions. The solutions were also adjusted with HCl in some reaction vessels to pH 3.2, whereas others were in pure water with a pH of 5.7. Duplicates were run for each set of conditions, and only slight Phe loss was observed (roughly 5% of $[Phe]_o$) after a 1-hour and 4-hour incubation in solutions of Mn^{2+} without H_2O_2 at pH 3.2. Incubations of Mn^{2+} containing H_2O_2 did not degrade Phe at either pH.

Similar to reactions in MnO_x slurries, formation of Tyr was not observed in any incubation of MnF_2 and Phe indicating $^{\cdot}OH$ was not involved in the minimal loss of Phe observed in solution. These observations were not consistent with prior results implicating $^{\cdot}OH$ in the loss of hexanol under similar conditions (Watts et al. 2005a). More important to this work, the absence of Tyr formation corresponding to Phe loss in incubations with Mn_2O_3 and MnO_2 are not in agreement with preliminary results from APF experiments conducted in a collaborating lab by Hylton et al (unpublished), which indicated likely presence of $^{\cdot}OH$ based on fluorescence measurements of a fluorescein. There are many possible reasons why the Phe and

APF probes may be indicating different levels of ·OH, and a detailed investigation should be conducted to determine whether the reactions of both probes in MnO_x slurries are dominated by simple second-order reaction with dissolved ·OH or other mechanisms. Considering MnO_x suspensions where the oxidation of organic compounds can proceed by different mechanisms, one might consider whether the APF probe is specific to reaction with ·OH in this case.

Although APF is highly sensitive for reactions with ·OH *in vitro* (Setsukinai et al. 2003) and pyrite slurries (Cohn et al. 2008), the probe is also sensitive to reaction under highly oxidizing as suggested by the developers Setsukinai et al. (2003), and can also be used as a probe with other strong oxidants including hypochlorous acid and peroxynitrite. APF has even been utilized to detect high levels of singlet oxygen (Setsukinai et al. 2003). It seems plausible that like other many other organic compounds, the highly oxidized surface of some MnO_x minerals might induce transformation of APF. In the case of Phe, although Tyr was not observed, the [Phe] did decrease with time, and reports of MnOx oxidation of organic acids indicate reaction mechanisms at or near the carboxyl group (Wang and Stone 2006). Therefore, other degradation products of Phe that might implicate ·OH were sought.

6.3.3. Degradation products of phenylalanine in manganese oxide slurries

Since formation of Tyr was not observed in any of the MnO_x incubations where Phe was lost, additional analyses were run to help identify any other dissolved degradation product of Phe that could implicate a reaction mechanism. The reductive dissolution of MnO_x that occurs through multiple electron-transfers (Equation 6.1 through 6.6) and ultimately lead oxidation of organic compounds are more selective than ·OH for reaction sites on molecules. However, it was presumed that reactions at the polar-end of Phe are preferred over the phenyl group (based on reaction rates from studies showing rapid reaction with organic acids (Wang and Stone 2006) and the lack of Tyr formed).

6.3.3.1. Extended HPLC-MS analyses

A review of the chromatograms and spectra did not reveal any additional compounds accumulating at later time points within the acquisition window. Therefore, an extended HPLC-MS method was run to look for additional compounds that would be less-polar than Phe (i.e., elute later than 8.8 minutes). Following reinjection of samples from Phe incubations with Mn_2O_3 and MnO_2, a single peak was observed at a retention time of about 12.1 minutes on the chromatogram (3.3 minutes after the Phe peak), which was not present at **t** = 0 hours and increased in area at later time points (Figure 6.4). Although no standards were available to positively identify the compound, the accurate mass calculation yielded a mass-to-charge ratio (m/z) of 136.068 ± 0.005 Daltons (Da) in the combined spectrum, corresponding to an $[M+H]^+$ of $C_8H_{10}NO^+$ (a loss of CH_2O from the molecular ion of Phe determined by ESI+ MS).

The number of potential structures is constrained by the fact that it was derived from Phe and the retention time increase observed with reverse-phase HPLC implies a less-polar molecule. In order to achieve a Phe reaction product with the observed mass, it is hypothesized that oxidative decarboxylation occurred at the alpha carbon. Two reaction mechanisms are proposed: 1) a net four-electron transfer involving hydrogen abstraction at the alpha-carbon that leads to oxidation by oxygen of MnO_x, followed by electron-transfer through to the manganese reduction and loss of CO_2; or 2) a net two-electron transfer involving direct oxidation of the alpha-carbon by MnOx oxygen with elimination of the carboxyl functional group as formic acid. It is theorized that these reactions result in the formation of 2-phenylacetamide.

Although no reports of Phe degradation to 2-phenylacetamide have been found, and in addition to the rationale given above, this theory is consistent with data from several publications that show: the potential for oxidation of organic compounds at the MnO_x surface within the pH range of this study (Rubert and Pedersen 2006; Zhang and Huang 2005); hydrogen abstraction by MnO_2 has been shown when coordinated (i.e., electron stabilization) (Yin et al. 2007); and extrapolation of amino acid rearrangement reactions to stabilize a free radical (Guitton et al. 1998; Hosamani et al. 2010). Interaction of the intermediate molecules at the MnO_x surface may have helped the intermediates avoid concomitant loss of the amine group (which is a commonly

shown to be removed as the carboxyl is lost). It should be noted that since the ESI+ MS methods could only detect ions with protonizable (i.e., the amine), functional group. Thus, if a deamination product were formed it, would not have appeared in the spectrum. Therefore, radio-labeled Phe was used with an in-line beta detector to search for the missing degradation products.

6.3.3.2. Radio-labeled phenylalanine

Experiments with 45 $\mu C_i\ L^{-1}$ of ^{14}C-labeled Phe were conducted to help identify compounds that may not have ionized with the HPLC-MS method. The same extended HPLC gradient was used for direct comparison of peaks to on the MS spectrum. Following 48-hour incubations of Phe in Mn_2O_3 and MnO_2, two peaks (other than Phe) were observed. One peak corresponded to the solvent front, or amount of time an unretained compound would take to reach the detector. The other peak was roughly 3 minutes after Phe, corresponding to the [theorized] 2-phenylacetamide peak identified with the extended HPLC-MS experiment. The peak at the solvent front may have been dissolved $^{14}CO_2$ or formic acid that evolved from the decarboxylation of Phe described above.

Most of the added radiolabel could be accounted for as resolvable peaks on the chromatographs. In the case of $Mn_2O_{3,}$, most of the radioactivity remained as Phe and the peaks observed at the solvent front and at 12 minutes were largest at the final (48-hour) time point, each representing roughly 3% of initial Phe (assessed by calculating peak areas). Results from incubations in MnO_2 revealed that the loss of Phe was greater and a large peak at the solvent front, accounting for roughly 50% of the 70% $[Phe]_o$ lost after 48 hours. The proposed 2-phenylacetamide peak only accounted for about 8% by-area of $[Phe]_o$ in the MnO_2 slurry. Unfortunately, no other peaks were identified throughout the entire 22-minute analysis. The missing radioactivity suggests that perhaps some CO_2 was generated and subsequently degassed, or some portion of Phe products adsorbed to the MnO_x surface. Non radio-labeled standards of 2-phenylacetamide and other hypothesized degradation products (i.e., reactions involving loss of the amine group) would be necessary to confirm the mechanism of Phe loss using the extended

HPLC-MS method. Alternate methods may also be needed to characterize more soluble and/or acidic reaction products that were not retained by HPLC or detected and insensitive to ionization in positive ionization mode.

6.3.3.3. Phenylalanine versus tyrosine loss

Incubations of 100 μM *p*-Tyr were run in slurries of Mn_2O_3 and MnO_2 to determine if Tyr may have been formed but rapidly degraded or adsorbed in the presence of these minerals following Phe degradation (as had been tested with sub-bituminous coals in Chapter 5). Figure 6.5 reveals that the rate of *p*-Tyr loss is roughly the same as that of Phe in the MnO_2 slurry. On the other hand, the rate of *p*-Tyr loss in the Mn_2O_3 slurry was significantly greater than that of Phe, suggesting that the mechanism for *p*-Tyr loss may have been slightly different than at the MnO_2 surface. This can be explained using interpretations made by Stone and Morgan (1984) which state that compounds of similar structure (and even isomers) can have significantly different reaction rates depending on the oxidation state of manganese and slight variations in functional groups. Thus, the phenol group appears to be a better target for reaction with the Mn_2O_3 surface.

Evidence for ·OH-hydroxylation of *p*-Tyr to dihydroxyphenylalanine (DOPA) was not observed in either incubation. Peaks corresponding to a decarboxylation of *p*-Tyr were also not observed, and would have appeared on the chromatogram after *p*-Tyr. Phe was also not observed in incubations of *p*-Tyr, which would have indicated reduction of Tyr (though this was not expected).

6.3.4. Manganese oxides in simulated lung fluid

Slurries of ground Mn_2O_3 and MnO_2 were added to the same solution of SLF used to test the ·OH-potential of pyrite in biological matrices in Chapter 4. Figure 6.6A shows that Phe did not degrade in slurries of Mn_2O_3 or MnO_2 with SLF at pH 7.4 or when adjusted to pH 4.6 with

HCl as it did in slurries of pure water (Figure 6.1). No loss of Phe was observed with the addition of 100 µM H_2O_2 (Figure 6.6B) to MnO_x slurries suspended in SLF at pH 4.6 (conditions that simulate the potential phagocytic response in alveolar fluid (Nyberg et al. 1992)) or pH 7.4.

As was observed with experiments with pyrite in Chapter 4, the salts and other components of the SLF (e.g., phosphate) likely interfered with the reactivity of the MnO_x surface. Interestingly, the phosphate buffer (pH 7.4) used in APF experiments discussed above did not prevent the formation of fluorescent degradation product(s), as it is known that phosphate can bind strongly to MnO_x (Yao and Millero 1996) and coordinate with Mn^{2+} (Stadtman et al. 1990). It is argued above that there may be other mechanisms operating that lead to the reaction of the APF probe in presence of MnO_x surfaces. It would be useful to determine the identities and rates of formation of APF degradation products in addition to fluorescein (it is even possible that some other products fluoresce at the same wavelengths) and contrast degradation pathways of APF with systems where ·OH is known to be the primary oxidant. Experiments to identify the effect of the individual components of SLF on the Phe loss kinetics (as was done with pyrite in Chapter 4) could help elucidate the factors that control the kinetics of MnO_x reactivity.

6.4. Summary

Results presented in this chapter suggest that the redox chemistry responsible for the apparent degradation of Phe in Mn_2O_3 and MnO_2 slurries (within the pH range of 3.2 to 5.5) is a result of surface catalysis, and is not related to Fenton-like reactions that generate ·OH. This is supported by the lack of Tyr formation indicative of Phe hydroxylation by ·OH observed in Fenton reactions and incubations with pyrite (Chapters 2 and 3). It is also supported by the identification of a decarboxylated reaction product of Phe, which is consistent with similar surface mediated redox reactions that have been observed with other carboxylic acid in the presence of MnO_x. Experiments in this chapter also showed that solutions of Mn^{2+} and H_2O_2 did not degrade Phe. Furthermore, H_2O_2 does not appear to be involved in the degradation of Phe when added to MnO_x slurries. These conclusions are in agreement with the majority of studies

that implicate oxidation of organic compounds at the MnO_x surface through mechanisms that also result in reductive dissolution of the mineral (Chien et al. 2009; Wang and Stone 2006).

The degradation rates of Phe in slurries of Mn_2O_3 were slower than in MnO_2 in a manner likely related to the redox potentials of manganese (i.e., +3 and +4 respectively), which affects their ability to sorb and oxidize Phe at the surface. This would also explain the lack of Phe loss in MnO, where reduction of Mn(II) in the mineral phase is not favorable. Interestingly, no loss of Phe was observed in $LiMn_2O_4$, despite high mixed-valence oxidation states (+3/+4). It was not determined why $LiMn_2O_4$ was not reactive, but it is likely related to the presence of lithium which may change the crystal structure to an unfavorable arrangement for the reductive dissolution of manganese. On the other hand, the oxidation potential of the manganese in this mineral with mixed metals may simply be less than in pure MnO_x phases.

Incubations of Phe in Mn_2O_3 and MnO_2 slurries with β-ME added showed no reactivity, which may have been a result of either the increase in pH to around 10 changing the redox potential or competition for the active sites of MnO_x as β-ME is known to be a good reductant. The loss of Phe observed in slurries of MnO (which was otherwise unreactive) with added β-ME was associated with gross changes in mineral chemistry that could be visualized.

The loss of *p*-Tyr compared to the loss of Phe showed that there was little difference in slurries of MnO_2 and a significant increase in slurries of Mn_2O_3, likely due the phenol functional group reacting preferentially at the surface. However, in both incubations, Tyr was persistent long enough that it should have been readily detectable if the mechanism of Phe loss was controlled by reaction with $^{\cdot}OH$.

Radical species are theorized to form as intermediates during the reductive dissolution of MnO_x by organic compounds that will continue to react either while adsorbed to the MnO_x surface or following desorption into solution (Equations 6.3 and 6.4). The oxidation of Phe may have been the result of preferential alignment at the MnO_x surface (i.e., the polar end of the molecule interacting with the surface). This alignment could explain oxidative decarboxylation without the loss of the amino group, believed to lead to the formation of 2-phenylacetamide. If

the proposed mechanisms (two- or four-electron transfer) are correct, the peak observed in the solvent-front in the radio-labeled ^{14}C-Phe experiment may be formic acid and/or dissolved CO_2 resulting from the oxidative decarboxylation of Phe. Future experiments with Phe and MnO_x should monitor for the evolution of CO_2, formic acid, and ammonia (resulting from deamination).

The use of Phe in MnO_x slurries has still proven to be useful a probe despite the lack of Tyr formation in slurries of all four forms of MnO_x. The results presented in this chapter suggest that APF may be reacting by a mechanism other than $^{\cdot}OH$ under these highly-oxidizing conditions. The fact that no loss of Phe in MnO_x suspensions with SLF at pH 4.6 or 7.4, with or without H_2O_2 added, may be important when considering that Mn^{2+} dissolution and the phagocytic response already contributes significantly to increased physiological stress. It may be that the surface of MnO_x is less reactive with biological molecules in the presence of strong buffering salts. On the other hand, this may also imply that application of MnO_x as a remediation tool may be hindered in some natural waters, since many of the same salts and buffers in SLF are also found in environmental matrices.

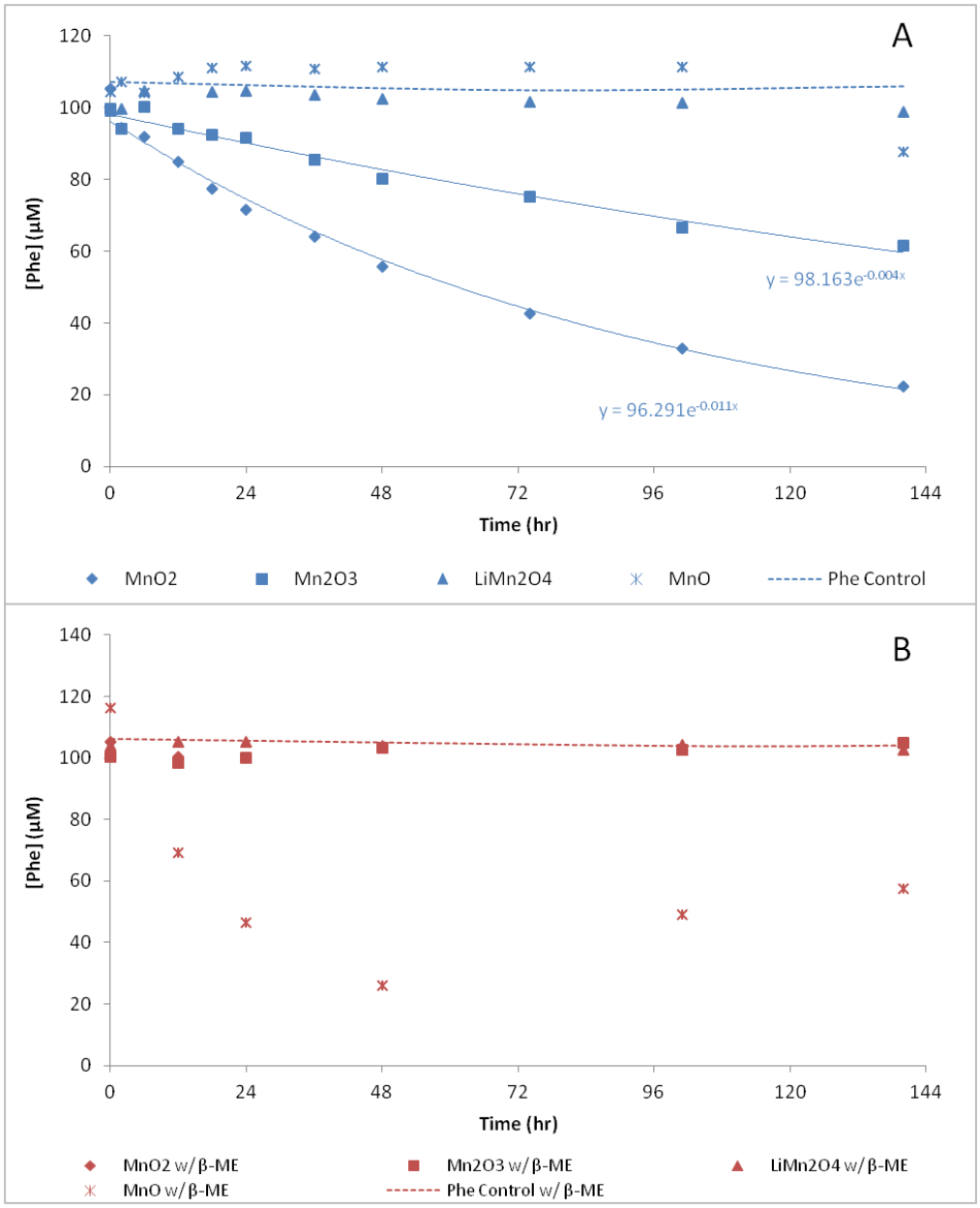

Figure 6.1. Loss of Phe in slurries of various MnO_x. The four different MnO_x were incubated with 100 µM Phe in suspensions of (**A**) pure water and (**B**) 0.1% β-ME. Loss of Phe was observed Mn_2O_3 and MnO_2 slurries made in pure water, and in MnO suspended in 0.1% β-ME.

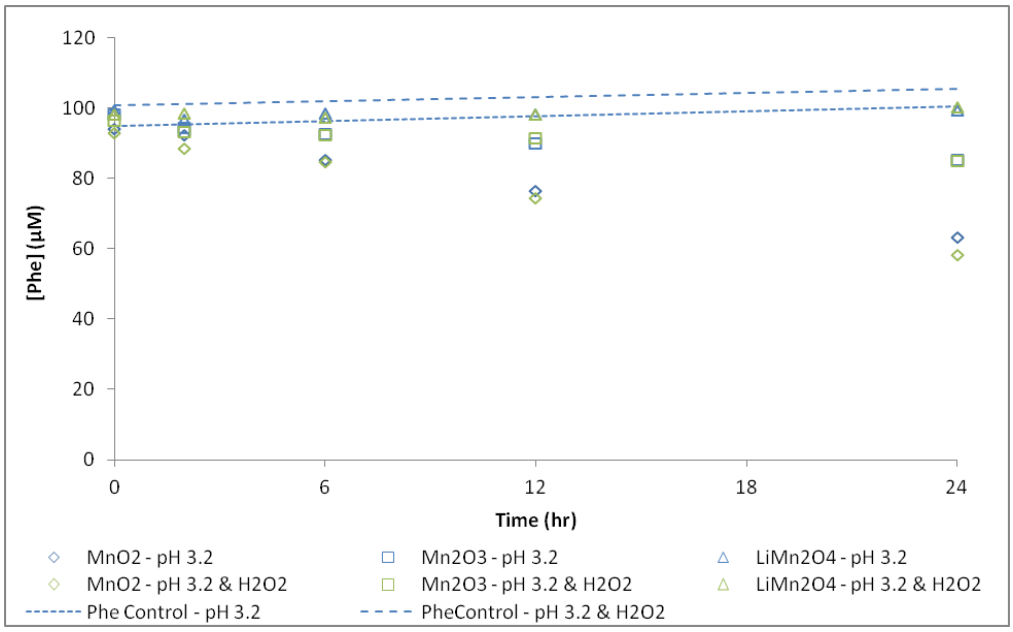

Figure 6.2. Loss of Phe in MnO_x slurries with an adjusted pH. Slurries with 100 g L^{-1} MnO_2, Mn_2O_3, or $LiMn_2O_4$ were each adjusted with HCl to pH 3.2 and showed similar rates of Phe loss to incubations at pH 5.5 (Figure 6.1). Similarly, there was little effect on Phe loss with added H_2O_2 to the MnO_x slurries.

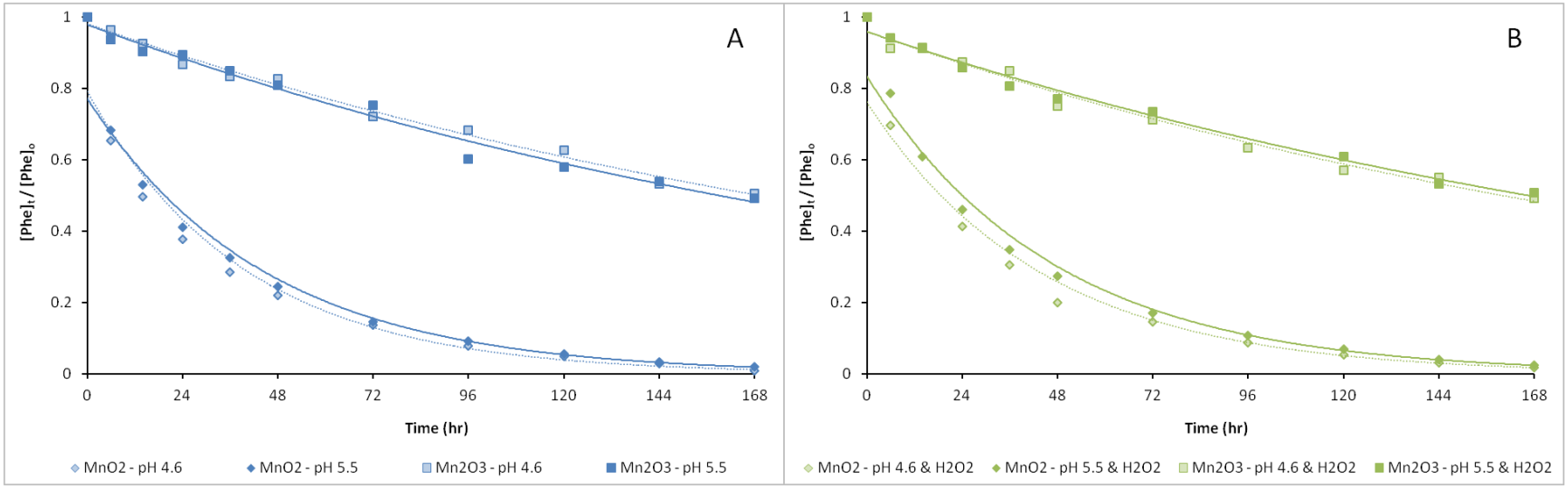

Figure 6.3. Comparison of Phe loss in MnO_x slurries in adjusted pH with increased surface area. (**A**) Loss of Phe in slurries with pH adjusted with HCl showed very slight increase in initial rate in MnO_2, but overall had similar kinetics. Loss of Phe in Mn_2O_3 did not appear to be affected by change in pH. (**B**) Loss of Phe with added H_2O_2 in pH-adjusted and pH-unadjusted slurries exhibited little difference in kinetics from solutions without H_2O_2 (Figure 6.2). Again, MnO_2 showed a slight increase in initial rate at pH 4.6, but overall the fitted curve was the same.

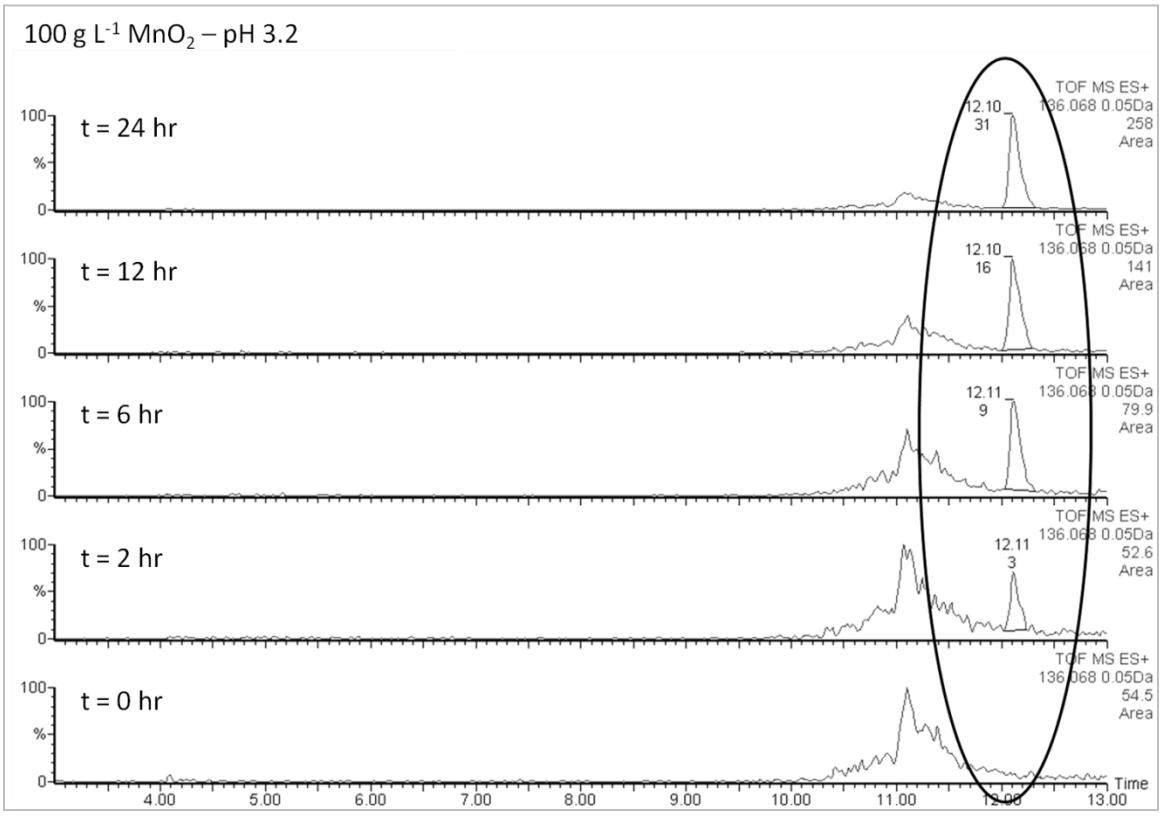

Figure 6.4. Extended chromatography of Phe in a MnO_2 slurry. A peak indicating formation of a less-polar degradation product of Phe with an m/z of 136.068 ± 0.005 Da (corresponding to a $[M+H]^+$ of $C_8H_{10}NO^+$) at 12.1 minutes into the run increased in area over the duration of the incubation in 100 g L^{-1} MnO_2 and Mn_2O_3 (not shown). Similar area counts were observed in MnO_2 (pH 3.2) with added H_2O_2 (not shown), indicating that Phe was not influenced by Fenton-like reactions during formation of this product.

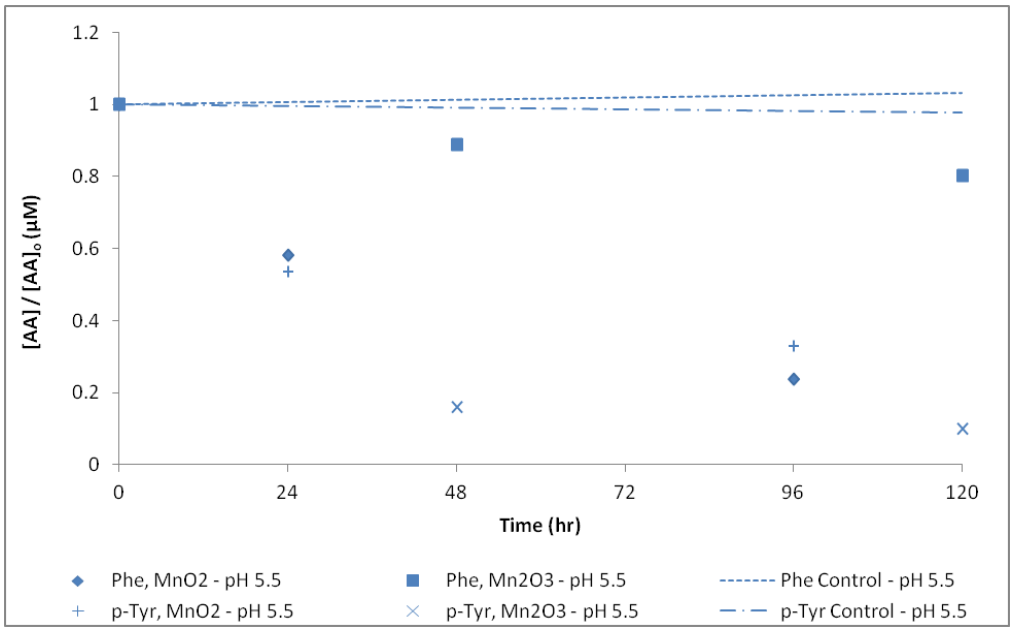

Figure 6.5. Incubations of Phe and *p*-Tyr in MnO_x slurries. The kinetics of *p*-Tyr loss in the MnO_2 slurry did not appear different than the loss of Phe. Loss of *p*-Tyr in the Mn_2O_3 slurry was significantly greater than loss of Phe after 48 hours, suggesting preferential degradation of *p*-Tyr, likely due to interactions of the phenol moiety. The formation of DOPA or Phe was not observed in the *p*-Tyr incubations, which would have suggested ·OH hydroxylation or reduction of the phenol to phenyl (respectively).

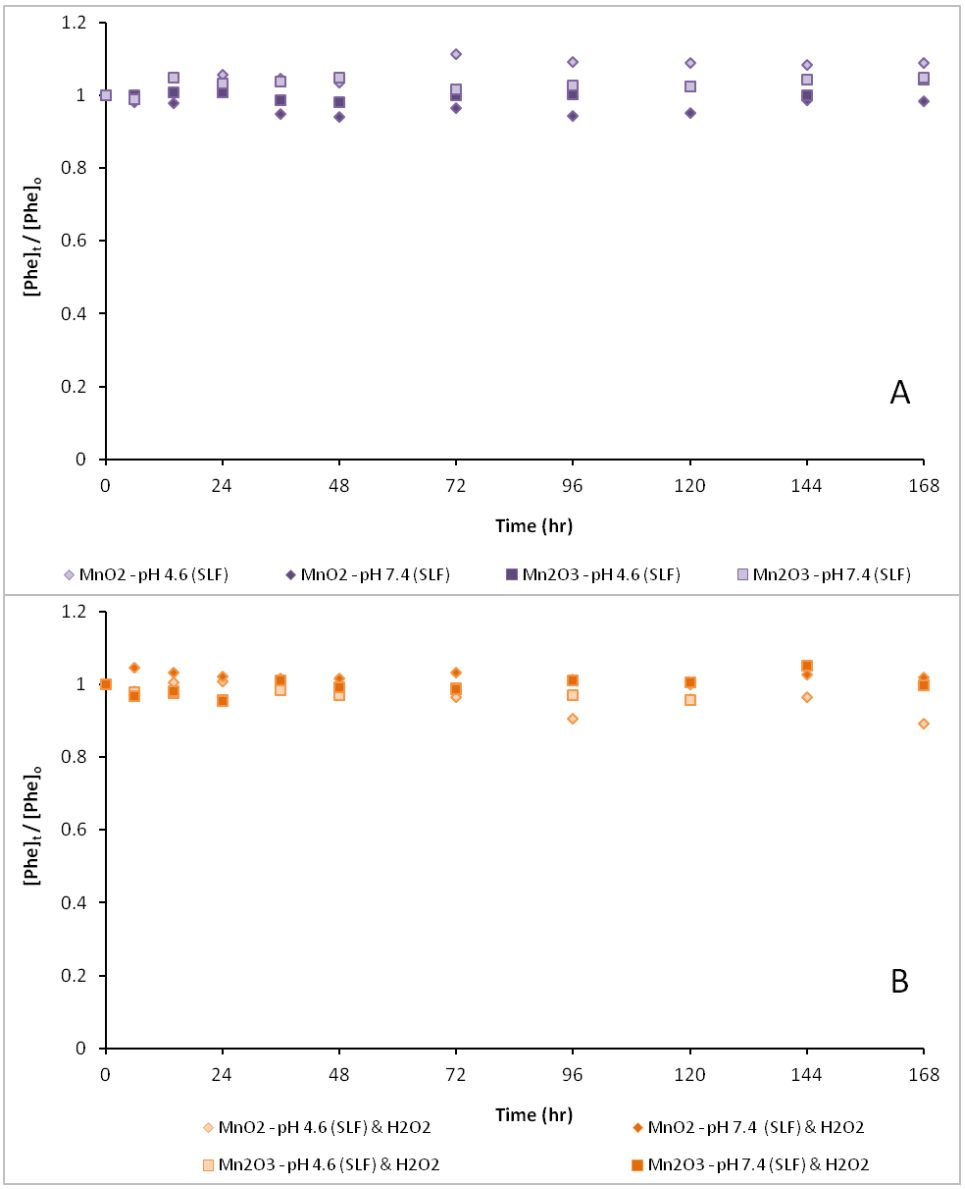

Figure 6.6. Slurries of MnO_x with increased surface areas in SLF with added H_2O_2 and adjusted pH. Incubations of 100 μM Phe in MnO_x suspended in (**A**) SLF and (**B**) SLF with H_2O_2. No loss of Phe was observed in any slurries containing SLF, suggesting that either the redox potential at the MnO_x surface was altered by the salts and/or high pH, or that the components of SLF out-competed Phe for redox active sites at the mineral surface.

Chapter 7

SUMMARY OF CONCLUSIONS AND FUTURE WORK

7.1 Summary of conclusions

Results presented in this dissertation provide evidence that phenylalanine (Phe) can be employed as an effective molecular probe to monitor hydroxyl radical (·OH) formation in slurries of pyrite and pyritic coals through time, as well as provide insight into alternative mechanisms of reaction in slurries of manganese oxide minerals (MnO_x) where ·OH had previously been implicated. To our knowledge, this is the first study to use a probe that relies on phenyl hydroxylation in mineral slurries to assess ·OH production and fate. Formation of *ortho*- and *meta*-tyrosine (*o*-Tyr and *m*-Tyr) in the presence of ·OH is a well-established sign of oxidative stress *in vivo*, and their detection, along with *para*-Tyr (*p*-Tyr), provided evidence that ·OH was being produced in slurries of pyrite and pyritic coal. The ratios of the three-isomers of Tyr in pyrite were shown to be very similar to those resulting from aqueous-phase, homogeneous ·OH formation through Fenton chemistry. The absence of Tyr in slurries of MnO_x confirmed that ·OH was not being generated and that the loss of Phe was most likely the result of reductive dissolution at the surface of MnO_x.

The analytical method developed in this study (described in Chapter 2) offers several advantages over other methods currently being used to probe for ·OH in mineral slurries, including confirmation of degradation products, analytic sensitivity, and concurrent

quantification of parent and degradation products. Unlike some procedures that require separate analyses of the reactant and degradation products (e.g., trichloroethylene (TCE) (Pham et al. 2009)), the combination of high-performance liquid chromatography (HPLC) and Time-of-Flight (ToF) electrospray mass spectrometry (ESI+ MS) allows for detection and quantification of Phe, the three isomers of Tyr, and dihydroxyphenylalanine (DOPA) in the nanomolar range with a single run. The sensitivity achieved with HPLC-ToF-MS was substantially greater than HPLC-fluorescence (near-millimolar levels of Phe were required to monitor degradation kinetics). The mass resolution of the ToF-MS (roughly 6000) allows for greater specificity and selectivity than standard UV/fluorescence, as well as the ability to estimate the accurate mass of a compound within a few milliDaltons, which is useful for characterizing observed degradation products for which standards are not available (e.g., 2-phenylacetamide theorized to formed in some MnO_x slurries). HPLC retention provides additional selectivity for identification of reactants while also separating salts, dissolved metals, and other constituents that can interfere with quantification in methods that employ fluorescence monitoring.

Another advantage of the method was that it required minimal sample processing, which allowed for a large number of samples to be analyzed and more reliable recovery of both targeted and non-targeted analytes. Filtered aliquots were preserved in HPLC vials with 5% methanol at low pH for injection directly on-column without the need for further purification (even when slurries contained complex mixtures such as simulated solutions and dissolved organic matter (i.e., humic acid (HA)). Furthermore, the required pH-adjustment for MS analysis is made in the HPLC vial, and thus incubations with Phe are not restricted to a narrow pH-range required for application of some fluorogenic probes.

Phenylalanine in pyrite slurries

Phenyl hydroxylation of Phe provided selectivity for $^{\cdot}OH$ in pyrite slurries with significant yields of total-Tyr (ΣTyr) that accounted for about 50% of the Phe degraded. Suspension of pyrite in pure water yielded Tyr-isomer ratios consistent with those found in homogeneous solutions containing Fenton reagents (dissolved ferrous iron (Fe^{2+}) and hydrogen peroxide (H_2O_2)). The fact that the rate of Phe degradation did not change following addition of

Fe^{2+} salt to pyrite slurries indicates that iron dissolution is sufficient to catalytically generate ·OH as H_2O_2 becomes available from the surface (i.e., the rate of ·OH formation, as well as the rate of ·OH-mediated reactions, is limited by the flux of peroxide). Similarly, the rapid loss of Phe when H_2O_2 was added to pyrite slurries is consistent with the net flux of H_2O_2 into solution acting as the rate-limiting factor contributing to ·OH formation (in the absence of compounds that may limit dissolved iron concentration). Prior work indicates that since H_2O_2 reacts so rapidly in pyrite slurries, it can only be measured in pyrite slurries when iron is chelated with ethylenediaminetetraacetic acid (EDTA), which effectively halts the Fenton reaction. These results, along with a lack of sorption of Phe to pyrite, provide strong evidence for ·OH-formation in the aqueous phase.

One important discovery in this work was that the rate of Phe degradation was not proportional to its initial concentration. Earlier studies with pyrite only monitored disappearance of RNA, adenine, or TCE at a single initial concentration of substrate and interpreted the observed exponential losses of target compounds as evidence for first-order kinetics (Cohn et al. 2006b; Cohn et al. 2010; Pham et al. 2009). Results presented in this dissertation have shown that the rate of Phe loss as a function of initial Phe concentration ($[Phe]_o$) was much-less than first-order, and plotting the initial rates of Phe degradation ($\boldsymbol{R_o}$) as a function of $[Phe]_o$ produces a hyperbolic curve that can be described using the Langmuir-Hinshelwood equation (L-H) (Chapter 2). When reaction kinetics involving ·OH can be described by the L-H equation, as is the case of photo-catalytic reactions with titanium oxides (Turchi and Ollis 1990), mechanisms that involve surface catalysis are generally cited. However, in this dissertation, the overall kinetics and the effect of initial concentration were explained by an alternative model where reaction with ·OH occurs in the bulk aqueous phase. In the aqueous phase, the [·OH] decreases with increasing $[Phe]_o$ and is controlled by the balance between: rate limiting production, which depends on release of H_2O_2 into solution; and loss, which is a function of the product of concentration of reactants (Phe and its reactive degradation products) and their respective second-order reaction rates with ·OH. The apparent first-order loss of Phe as a function of time (i.e., exponential decay) could then be explained if one assumes that the total pool of Phe and its oxidizable degradation products remains relatively unchanged throughout most of the incubation,

and those reaction products are characterized by similar second-order rate constants for reaction with ·OH.

A simplified pseudo first-order model was developed that could predict both the [Phe] and [ΣTyr] through time across a wide range of reaction conditions with a given batch of pyrite. Rate constants specific to each pyrite sample are proportional to pyrite loading and inversely related to $[Phe]_o$ (as in the L-H equation). The model was supported and constrained by experimental observations related to the relative reactivity of Tyr products and ranges of reaction yields. Simplification of the kinetic model involved several key, but not unreasonable, assumptions to hold over the time-course of the experimental observations: the [·OH] is at steady state, as is the flux of its precursor H_2O_2; the total concentration of reactants (Phe, Tyr and other degradation products) that compete for ·OH remains unchanged over time and is equal to $[Phe]_o$; and, the second-order rate constants for reaction with ·OH of those reactants are the same. If the degradation products were not susceptible to competitive reaction with ·OH (e.g., the final product of Phe oxidation, carbon dioxide (CO_2), does not effectively compete with for ·OH), the degradation curve of Phe would be linear with time (zero-order) at higher $[Phe]_o$, with the loss dependent only on the constant rate of ·OH formation. Furthermore, loss of Phe in reactions with would be faster if the continued formation of subsequent degradation products of Phe did not compete. While oxidized products may compete less effectively, there is a limit to how much better a potential degradation product can compete for ·OH because second-order rate constants measured with both Phe and Tyr are comparable, very fast, and near diffusion-rate limited. The sensitivity of assumptions made to develop the simplified kinetic model was evaluated in numerical simulations (see Appendix) that more explicitly included effects of reaction path-lengths and assumptions concerning the relative reactivity of competitors in more complex matrices.

The multiple sets of incubations conducted to determine the kinetics of Phe degradation also revealed that subtle variations in the acid-pretreatment conditions used to prepare pyrite on different dates appeared to have significant effects on the pyrite reactivity. A likely explanation for these observations was presented by Schoonen et al. (2010), who suggested that a certain amount of oxidized iron (i.e., patches of Fe(III) oxide) at the pyrite surface is required, in addition to Fe(II), for the electron transport within the pyrite to be optimal. Thus it is suggested

that more-extensive acid treatment or a very low pH would reduce too much iron, while a high pH would result in a surface too oxidized to reduce dissolved oxygen at the surface. Along these lines, it is noteworthy that in experiments with pyrite, degradation rates of Phe in unbuffered suspensions were reduced when acid was added to adjust initial pH to less than 3, where preservation or accumulation of Fe(III) oxide patches would be less favored. The fastest rates of Phe degradation were observed in unadjusted solutions in which oxidative dissolution of pyrite led to pH decreasing to values between approximately 3.0 and 5.5 (low pyrite loading). Interestingly, when normalized for the mass loading of pyrite, reaction rates appeared to be independent of pH in this range (i.e, ·OH formation and reaction with Phe was first-order in pyrite loading). Working at the high end of this pH range, Cohn et al. (2010) showed the loss of adenine can occur for up to three weeks in low pyrite loadings of 1 g L^{-1} and 10 g L^{-1}. However, corresponding formation of ·OH-specific degradation products were not determined for the incubation with adenine at later time points. Experiments with Phe and pyrite loadings of 1 g L^{-1} and 10 g L^{-1} in this study revealed appreciable amounts of Tyr over 6 and 10 days of incubation respectively. These results are significant in that they provide additional evidence for the extended catalytic formation of ·OH that had been reported in earlier studies that relied on disappearance of probe molecules rather than production of diagnostic products.

The experiments conducted to determine reaction kinetics for Phe and Tyr transformations in pyrite suspended in pure water laid the groundwork for examining the influence of additional variables such as salinity and the presence of dissolved organic matter, which had not been previously reported. Incubations with various loadings of simulated seawater (SSW) and organic humic substances (i.e., HA) were run to test the ability of pyrite to degrade Phe in the presence of high salt and dissolved organic matter relevant to environmental conditions (Chapter 4). Results revealed that high concentrations of the inorganic salts (up to 32 parts-per-thousand salt) that comprise seawater slow, but do not halt, the rate of ·OH formation in pyrite slurries. Although $[\Sigma Tyr] / [Phe]_o$ ratios were proportionally lower with increasing salt content, Tyr formation was observed at significant quantities – even in slurries with a salt content of true seawater that was well buffered, such that pH did not decrease below 7.6. Hydroxylation of Phe was also observed in pyrite slurries containing very high levels of dissolved HA (400 mg L^{-1}). The effect of increasing HA concentration on Phe reaction rates was attributed to direct

competition for ·OH, in agreement with predictions based on estimates of a second-order rate constant and the range of molar-masses for the complex organic matter of HA assigned by the manufacturer (Sigma Aldrich). This suggests that the surface of pyrite was still capable of generating H_2O_2 and that the Fenton reaction is still effective in the presence of natural organic matter with iron-chelating properties. Since the dissolved HA used in this study is an oxidized form of lignite (an immature type of coal), it is interesting to note that an earlier study by Cohn et al. (2006a) found that particulate organic matter in the form of sub-bituminous non-pyritic coal did not appear to compete for ·OH with 3'-(*p*-aminophenyl) fluorescein (APF). Together, these findings are significant in that they show pyrite has potential to produce ·OH under a wide range of natural water conditions – even those containing high organic matter such as wastewater where pyrite may be considered for use as a remediation tool – and that Phe is a useful probe under such conditions.

Initial experiments with pyrite suspended in simulated lung fluid (SLF) showed that although the rate of Phe loss was very slow, trace amounts of *o*-Tyr and *m*-Tyr were detected, and therefore ·OH is still a potential threat to biomolecules in cells exposed to pyrite dust (Chapter 4). Later work with pyrite and SLF conducted by collaborating investigators used APF, which provided more evidence that ·OH production is greatly limited and was likely due to the presence of citrate and other complexing ions (Harrington et al. 2011). The effects of SLF on ·OH estimated by APF were much less than observed in this work with Phe and Tyr, which may have been due to a different reaction mechanism for Phe loss, or reaction of APF with oxidants other than ·OH. More experiments with both probes to determine the extent to which solution chemistry affects their degradation pathways would be useful for understanding the differences in observations.

Additional work examined the effects of individual components of SLF, many of which had never been tested in pyrite slurries for their effects on ·OH formation. Each affected degradation of Phe differently. Consistent with results from SSW, high concentrations of chloride (greater than 120 mM) added to pyrite slurries did not greatly affect the amount of ·OH available for reaction with Phe. The competitive effect of chloride was found to be much less than the second-order rate constant for reaction with ·OH suggests. This is attributed to the fact that reaction of chloride with ·OH in solution that forms hypochlorous acid radical is reversible

to different extents based on pH (Jayson et al. 1973). Calculations based on relative rates of Phe loss in pyrite slurries containing chloride or pure water, along with the Jayson et al. (1973) study, indicate that the observed difference was due to competition for ·OH; thus by extension, it was shown that chloride does not significantly interfere with the formation of H_2O_2 at the pyrite surface. The effect of adding high concentrations of the simple amino acid glycine, which has a much lower second-order rate constant for reaction with ·OH than does Phe, was also very close to that expected only from competition for ·OH.

It can be difficult to determine if the reduced reactivity observed when adding a complex ion is the result of competition for ·OH, an effect on the catalytic properties of the pyrite surface, or an effect on the concentration or species of iron that catalyzes the production of ·OH from H_2O_2. The rates of Phe loss in slurries containing carbonate and phosphate buffers were affected more than their second-order rate constants for reaction with ·OH suggests, which means the net flux of ·OH was hindered by a decrease in the catalysis of either dissolved oxygen to H_2O_2 at the surface, H_2O_2 by Fe^{2+} in solution, or a combination of both. Further complicating the interpretation is the change in pH these salts induce, as pH has already been shown to effect ·OH formation. Similarly, the coordination of Fe^{2+} in solution by citrate and its effect on the Fenton reaction is most likely the reason for the decrease in net ·OH (Harrington et al. 2011) available for reaction with Phe; though some of the decrease in reactivity could be attributed to competition, as citrate has a second-order rate constant for reaction with ·OH that is similar to that of Phe.

The extent that ·OH formation is affected by components of biological solutions is important when considering the effect of pyrite dust has on human health. It is clear from these results that there is a need to better understand the mechanisms by which pH and dissolved species affect reactions that control H_2O_2 formation and production of ·OH occurring either at the surface or in solution. Of particular importance appears to be complex ions (i.e., carbonate and phosphate salts, citrate) and pH and their affect on the speciation of iron (Hamm et al. 1954; Konigsberger et al. 2000) and on Fenton chemistry (Zhang et al. 2006).

Phenylalanine in coal slurries

Few studies have evaluated the formation and fate of ·OH generated by pyritic coal. Schoonen, Cohn, and others (2006a) were among the first to study ·OH-formation in coal samples containing variable amounts of pyrite. Experiments in this study have supplemented and expanded upon their work through measurements of ·OH reaction products as a function of time and experiments aimed at better determining effects of pH (Chapter 5).

The concentration of Phe decreased through time in suspensions of all six coals tested, but Tyr formation was only observed in the four bituminous coal samples, all of which contain pyrite. Loss of Phe in the two sub-bituminous coals was attributed to sorption reactions. Initial degradation rates of Phe among the different pyritic coals were not found to be proportional to their sulfur or pyrite content, which may be the result of variations in the composition of solid organic matter, association of the solid organic matter with pyrite, or the extent of pyrite surface oxidation. One important finding was that despite the low pyrite content, normalized reaction rates of Phe hydroxylation in aqueous suspensions were faster with samples of pyritic coal than the pure-pyrite samples used in this study. The faster normalized rates of Phe loss (and Tyr formation) in pyritic coal is speculated to be due to the pyrite mineral morphology (i.e., framboidal) in coal, which has a greater surface area than the samples of cubic pyrite used in this study. The greater reactivity of coal pyrite is impressive considering that most of the pyrite surface is likely in contact with the solid organic matter and not directly exposed to water.

As mining is one of the main routes for human exposure to coal (and possibly pyrite), there has been considerable attention paid to the prolonged effects of inhaled particles. Prolonged generation of ·OH indicated by hydroxylation of Phe for up to 14 days highlights the potential for inhaled pyritic coal to continue to cause lung damage for several weeks. Furthermore, an incubation of pyritic coal at a constant pH of 7.4 exhibited an initial burst of ·OH (as evidenced by Tyr formation), with a greater amount of Tyr formation over the first hour than was measured at lower pH. A similar experiment at constant pH 4.5 revealed reactions that continued for over a day and where the production of ·OH was greater than in incubations where the pH was allowed to decrease from pH 3.8 to 3.3 over the first 24 hours. This is an important finding considering that phagocytes in the lungs could induce an even greater flux of ·OH (perhaps for a longer period) by not only creating low pH environments near the particle interface, but also by releasing H_2O_2, effectively short-cutting the rate-limiting H_2O_2 formation process at the pyrite

surface. Taken together, these findings indicate that the potential of ·OH damage to epithelial cells from pyritic coal may be greater than anticipated based on studies of pure pyrite.

An unexpected, and as yet unexplained, observation made while testing slurries of pyritic coals was that the incubations containing 1% beta-mercaptoethanol (β-ME) by-volume did not appear to completely quench ·OH (as evidenced by the hydroxylation of Phe to the three isomers of Tyr); whereas 0.1% β-ME was effective at stopping Phe reactions in pyrite-only experiments. In comparison, addition of ethanol did quench the reactions in two of the pyritic coals, but again was not completely effective at quenching ·OH as all three isomers of Tyr could eventually be detected after several hours in the presence of two other pyritic coals. There are possible reactions for both chemicals with organic and inorganic components of the coal surface that may have removed some of these agents from the aqueous phase; especially β-ME, where the exchange of free radicals from coal organic matter to the thiol moiety may have significant consequences the fate of β-ME (Zhang et al. 2004; Zheng et al. 2012). However, the number of moles of β-ME and ethanol should have greatly exceeded possible organic or inorganic reaction sites; thus, unless removal from solution phase was rapid and catalytic in some way, it is difficult to imagine how aqueous concentrations of these quenching agents starting at over 100 mM could be reduced enough such that they would not greatly outcompete 100 µM Phe for ·OH present in the aqueous phase.

The results pose the question as to whether hydroxylation of Phe in pure-pyrite and pyritic coal samples occurs by the same mechanism, and whether or not reactions in either pyritic coal and/or pyrite occur in the aqueous phase as opposed to reactions that might be catalyzed at the pyrite surface. It may be possible that β-ME and ethanol compete less than Phe for active-sites or surface phases, for example if the reaction was with adsorbed rather than dissolved ·OH. In any case, these results seem to suggest that there are more complicated interactions in coal slurries than pyrite alone, possibly due to the presence of solid organic matter in which the pyrite is embedded. It may be that there is greater importance of surface-bound ·OH than has been hypothesized in this study and by others, and that the presence of coal organic matter somehow restricts the region of elevated ·OH-flux to near the mineral surface. The potential for formation of ·OH adsorbed at the pyrite surface has been proposed by Borda et al. (2003) and Schoonen et al. (2010) but not yet confirmed in published studies.

Phenylalanine in manganese oxide slurries

The oxidation of organic compounds have been shown in the presence of MnO_x and attributed to reactions involving the reductive dissolution of the mineral. Although there is little evidence supporting the formation of ·OH in slurries containing only MnO_x, several studies suggest different mechanisms by which ·OH may be formed with added dissolved manganese (Mn^{2+}) and/or H_2O_2 (Schoonen et al. 2006; Watts et al. 2005a). One study by Watts et al. (2005a) attributed the observed loss of hexanol in a solution of Mn^{2+} and H_2O_2, and in slurries of MnO_x and H_2O_2, to ·OH formation (though the evolution of CO_2 was the only degradation product observed, which has also been shown to form by mechanisms that involve electron-transfer reactions with organic compounds at the MnO_x surface (Wang and Stone 2006)). On the other hand, it was hypothesized in another study that Mn^{2+} might be a better oxidant as an adsorbed species and perhaps be involved in ROS formation (Schoonen et al. 2006). This provided an explanation for observations with APF reacting to form fluorescein in slurries of several different types of MnO_x (Hylton et al. unpublished).

Phenylalanine was degraded in the presence of the more oxidized MnO_x minerals tested (MnO_2 and Mn_2O_3). The lack of Tyr formation in those slurries where a significant amount of Phe was lost discounted ·OH as a reactant, even with added Mn^{2+} and/or H_2O_2 at low pH (Chapter 6). The observed degradation rates of Phe in MnO_2 and Mn_2O_3 are consistent with prior studies of MnO_x minerals (mostly with +3 and/or +4 manganese oxidation states) that show oxidation of organic compounds are catalyzed at the surface; consistent with reductive dissolution (Stone and Morgan 1984a; Wang and Stone 2006). Similarly, formation of a Phe degradation product theorized to be 2-phenylacetamide (based on chromatography and mass) is likely to be the result of oxidative decarboxylation as the charged amino and carboxylic groups interact at the MnO_x surface (Chapter 6). It is hypothesized that the formation of fluorescent compounds measured following MnO_x incubations with APF was the result of direct surface redox reactions, which created a false positive for ·OH formation.

Similar to observations of pyrite suspended in SLF at pH 7.4, rates of Phe loss were greatly affected when SLF was added to slurries of MnO_2 and Mn_2O_3. In fact, no significant loss of Phe was observed in SLF, even at pH 4.6 with H_2O_2 added to the MnO_x slurries. It appears that there was sufficient competition for surface interaction among the components of SLF, which limited Phe exposure because of either greater redox potential or surface adsorption. Overall, the use of Phe as a probe for ·OH worked well in slurries of MnO_x in that the products formed support mechanisms other than ·OH-formation for the observed disappearance of Phe.

7.2 Future Work

There are factors that contribute to the formation of ·OH in pyrite and pyritic coal slurries that require further investigation. Although strong evidence has been presented for the formation of ·OH occurring in the aqueous phase in experiments conducted with pyrite, adsorbed ·OH formation and reactivity cannot be completely ruled out. It is not clear how to best design experiments that would distinguish between reactions occurring in bulk solution from those occurring near the mineral-water interface. It might be possible to experimentally determine and model the fate of structural analogs of Phe with different rates or energies of adsorption to the pyrite surface.

Considering and isolating the various roles acid pretreatment (and more generally pH) has on pyrite-induced formation of ROS and specifically ·OH is difficult and requires much greater attention. It is suggested that future efforts should include: studies of surface mineralogy; determination of dissolved and surface associated iron speciation; and, utilization of more pH-stat experiments that control pH. A better understanding of the iron speciation at the pyrite surface with respect to pretreatment with acid would be helpful in determining causes of variation in rates of Phe loss among different pyrite samples, initial lags (Chapter 3 aging experiment), and initial bursts (coal at pH 7.4) of ·OH observed in some experiments. Maintaining a constant pH would help differentiate the changes in Phe loss that are the result of pH without buffering ions that can affect iron availability, reaction mechanism, or compete for ·OH.

More experiments should be conducted to help explain the curious lack of ·OH-quenching by high concentrations of β-ME and ethanol in pyritic coal slurries. If the explanation does not lie with the effect of complex organic matrices of coal reducing the activity of the quenching agents, then it will likely implicate the complex organics interacting to some extent with the embedded pyrite and changing the fate and/or formation of ·OH such that it is preferentially available to less polar compounds like Phe. There should also be a more detailed investigation into the high reactivity of pyritic coal, including estimates of pyrite surface chemistry and surface area using scanning electron microscopy for comparison between coal samples. The possibility separating the pyrite from the coal using physical methods should be considered in order to test the pyrite portion free of organic matter.

The continued use of Phe as a biologically and environmentally-relevant probe in mineral slurries suspected of ·OH formation is recommended. However, due to the natural presence of L-Phe and L-*p*-Tyr, use of the dextro enantiomer of Phe (D-Phe) for experiments with pyrite or other minerals suspended in biologically-active solutions may be more beneficial. This would allow for determination of the same reaction kinetics and product-ratios as Phe with less potential for incorporation into cells and enzymatic loss of D-Phe to the production of D-*p*-Tyr (Biondi et al. 2001) (though initial experiments would need to be conducted to monitor other forms of potential biological degradation).

Since Tyr, DOPA, and 2-phenylacetamide (theorized degradation product of Phe in MnO_2 and Mn_2O_3 slurries – based on molecular formula, retention time, and proposed reaction mechanism) were the only degradation products of Phe observed with the ESI+ MS method used in this study, improved detection methods for other degradation products should be explored. Newer models of mass spectrometers are available that can achieve sensitivity and resolution orders-of-magnitude higher than the ToF. Some even include real-time ionization switching, which allows for detection of positively- and negatively-charge compounds throughout the same run. Application of a more powerful MS could easily bring detection limits for Phe, Tyr, and DOPA closer to the picomolar range. Coupled with the advances in separation science (i.e., ultra-performance liquid chromatography (UPLC)), more samples could be processed and analyzed in a shorter amount of time. In the absence of a MS, fluorescent reagents (added post-filtration) that derivatize amino acid functional groups could be used as a way to increase fluorescence

sensitivity for analysis of Phe, Tyr, and other potential degradation products (provided they still retain the reactive functional groups) and might be worth considering for reactions with sub-millimolar levels of Phe.

The ongoing research focused on mineral-mediated ·OH is clearly warranted. Along with the detrimental human and ecological health impacts previously mentioned, an understanding of basic and advanced interactions of earth minerals with organic compounds may also help explain how life on Earth began. Interest in advanced oxidation methods (such as Fenton and Fenton-like reagents and minerals) in the environmental remediation field continues to grow as new methods for generating *in-situ* ROS for degradation of persistent pollutants are being investigated and implemented. Results presented in this study have contributed useful insight into the fate and formation of ·OH in a variety of solutions that mimic physiological and ecological conditions that can help advance these fields.

References

Albarran, G., Bentley, J. and Schuler, R. H. (2003). "Substituent effects in the reaction of OH radicals with aromatics: Toluene." *Journal of Physical Chemistry A* **107**(39): 7770-7774.

Albrecht, C., Borm, P. J. A., Adolf, B., Timblin, C. R. and Mossman, B. T. (2002). "In vitro and in vivo activation of extracellular signal-regulated kinases by coal dusts and quartz." *Toxicology and Applied Pharmacology* **184**(1): 37-45.

Altschuler, Z. S., Schnepfe, M. M., Silber, C. C. and Simon, F. O. (1983). "Sulfur diagenesis in Everglades peat and origin of pyrite in coal." *Science* **221**(4607): 221-227.

Atkinson, M. J. and Bingman, C. (1998). "Elemental composition of commercial seasalts." *Journal of Aquariculture and Aquatic Sciences* **VIII**(2): 39-43.

Baral, S., Lumepereira, C., Janata, E. and Henglein, A. (1986). "Chemistry of colloidal manganese oxides. 3. Formation in the reaction of hydroxyl radicals with Mn2+ ions." *Journal of Physical Chemistry* **90**(22): 6025-6028.

Bebie, J. and Schoonen, M. A. A. (1999). "Pyrite and phosphate in anoxia and an origin-of-life hypothesis." *Earth and Planetary Science Letters* **171**(1): 1-5.

Biondi, R., Xia, Y., Rossi, R., Paolocci, N., Ambrosio, G. and Zweier, J. L. (2001). "Detection of hydroxyl radicals by D-phenylalanine hydroxylation: A specific assay for hydroxyl radical generation in biological systems." *Analytical Biochemistry* **290**(1): 138-145.

Bonifacic, M., Schoneich, C. and Asmus, K. D. (1991). "Halsogenated peroxyl radicals as multielectron oxidants - Pulse-radiolysis study on the reaction of trichloromethyl perxyl radicals with iodide." *Journal of the Chemical Society-Chemical Communications*(16): 1117-1119.

Borda, M. J., Elsetinow, A. R., Strongin, D. R. and Schoonen, M. A. (2003). "A mechanism for the production of hydroxyl radical at surface defect sites on pyrite." *Geochimica Et Cosmochimica Acta* **67**(5): 935-939.

Burbano, A. A., Dionysiou, D. D., Suidan, M. T. and Richardson, T. L. (2005). "Oxidation kinetics and effect of pH on the degradation of MTBE with Fenton reagent." *Water Research* **39**(1): 107-118.

Buxton, G. V. and Sellers, R. M. (1975). "Pusle-radiolysis study of monovalent cadmium, cobalt, nickel and zinc in aqueous solution. 1. Formation and decay of monovalent ions." *Journal of the Chemical Society-Faraday Transactions I* **71**(3): 558-567.

Buxton, G. V., Sellers, R. M. and McCracken, D. R. (1976). "Pulse radiolysis study of monovalent cadmium, cobalt, nickel and zinc in aqueous solution. 2. Reactions of the

monovalent ions." *Journal of the Chemical Society-Faraday Transactions I* **72**: 1464-1476.

Buxton, G. V. and Elliot, A. J. (1986). "Rate-constant for reaction of hydroxyl radicals with bicarbonate ions." *Radiation Physics and Chemistry* **27**(3): 241-243.

Buxton, G. V., Greenstock, C. L., Helman, W. P. and Ross, A. B. (1988). "Critical-review of rate constants for reaction of hydrated electrons, hydrogen atoms and hydroxyl radicals (.OH/.O-) in aqueous-solutions." *Journal of Physical and Chemical Reference Data* **17**(2): 513-886.

Campbell, N. A., Reece, J. B. and Mitchell, L. G. (1999). Biology, Fifth Edition. Addison Wesley Longman, Inc., Menlo Park, CA. 802, **pp:** 1175.

Chang, C. Y., Hsieh, Y. H., Cheng, K. Y., Hsieh, L. L., Cheng, T. C. and Yao, K. S. (2008). "Effect of pH on Fenton process using estimation of hydroxyl radical with salicylic acid as trapping reagent." *Water Science and Technology* **58**(4): 873-879.

Chen, C. C., Wu, R. J., Tzeng, Y. Y. and Lu, C. S. (2009). "Chemical Oxidative Degradation of Acridine Orange Dye in Aqueous Solution by Fenton's Reagent." *Journal of the Chinese Chemical Society* **56**(6): 1147-1155.

Chen, G., Hoag, G. E., Chedda, P., Nadim, F., Woody, B. A. and Dobbs, G. M. (2001). "The mechanism and applicability of in situ oxidation of trichloroethylene with Fenton's reagent." *Journal of Hazardous Materials* **87**(1-3): 171-186.

Chen, R. Z. and Pignatello, J. J. (1997). "Role of quinone intermediates as electron shuttles in Fenton and photoassisted Fenton oxidations of aromatic compounds." *Environmental Science & Technology* **31**(8): 2399-2406.

Cheney, M. A., Sposito, G., McGrath, A. E. and Criddle, R. S. (1996). "Abiotic degradation of 2,4-D (dichlorophenoxyacetic acid) on synthetic birnessite: A calorespirometric method." *Colloids and Surfaces a-Physicochemical and Engineering Aspects* **107**: 131-140.

Chien, S. W. C., Chen, H. L., Wang, M. C. and Seshaiah, K. (2009). "Oxidative degradation and associated mineralization of catechol, hydroquinone and resorcinol catalyzed by birnessite." *Chemosphere* **74**(8): 1125-1133.

Cohen, G., Yakushin, S. and Dembiec-Cohen, D. (1998). "Protein L-Dopa as an index of hydroxyl radical attack on protein tyrosine." *Analytical Biochemistry* **263**(2): 232-239.

Cohn, C. A., Borda, M. J. and Schoonen, M. A. (2004). "RNA decomposition by pyrite-induced radicals and possible role of lipids during the emergence of life." *Earth and Planetary Science Letters* **225**(3-4): 271-278.

Cohn, C. A., Pak, A., Strongin, D. and Schoonen, M. A. (2005). "Quantifying hydrogen peroxide in iron-containing solutions using leuco crystal violet." *Geochemical Transactions* **6**(3): 47-51.

Cohn, C. A., Laffers, R., Simon, S. R., O'Riordan, T. and Schoonen, M. A. A. (2006a). "Role of pyrite in formation of hydroxyl radicals in coal: possible implications for human health." *Particle and Fibre Toxicology* **3**(1): 16.

Cohn, C. A., Laffers, R. and Schoonen, M. A. A. (2006b). "Using yeast RNA as a probe for generation of hydroxyl radicals by earth materials." *Environmental Science & Technology* **40**(8): 2838-2843.

Cohn, C. A., Mueller, S., Wimmer, E., Leifer, N., Greenbaum, S., Strongin, D. R. and Schoonen, M. A. A. (2006c). "Pyrite-induced hydroxyl radical formation and its effect on nucleic acids." *Geochemical Transactions* **7**: 11.

Cohn, C. A., Simon, S. R. and Schoonen, M. A. A. (2008). "Comparison of fluorescence-based techniques for the quantification of particle-induced hydroxyl radicals." *Particle and Fibre Toxicology* **5**: 9.

Cohn, C. A., Pedigo, C. E., Hylton, S. N., Simon, S. R. and Schoonen, M. A. A. (2009). "Evaluating the use of 3 '-(p-Aminophenyl) fluorescein for determining the formation of highly reactive oxygen species in particle suspensions." *Geochemical Transactions* **10**: 9.

Cohn, C. A., Fisher, S. C., Brownawell, B. J. and Schoonen, M. A. A. (2010). "Adenine oxidation by pyrite-generated hydroxyl radicals." *Geochemical Transactions* **11**: 8.

Dalal, N. S., Newman, J., Pack, D., Leonard, S. and Vallyathan, V. (1995). "Hydroxyl radical generation by coal-mine dust - possible implication to Coal-Workers Pneumoconiosis (CWP)." *Free Radical Biology and Medicine* **18**(1): 11-20.

Davies, M. J. (2005). "The oxidative environment and protein damage." *Biochimica Et Biophysica Acta-Proteins and Proteomics* **1703**(2): 93-109.

Davies, S. H. R. and Morgan, J. J. (1989). "Manganese(II) oxidation-kinetics on metal-oxide surfaces." *Journal of Colloid and Interface Science* **129**(1): 63-77.

de la Cruz Moreno, M. P., Oth, M., Deferme, S., Lammert, F., Tack, J., Dressman, J. and Augustijns, P. (2006). "Characterization of fasted-state human intestinal fluids collected from duodenum and jejunum." *Journal of Pharmacy and Pharmacology* **58**(8): 1079-1089.

De Laat, J. and Gallard, H. (1999). "Catalytic decomposition of hydrogen peroxide by Fe(III) in homogeneous aqueous solution: Mechanism and kinetic modeling." *Environmental Science & Technology* **33**(16): 2726-2732.

Deegan, A. M., Shaik, B., Nolan, K., Urell, K., Oelgemoller, M., Tobin, J. and Morrissey, A. (2011). "Treatment options for wastewater effluents from pharmaceutical companies." *International Journal of Environmental Science and Technology* **8**(3): 649-666.

Demers, L. M. and Kuhn, D. C. (1994). "Influence of mineral dusts on metabolism of arachidonic-acid by alveolar macrophage." *Environmental Health Perspectives* **102**: 97-100.

Descostes, M., Vitorge, P. and Beaucaire, C. (2004). "Pyrite dissolution in acidic media." *Geochimica Et Cosmochimica Acta* **68**(22): 4559-4569.

Descostes, M., Vitorge, P. and Beaucaire, C. (2006). "Response to the Comment by G. Druschel and M. Borda on "Pyrite dissolution in acidic media"." *Geochimica Et Cosmochimica Acta* **70**(20): 5251-5252.

Devoe, H. and Wasik, S. P. (1984). "Aqueous solubilities and enthalpies of solution of adenine and guanine." *Journal of Solution Chemistry* **13**(1): 51-60.

Dorfman, L. M. and Adams, G. E. (1973). "Reactivity of the hydroxyl radical in aqueous solutions." National Bureau of Standards Data System. National Bureau of Standards, U.S. Department of Commerse, **pp:** 63

Druschel, G. and Borda, M. (2006). "Comment on "Pyrite dissolution in acidic media" by M. Descostes, P. Vitorge, and C. Beaucaire." *Geochimica Et Cosmochimica Acta* **70**(20): 5246-5250.

Eastes, W., Morris, K. J., Morgan, A., Launder, K. A., Collier, C. G., Davis, J. A., Mattson, S. M. and Hadley, J. G. (1995). "DISSOLUTION OF CLASS FIBERS IN THE RAT LUNG FOLLOWING INTRATRACHEAL INSTILLATION." *Inhalation Toxicology* **7**(2): 197-213.

Eastes, W. and Hadley, J. G. (1995). "Dissolution of fibers inhaled by rats." *Inhalation Toxicology* **7**(2): 179-196.

Elder, A., Gelein, R., Silva, V., Feikert, T., Opanashuk, L., Carter, J., Potter, R., Maynard, A., Finkelstein, J. and Oberdoerster, G. (2006). "Translocation of inhaled ultrafine manganese oxide particles to the central nervous system." *Environmental Health Perspectives* **114**(8): 1172-1178.

Elsetinow, A. R., Schoonen, M. A. A. and Strongin, D. R. (2001). "Aqueous geochemical and surface science investigation of the effect of phosphate on pyrite oxidation." *Environmental Science & Technology* **35**(11): 2252-2257.

Evangelou, V. P., Seta, A. K. and Holt, A. (1998). "Potential role of bicarbonate during pyrite oxidation." *Environmental Science & Technology* **32**(14): 2084-2091.

Fenton, H. J. H. (1894). *Journal of Chemical Society Transactions* **65**: 899.

Fisher, S. C., Schoonen, M. A. A. and Brownawell, B. J. (2012). "Phenylalanine as a hydroxyl radical-specific probe in pyrite slurries." *Geochemical Transactions* **13**(3): 18.

Freire, A. C., Basit, A. W., Choudhary, R., Piong, C. W. and Merchant, H. A. (2011). "Does sex matter? The influence of gender on gastrointestinal physiology and drug delivery." *International Journal of Pharmaceutics* **415**(1-2): 15-28.

Frejaville, C., Karoui, H., Tuccio, B., Lemoigne, F., Culcasi, M., Pietri, S., Lauricella, R. and Tordo, P. (1995). "5-(Diethoxyphosphoryl)-5-methyl-1-pyrroline N-oxide - A new efficient phosphorylated nitrone for the in-vivo and in-vitro spin-trapping of oxygen-centered radicals." *Journal of Medicinal Chemistry* **38**(2): 258-265.

Friedman, M. (2010). "Origin, Microbiology, Nutrition, and Pharmacology of D-Amino Acids." *Chemistry & Biodiversity* **7**(6): 1491-1530.

Gluskoter, H. J. and Simon, J. A. (1968). "Sulfur in Illinois coals." Department of Registration and Education, **pp:** 32

Goldstein, S., Czapski, G., Cohen, H. and Meyerstein, D. (1992). "Deamination of beta-alanine induced by hydroxyl radicals and monovalent copper ions - A pulse-radiolysis study." *Inorganica Chimica Acta* **192**(1): 87-93.

Goldstone, J. V., Pullin, M. J., Bertilsson, S. and Voelker, B. M. (2002). "Reactions of hydroxyl radical with humic substances: Bleaching, mineralization, and production of bioavailable carbon substrates." *Environmental Science & Technology* **36**(3): 364-372.

Gonzalez-Davila, M., Santana-Casiano, J. M. and Millero, F. J. (2005). "Oxidation of iron(II) nanomolar with H2O2 in seawater." *Geochimica Et Cosmochimica Acta* **69**(1): 83-93.

Graham, R. M., Morgan, E. H. and Baker, E. (1998). "Characterisation of citrate and iron citrate uptake by cultured rat hepatocytes." *Journal of Hepatology* **29**(4): 603-613.

Grebel, J. E., Pignatello, J. J. and Mitch, W. A. (2010). "Effect of Halide Ions and Carbonates on Organic Contaminant Degradation by Hydroxyl Radical-Based Advanced Oxidation Processes in Saline Waters." *Environmental Science & Technology* **44**(17): 6822-6828.

Greene, A. C. and Madgwick, J. C. (1991). "Microbial formation of manganese oxide." *Applied and Environmental Microbiology* **57**(4): 1114-1120.

Grigorev, A. E., Makarov, I. E. and Pikaev, A. K. (1987). "Formation of Cl_2^- in the bulk solution during the radiolysis of concentrated aqueous-solutions of chlorides." *High Energy Chemistry* **21**(2): 99-102.

Guitton, J., Tinardon, F., Lamrini, R., Lacan, P., Desage, M. and Francina, A. (1998). "Decarboxylation of [1-C-13]leucine by hydroxyl radicals." *Free Radical Biology and Medicine* **25**(3): 340-345.

Hamm, R. E., Shull, C. M. and Grant, D. M. (1954). "Citrate complexes with iron(II) and iron(III)." *Journal of the American Chemical Society* **76**(8): 2111-2114.

Harrington, A. D., Hylton, S. and Schoonen, M. A. A. (2011). "Pyrite-driven reactive oxygen species formation in simulated lung fluid: implications for coal workers' pneumoconiosis." *Environmental Geochemistry and Health*: 12.

Harrison, J. D., Morris, D. L. and Hardcastle, J. D. (1993). "Screening for gastric-carcinoma in coal-miners." *Gut* **34**(4): 494-498.

Hosamani, R. R., Hegde, R. N. and Nandibewoor, S. T. (2010). "Mechanistic study on the oxidation of L-phenylalanine by copper(III) in aqueous alkaline medium: a kinetic approach." *Monatshefte Fur Chemie* **141**(10): 1069-1076.

Houghton, A. M., Mouded, M. and Shapiro, S. D. (2008). "Common origins of lung cancer and COPD." *Nature Medicine* **14**(10): 1023-1024.

Huang, X., Li, W. H., Attfield, M. D., Nadas, A., Frenkel, K. and Finkelman, R. B. (2005). "Mapping and prediction of coal workers' pneumoconiosis with bioavailable iron content in the bituminous coals." *Environmental Health Perspectives* **113**(8): 964-968.

Huang, X. and Finkelman, R. B. (2008). "Understanding the chemical properties of macerals and minerals in coal and its potential application for occupational lung disease prevention." *Journal of Toxicology and Environmental Health-Part B-Critical Reviews* **11**(1): 45-67.

Jayson, G. G., Stirling, D. A. and Swallow, A. J. (1971). "Pulse-radiolysis and X-radiolysis of 2-mercaptoethanol in aqueous solution." *International Journal of Radiation Biology and Related Studies in Physics Chemistry and Medicine* **19**(2): 143-&.

Jayson, G. G., Parsons, B. J. and Swallow, A. J. (1973). "Some simple, highly reactive, inorganic chlorine derivatives in aqueous-solution - Their formation using pulses of radiation and their police in mechanism of Fricke Dosimeter." *Journal of the Chemical Society-Faraday Transactions I*(9): 1597-1607.

Ji, P. and Feng, W. (2008). "Solubility of amino acids in water and aqueous solutions by the statistical associating fluid theory." *Industrial & Engineering Chemistry Research* **47**(16): 6275-6279.

Jokic, A., Frenkel, A. I., Vairavamurthy, M. A. and Huang, P. M. (2001). "Birnessite catalysis of the Maillard reaction: Its significance in natural humification." *Geophysical Research Letters* **28**(20): 3899-3902.

Jung, Y. S., Lim, W. T., Park, J. Y. and Kim, Y. H. (2009). "Effect of pH on Fenton and Fenton-like oxidation." *Environmental Technology* **30**(2): 183-190.

Kaur, H., Fagerheim, I., Grootveld, M., Puppo, A. and Halliwell, B. (1988). "Aromatic hydroxylation of phenylalanine as an assay for hydroxyl radicals - Application to activated human-neutrophils and to the heme protein leghemoglobin." *Analytical Biochemistry* **172**(2): 360-367.

King, D. W. and Farlow, R. (2000). "Role of carbonate speciation on the oxidation of Fe(II) by H2O2." *Marine Chemistry* **70**(1-3): 201-209.

Konigsberger, L. C., Konigsberger, E., May, P. M. and Hefter, G. T. (2000). "Complexation of iron(III) and iron(II) by citrate. Implications for iron speciation in blood plasma." *Journal of Inorganic Biochemistry* **78**(3): 175-184.

Kos, L., Michalska, K. and Perkowski, J. (2010). "Textile Wastewater Treatment by the Fenton Method." *Fibres & Textiles in Eastern Europe* **18**(4): 105-109.

Kumara, M. N., Mantelingu, K., Bhadregowda, D. G. and Rangappa, K. S. (2011). "Oxidation of L-Amino Acids by Metal Ion (Mn(3+)) in Sulfuric Acid Medium: Effect of Nucleophilicity and Hydrophobicity on Reaction Rate." *International Journal of Chemical Kinetics* **43**(11): 599-607.

Kwan, W. P. and Voelker, B. M. (2003). "Rates of hydroxyl radical generation and organic compound oxidation in mineral-catalyzed Fenton-like systems." *Environmental Science & Technology* **37**(6): 1150-1158.

Lalvani, S. B. and Zhang, G. (1994). "Mitigation of pyrite dissolution due to humic acids addition." *Fuel Science & Technology International* **12**(7-8): 963-982.

Liao, C. H., Kang, S. F. and Wu, F. A. (2001). "Hydroxyl radical scavenging role of chloride and bicarbonate ions in the H2O2/UV process." *Chemosphere* **44**(5): 1193-1200.

Lindsey, M. E. and Tarr, M. A. (2000). "Inhibition of hydroxyl radical reaction with aromatics by dissolved natural organic matter." *Environmental Science & Technology* **34**(3): 444-449.

Little, C. D., Palumbo, A. V., Herbes, S. E., Lidstrom, M. E., Tyndall, R. L. and Gilmer, P. J. (1988). "Trichloroethylene Biodegradation by a Methane-oxidizing Bacterium." *Applied and Environmental Microbiology* **54**(4): 951-956.

Liu, S.-Y., Xie, J., Zheng, Y.-X., Cao, G.-S., Zhu, T.-J. and Zhao, X.-B. (2012). "Nanocrystal manganese oxide (Mn3O4, MnO) anchored on graphite nanosheet with improved electrochemical Li-storage properties." *Electrochimica Acta* **66**: 271-278.

Lyons, P. C., Whelan, J. F. and Dulong, F. T. (1989). "Marine origin of pyritic sulfur in the Lower Bakerstown coal bed, Castleman coal field, Maryland (USA)." *International Journal of Coal Geology* **12**(1-4): 329-348.

Maruthamuthu, P. and Neta, P. (1978). "Phosphate radicals - Spectra, acid-base equilibria, and reactions with inorganic compounds." *Journal of Physical Chemistry* **82**(6): 710-713.

Marvin, L. F., Delatour, T., Tavazzi, I., Fay, L. B., Cupp, C. and Guy, P. A. (2003). "Quantification of o,o '-dityrosine, o-nitrotyrosine, and o-tyrosine in cat urine samples by LC/electrospray ionization-MS/MS using isotope dilution." *Analytical Chemistry* **75**(2): 261-267.

Matayatsuk, C., Poljak, A., Bustamante, S., Smythe, G. A., Kalpravidh, R. W., Sirankapracha, P., Fucharoen, S. and Wilairat, P. (2007). "Quantitative determination of ortho- and meta-tyrosine as biomarkers of protein oxidative damage in beta-thalassemia." *Redox Report* **12**(5): 219-228.

Matta, R., Hanna, K. and Chiron, S. (2007). "Fenton-like oxidation of 2,4,6-trinitrotoluene using different iron minerals." *Science of the Total Environment* **385**(1-3): 242-251.

Moller, P., Jacobsen, N. R., Folkmann, J. K., Danielsen, P. H., Mikkelsen, L., Hemmingsen, J. G., Vesterdal, L. K., Forchhammer, L., Wallin, H. and Loft, S. (2010). "Role of oxidative damage in toxicity of particulates." *Free Radical Research* **44**(1): 1-46.

Molnar, G. A., Nemes, V., Biro, Z., Ludany, A., Wagner, Z. and Wittmann, I. (2005a). "Accumulation of the hydroxyl free radical markers meta-, ortho-tyrosine and DOPA in cataractous lenses is accompanied by a lower protein and phenylalanine content of the water-soluble phase." *Free Radical Research* **39**(12): 1359-1366.

Molnar, G. A., Wagner, Z., Marko, L., Koszegi, T., Mohas, M., Kocsis, B., Matus, Z., Wagner, L., Tamasko, M., Mazak, I., et al. (2005b). "Urinary ortho-tyrosine excretion in diabetes mellitus and renal failure: Evidence for hydroxyl radical production." *Kidney International* **68**(5): 2281-2287.

Moncur, M. C., Jambor, J. L., Ptacek, C. J. and Blowes, D. W. (2009). "Mine drainage from the weathering of sulfide minerals and magnetite." *Applied Geochemistry* **24**(12): 2362-2373.

Monks, P. S., Granier, C., Fuzzi, S., Stohl, A., Williams, M. L., Akimoto, H., Amann, M., Baklanov, A., Baltensperger, U., Bey, I., et al. (2009). "Atmospheric composition change - global and regional air quality." *Atmospheric Environment* **43**(33): 5268-5350.

Motohashi, N. and Saito, Y. (1993). "Competitive measurement of rate constants for hydroxyl radical reactions using radiolytic hydroxylation of benzoate." *Chemical & Pharmaceutical Bulletin* **41**(10): 1842-1845.

Nair, U. J., Nair, J., Friesen, M. D., Bartsch, H. and Ohshima, H. (1995). "orhto-Tyrosine and meta-tyrosine formation from phenylalanine in human saliva as a marker of hydroxyl radical generation during betel quid chewing." *Carcinogenesis* **16**(5): 1195-1198.

Ng, A. W., Bidani, A. and Herring, T. A. (2004). "Innate host Defense of the lung: Effects of lung-lining fluid pH." *Lung* **182**(5): 297-317.

Nyberg, K., Johansson, U., Johansson, A. and Camner, P. (1992). "Phagolysosomal pH in alveolar macrophages." *Environmental Health Perspectives* **97**: 149-152.

Ono, Y., Matsumura, T. and Fukuzumi, S. (1977). "Electron-spin resonance studies on mechanism of formation of para-benzosemiquinone anion over manganese dioxide." *Journal of the Chemical Society-Perkin Transactions 2*(11): 1421-1424.

Oturan, M. A. and Pinson, J. (1995). "Hydroxylation by electrochemically generated OH radicals - monohydroxylation and polyhydroxylation of benzoic acid - products and isomer distribution." *Journal of Physical Chemistry* **99**(38): 13948-13954.

Pant, P. and Pant, S. (2010). "A review: Advances in microbial remediation of trichloroethylene (TCE)." *Journal of Environmental Sciences-China* **22**(1): 116-126.

Petigara, B. R., Blough, N. V. and Mignerey, A. C. (2002). "Mechanisms of hydrogen peroxide decomposition in soils." *Environmental Science & Technology* **36**(4): 639-645.

Pham, A. N. and Waite, T. D. (2008). "Modeling the kinetics of Fe(II) oxidation in the presence of citrate and salicylate in aqueous solutions at pH 6.0-8.0 and 25 degrees C." *Journal of Physical Chemistry A* **112**(24): 5395-5405.

Pham, H. T., Kitsuneduka, M., Hara, J., Suto, K. and Inoue, C. (2008). "Trichloroethylene transformation by natural mineral pyrite: The deciding role of oxygen." *Environmental Science & Technology* **42**(19): 7470-7475.

Pham, H. T., Suto, K. and Inoue, C. (2009). "Trichloroethylene Transformation in Aerobic Pyrite Suspension: Pathways and Kinetic Modeling." *Environmental Science & Technology* **43**(17): 6744-6749.

Post, J. E. (1999). "Manganese oxide minerals: Crystal structures and economic and environmental significance." *Proceedings of the National Academy of Sciences of the United States of America* **96**(7): 3447-3454.

Pratt, E. F. and Vandecasteele, J. F. (1961). "Oxidation by solids. I. Oxidation of selected alcohols by manganese dioxide." *Journal of Organic Chemistry* **26**(8): 2973-2975.

Pratt, E. F. and Suskind, S. P. (1963). "Oxidation by solids. II. The preparation of either tetraarylethanes or diaryl ketones by the oxidation of diarylmethanes with manganese dioxide." *Journal of Organic Chemistry* **28**(3): 638-642.

Pratt, E. F. and McGovern, T. P. (1964). "Oxidation by solids. III. Benzalanilines from N-benzylanilines and related oxidations by manganese dioxide." *Journal of Organic Chemistry* **29**(6): 1540-1543.

Rao, K. S. (2009). "Free Radical Induced Oxidative damage to DNA: Relation to Brain Aging and Neurological Disorders." *Indian Journal of Biochemistry & Biophysics* **46**(1): 9-15.

Rimstidt, J. D. and Vaughan, D. J. (2003). "Pyrite oxidation: A state-of-the-art assessment of the reaction mechanism." *Geochimica Et Cosmochimica Acta* **67**(5): 873-880.

Risser, J. A. and Bailey, G. W. (1997). "Spectroscopic study of soil particle surface redox reactions." *Bulletin of Environmental Contamination and Toxicology* **58**(3): 356-363.

Roels, H. A., Ghyselen, P., Buchet, J. P., Ceulemans, E. and Lauwerys, R. R. (1992). "Assessment of the permisible exposure level to manganese in workers exposed to manganese dioxide dust." *British Journal of Industrial Medicine* **49**(1): 25-34.

Rosso, K. M., Becker, U. and Hochella, M. F. (1999). "The interaction of pyrite {100} surfaces with O-2 and H2O: Fundamental oxidation mechanisms." *American Mineralogist* **84**(10): 1549-1561.

Rubert, K. F. and Pedersen, J. A. (2006). "Kinetics of oxytetracycline reaction with a hydrous manganese oxide." *Environmental Science & Technology* **40**(23): 7216-7221.

Samuni, A., Meisel, D. and Czapski, G. (1972). "The kinetics of the oxidation of chromium(II), titanium(III), and vanadium(IV) by hydrogen peroxide and hydroxyl radicals." *Journal of the Chemical Society-Dalton Transactions*(12): 1273-&.

Saran, M. and Summer, K. H. (1999). "Assaying for hydroxyl radicals: Hydroxylated terephthalate is a superior fluorescence marker than hydroxylated benzoate." *Free Radical Research* **31**(5): 429-436.

Sawyer, D. T. and Valentine, J. S. (1981). "How super is superoxide?" *Accounts of Chemical Research* **14**(12): 393-400.

Scholes, G., Shaw, P., Willson, R. L. and Ebert, M. (1965). Pulse radiolysis studies of aqueous solutions of nucleic acid and related substances. Academic Press, New York. 151-164

Schoonen, M. A. A. (2004). "Mechanisms of sedimentary pyrite formation." *Geological Society of America* **Special Paper**(379): 18.

Schoonen, M. A. A., Cohn, C. A., Roemer, E., Laffers, R., Simon, S. R. and O'Riordan, T. (2006). "Mineral-induced formation of reactive oxygen species." *Medical Mineralogy and Geochemistry* **64**: 179-221.

Schoonen, M. A. A., Harrington, A. D., Laffers, R. and Strongin, D. R. (2010). "Role of hydrogen peroxide and hydroxyl radical in pyrite oxidation by molecular oxygen." *Geochimica Et Cosmochimica Acta* **74**(17): 4971-4987.

Setsukinai, K., Urano, Y., Kakinuma, K., Majima, H. J. and Nagano, T. (2003). "Development of novel fluorescence probes that can reliably detect reactive oxygen species and distinguish specific species." *Journal of Biological Chemistry* **278**(5): 3170-3175.

Sigma Aldrich (2008a). Certificate of Analysis: Humic acid - Lot #1307944. www.sigmaaldrich.com.

Sigma Aldrich (2008b). Certificate of Analysis: Humic acid, sodium salt - Lot #09213LD. www.sigmaaldrich.com.

Sigma Aldrich (2010). Phone conversion regarding source of humic acid.

Smith, B. A., Teel, A. L. and Watts, R. J. (2004). "Identification of the reactive oxygen species responsible for carbon tetrachloride degradation in modified Fenton's systems." *Environmental Science & Technology* **38**(20): 5465-5469.

Sommerville, K. and Preston, T. (2001). "Characterisation of dissolved combined amino acids in marine waters." *Rapid Communications in Mass Spectrometry* **15**(15): 1287-1290.

Stadtman, E. R., Berlett, B. S. and Chock, P. B. (1990). "Manganese-dependent disproportionation of hydrogen peroxide in bicarbonate buffer." *Proceedings of the National Academy of Sciences of the United States of America* **87**(1): 384-388.

Stone, A. T. and Morgan, J. J. (1984a). "Reduction and dissolution of manganese(III) and manganese(IV) oxides by organics 2. Survey of the reactivity of organics." *Environmental Science & Technology* **18**(8): 617-624.

Stone, A. T. and Morgan, J. J. (1984b). "Reduction and dissolution of manganese(III) and manganese(IV) oxides by organics 1. Reaction with hydroquinone." *Environmental Science & Technology* **18**(6): 450-456.

Stone, A. T. (1987). "Reductive dissolution of manganese(III/IV) oxides by substituted phenols." *Environmental Science & Technology* **21**(10): 979-988.

Struyk, Z. and Sposito, G. (2001). "Redox properties of standard humic acids." *Geoderma* **102**(3-4): 329-346.

Stuglik, Z. and Zagorski, Z. P. (1981). "Pulse-radiolysis of neutral iron(II) solutions - Oxidation of ferrous ions by OH radicals." *Radiation Physics and Chemistry* **17**(4): 229-233.

Sukhov, N. L. and Ershov, B. G. (1982). "Pulse-radiolysis of aqueous solutions of Pb(II)." *High Energy Chemistry* **16**(6): 395-399.

Swaen, G. M. H., Meijers, J. M. M. and Slangen, J. J. M. (1995). "Risk of gastric-cancer in pneumoconiotic coal-miners and the effect of respiratory impairment." *Occupational and Environmental Medicine* **52**(9): 606-610.

Thiruvenkatachari, R., Kwon, T. O. and Moon, I. S. (2006). "Degradation of phthalic acids and benzoic acid from terephthalic acid wastewater by advanced oxidation processes." *Journal of Environmental Science and Health Part a-Toxic/Hazardous Substances & Environmental Engineering* **41**(8): 1685-1697.

Tizaoui, C., Karodia, N. and Aburowais, M. (2010). "Kinetic study of the manganese-based catalytic hydrogen peroxide oxidation of a persistent azo-dye." *Journal of Chemical Technology and Biotechnology* **85**(2): 234-242.

Turchi, C. S. and Ollis, D. F. (1989). "Mixed reactant photocatalysis - Intermediates and mutual rate inhibition." *Journal of Catalysis* **119**(2): 483-496.

Turchi, C. S. and Ollis, D. F. (1990). "Photocatalytic degradation of organic-water contaminants - Mechanisms involving hydroxyl radical attack." *Journal of Catalysis* **122**(1): 178-192.

Turrens, J. F. (1997). "Superoxide production by the mitochondrial respiratory chain." *Bioscience Reports* **17**(1): 3-8.

Ulrich, H. J. and Stone, A. T. (1989). "Oxidation of chlorophenols adsorbed to manganese oxide surfaces." *Environmental Science & Technology* **23**(4): 421-428.

Umar, M., Aziz, H. A. and Yusoff, M. S. (2010). "Trends in the use of Fenton, electro-Fenton and photo-Fenton for the treatment of landfill leachate." *Waste Management* **30**(11): 2113-2121.

Usher, C. R., Cleveland, C. A., Strongin, D. R. and Schoonen, M. A. (2004). "Origin of oxygen in sulfate during pyrite oxidation with water and dissolved oxygen: An in situ horizontal attenuated total reflectance infrared spectroscopy isotope study." *Environmental Science & Technology* **38**(21): 5604-5606.

Valavanidis, A., Vlachogianni, T. and Fiotakis, K. (2009). "Tobacco Smoke: Involvement of Reactive Oxygen Species and Stable Free Radicals in Mechanisms of Oxidative Damage, Carcinogenesis and Synergistic Effects with Other Respirable Particles." *International Journal of Environmental Research and Public Health* **6**(2): 445-462.

Vallyathan, V. (1994). "Generation of oxygen radicals by minerals and its correlation to cytotoxicity." *Environmental Health Perspectives* **102**: 111-115.

van Maanen, J. M. S., Borm, P. J. A., Knaapen, A., van Herwijnen, M., Schilderman, P., Smith, K. R., Aust, A. E., Tomatis, M. and Fubini, B. (1999). "In vitro effects of coal fly ashes:

Hydroxyl radical generation, iron release, and DNA damage and toxicity in rat lung epithelial cells." *Inhalation Toxicology* **11**(12): 1123-1141.

van Spronsen, F. J. (2010). "Phenylketonuria: a 21(st) century perspective." *Nature Reviews Endocrinology* **6**(9): 509-514.

Vidrio, E., Jung, H. and Anastasio, C. (2008). "Generation of hydroxyl radicals from dissolved transition metals in surrogate lung fluid solutions." *Atmospheric Environment* **42**(18): 4369-4379.

Vione, D., Ponzo, M., Bagnus, D., Maurino, V., Minero, C. and Carlotti, M. E. (2010). "Comparison of different probe molecules for the quantification of hydroxyl radicals in aqueous solution." *Environmental Chemistry Letters* **8**(1): 95-100.

Walling, C. (1975). "Fenton's reagent revisited." *Accounts of Chemical Research* **8**(4): 125-131.

Wang, Y. and Stone, A. T. (2006). "Reaction of Mn(III,IV) (hydr)oxides with oxalic acid, glyoxylic acid, phosphonoformic acid, and structurally-related organic compounds." *Geochimica Et Cosmochimica Acta* **70**(17): 4477-4490.

Watts, R. J., Sarasa, J., Loge, F. J. and Teel, A. L. (2005a). "Oxidative and reductive pathways in manganese-catalyzed Fenton's reactions." *Journal of Environmental Engineering-Asce* **131**(1): 158-164.

Watts, R. J., Howsawkeng, J. and Teel, A. L. (2005b). "Destruction of a carbon tetrachloride dense nonaqueous phase liquid by modified Fenton's reagent." *Journal of Environmental Engineering-Asce* **131**(7): 1114-1119.

Williams, L. B., Metge, D. W., Eberl, D. D., Harvey, R. W., Turner, A. G., Prapaipong, P. and Poret-Peterson, A. T. (2011). "What Makes a Natural Clay Antibacterial?" *Environmental Science & Technology* **45**(8): 3768-3773.

Wing, M. R., Stromvall, E. J. and Lieberman, S. H. (1990). "Real-time determination of Dissolved free amino-acids and primary amines in seawater by time-resolved fluorescence." *Marine Chemistry* **29**(4): 325-338.

Wu, J. J., Muruganandham, M., Yang, J. S. and Lin, S. S. (2006). "Oxidation of DMSO on goethite catalyst in the presence of H2O2 at neutral pH." *Catalysis Communications* **7**(11): 901-906.

Xi, L. J., Wang, H.-E., Lu, Z. G., Yang, S. L., Ma, R. G., Deng, J. Q. and Chung, C. Y. (2012). "Facile synthesis of porous LiMn(2)O(4) spheres as positive electrode for high-power lithium ion batteries." *Journal of Power Sources* **198**: 251-257.

Yao, W. S. and Millero, F. J. (1996). "Adsorption of phosphate on manganese dioxide in seawater." *Environmental Science & Technology* **30**(2): 536-541.

Yin, G. C., Danby, A. M., Kitko, D., Carter, J. D., Scheper, W. M. and Busch, D. H. (2007). "Understanding the selectivity of a moderate oxidation catalyst: Hydrogen abstraction by a fully characterized, activated catalyst, the robust dihydroxo manganese(IV) complex of a bridged cyclam." *Journal of the American Chemical Society* **129**(6): 1512-+.

Yoshimura, Y., Matsuzaki, Y., Watanabe, T., Uchiyama, K., Ohsawa, K. and Imaeda, K. (1992). "Effects of buffer solutions and chelators on the generation of hydroxyl radical and the lipid-peroxidation in the Fenton reaction system." *Journal of Clinical Biochemistry and Nutrition* **13**(3): 147-154.

Zegota, H., Kolodziejczyk, K., Krol, M. and Krol, B. (2005). "o-Tyrosine hydroxylation by OH center dot radicals. 2,3-DOPA and 2,5-DOPA formation in gamma-irradiated aqueous solution." *Radiation Physics and Chemistry* **72**(1): 25-33.

Zehavi, D. and Rabani, J. (1972). "Oxidation of aqueous bromide ions by hydroxyl radicals - Pulse radiolytic investigation." *Journal of Physical Chemistry* **76**(3): 312-&.

Zepp, R. G., Faust, B. C. and Hoigne, J. (1992). "Hydroxyl radical formation in aqueous reactions (pH 3-8) of iron(II) with hydrogen-peroxide - The photo-Fenton reaction." *Environmental Science & Technology* **26**(2): 313-319.

Zhang, C., Wang, L., Wu, F. and Deng, N. (2006). "Quantitation of hydroxyl radicals from photolysis of Fe(III)-citrate complexes in aerobic water." *Environmental Science and Pollution Research* **13**(3): 156-160.

Zhang, H. C. and Huang, C. H. (2003a). "Oxidative transformation of triclosan and chlorophene by manganese oxides." *Environmental Science & Technology* **37**(11): 2421-2430.

Zhang, H. C. and Huang, C. H. Manganese oxide-facilitated oxidative transformation of antibacterial agents. 3rd International Conference on Pharmaceuticals and Endocrine Disrupting Chemicals in Water, National Ground Water Association, Minneapolis, MN, March 19-21, 2003.

Zhang, H. C. and Huang, C. H. (2005). "Oxidative transformation of fluoroquinolone antibacterial agents and structurally related amines by manganese oxide." *Environmental Science & Technology* **39**(12): 4474-4483.

Zhang, H. C., Chen, W. R. and Huang, C. H. (2008). "Kinetic modeling of oxidation of antibacterial agents by manganese oxide." *Environmental Science & Technology* **42**(15): 5548-5554.

Zhang, J. Z., Wang, F. Y., House, J. D. and Page, B. (2004). "Thiols in wetland interstitial waters and their role in mercury and methylmercury speciation." *Limnology and Oceanography* **49**(6): 2276-2286.

Zheng, W., Liang, L. Y. and Gu, B. H. (2012). "Mercury Reduction and Oxidation by Reduced Natural Organic Matter in Anoxic Environments." *Environmental Science & Technology* **46**(1): 292-299.

Zhu, H., Li, H. L., Ou, Z. S. and Wang, D. Z. (2002). "Analysis of surface modification on coal pyrite." *Journal of the South African Institute of Mining and Metallurgy* **102**(5): 315-318.

Appendix

Supplemental Information File from:

Fisher, S.C., Schoonen M.A.A., Brownawell, B.J. 2012. Phenylalanine as a hydroxyl radical-specific probe in pyrite slurries. Geochemical Transactions 13(3):18p.

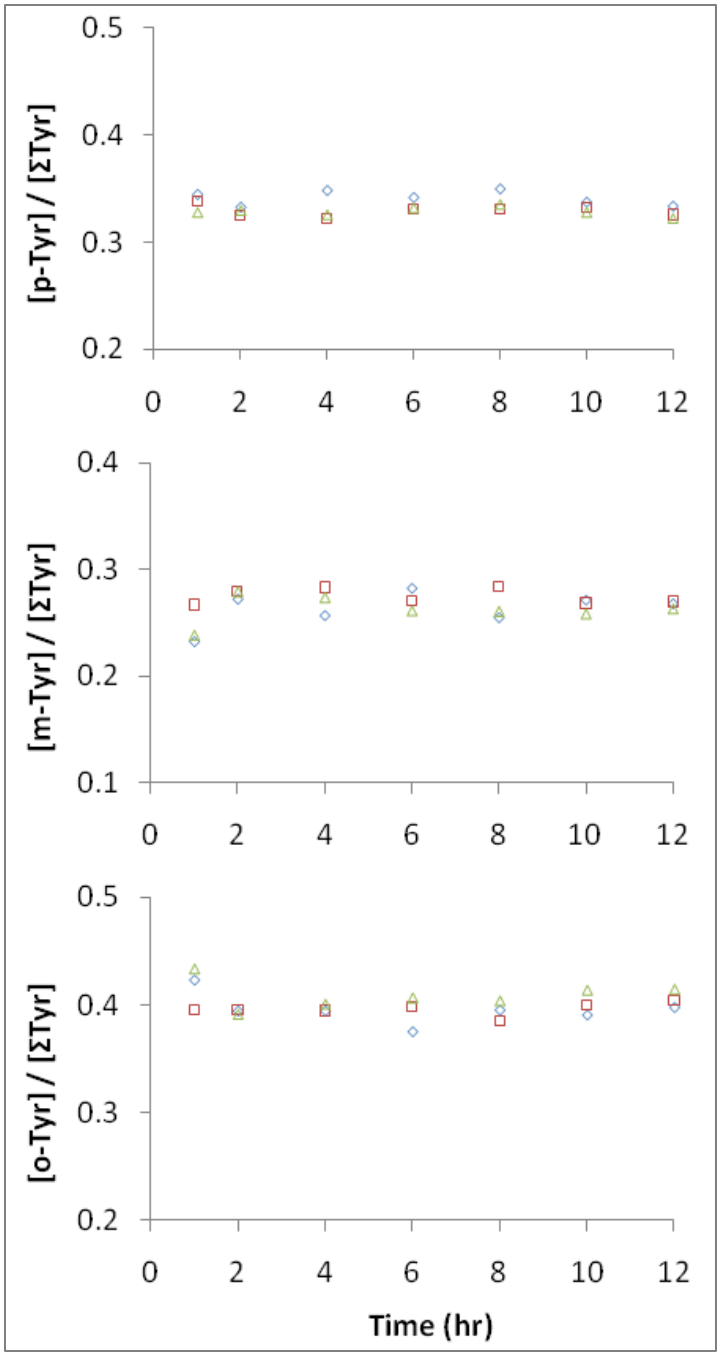

Figure A.1. Tyr-isomer ratios relative to ΣTyr during 100 µM Phe degradation (Exp. D). The proportions of each Tyr isomer are uniform among samples and are independent of $[Phe]_o$ and pyrite loading, with *p*-Tyr as 32%, *m*-Tyr as 28%, and *o*-Tyr as 40% of the ΣTyr. These results from experiment D of three different sets of 100 µM Phe experiments with **25 g L^{-1}** (◇), **50 g L^{-1}** (□), **100 g L^{-1}** (Δ) pyrite loading are characteristic of observed experimental results where Phe was still present.

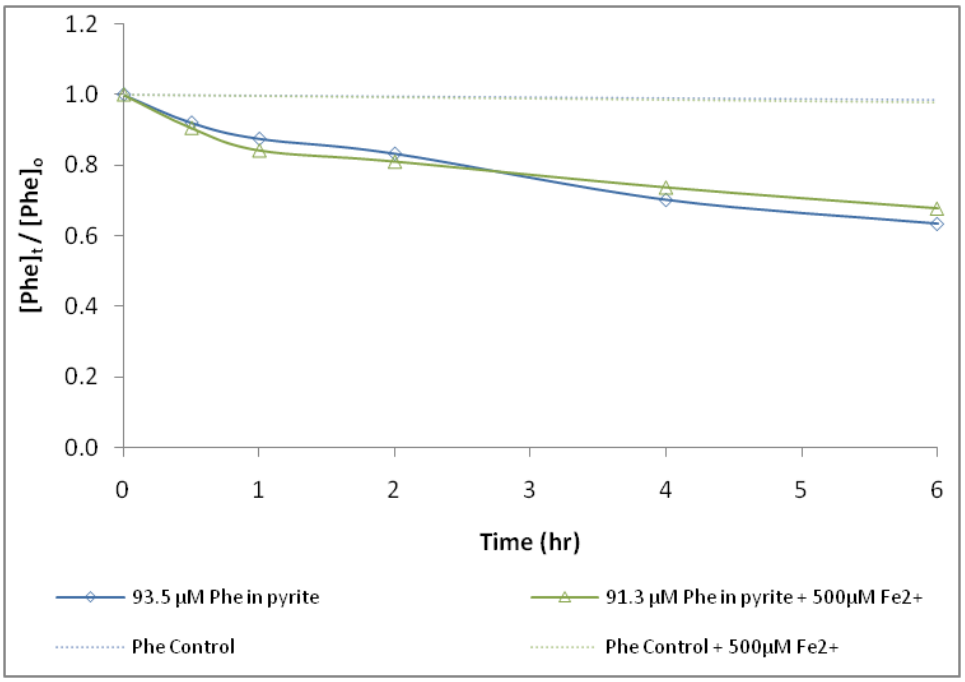

Figure A.2. Loss of Phe in 50 g L^{-1} pyrite with and without additional 500 µM Fe^{2+}. Results from incubations of Phe in 50 g L^{-1} pyrite with and without 500 µM Fe^{2+} (in the form or Mohr's salt) indicate that there is no significant differences in the rate of Phe loss over time. No loss of Phe was observed in two different control incubations without pyrite, and the production of expected levels of Tyr were also determined (data not shown). This confirms that ferrous iron is not the limiting factor in the formation of ·OH (via the Fenton reaction) in pyrite slurries.

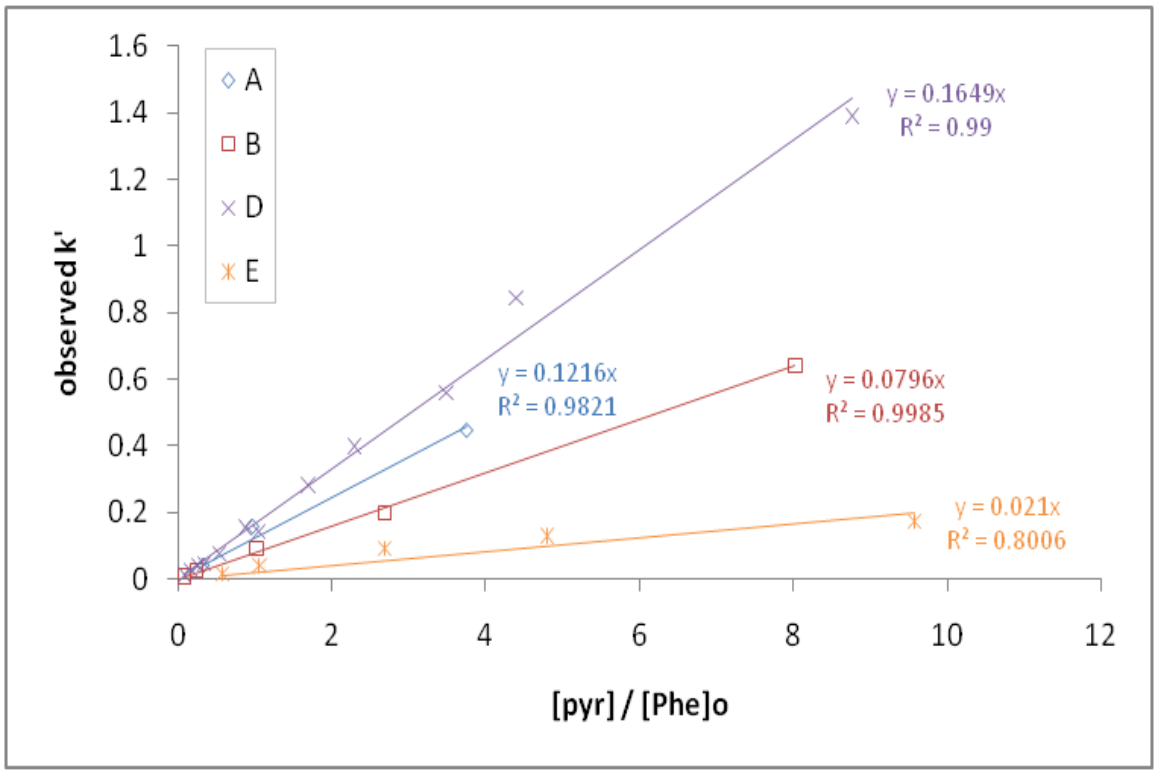

Figure A.3. Determination of estimated pyrite reactivity constant, K_{pyr} , for a given pyrite sample. Pseudo first-order rate constant ***k'*** (obtained empirically by fitting ln[Phe] versus **t**) versus pyrite loading over $[Phe]_o$; the resulting slopes correspond to the $\mathbf{K_{pyr}}$ of the sample of pyrite in a given experiment (A, B, D, or E) that can be used to model the data.

Numerical simulation

In contrast to the simplified model discussed in the main text, numerical simulations formulated to test some of the assumptions do not necessarily assume that $[Phe]_t + [Tyr]_t + \Sigma[i]_t \approx [Phe]_o$ (i.e. formation of CO_2 is permitted and removed from the equation). CO_2 formation decreases the reactant pool of reactive intermediates competing for ·OH. Two hypothesized reaction pathways (Figures A.4 and A.5) were compared to test the differences between a reaction pathway where Phe is completely degraded in just four steps to CO_2 (short pathway, Figure A.4), and one requiring a greater number of reactions and intermediates (long pathway, Figure A.5). Reaction Figure A.5 would seem more reasonable given the number of carbons in Phe, Tyr, and DOPA that would need to be fully oxidized to CO_2.

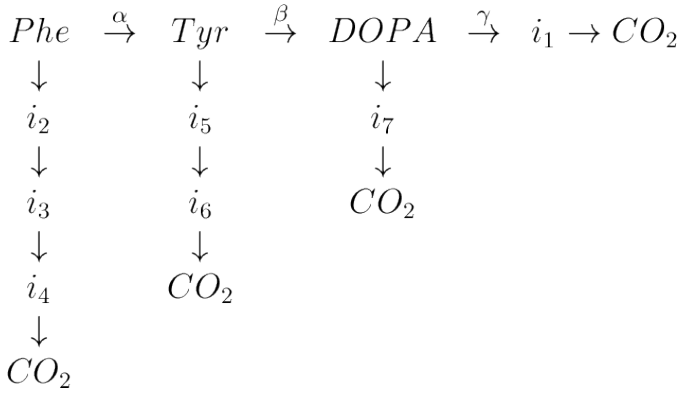

Figure A.4. Hypothetical reaction scheme with nine reaction intermediates "short pathway". Theoretical "short" pathway for the reaction of ·OH with Phe and three subsequent intermediates where all reactants are susceptible to ·OH reaction oxidation until CO_2 is formed and removed from competition.

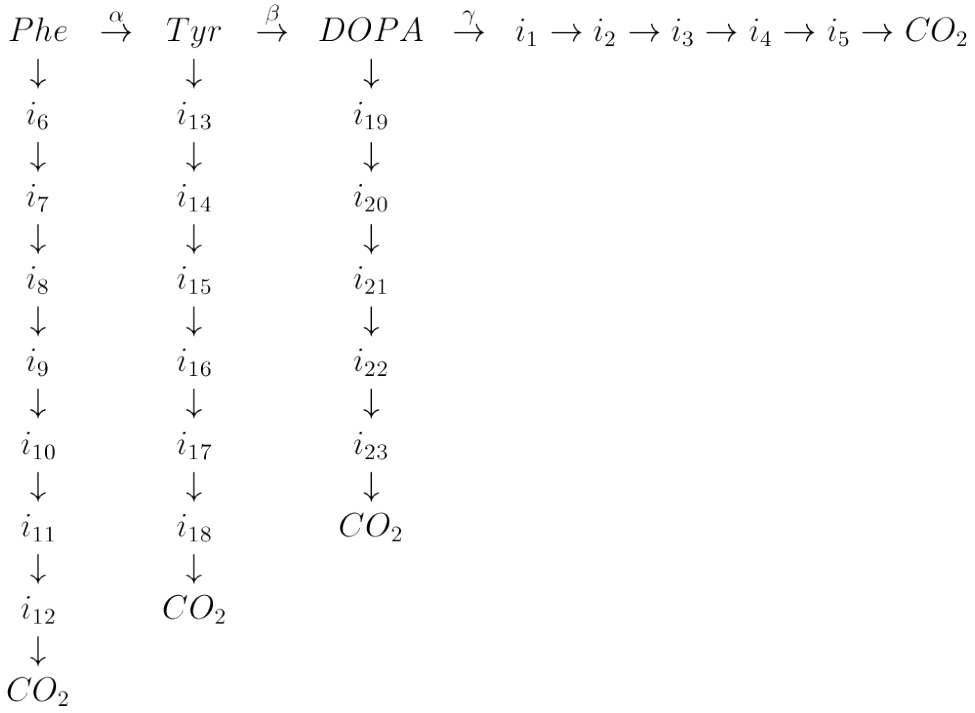

Figure A.5. Hypothetical reaction scheme with 25 reaction intermediates "long pathway". Theoretical "long" pathway for the reaction of ·OH with Phe and seven subsequent intermediates where all reactants are susceptible to ·OH reaction oxidation until CO_2 is formed and removed from competition. This pathway seems more realistic as there are many carbon atoms to oxidize before complete mineralization of Phe can be achieved.

To assess the effect of varying the individual rate constants for each reactant, the simulation solves competitive equations (analogous to Equation 2.12 for Tyr) iteratively for Phe, Tyr, DOPA, and i_n (where n can equal 1-7 or 5-23 depending on the pathway). The percentage of total ·OH-flux that is consumed by an individual reactant is determined by the product of its relative rate constant, ***f*** (defined here as the ratio of the second-order rate constant of a reactant relative to the rate constant for Phe (e.g. $\boldsymbol{f_i = k_i / k_{Phe}}$)), and its concentration divided by the sum of analogous terms for all competing reactants.

Calculations for the numerical simulation were done in Microsoft® Excel® 2007 using Equations A.1 for [Phe] and A.2 for [ΣTyr] at each time interval. Concentrations of additional degradation products (represented as "i_n" (includes DOPA in the Equations)) were calculated with similar formulas to for each species represented by Figures A.4 and A.5 ("short" and "long" degradation pathways, respectively).

$$[\mathrm{Phe}]_t = [\mathrm{Phe}]_{t-1} - [\cdot\mathrm{OH}]_t \left(\frac{k_{\mathrm{Phe}}[\mathrm{Phe}]_{t-1}}{k_{\mathrm{Phe}}[\mathrm{Phe}]_{t-1} + k_{\mathrm{Tyr}}[\mathrm{Tyr}]_{t-1} + \Sigma\, k_{i_n}[i_n]_{t-1} + K} \right) \quad \text{(A.1)}$$

$$[\mathrm{Tyr}]_t = \alpha\,([\mathrm{Phe}]_t - [\mathrm{Phe}]_{t-1}) + [\mathrm{Tyr}]_{t-1} - \left([\cdot\mathrm{OH}]_t \left(\frac{k_{\mathrm{Tyr}}[\mathrm{Tyr}]_{t-1}}{k_{\mathrm{Phe}}[\mathrm{Phe}]_{t-1} + k_{\mathrm{Tyr}}[\mathrm{Tyr}]_{t-1} + \Sigma\, k_{i_n}[i_n]_{t-1} + K} \right) \right. \quad \text{(A.2)}$$

Analytical results and estimated $\mathbf{K_{pyr}}$ from Experiment D were compared to predictions by both analytical solution of the model presented above (Equations 2.11 and 14; Figure A.6) and numerical simulations described here (Figure A.7). Predictions from the simplified model was examined first alongside observed data points for Phe and Tyr for 29.5 μM $[Phe]_o$ in 50 $g\ L^{-1}$ pyrite loading (Figure A.6A) and 94.5 μM $[Phe]_o$ in 100 $g\ L^{-1}$ pyrite loading (Figure A.6B), respectively.

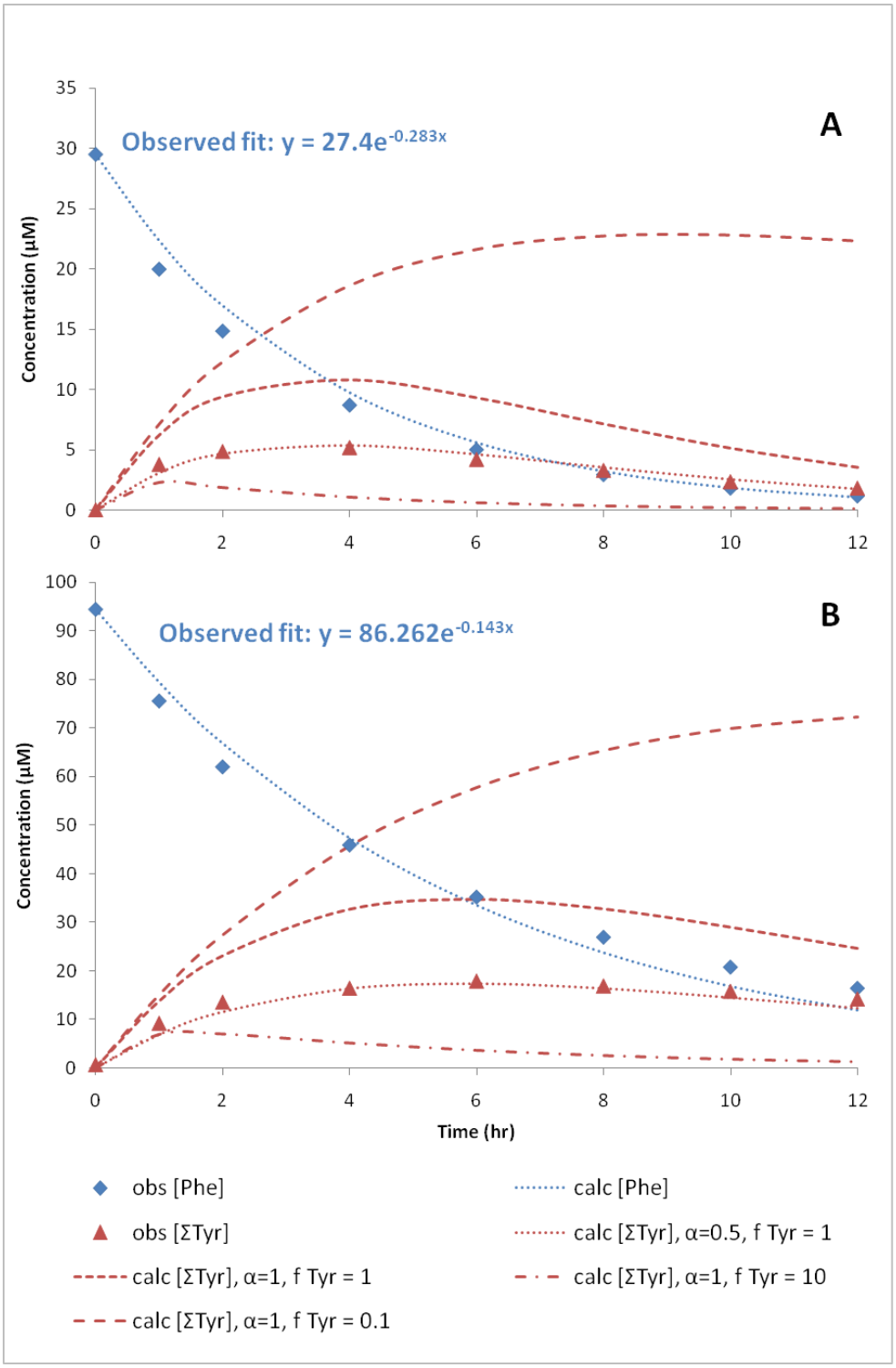

Figure A.6. Calculations for the simplified model based on experimental data. Kinetic data from experiment D is plotted with $[Phe]_o$ of 29.5 µM (A) and 94.5 µM (B) and pyrite loading of 50 g L^{-1} and 100 g L^{-1}, respectively. Values of **α** are either 0.5 or 1 and values of f_{Tyr} were set to 0.1, 1, or 10; values of f_i were all assumed to equal 1 for the purposes of this exercise.

The models showed no change in the kinetics of Phe loss when $\boldsymbol{\alpha}$ or $\boldsymbol{f_{Tyr}}$ were varied because the underlying assumptions that led to Equation 2.11 have not been changed. However, ΣTyr calculated when $\boldsymbol{\alpha}$ = 0.5 or 1 and $\boldsymbol{f_{Tyr}}$ = 0.1, 1, or 10 were dramatically different, and reveal the closest fit to the actual data when $\boldsymbol{\alpha}$ = 0.5 and $\boldsymbol{f_{Tyr}}$ = 1. Predicted ΣTyr, when $\boldsymbol{k_{Tyr}}$ did not equal $\boldsymbol{k_{Phe}}$, were not possible with Equation 2.14. Instead, integration of a more general rate expression for consecutive reactions was used (Equation A.3).

$$[\mathrm{Tyr}]_t = \alpha\,[\mathrm{Phe}]_o \left(\frac{\frac{K_{pyr}\,[pyr]}{[\mathrm{Phe}]_o}}{k'_{\mathrm{Tyr}} - \frac{K_{pyr}\,[pyr]}{[\mathrm{Phe}]_o}} \right) \left(e^{-k'_{\mathrm{Tyr}}\,t} - e^{-\frac{K_{pyr}\,[pyr]}{[\mathrm{Phe}]_o}\,t} \right) \tag{A.3}$$

The numerical simulation was used to test the assumption $\boldsymbol{k_{Tyr} \approx k_{Phe}}$ made in the simplified first-order model for [Tyr] through time (Equations 2.13 and 2.14). Assuming that $\boldsymbol{k_{Tyr} \neq k_{Phe}}$ results in a different integration for determining [Tyr] (Equation A.3). However, when simulations were run with a realistic range of $\boldsymbol{k_{Phe}}$ / $\boldsymbol{k_{Tyr}}$, the predicted [Tyr] did not appreciably differ from predictions using the assumption that the rate constants were equal (Equation 2.14).

Simulations were then examined in Figure A.7 with the same $[\mathrm{Phe}]_o$ and pyrite loadings shown in Figure A.6. Figure A.7 also considers the short and long pathways (Figures A.4 and A.5) and shows simulations of CO_2 concentration formed over time. In agreement with the predictions from the model (Figure A.6), an excellent fit to the observed data is also represented by the simulations that set $\boldsymbol{\alpha}$ = 0.5 and $\boldsymbol{f_{Tyr}}$ = 1 (Figures A.7A & E) with the powers of the exponential fits similar. Phe concentration through time when $\boldsymbol{\alpha}$ is increased to 1 (Figures A.7B & D) are identical to those determined when $\boldsymbol{\alpha}$ = 0.5 (Figures A.7A & E); however, Tyr concentration at each time point doubles as a result of $\boldsymbol{\alpha}$ = 1 channeling all Phe degradation through Tyr.

Figures A.7C & G illustrate the effect of increasing the reactivity of Tyr in comparison to Phe and represent a $\boldsymbol{k_{Tyr}}$ that is 10-times faster than $\boldsymbol{k_{Phe}}$ ($\boldsymbol{f_{Tyr}}$ = 10) when all the Phe in the system forms Tyr ($\boldsymbol{\alpha}$ = 1). Not only is measured $[\mathrm{Tyr}]_t$ under-predicted by the model, but $[\mathrm{Phe}]_t$ is over-predicted as expected, the latter due to increased competition for ·OH even at lower concentrations of Tyr. Similarly, where $\boldsymbol{k_{Tyr}}$ is one-tenth the value of $\boldsymbol{k_{Phe}}$ ($\boldsymbol{f_{Tyr}}$ = 0.1) and $\boldsymbol{\alpha}$ = 1, the simulated results show a faster, near zero-order loss of Phe over much of the time and a relatively large build-up of Tyr (Figures A.7D & H). Compared to other the simulations where CO_2 production is only observed when modeling the short pathway, CO_2 evolves more rapidly when $\boldsymbol{f_{Tyr}}$ is small, and appreciable amounts are even projected to form over the long pathway.

Overall, there are not significant differences in the loss of Phe through time when the short and long pathways are compared with the assumptions used. Variations in $\boldsymbol{\alpha}$ and $\boldsymbol{f_{Tyr}}$ can change the apparent kinetics in both the numerical simulations and the analytical models. Accumulation of CO_2 in the short pathway is much more rapid; however, it does not appreciably influence the loss of Phe because the pool of oxidizable reactants is not greatly depleted over the

timescale of Phe degradation. This is also generally the case for Tyr, with the notable exception of the simulation illustrated in Figure A.7D corresponding to greater amounts of CO_2 produced and loss of competing reactants.

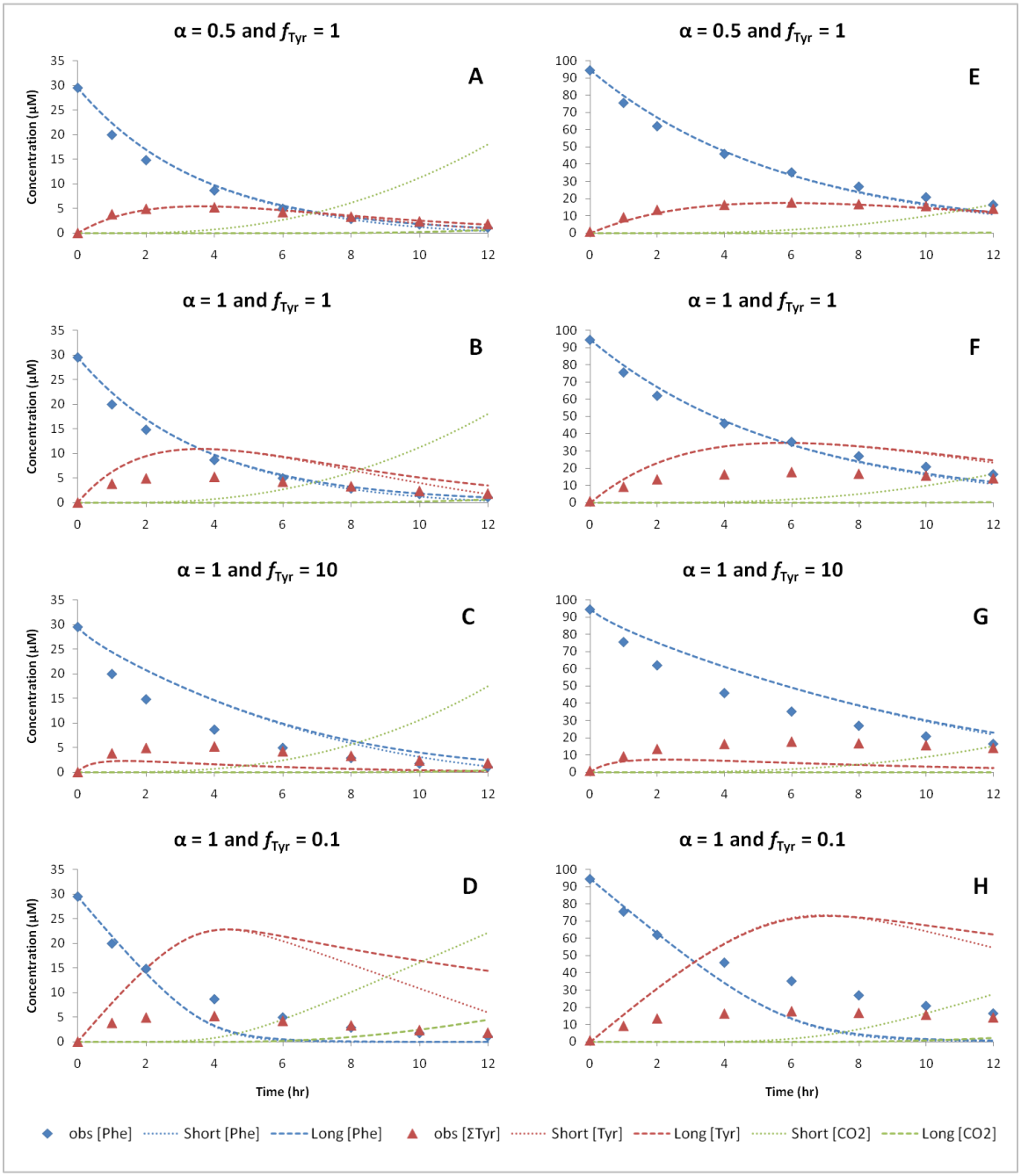

Figure A.7. Simulations of kinetic curves for experiment D. Simulations presented with $[Phe]_o$ of 29.5 μM (A-D) and 94.5 μM (E-H) and pyrite loading of 50 g L^{-1} and 100 g L^{-1}, respectively. Values of **α** are either 0.5 or 1 and values of f_{Tyr} was set to 0.1, 1, or 10.